UNIVERSITY OF Southampton

University of Southampton Research Repository
ePrints Soton

Copyright © and Moral Rights for this thesis are retained by the author and/or other copyright owners. A copy can be downloaded for personal non-commercial research or study, without prior permission or charge. This thesis cannot be reproduced or quoted extensively from without first obtaining permission in writing from the copyright holder/s. The content must not be changed in any way or sold commercially in any format or medium without the formal permission of the copyright holders.

When referring to this work, full bibliographic details including the author, title, awarding institution and date of the thesis must be given e.g.

AUTHOR (year of submission) "Full thesis title", University of Southampton, name of the University School or Department, PhD Thesis, pagination

http://eprints.soton.ac.uk

UNIVERSITY OF SOUTHAMPTON

FACULTY OF ENGINEERING AND THE ENVIRONMENT

School of Civil Engineering and the Environment

A study of the structure in solid wastes and some implications for fluid flow in landfills

By

Diana Milena Caicedo

Thesis for the degree of Doctor of Philosophy

June 2013

UNIVERSITY OF SOUTHAMPTON

<u>**ABSTRACT**</u>

FACULTY OF ENGINEERING AND THE ENVIRONMENT
School of Civil Engineering and the Environment

A STUDY OF THE STRUCTURE IN SOLID WASTE AND SOME IMPLICATIONS FOR FLUID FLOW IN LANDFILLS
by Diana Milena Caicedo

The search for alternative landfill operation and management strategies has triggered the development of the concept of a landfill as a bioreactor. The application of the concept requires the recirculation of liquids and hence a better understanding of fluid flow and transport processes that are strongly controlled by the physical structure of the media. It is generally accepted that as a result of the deposition in progressive layers, compaction and heterogeneity; solid waste develops a strong and anisotropic structure. Also, that due to their flat shape and orientation, materials such as plastics and textiles can influence flow behavior. The aim of this research was to provide a better understanding of the structure that develops when solid wastes are landfilled and the influence of this structure on fluid flow. The research included a characterization and description of specimens of raw household waste (MSW) and pretreated wastes (MBT) using PSD mathematical models, an study of the changes caused to particle size and shape by degradation processes, a study of the effect that flat shaped particles have on the fluid flow characteristics of a porous medium, and an investigation of the structure of a MSW specimen applying invasive and non-invasive radiographic techniques.

The study revealed that the characteristics of particle size and shape differ between waste materials and also change with degradation. An MBT specimen that had gone a dual anaerobic aerobic treatment showed statistically insignificant changes in particle size and shape with degradation, whilst partially treated MBT and MSW specimens showed significant changes in the particle size and in the content of flat shaped materials. PSD models were successfully fitted to the different specimens investigated suggesting that analytical expressions can be incorporated into existing waste behavioural mathematical models to characterise the particle size. Flat shaped particles that comply to be at least 15 times larger than the matrix particles and constitute at least 7.3% by dry mass were found to reduce the hydraulic conductivity by a factor of more than 30%. The reduction factor is controlled by the relative content and size of the intrusive particles and it is always within one order of magnitude.

The use of dye tracer visualization, thin sectioning and μCT techniques were pioneered during this research for the study of preferential flow and the structure in solid waste. This

study evidenced that the presence of high content of inert coarse flat shaped materials in a specimen of MSW resulted in the development of a strongly layered structure, with large pores horizontally connected and that favoured preferential flow.

Table of contents

List of Tables

List of Figures

Declaration Of Authorship

I, Diana Milena Caicedo Concha, declare that the thesis presented in this document named "**A study of the structure in solid wastes and some implications for fluid flow in landfills**" and the work presented in it are my own and has been generated by me as the result of my own original research.

I confirm that:

1. This work was done wholly or mainly while in candidature for a research degree at the University of Southampton ;

2. I have acknowledged all main sources of help. A special contribution has been acknowledged in Chapter 4 to Professor John Barker for his contribution in developing a model that explains the impact of the inclusion of 2D particles in the hydraulic conductivity of a matrix. Further details of Professor Barker contribution are given in the introductory part of Chapter 4;

3. Where any part of this thesis has previously been submitted for a degree or any other qualification at this University or any other institution, this has been clearly stated;

4. Where I have consulted the published work of others, this is always clearly attributed;

5. Where I have quoted from the work of others, the source is always given. With the exception of such quotations, this thesis is entirely my own work;

6. Where the thesis is based on work done by myself jointly with others, I have made clear exactly what was done by others and what I have contributed myself;

7. Either none of this work has been published before submission, or parts of this work have been published as

CAICEDO, D. M., WATSON, G. V. R., RICHARDS, D. J. & POWRIE, W. 2011. Exploring the use of Micro-focus Computed Tomography for a better conceptual understanding of structure in landfilled waste in the context of post-closure management for landfills. *Sustainable Environmental Research*, 21**,** 1-10.

CAICEDO, D. M., SANDOVAL, J. J., WATSON, G. V. R., RICHARDS, D. J. & POWRIE, W. 2010. Exploring the use of a modified dye-adsorption method for the study of landfilled waste structure and some implications for post-closure management in landfills. *Global Waste Management Symposium.* San Antonio, Texas.

CAICEDO, D. M., WATSON, G. V. R., RICHARDS, D. J. & POWRIE, W. 2010. Exploring the use of Micro-focus Computed Tomography for a better conceptual understanding of flow and structure in landfilled waste in the context of post-closure management for landfills. *1st International Conference on Final Sinks.* Vienna, Austria.

VELKUSHANOVA, K., CAICEDO, D., RICHARDS, D. J. & POWRIE, W. A detailed characterisation of an MBT waste. Proceedings Sardinia 2009, Twelfth International Waste Management and Landfill Symposium, 5-9 October 2009 2009 S. Margherita di Pula, Cagliari, Italy.

These publications can be found within this document in Chapter 9

Signed:

Date: June of 2013

Acknowledgement

Praise be to God almighty that makes possible the impossible things.

I am heartily thankful to all the people who in one way or another have been involved with the work conducted during this research. My main gratitude is for my supervisors, William Powrie and David Richards , whose guidance enabled me to attain understanding of the subject and to develop important skills.

This thesis would not have been possible without the help of the research staff in the School of Civil Engineering and Environment at the University of Southampton, and in particular the members of the Waste Management Research Group. A special acknowledgement is indebted to Geoff Watson and Harvey Skinner who have made available their support in different but equally important ways.

Thanks to my beloved husband John and his constant love and support, this would have been unimaginable without his presence.

This work was funded by EPSRC grant: EP/E041965/1: "Science and strategies for the long-term management and remediation of landfills"

Abbreviations

Abbreviation	*Definition*		*Abbreviation*	*Definition*
CAR	Consolidating Anaerobic Reactor		RR	Rosin-Rammler Distribution
DO	Dissolved oxygen		RS	Relative size of 2D particles to the matrix material
German MBT	Sample collected in Germany from an MBT process		SD	Standard deviation during material characterisation
LB-b	Leighton Buzzard sand fraction b		STDEV	Standard deviation of the replicates taken in the sieving analysis
LB-d	Leighton Buzzard sand fraction d		t-test	Statistical test that compares the difference in the mean of two distributions
MBT	Mechanical and Biological Treatment		UK MBT	Sample collected in the UK from an MBT process
MSW	Sample of Municipal Solid Waste		AR	Aspect Ratio
NORMDIST	Normal distribution		VC	Volumetric Content
NORMINV	Inverse Normal distribution		PSD	Particle size distribution
PDF	Probability density function		CT and μCT	Computed Tomography and Microfocus CT

Notation

Greek Symbols

Symbol	*Definition*
α	Proportionality constant (in application of Maxwell equation) that relates the volume proportion on 2D particles embedded in a matrix with the diameter of the matrix and 2D particles
α_1	Radius of the embedded particles in Maxwell equation
α_2	Radius of the matrix particles in Maxwell equation
β	An exponent in Equation 2-4 frequently taking of approximate ≈ 2
Δl	Distance between the manometer intakes
ε	Power coefficient applicable to D and d to ensure correct dimensionality in the application of Maxwell equation
μ	Dynamic viscosity
μ	Linear x-ray attenuation coefficient
ν	The specific discharge (Darcy´s Law)
ρ	Fluid density. Electron density in x-ray attenuation equations
ρ_{dry}	Solid dry mass density
ρ_M	Material density

Roman symbols

Symbol	*Definition*
a_i	Area of flow as a contribution of one particle in a range size
A	Cross section area in Darcy´s law
A_E	Area of the elemental volume
A_i	Total channel flow area as a contribution of all the particles in a range size
C	Dimensionless numerical coefficient whose value depends on geometrical shape of the internal structure of the medium

Symbol	*Definition*
d	Characteristic length of the system that can indicate the effective particle size, the coarseness of the solid matrix or the capillary tube diameter
D	Fractal dimension or diameter of the 2D particles (polystyrene discs)
d'	A parameter in the RR model that corresponds to the size of the particles where 63.2% by mass are smaller
D_{discs}	Diameter of the 2D particles (polystyrene discs)
D_i	Channel diameter
D_{10}	The finest 10% fraction in particulate solid media
D_{25}	The finest 25% fraction in particulate solid media
D_{50}	The finest 50% fraction in particulate solid media
D_{60}	The finest 60% fraction in particulate solid media
d_i	Minimum size in a range of sizes
d_{min}	Minimum diameter of the particles that constitute the matrix (sand grains)
d_{max}	Maximum diameter of the particles that constitute the matrix (sand grains)
E	Energy of incoming x-ray beam
e	Void ratio
$f_D(\bar{d}_i)$	Size dependent function that relates the particles average size with the diameter of a channel element
$f_L(\bar{d}_i)$	Size dependent function that relates the particles average size with the length of a channel element
$f_1(shape)$	A function of the pore or particle shape which includes characteristics such as the sphericity, roundness, packing and flow path tortuosity
$f_2(n)$	A function of the porosity of the media
g	Gravity acceleration
G_s	Relative density of solid particles that constitute a porous media
$\bar{G}_s$	Relative density of a mixture that constitute a porous media
h	Hydraulic head
h_i	Elevations of the fluid levels in each manometer (Darcy´s Law)

Symbol	*Definition*
I_0	Initial beam intensity
$I_{(x)}$	Transmitted beam intensity
i	Hydraulic gradient (Darcy´s Law)
k	Intrinsic permeability
K	Hydraulic conductivity in Darcy`s law
K_i	Effective permeability for the group of channels within the network
K_{discs}	Hydraulic conductivity of the embedded particles (discs in the application of Darcy`s law)
K_0	Hydraulic conductivity of the matrix in Darcy`s law
K_{ck}	Hydraulic conductivity estimated using the Carman-Kozeny model
$K_{saturated}$	Hydraulic conductivity at saturated conditions
l	Element of channel length
L_e	Length of the elemental volume or average effective path in Carman-Kozeny model
L	Length of an hypothetical particle moving through a straight line in the Carman-Kozeny model
L_i	Total channel length
$\frac{M(x < x_{max})}{M_T}$	In the fractal mode it is the mass fraction of material with a size less than the sieve size x_{max}
n	Porosity
N	Total number of particles (spheres or 2D particles in Maxwell equation) embedded in a matrix
N_i	Total number of particles in a range of sizes
N_0	Total number of 2D particles in the sample
NSE	Nash-Sutcliffe model efficiency coefficient
p	Volume proportion of the embedded particles in a matrix
q_i	Flow rate for the group of channels within the network

Symbol	*Definition*
Q	Fluid Flow rate
$Q_{saturated}$	Fluid Flow rate at saturated conditions
$Q_{experimental}$	Fluid Flow rate at unsaturated experimental conditions
$Q_{average}$	Fluid Flow rate at average experimental conditions
r	Effective specific resistance of a medium comprised of matrix and embedded particles (Maxwell equation)
r_1	Resistance of the embedded particles in Maxwell equation
r_2	Resistance of the matrix particles in Maxwell equation
R^2	Coefficient of determination for a linear regression
RS	Relation of sizes between the 2D particles and matrix material
S	Standard deviation of the distribution (in the variable x)
s_g	Standard deviation of the distribution transformed according to the log-normal law (in the variable z)
S_{diff}	Difference of the standard deviations of the distributions before and after degradation
S_1	Standard deviation of the distribution before degradation
S_2	Standard deviation of the distribution after degradation
v	A parameter in the RR model that corresponds to the slope of the linear representation Y vs X
v	Velocity of a hypothetical particle in the Carman-Kozeny model
$\mathrm{v_p}$	Velocity of an actual particle in the Carman-Kozeny model
V	Specimen volume
VC	Volumetric content of 2D particles in the matrix material
V_{discs}	Volumetric content of 2D particles
V_E	Elemental volume

Symbol	***Definition***
V_{sand}	Volumetric content of sand grains
x	Sieve size and length of x-ray path through a material
x_{max}	The maximum sieve size in the fractal model
x_{mean1}	Sieve size mean value before the degradation
x_{mean2}	Sieve size mean value after the degradation
$y_{average}$	Arithmetic mean for the material mass fraction that is retained or passes through a sieve
$y_{estimated}$	Material mass fraction estimated with a mathematical model
$y_{measured}$	Material mass fraction measured experimentally
$y_{passing}$	Material mass fraction that passes through a sieve of a certain size
$y_{retained}$	Material mass fraction retained in each of the sieves of a stack
z	Logarithmic transformation of the sieve size to make a log-normal distribution
z_i	Elevation of the manometer intake (Darcy´s Law)
z_{mean}	Mean of the values of sieve size logarithmically transformed
Z	Effective atomic number

1. Introduction

Landfilling is generally considered the least desirable option for final disposal of solid waste. Nevertheless, in many countries, landfilling remains the final disposal route for solid wastes. Recalcitrant contaminants in landfill sites are likely to persist for centuries rather than decades and liner and leachate collection systems are likely to fail before this time (Hall et al., 2007). Thus the risk of pollution posed by active and closed landfill sites extends well beyond the operational period for the site (Hudgins and Harper, 1999).

The search for alternative landfill operation and management strategies has triggered the development of the concept of a landfill as a bioreactor, aiming to enhance biodegradation, which has many advantages. These include improved site utilization (through accelerated settlement), leachate management, physicochemical stabilization and removal of contaminants. The application of the concept requires the recirculation of liquids and hence a better understanding of fluid flow and transport processes in landfills.

Research in porous media including soils, packed beds and foams, has revealed that flow and transport processes are strongly controlled by the physical structure of the media. The term structure refers to the particles' arrangement or organization, which is determined by their geometrical properties, i.e. size and shape. The geometry of the solid matrix in turn controls the architecture of the pore space, i.e. total porosity, geometry and interconnectivity of the pore space, through which fluids flow (Collins, 1961, Beven and Germann, 1982, Dullien, 1992, Hillel, 1998).

Municipal solid waste (MSW) is a porous medium comprising a mixture of highly diverse materials (e.g. plastics, textiles, glass and organic waste). It is recognized that like geological materials and as a result of the deposition in progressive layers, compaction and heterogeneity, MSW develops a strong (Dixon and Jones, 2005) and anisotropic structure (Hudson, 2007). It is also accepted that plastics and textiles, due to their flat shape, tensile strength and orientation, can enhance the strength (Kölsch, 1995, Dixon et al., 2008), and it has been argued that they could also influence flow behaviour by diverting fluid flow (Xie et al., 2006, Velkushanova et al., 2009). The introduction of the European Landfill Directive (1999), aiming to reduce the amount of biodegradable waste sent to landfill, has produced a new range of mechanical and biological pre-treated wastes (e.g. generically referred as MBTs) that will develop a different structure in landfills (Powrie et al., 2007). Additionally, as degradation progresses and in common with other organic materials (e.g. organic soils and peat), changes in the waste structure can be expected that will produce alterations in the pore space and in the hydraulic properties that control flow and transport processes (White and Beaven, 2008).

All this indicates that the structure of solid wastes plays an important role in flow and transport processes, and stresses the need for improving the current understanding of its nature and influencing factors. The structure of solid wastes, as it happens with any porous medium, is influenced by the properties of the material at different levels which range from the particle to the packed bed material (Beven and Germann, 1982, Donohue and Wensrich, 2009, Dullien, 1992, Felske et al., 2001). Therefore, the study of the structure in solid wastes should involve the investigation of properties at least at these two levels. Additionally, the structure can be indirectly studied by understanding material behaviour through, for example, the investigation of fluid flow properties.

At the particle level, geometric and physical characteristics are of relevance for structure development. This group of properties includes the particle size, particle shape, specific surface, roughness, bulk density, water absorption and water content (Felske et al., 2001). Knowledge of these properties gives an indication of the nature of the structure created once the material is placed (Donohue and Wensrich, 2008, Donohue and Wensrich, 2009). For example, a material with particles distributed over a range of sizes show better packing properties (e.g. smaller porosity) than a material with uniform size particles (i.e. the smaller particles can fill the pores formed between the coarser particles). At the packed bed level, properties such as the degree of packing, porosity, pore size distribution, degree of networking and tortuosity describe the characteristics of the structure created. At the level of fluid flow behaviour, properties such as the hydraulic conductivity, fluid distribution and retention time can be used to enhance the understanding of the characteristics of the in situ structure (Beven and Germann, 1982, Flury et al., 1994).

The research detailed in this thesis is based on an experimental programme that included tests in solid wastes at different levels. The study comprised the investigation at the particle level with the analysis of the size and shape in specimens of solid waste from diverse sources (i.e. MSW, MBT from a facility in the UK and in Germany). At the level of the packed bed, the characteristics of the structure of a specimen of MSW were studied with the use of a non-invasive direct technique (i.e. computed tomography). In the same specimen and at the fluid flow behaviour level, dye tracers were used to understand fluid paths. Also, analogous specimens (i.e. sand and flat particles) were prepared in the laboratory for a systematic study of the impact of flat shape materials on the hydraulic conductivity. This investigation component was also used to examine the porosity at the packed bed level. The properties investigated and the relationship between the levels of investigation and research objectives are presented in Table 1-1. The research objectives are detailed and justify in the next paragraphs.

Table 1-1 Levels of investigation and correspondence with research objectives

Level of Investigation	Properties Investigated	Samples /Specimens	Knowledge Gaps	Research Objective	Chapter
PARTICLE	Particle size distribution	MSW	a,b,d	i	2
		UK MBT			
		German MBT			
	Particle shape	MSW			3
		UK MBT			
		German MBT			
PACKED BED	Pore space	MSW	c,d	iii	5
	Pore size distribution				
	Degree of networking				
	Porosity	Analogues			4
FLUID FLOW BEHAVIOUR	Hydraulic conductivity	Analogues	e	ii	4
	Flow paths	MSW			5

Existing knowledge in the area of waste structure includes the following subjects where our detailed understanding is still limited:

a. the geometrical characteristics of the particles in solid wastes

b. how the geometry of the particles varies between residues from different origins

c. the structure that develops once solid waste is placed into landfills

d. how the structure changes with degradation

e. and how that influences fluid flow

Characterisation of solid waste has traditionally been performed with the purpose of assessing waste management strategies and developing criteria for admission of residues to landfill sites. Consequently, most classification systems emphasise the material type and degradability (Landva and Clark, 1990, Siegel et al., 1990, Grisolia, 1995), and only limited attention has been given to properties such as particle size and shape. Characterisation of solid waste for geotechnical applications has however became a matter of research interest during the last few years. Particle size and shape are recognised to influence the mechanical and fluid flow properties in residues (Kölsch, 1995, Dixon and Jones, 2005) and are considered in the most recent classification systems (Dixon and Langer, 2006). Dixon and Langer (2006) proposed a comprehensive procedure where by material type, particle size and shape are all considered in grouping components according to their compressibility and reinforcing properties. The benefits of the Dixon and Langer (2006) system are recognised; however, the number of studies that have used it and therefore comprehensive information of particle size, material type and particle shape in wastes remains limited.

Another limitation arises from the fact that none of the classification systems has attempted to relate the characteristics of the waste particles to their influence on fluid flow properties. This has been the subject of research in more conventional porous media. These studies provide some general understanding of the role of particle size and shape on the hydraulic conductivity, but the unique and highly heterogeneous nature of solid wastes limits the direct applicability of results.

A further knowledge gap identified is that the structure that develops during landfilling solid waste has been little explored. This is due to the experimental difficulties associated with the preservation of the structure during sampling (Clayton et al., 1982) and the lack of transference of methodologies from other areas of research. Traditionally, the structure in soils has been studied using indirect and invasive methods (e.g. field observation, thin sectioning, breakthrough curves and dye staining). The use of these techniques has provided with essential understanding of structural characteristics such as macroporosity and layering (Beven and Germann, 1982, Allaire et al., 2009). The study of preferential flow, a mechanism which causes the transport of fluids and contaminants to be associated primarily with a small fraction of the total pore space, has also benefited from the application of indirect techniques (Morris and Mooney, 2004, Flury et al., 1994). The introduction in early 1990's of non-invasive direct techniques from the field of diagnostic medicine, i.e. X-ray Computed Tomography (CT) and high resolution Computed Tomography (μCT), has provided major advances in understanding the micro level structure of porous media. Detailed information on the structure, pore space architecture, fluid flow and porous medium interaction processes in soils are extensively reported in the literature (Kettridge and Binley, 2008, Heijs et al., 1995, Amos et al., 1996, Mooney and Morris, 2008, Sato and Suzuki, 2003). However, CT has seen limited use in the study of waste structure and fluid flow phenomena with Watson et al. (2006) and Watson et al. (2007) being the only references identified at the time of writing this thesis.

The study of preferential flow has relevance for solid wastes. Preferential routes may accelerate or delay the movement of dissolved matter and contaminants and thus have significant implications for the remediation of landfill sites. Experimental work in waste packed columns has indicated the presence of channelling (Johnson et al., 2001, Korfiatis, 1984, Zeiss and Major, 1992, Bendz and Singh, 1999). However, since little information on the characteristics of the residue, i.e. material composition and particle size, is provided in these studies, the possibility to establish links between preferential flow, waste characteristics and waste structure is limited.

Considering the gaps in the knowledge discussed, the objectives of this research were established as:

i. The development of a detailed characterization of the geometrical properties of particles in solid wastes from different sources, i.e. MSW and MBT, and an analysis of the changes in particle size and shape caused by degradation

ii. A study of the effect that flat shaped particles, e.g. plastics and textiles, have on the fluid flow characteristics of a porous medium

iii. The development of methods for the characterization of structure in solid wastes and the application of such methods to wastes

The characterisation of MSW and MBT is detailed in Chapters 2 and 3. This required the development of methods to describe, in simple yet meaningful terms, the size and shape of the particles in solid wastes. Results revealed that the content of flat particles is considerable and increases with degradation. Flat particles are thought to influence flow behaviour; however, the lack of studies in the topic limits the ability to estimate the magnitude of this. Thus, a study was designed to understand he effect of flat particles on the hydraulic conductivity. Analogue specimens were formulated considering the ranges in particle content and size revealed during the characterisation. This is discussed in Chapter 4. The study proved that the presence of flat shape particles reduces the hydraulic conductivity of solid wastes. However, this is probably not their only effect on fluid flow. Evidence from columns packed with solid waste suggests the presence of preferential flow paths (Zeiss and Major, 1992, Korfiatis, 1984) and anisotropy in the hydraulic conductivity (Hudson, 2007). Flat particles could be the explaining cause as they could divert flow, change the structure and favour some flow paths. An investigation to examine the structure and visualise preferential flow paths in a specimen of waste fully characterised was introduced during this research and published in Caicedo et al.(2010). Also, the use of μCT was pioneered during this research and published in Caicedo et al.(2011). These publications can be found in Chapter 9. Further details of this investigation are detailed in Chapter 5.

Further details on the contents of each chapter follow:

Chapter 2 is dedicated to the characterisation of particle size. The description of particle size was based on mathematical analysis of the cumulative particle size distributions (PSD) using a series of models traditionally applied to particulate matters and soils. The use of mathematical models offers several advantages. It allows the analytical representation of the entire PSD. The type of model that best fit the data set reveals details of the process followed to reach such PSD, and the model parameters can assist in the calculation of the intrinsic permeability. Nevertheless, mathematical PSD models are rarely used in geotechnical engineering where the description of particle size is commonly based on ratios between specific points of the distribution. So far, the use of PSD mathematical models had been missed in the literature for solid wastes. The research presented in this chapter is innovative in at least four aspects:

- It presents a comprehensive characterisation of particle size for solid wastes from different sources
- It provides an analysis of the changes that degradation produces in particle size

- It introduces the use of mathematical models for the description of PSD in solid wastes and
- it uses the model information to infer some characteristics of the transformation processes, i.e. degradation and mechanical pre-treatment, that result in changes in particle size

Chapter 3 focuses on the characterisation of particle shape. The characterisation followed a classification system proposed as part of this research and published in Velkushanova et al.(2009). The system extended the Dixon and Langer (2006) scheme by considering the effect of particle shape on fluid flow. Particle shape was defined according to the dimensionality, following Kölsch (1995), as 0D, 1D, 2D or 3D. 2D particles (e.g. plastic sheets) were assumed to have the potential to alter fluid flow properties. This assumption is supported by the research by Xie et al. (2006) and further investigated in Chapter 4. This chapter explores the application of the Velkushanova et al.(2009) framework to samples of MSW and MBT before and after degradation. Differences between samples and the changes in composition caused by degradation are discussed. The chapter emphasises the significant content of 2D particles in solid waste (>30% dry mass) and how this content sees a further increase with degradation.

Chapter 4 investigates the effect of 2D particles on the hydraulic conductivity. Mixtures of sand systematically modified with 2D plastic discs were used. The hydraulic conductivity of each mixture was determined experimentally. Two parameters were investigated: the 2D/sand relative size and the relative content of 2D particles. Two further factors were considered for discussion: the angle formed between 2D particles and the plane normal to the flow direction and the porosity. The study showed that the inclusion of 2D particles reduces the hydraulic conductivity by a factor that increases with both the relative content and size of the particles, and is always within one order of magnitude. It provided also a quantification of the size and content of 2D particles above which significant changes in the hydraulic conductivity start. These results can be used to develop the criteria introduced in Velkushanova et al. (2009) to classify materials according to their potential to influence fluid flow. A further analysis was carried out comparing the experimental data against a model proposed by Maxwell (1954) for conduction through heterogeneous media. The investigation revealed that the reduction in the hydraulic conductivity can be expressed in terms of a single term p, the proportion by volume of 2D particles calculated from the number of particles and their size. The outcome of this analysis suggests that p is a reasonable factor to use to quantify the magnitude of the reduction in the hydraulic conductivity.

Chapter 5 focuses on the study of preferential flow phenomena and the structure in a specimen of MSW. The investigation combined the use of invasive and non-invasive techniques and required the production of a representative specimen with a well preserved structure. A cored sample of a specimen of MSW fully characterised in Chapters 2 and 3 was selected. Preferential flow was studied using dye staining methods to facilitate the visualisation of flow paths and the diversion caused by flat shaped materials. The results of this study were published in Caicedo et al. (2010). The structure was studied at two different scales. At centimetre scale, 8 cm thick slices were produced by sectioning following a procedure carefully designed to ensure sharp cuts. At millimetre scale, one of the 80mm thick slices was investigated using μCT. This step required the development of an examination procedure appropriated for the characteristics of solid waste as detailed in Caicedo et al. (2011). The use of μCT revealed details in the structure of the specimen down to 0.125 mm. The study evidenced the presence of preferential flow channels, flow diversion caused by flat shape materials, a layered structure and pores better connected in the horizontal than in the vertical direction. It was possible to reveal high level of details using μCT, this itself is innovative as not previous studies have been reported using this technique for solid waste. The combination of invasive and non-invasive methods for the study of the structure of solid waste is innovative and provides the first study of this nature.

Chapter 6 presents general conclusions, recommendations, links between the different chapters and highlights future areas of investigation.

2. The nature of particle size in solid waste and its role on waste behaviour

The physical structure of a solid medium plays an important role in a range of phenomena such as fluids conduction and biodegradation which are both of relevance in the context of solid wastes. The term structure refers to the geometry of the solid particles and includes aspects such as their size, shape and orientation as well as the geometry and architecture of the resulting pores (Hillel, 1998). This chapter concerns the study of particle size in solid waste and discusses the potential effects on waste behaviour, particularly on fluids flow. The introductory part of this chapter discusses first the role of the structure on fluid flow processes, then examines the importance of considering the nature of structure during biodegradation processes and finishes with a review of the nature of the changes expected in the structure with the biodegradation.

2.1. The role of structure on fluid flow and biodegradation processes

2.1.1. The role of structure on fluid flow processes

The influence of solid particles on fluid flow has been extensively studied in porous media. For example, in Darcy's law (Equation 2-1) the hydraulic conductivity K is a function of the intrinsic permeability k which depends entirely on the properties of the solid medium (see Equation 2-3).

$$Q = -KAi \qquad \text{Equation 2-1}$$

$$K = \frac{k\rho g}{\mu}$$ Equation 2-2

where ρ and μ are the fluid density and the dynamic viscosity respectively and g the acceleration due to gravity.

A theoretical deduction of an expression for k in terms of the particle size and shape (Equation 2-3) was obtained by Hubbert (1940) who considered the forces that act on a microscopic fluid element and used a dimensional analysis. In Equation 2-3, d is a characteristic length of the system that indicates the coarseness of the solid matrix, and C a dimensionless numerical coefficient whose value depends upon the geometrical shape of the internal structure of the medium. Further explanation on Hubbert' (1940) work can be found in Chapter 4.

$$k = Cd^2$$ Equation 2-3

A number of equations agree with Hubbert (1940) expression in relating k to the size and shape of particles and pores (Hazen, 1911, Krumbein and Monk, 1942). The equations discussed can be well represented with the form of Equation 2-4, where $f_1(shape)$ is a function of the pore or particle shape which includes characteristics

$$k = f_1(shape)d^{\beta} f_2(n)$$ Equation 2-4

such as the sphericity, roundness, packing and flow path tortuosity. In Equation 2-4, the term d is an effective particle size or capillary tube diameter, whilst the exponent β is the power value for d which generally takes values close to 2. This agrees with the theoretically based Equation 2-3. The term $f_2(n)$ is a function of the porosity of the media. It is interesting to notice that k in both Equation 2-3 and Equation 2-4 is related to d , a parameter that indicates a characteristic length or an effective particle size, which varies according to the specific media under study (e.g. D_{10} for sandy soils). Some questions that subsequently arise from Equation 2-4 are how could d be better described in solid wastes and which would be the form of $f_1(shape)$ and $f_2(n)$ in solid wastes. This chapter discusses some background that could aid in answering that question.

Like other porous media, solid wastes are expected to have k influenced by the size and shape of the solid particles. Yet, as only a limited amount of studies in the topic can be found in the literature (Felske et al. 2001, White et al. 2004, McDougall 2007) the nature of such influence remains highly unexplored and general equations to estimate k unavailable. However, research over the last decade has added information to understand the influence of the characteristics of landfilled waste on fluid flow and more specifically to understand the nature of $f_2(n)$ (e.g. Powrie and Beaven (1999)).

Powrie and Beaven (1999) investigated the hydraulic conductivity in raw and pulverised pre-landfill directive household solid wastes over a stress range of 0- 600 kPa, where the residues investigated displayed a decrease in K of three orders of magnitude. The results by Powrie and Beaven (1999) showed that the porosity, which results from the effective stress conditions, controls the vertical saturated hydraulic conductivity. Mathematical expressions were obtained that relate effective stress to porosity and porosity to intrinsic permeability.

Little differences between raw and pulverised pre-treated samples were reported in Powrie and Beaven (1999), which on first examination seems to suggest that the size and shape of the particles have only a minor influence on the hydraulic conductivity of solid waste, i.e. a reduction in particle size by pulverisation caused little changes in K. However, when the results are examined in more detail, some features emerge that need further analysis (see Annex 2-1). For example, below the D_{25} (the finest 25% fraction) the PSDs for the waste samples investigated are very similar, i.e. D_{10} is approximately 15mm for both. In many types of soils, i.e. sandy soils, D_{10} controls the hydraulic conductivity (Hazen, 1911). The D_{10}

fraction could influence the hydraulic conductivity of landfilled solid wastes as it does in soils. This would imply that when D_{10} is constant only minor variations in the hydraulic conductivity are expected, i.e. within one order of magnitude. Another observation is that raw and pulverised samples originated at different sources. The material characterisation demonstrated differences in the mass content of paper (39 vs 49%), film plastics (4.4 vs 8.3%), glass (7 vs 1.3%) and putrescibles (13 vs 6.5%). This limits comparisons to estimate the influence of particle size on hydraulic conductivity, i.e. it cannot be isolated from factors such as the composition and particle shape.

The analysis above suggests that although the study by Powrie and Beaven (1999) evidences the dominant role of the porosity on fluid flow in solid wastes, it also emphasises the need for further research to understand the role of complementary factors such as the size and shape of the waste particles. For instance, it might be that in solid wastes variations in porosity explain the large changes in hydraulic conductivity (e.g. changes in the order of magnitude), whilst changes in size and shape might explain variations in the hydraulic conductivity within one order of magnitude.

Not only would the estimation of k benefit from a more comprehensive understanding of the controlling factors, but also properties such as the hydraulic conductivity (White et al., 2004, McDougall, 2007).

As previously mentioned, the estimation of k needs a sensible description of d. This is where this chapter focuses by investigating the nature of the particle size distribution in solid wastes. Some of the specific objectives are justified in the following paragraphs:

1. The study of the nature of the particle size distribution (PSD) in solid wastes.

For that, PSDs of samples of pre and post landfill directive wastes were analysed using two approaches: conventional methods from geotechnical engineering (i.e. cumulative curves) and methods from the powder manufacturing industry (i.e. adjustment of the experimental curve to a reference model (BS ISO 9276-3, 2008)). The need for using different methods is justified. Like most particulate materials, solid waste is a non uniform material with particles distributed over a very wide range of sizes (e.g. three orders of magnitude). Size data is thus available as a distribution rather than as a single figure. This creates difficulties for the estimation of the effective size d required to calculate k (i.e. Equation 2-4). This difficulty can be dealt with by applying the following two approaches:

- Determination of the size of the fraction that dominates the flow, and use of that value as the effective size d. For example, in sandy soils (Hazen, 1911) observed that the size of the 10% finest fraction dominated liquid flow. The well-known Hazen equation that relates k with d is based on this finding (Equation 2-3 with $d = D_{10}$). Similarly, Slichter (1898) proposed an expression to calculate k as a function of the 30% finest fraction (Dullien, 1992).

- Determination of the type of mathematical model that best describes the experimental curve, e.g. normal, log-normal, etc. (BS ISO 9276-3, 2008). Then, the fitted mathematical expression is used to calculate some curve parameters that are useful to estimate the effective size d. For example, if data follows a normal distribution, the mean and the standard deviation can be used to fully represent the distribution (Herdan, 1960). Krumbein and Monk (1942) adopted this approach and obtained an expression for k in terms of the mean size and the standard deviation for normally distributed grains of unconsolidated sands. They found that, as distributions have higher standard deviations (i.e. had particles spread over a wider range of sizes), the smaller grains fill the pores formed by the coarser particles and create a media with less pore space and a resulting lower hydraulic conductivity. If the particle size distribution (PSD) follows an alternative mathematical model (e.g. Rosin-Rammler, Fractal, etc.) analogous analyses are possible and the analytical description of the distribution is achieved using the model parameters.

A discussion of the two approaches in the context of solid waste follows. Particles in solid waste are highly heterogeneous. Hence, it is likely that more than one fraction controls the hydraulic conductivity, e.g. fines filling the pores and coarse-impermeable fraction restricting the flow (this will be further discussed in Chapter 3). Therefore, representations of PSDs using mathematical models and the acquisition of the model parameters may be a more sensible approach towards the description of d for solid wastes. This was therefore the approach selected during the experiments described along this chapter. Some mathematical models were evaluated to describe the PSD of different samples of waste, then the one with the best fit was identified and the distribution described using the parameters of the model that was selected. Some background about the use of mathematical models, the type of models that are frequently used to describe particle size distributions and experiences in the application in solid wastes are discussed in the following paragraphs.

The use of mathematical models to represent the distribution of particle sizes is a common practice in the powder manufacturing industry (Herdan, 1960, BS ISO 9276-3, 2008) and in research into particulate materials such as soils and sediments (Krumbein, 1936a, Herdan, 1960). This is however unusual in geotechnical engineering where frequently, a PSD is described in terms of coefficients such as the uniformity and curvature which measure the ratios between specific points of the distribution curve. For example, the uniformity coefficient is calculated as the ratio between D_{60} and D_{10}, which are the finest 60% and 10% fractions respectively (Powrie, 1997).

The normal or Gaussian distribution of particle sizes has been found to describe reasonably well natural products such as pollens and powders obtained by precipitation and condensation processes. Whereas sediments, soils and powders obtained by grinding or crushing have been found to be well described by log-normal distributions, i.e. the distribution is normal after the particle size has been logarithmically transformed (Krumbein, 1938a). Alternative distributions are generally used when significant deviations from the log-normal distribution are observed. For example, the Rosin-Rammler distribution (RR) is considered suitable to describe the particle size of mechanically processed particulate materials (Washington, 1992, BS ISO 9276-3, 2008, Herdan, 1960). Annex 2-2 illustrates the characteristics of different PSD mathematical models.

In solid wastes, systematic studies to characterise the constituting particulate materials and describe their PSDs using model distributions are rare. Felske et al. (2001) and Nakamura et al. (2005) are two of such documents in this area. Felske et al. (2001) used the RR to investigate PSDs in samples of landfilled waste and to estimate a number of properties of relevance in fluid flow (e.g. average pore size). However, Felske et al. (2001) did not discuss the reasons for selecting this distribution nor provided details on mathematical processing of the data. In the other hand, Nakamura et al. (2005) used a derivation of the Gaussian distribution, the Gamma distribution, to describe the number PSD (i.e. PSD obtained from the number of particles with a certain size) for MSW and ashes. In Nakamura et al. (2005)′ study, the analysis of particle size was carried by image analysis and not information (i.e. particles density) was reported to obtain a mass PSD (i.e. mass of particles with a certain size). From the research by Nakamura et al. (2005), it remains uncertain whether the Gaussian model could give a sensible representation of the mass PSD, the standard format for particle size data.

It is clear that the number of studies that investigate the nature of particle size in solid wastes is still limited and that more research to mathematically model the PSD and improve the analytical description of the particle size in solid wastes is needed. Consequently, the second objective of this chapter is :

2. To investigate the use of standard mathematical models for particle size distribution, i.e. normal, log-normal and RR, for a better description of the PSD of pre and post landfill directive residues.

Alternative mathematical models to describe particle size in soils, and particularly the use of fractal geometry, have gained research attention during the last decade (Wu et al., 1993, Tyler and Wheatcraft, 1992, Perfect and Kay, 1995). Fractal geometry was originated by Mandelbrot (1982) after finding that patterns observed in diverse systems and at different spatial scales could be related to each other by a power function. He called the exponential of the function the fractal dimension. Turcotte (1986) extended this concept to explain the random fragmentation process using a power law between the number of fragments and their mass. His relationship was confirmed for materials such as powders, crushed materials and sediments. Tyler and Wheatcraft (1989) developed further the concept to describe soils PSDs using a power relation between the mass of grains and the ratio between the upper and lower sieve diameter with the equation power being a function of the fractal dimension (i.e. Equation 2-18). Later work confirmed that the power relationship represents well the PSD in many diverse types of soils (Wu et al., 1993, Tyler and Wheatcraft, 1992). A PSD that follows a fractal relationship implies that across a wide range of scales the size of the solid particles appear similar so it can be referred as a self similar system (Tyler and Wheatcraft, 1992). The use of fractal geometry for describing PSD in solid wastes has not previously been considered. This chapter discusses the relevance of this approach in solid wastes. The third objective of the chapter is therefore

3. The use of fractal scaling concepts for the description of PSDs in pre and post-directive refuses

2.1.2. The role of structure on biodegradation processes

Fractal geometry concepts have strong physical grounds (Korvin, 1992, Mandelbrot, 1982) and have therefore being applied to describe a very broad spectrum of soil properties, e.g. bulk density, pore size distribution, pore surface area and particle shape (Perfect and Kay, 1995, Hyslip and Vallejo, 1997) as well as to describe processes such as adsorption, diffusion and transport of water and solutes (Crawford et al., 1993, Perfect and Kay, 1995).

The application of fractal geometry concepts to diffusion may be of relevance in the context of biodegradation of landfilled solid wastes. Biodegradation of solid wastes is based on the transformation of solid organic matter to biogas. This transformation involves solubilisation of organic matter by the microbial action and the diffusion of the solubilised matter from the solid matrix to the solid-liquid interface and the liquid phase where reactions to produce biogas take place (Wall and Zeiss, 1995, Barlaz et al., 1990).

This type of diffusion where the diffusing molecules have to travel through different phases and where the reactions take place at the interface of the different phases is an example of heterogeneous or abnormal diffusion (Kopelman, 1988). This is in opposition to homogeneous or normal diffusion where the diffusing molecules follow traditional Brownian paths and where reactions take place in a homogeneous phase. The study of processes where heterogeneous reactions take place (i.e. at the interface between phases) have seen increasing research interest during the last decades (Kopelman, 1988, Meraz et al., 2004, Wang and Feng, 2010, Wang et al., 2011, Xu and Ding, 2007), and have included the study in areas as diverse as industrial surface-catalysis, industrial electrode reactions, bioenzymatic, membrane reactions and some geochemical and atmospheric reactions.

Homogeneous and heterogeneous reactions differ substantially at the fundamental level. Classical homogeneous kinetics assumes a well stirred system, a condition that is achieved by the convective stirring caused by the fluids' motion. This condition cannot always be attained for reactions in or on media that are solid, viscous, porous or structured. In the absence of convective stirring, there is still diffusive stirring (i.e. produced by molecular diffusion). However, under dimensional constraints (i.e. surface reactions) or topological constraints (solid-state reactions), the diffusive stirring may be insufficient to ensure an adequate system mixing. Moreover, in classical homogeneous kinetics, the reaction rate is a constant independent of time; whilst in heterogeneous systems experimental data have shown anomalous results in which the rate constants are time dependent (Klymko and Kopelman, 1982, Kopelman, 1986).

Kopelman (1988) pioneered the study of heterogeneous reaction kinetics and considered the rate constant time dependence using the concepts of fractal geometry. Time dependence is a central consideration in fractal like kinetics. The reaction rate coefficient is not a constant, but is rather a function of the rate constant and the time powered at the negative value of the fractal dimension, which causes a reaction rate coefficient time decline.

The concepts developed by Kopelman (1988) have been increasingly adopted to explain heterogeneous reactions such as the enzymatic saccharification of cellulose (Xu and Ding, 2007, Wang and Feng, 2010, Wang et al., 2011), the degradation of particulate food material (Devaux et al., 2006), industrial biocatalytic reactions (Xu and Ding, 2007) and in geochemical processes such as the sorption of dissolved contaminants in liquid phase (Brouers and Sotolongo-Costa, 2006).

Experiences gained in the application of fractal kinetics for the enzymatic saccharification of cellulose and for the degradation of particulate food material are relevant in solid waste science. Cellulose and hemicellulose account for a high proportion of the organic matter and could be up to 90% in domestic refuses (Barlaz et al., 1989). Like the enzymatic saccharification of cellulose, landfill degradation of solid wastes is a biological reaction where anaerobic bacteria digest the organic matter. Besides, food waste can account for up to 40% by mass in raw refuses and constitute the highest proportion of the readily biodegradable fraction (Eleazer et al., 1997). Given these similarities, it is reasonable to expect the biodegradation of solid wastes to be highly influenced by the degradation of food waste and cellulose and to exhibit comparable reaction kinetics.

The experiments that built the concepts of fractal kinetics (Klymko and Kopelman 1982 and Kopelman (1986) were conducted in fractal systems (i.e. objects with fractal dimensions) which are considered ideal testing grounds for heterogeneous kinetics. The results of such experiments suggest that if a heterogeneous system can be characterised as a fractal and the system undergoes a chemical reaction, that reaction is expected to follow a fractal like kinetics. In the research discussed along this chapter, fractal geometry was applied to describe the size distribution of particles of solid waste materials.

Landfill solid waste is by nature a system with a heterogeneous structure. Compaction creates water spatial variation. Additionally, the very diverse materials in solid wastes create a structure that is constituted by agglomerates of readily degradable organics (e.g. food, green waste) mixed with slowly degradable materials (e.g. paper, textiles, wood) and inert components (e.g. plastics, glass, metals, debris, etc.). In this scenario, the solubilised molecules of organic matter diffuse and find diverse obstacles (e.g. inert particles) to divert before they reach the final targeted interface. The heterogeneous nature of the waste structure suggests that the reaction processes could follow a fractal kinetics mechanism.

Although the heterogeneity of landfilled waste is widely acknowledge by landfill modellers, studies to formally incorporate it in landfill modelling remain limited (Martin, 1999, Martin, 2001, Meraz et al., 2004). Biodegradation has been traditionally studied in liquid phase where there is no need to consider heterogeneity (i.e. in the context of waste waters and slurries). Some progress has been done in the last decade with the study of biodegradation in solid phase (Martin, 1999, Martin, 2001). Those studies have concentrated on the heterogeneous spatial chemical reactivity in landfills, the decisive role of heterogeneity as a structural characteristic in solid waste, the increased mass transfer resistance caused by the heterogeneous structure and the consequent variation of the reaction rate coefficient with time (Martin, 1999, Martin, 2001).

Introduction of the heterogeneity of solid waste in landfill modelling and particularly the application of fractal kinetics for the biodegradation of landfill solid waste was introduced by Meraz et al. (2004) who proposed a fractal-like kinetic equation for landfill methane production. Meraz et al. (2004) argued that conventional models to estimate methane yield (e.g. Hoeks model and USEPA) consider total conversion of the organic matter and homogeneous spatial chemical activity. This is an inadequate assumption for landfilled solid waste and could be the reason for the overestimation of the time span for methane production in some of the commercial models.

Meraz et al. (2004) argued the need to explicitly consider the heterogeneous nature of the solid waste structure using the concepts of fractal kinetics developed by Kopelman (1988). Meraz et al. (2004) performed a series of modelling experiments to estimate the methane production from an operating landfill site (e.g. located in Mexico city) and used three different models for that purpose, i.e. USEPA, Hoeks equation and Hoeks modified according to fractal kinetics. The USEPA and Hoeks equations are based on a first order decay for the organic matter. In the modification of the Hoeks equation proposed by Meraz et al. (2004), the reaction rate coefficient was no longer a constant but rather a function of time (i.e. time powered to the fractal dimension) as it is established in the fractal like kinetics mechanism (Kopelman, 1988). The results reported by Meraz et al. (2004) showed that the time span predicted by the USEPA and Hoeks models were unrealistic and exceeded, by several decades, the time for methane production observed in landfills with comparable characteristics (e.g. 50 years methane production in tropical landfills (Pelt et al., 1990)). However, the results obtained with the fractal like kinetics model showed a better agreement with the observations in both time and total methane yield.

The study by Meraz et al. (2004), that incorporated the concepts of fractal kinetics in solid wastes, offers a sound alternative to consider the heterogeneous nature of solid waste structure in landfill modelling. Although the fractal kinetics in solid wastes still needs an important amount of research and the evaluation of aspects such as landfill operation conditions, variation in waste composition, etc., it has been developed from strong theoretical bases for heterogeneous systems as to expect it to be a promising alternative in landfill modelling.

The study of fractal geometry concepts in solid waste could enhance our current understanding of the mechanisms controlling the biodegradation process. It was discussed by Klymko and Kopelman (1982) and Kopelman (1988) that reactions occurring in a fractal heterogeneous system are well modelled with fractal like kinetics. The research presented in this thesis could add new information in this area.

2.1.3. The change in structure with biodegradation processes

As degradation processes occur and in common with other organic materials, e.g. organic soils and peat (Rezanezhad et al., 2010, Kettridge and Binley, 2011), transformations in the structure of waste would be expected. For example, degradable solid particles might change from solid to liquid and gas phases, altering both the overall size and shape of the particles as well as the pore space architecture. Research in this area is limited, with few studies available in soil science, i.e. impact of soil conditioners in soil structure (De Gryze et al., 2006, Pagliai and Vittori, 1993, Emerson and McGarry, 2003), and in peat degradation (Kettridge and Binley, 2011, Rezanezhad et al., 2010, Quinton et al., 2008).

Some theoretical concepts have been developed for landfilled solid wastes that link waste structure with degradation using a decomposition-induced void change parameter (McDougall, 2007, McDougall and Pyrah, 2004). In Mcdougall and Pyrah (2004) model, degradable soils (i.e. solid wastes can be considered as an example of degradable soils) are considered as a three phase system composed by a decomposable solid phase, and inert solid phase and voids. As the effective stress increases and the biodegradation progresses, volumetric changes are experienced. A higher effective stress reduces the volume occupied by the voids. As biodegradation develops, the absolute volume of the decomposable fraction is reduced whilst the absolute volume for the inert fraction remains unaltered. This creates a progressive change in the relative ratio between the solid phases.

An alternative approach is presented by White and Beaven (2008) where the pore space structure is estimated, i.e. channels length and area, from the PSD. The channels length and area are used for the estimation of *K*. The changes in the PSD with landfilling are conceptualised through a modification in the geometry of the PSD produced by the crushing of the coarser pieces and the biodegradation of the materials with some organic content. The resulting PSD shows a shift towards the left, and in both before and after degradation, the PSD is adjusted to a potential equation tuned to reflect the general S shape of the PSDs. The model used however does not have a physical backup to explain the distribution of the size of particles and the representation of the resulting distribution is arbitrary.

The methods by McDougall and Pyrah (2004) and White and Beaven (2008) were at the time of writing the only two approaches that consider the changes with degradation in the structure of solid wastes. The scarce literature in the area indicates the need for further research in the topic. This chapter aims to provide information about the evolution in the structure of waste by:

4. a systematic study of the nature and changes occurring with degradation in the particle size of pre and post landfilled directive wastes

Three samples are discussed and are referred to as UK MBT, German MBT and MSW. The names selected for each of the samples reflect the origin of the sample (i.e. from a waste facility if the UK or Germany) and whether they had been the subject to any treatment (e.g. MBT for Mechanically and Biologically treated wastes). The names used therefore are referred to a particular specimen of waste and although the results for each of the samples could give an indication of the possible characteristics of similar materials, the discussion and conclusions are better place in the context of the particular samples examined. More research would be needed to extend the observations outside these limits. All of the wastes were subjected to controlled degradation processes as part of a wider research programme. Analysis of particle size was carried on both before and after the degradation process. To discriminate between the results obtained before and after degradation samples are identified with the notations of B4 and AF respectively. Sieve analysis of UK MBT and German MBT B4 were carried out as part of the research published in Velkushanova et al. (2009).

Velkushanova et al. (2009) did not explore the use of conventional distributions and fractal scaling to describe PSDs which was introduced in the current research. Analyses of the remaining samples were carried out during this research with the exception of MSW B4 which was reported by Ivanova (2007).

2.2. Materials and methods

2.2.1. Materials

2.2.1.1. UK MBT

MBT stands for mechanically and biologically treated waste. This type of waste treatment was introduced in Europe to fulfil the requirements of the EU Landfill Directive (1999/31/EC), which sets targets for reducing the amount of biodegradable waste sent to landfills. Approximately 500 kg of the sample referred as UK MBT was obtained from a waste treatment facility in southern England which receives fresh municipal solid waste (MSW) and treats it through a process of mechanical removal of recyclables and aerobic stabilization. The facility is at the front in the development of technologies for the treatment of MSW in the UK, and it is considered as an adequate representation of the state of the art in MBT technology in the country. The sample UK MBT was obtained from a standard production bath of approximately 2000 kg which was thoroughly mixed for homogenization. The treatment process is detailed in Annex 2-3. MSW is received, shredded and screened through a 80mm mesh. Ferrous materials are removed using magnets. The remaining fraction, <80mm, is transferred to a bio-stabilization hall where aerobic degradation takes place over a period of 6 weeks. Degradation is achieved through a process of continuous air injection, irrigation and waste turning. Remaining recyclables are removed. The final product is mixed with composted green waste, its quality is not assessed as in the UK there are no regulations for landfilling MBT wastes other than to demonstrate diversion. It is important to notice that the type of MBT treatment developed in this facility is based in the extraction of recyclables and the stabilization of the biodegradable fraction through only aerobic process.

A representative sub-sample of 2 kg, from the 500 kg received, was obtained by quartering following BS ISO 23909 (2008) (section 6.3.2 method 2). The quantity of waste available for PSD analysis was constrained by the demand from other researchers and the capacity of the sieving equipment (see 2.2.2). Calculation of the quantity of material required for PSD analysis followed the recommendation in BS 1377-2 (1990) (Table 3): 0.5 kg as the minimum sample quantity for sieving materials with a proportion > 10% of materials retained in 10 mm sieve. The appropriateness of this initial amount was confirmed after a preliminary PSD analysis.

Controlled degradation of UK MBT was undertaken by Siddiqui (2011) as part of a study into the settlement and degradation properties of MBT waste over a period of 347 days. The process was carried out in a Consolidating Anaerobic Reactor (CAR), which is a Perspex cylinder (935 mm height and 480 mm ID) with a loading system that applies a constant surcharge to the waste. The design of the reactor is described by Parker et al. (1999). The stress was set at 50 kPa and 150 kPa, which would be equivalent to a depth of 5 m and 15 m in a landfill assuming a bulk unit weight of 10 kN/m^3. This sample is referred to as UK MBT AF. The fresh waste is referred to as UK MBT B4.

The CAR was loaded with approximately 20 kg of a well homogenised subsample from the 500 kg available in total. Once degradation had finished, the sample was carefully extruded into a spare cell of similar diameter to preserve its structure for future investigation. A bottom layer of approximately 2 kg was carefully removed and analysed for comparison with the fresh waste. The amount of sample taken followed the recommendation in BS 1377-2 (1990) and was comparable with the amount of waste sampled before the degradation (i.e. 2 kg in both cases). Ideally, the sample after degradation should have been obtained from the homogenization of the totality of the material remained in the CAR after degradation.

However, other pressures within the broader research programme made this unfeasible. The vertical variation of the biodegradation process (i.e. differences in chemical reactivity between the top and bottom layers) and the migration of fines from bottom to top (i.e. the flow direction for the leachate recirculation stream) were initially considered as potential downsides when sampling the bottom layer. However, they were both disregarded after an analysis of the material composition and particle size, at different levels within the CAR, was made with two more samples of solid waste (i.e. MBT from Germany and MSW).

Each of the 2 kg samples referred as to UK MBT B4 and UK MBT AF underwent a sieving analysis according to the method described in Section 2.2.2. Three subsamples were prepared to produce a PSD analysis with 3 replicates for each sample.

2.2.1.2. **German MBT**

120 kg of MBT waste of a sample referred as to German MBT was obtained from a facility situated near Hannover Germany, a facility that has been providing MBT treatment for several years to the Hannover province and that is considered to be at the front in the development of MBT technologies in Germany. The mechanical part of the treatment process is based on separation of recyclables and ferrous materials using screens and magnets. The biological component differs substantially from that used in the UK MBT process in that the waste is first anaerobically and then aerobically treated, so it can be described as a dual anaerobic-aerobic treatment. Anaerobic digestion takes place over a period of 3 weeks in fermentation tanks. It follows an aerobic post-treatment process where the fermented waste is composted in enclosed windrows during 6 weeks. The quality of the final product is assessed according to the waste storage ordinance which defines criteria for waste to be landfilled (AbfAbIV, 2001).

The 120 kg of sample were obtained from a thoroughly mixed production batch of approximately 1200 kg. Then a representative sub-sample of 5 kg, from the 120 kg received, was obtained by quartering following BS ISO 23909 (2008) (section 6.3.2 method 2). The minimum amount of material required for PSD analysis was calculated using BS 1377-2 (1990) (Table 3), which recommends 2 kg minimum sample for sieving materials with a maximum size of 20 mm.

Controlled degradation reported by Siddiqui (2011) took place over 279 days in the same conditions as for UK MBT. Once degradation had finished, a subsample of approximately 5 kg was carefully removed from the top of the reactor. This sample is referred to as German MBT AF; and the original as German MBT B4. The amount of sample taken after degradation followed the recommendation in BS 1377-2 (1990) and was comparable to the amount of waste sampled before the degradation (i.e. 5 kg in both cases). Like in the case of UK MBT, the totality of the material remained in the CAR could not be sampled because of other pressures within the broader research programme. The analysis of PSD (Chapter 2) and material composition (Chapter 3) of the German MBT AF showed that the variation with degradation was statistically un-significant. This was a good indication that both the vertical variation and the migration of fines during the biodegradation could be considered to be unimportant processes.

Each of the 5 kg samples referred as to German MBT B4 and German MBT AF underwent a sieving analysis according to the method described in Section 2.2.2. Five subsamples were prepared to produce a PSD analysis with 5 replicates for each sample.

2.2.1.3. **MSW**

A sample of fresh MSW from White's Pit Landfill facility in Dorset, UK was used in an investigation of settlement and degradation properties by Ivanova (2007). Ivanova (2007) described the conditioning and degradation process in which large particles >40mm were removed and shredded. Then the specimen was degraded in a CAR following a process similar to that for UK MBT but with a maximum applied stress of 50 kPa. The sample served as a control sample. Once placed inside the CAR, acidic leachate was intermittently recirculated through the waste to inhibit the degradation during the initial 345 days of the 919 days of total experimentation.

The degraded MSW was available at the start of this study. The sample was carefully extruded from the CAR. A resulting core was used for the study of structure and flow paths detailed in Caicedo et al. (2010) (see Chapter 9). The dry mass of the core was estimated by Ivanova (2007) as approximately 20 kg. 2kg of a composite sample was created from the extruded sample. The PSD reported in Table 5.3 of Ivanova (2007) shows that the waste had a maximum size of material present in a significant proportion (more than 10%) of 20 mm. According to Table 3 in BS 1377-2 (1990) a 2 kg sample size is required for the sieving analysis of materials with this maximum significant particle size. The rest of the sample was kept substantially intact for structure and flow studies.

The 2 kg sample referred as to MSW AF underwent a sieving analysis according to the method described in Section 2.2.2. Five subsamples were prepared to produce a PSD analysis with 5 replicates. The data used as PSD analysis for MSW B4 was carried out and reported by Ivanova (2007).

2.2.2. Sieving analysis

Solid waste is a highly heterogeneous material with particles ranging in sizes from cobbles (>30mm) to fine sands (≈0.06 mm, BS 1377-2, 1990: Form 2.N). This is true even for MBT wastes. Particle sizes within this range are suitable for analysis using both wet and dry sieving methods according to BS 1377-2 (1990). The samples were oven dried at 70°C until the mass varied by less than 1% over a period of 24 hours. A stack of test sieves of 200 mm diameter and apertures of 75, 63, 37.5, 20, 10, 6.3, 3.35, 2, 1.18, 0.6, 0.3, 0.15 and 0.063 mm were used. Two aspects concerning the nature of solid waste were considered during sieving:

1. Agglomeration, which refers to the tendency of particles to group together and form bigger clumps. In soils, the presence and degradation of organic matter increases both the degree of aggregation of primary soil particles and the strength of their bonds (Wilson, 1991). The stability of such aggregates highly depends on the type of binding agents (e.g. polysaccharides, fungal filaments and other complex organic substances). In solid waste, aggregation could be initiated by the presence of organics and enhanced by fibrous materials and stress conditions. For example, textiles can bind to organic particles, be stress-compacted and form stable agglomerates. Results from particle size analysis can then be affected by the presence of these agglomerates. An approach commonly followed in soils, is pre-treatment with a dispersant solution that helps to separate the individual particles without breaking them. This is the purpose of wet sieving.

2. Particle shape, which refers to the presence of elongated particles (i.e. 1D and 2D as defined in Chapter 3) coming from materials such as plastics that can influence results from sieving analyses. For example, plastic sheets are malleable and can easily re-orientate, deform and pass through mesh holes smaller than their nominal size. Long rigid plastic pieces can remain on a sieve until a bi-directional movement places them with their smaller side perpendicular to the mesh opening allowing them to pass through the sieve aperture.

Agglomeration was addressed using wet sieving. Waste samples were submerged during 1 hour in a 2g/l aqueous solution of sodium hexametaphosphate. BS 1377-2 (1990) explains that in soils, this promotes the detachment of smaller particles and generally gives a better estimate of the content of fines. In solid wastes, there are no reported advantages of using dispersants during sieving. This study was used to compare results from dry and wet sieving and estimate the relative error in dry sieving. Results are summarised in Annex 2-4; they suggest that the magnitude of the underestimation of fines does not exceed the magnitude of other experimental errors, indicating that waste aggregates are stable and not easily dispersed during wet sieving. Aggregates are expected to form during degradation (Wilson, 1991) making difficult to judge what the real state is under landfilling conditions, i.e. individual particles or aggregates. Aggregated state could be a more realistic description of landfilled waste and, dry sieving an appropriated method for the analysis of particle size. Health and safety must also be considered. Wetting waste particles can generate offensive and possibly toxic odours and also possibly affect the nature of permeable materials such as paper. For all these reasons, dry sieving was preferred except for MSW, where the PSD before degradation was available only from wet sieving analysis.

Difficulties caused from particle shape were addressed with careful control of the sieving conditions and assessment of the retained materials, i.e. visual inspection and manual measurement of the particles dimensions. BS 1377-2 (1990) states the maximum sample mass as 915 g for a sieve stack diameter of 200 mm. Each sample was partitioned into well mixed subsamples of less than 915 g to prevent system overloading. Once the subsample had been loaded in the sieve stack, it was subjected to continuous vibration for 60 minutes in a Sievetronic Model YGM15418. Once finished, a continued manual vibration to each sieve, i.e. vertical and horizontal movement, followed until the amount of material continuing to pass through the mesh was judged to be negligible. Given the high content of 1D and 2D particles in the coarser fractions this step was particularly relevant for sieves with the biggest apertures. Materials retained in each sieve were visually inspected and doubtful particles identified, i.e. those with measured dimensions substantially higher than the sieve size, and accordingly re-located in the appropriated sieve. Doubtful particles were the exception rather than the rule. This extra step increased the analysis time but it proved to be repeatable, i.e. low standard deviation between subsamples, and provided reliable particle size results.

Each of the samples studied were first thoroughly mixed and then partitioned into a number of subsamples (i.e. 3 for UK MBT, and 5 for German MBT and MSW) to produce a PSD analysis that was the result of 3 replicates for UK MBT and 5 replicates for German MBT and MSW.

2.3. Data analysis

Once the material had been sorted through the sieves stack, the mass of the material retained in each sieve was determined by weighting with a precision of 0.01 g. The results for each subsample were added to obtain the data for the representative sample as a whole. A PSD was prepared according to the method in Section 2.2.2., and the standard deviation calculated with the 3 replicates for UK MBT and 5 replicates for German MBT and MSW.

Methods for the analysis of the data were taken from Herdan (1960), BS ISO 9276-1 (1998) and BS ISO 9276-2 (2001), BS ISO 9276-3 (2008) and BS ISO 9276-5 (2005) and are explained in the following paragraphs.

2.3.1. Graphical representation

The first step was the graphical representation of results in which the x axis corresponds to the sieve size (mm) and the y axis is either the material mass fraction retained in a specific sieve (y_{retained} for histogram representation) or the material mass fraction that passes through a sieve of a certain size (y_{passing} for cumulative distribution). The standard deviation ($STDEV$) for each sieve size was calculated according to equation Equation 2-5, where y is either y_{retained} or y_{passing} according to the type of graph reported. $y_{average}$ is the arithmetic mean, and n is the number of subsamples (i.e. 3 for UK MBT and 5 for German MBT and MSW). $STDEV$ was used as an estimation of the magnitude of errors involved in the measurement of the mass fractions.

$$STDEV = \sqrt{\frac{\sum (y - y_{average})^2}{(n-1)}} \qquad \text{Equation 2-5}$$

2.3.2. Significance in differences between PSD

Objective No.4 in this chapter investigates the changes that occur in PSD with degradation. The statistical significance of changes in PSD was evaluated using the t-test. This test compares the difference in the mean of two distributions against the standard deviation of the difference between their means. The evaluation is used to decide whether or not the observations in a second distribution are only a chance deviation from the mean value of a first distribution. It uses a dividing line to differentiate probable from improbable deviations from the mean of the first distribution. The dividing line taken for the analysis was t equal to 2. This value of t implies approximately ± 2 standard deviations from the mean of the first distribution. $t < 2$ denotes that 95 times out of 100 the mean of the second distribution could happen on pure chance and the differences between the two distributions are non-significant. Conversely, $t > 2$ denotes significant differences between the two distributions. Equation 2-6 and Equation 2-7 were used. x_{mean1} and x_{mean2} are the sieve size mean values of the distributions before (1) and after degradation (2). S_1 and S_2 are the standard deviations of the distributions before and after degradation and S_{diff} is the difference of the deviations calculated according to Equation 2-7.

$$t = \frac{x_{mean1} - x_{mean2}}{S_{diff}} \qquad \text{Equation 2-6}$$

$$S_{diff}^2 = S_1^2 + S_2^2 \qquad \text{Equation 2-7}$$

For comparison purposes, calculation of x_{mean} and S_{diff} followed two different methods. In the first approach, the mean was calculated as the arithmetic mean according to Equation 2-9, and the standard deviation S as the root mean of the variance S^2 according to Equation 2-9.

$$x_{mean} = \sum x_i \, y_{retained} \qquad \text{Equation 2-8}$$

$$S^2 = \sum (x_i - x_{mean})^2 y_{retained}$$ Equation 2-9

The second approximation considered that the cumulative particle size distribution follows the log-normal law. Accordingly, the variable z was defined as in Equation 2-10. Equation 2-12 and Equation 2-13 correspond to the normal distribution law, functions of the variable z, the logarithmically transformed sieve size x. s_g is the standard deviation for the z distribution and S the standard deviation for the x distribution defined according to Equation 2-11 (BS ISO 9276-2, 2001). Equation 2-13 was used to calculate the corresponding y for each z. Using the solver tool in excel z_{mean} and s_g were estimated minimising the sum of the squares of the differences between y experimentally obtained and y calculated with Equation 2-13.

$$z = \ln x$$ Equation 2-10

$$s = \ln s_g$$ Equation 2-11

$$y_{retained}(z) = \frac{1}{s_g \sqrt{2\pi}} \int_{z_n}^{z_{n+1}} \exp . \left(\frac{(z - z_{mean})^2}{2s_g^2} \right) dz$$ Equation 2-12

$$y_{passing}(z) = \frac{1}{s_g \sqrt{2\pi}} \int_{-\infty}^{z'} \exp . \left(\frac{(z - z_{mean})^2}{2s_g^2} \right) dz$$ Equation 2-13

2.3.3. Comparison of the experimental PSD to a reference model

The third part during data analysis targeted objectives 2 and 3 in this chapter, which refer to the evaluation of mathematical models, i.e. log-normal, Rosin-Rammler and fractal models (Annex 2-2) shows graphically the differences between those distributions). The experimental PSDs for the six samples of waste described following the method described in Section 2.2.2. were compared against these three reference distributions. The methods followed are discussed.

2.3.3.1. Log normal distribution

An initial screening to analyse the normality agreement of the PSDs was carried out using the graphical method introduced by Hazen (1914). In this method, the cumulative distribution is plotted in a probabilistic scale in which the spacing lines of the y axis are computed from probability curve tables or by numerical integration of Equation 2-13 (e.g. z tables as Table A.1 in BS ISO 9276-5, 2005). The method is a useful tool to assess when a data series follows the normal law with minimal arithmetical labour. If the data correspond strictly with the normal law, the points plotted on this type of scale lie in a straight line (BS ISO 9276-5, 2005, Herdan, 1960). PSDs of mechanically produced particulate materials and some soils and sediments have been shown to follow the log-normal law. This means that after taking the logarithm of the size, the distribution follows the normal law. For comparison purposes, plots were produced in linear and logarithmic scales. The method allowed the identification of portions within the distribution that follow reasonably well the log-normal law and others that show deviations from it. Afterwards, the log-normal model was evaluated using linear regressions. Plots were created such that their y axis was the product of the numerical integration of Equation 2-13 (e.g. using the NORMINV function in excel) and the x axis was the natural logarithm of the sieve size.

The log-normal law model requires two parameters z_{mean} and s_g which were estimated as explained in Section 2.3.2. $y_{retained}$ was estimated using Equation 2-13 (e.g. with the NORMDIST function in excel) and the results compared against data obtained experimentally. Two evaluations of the goodness of fit of the model were carried out. The first was in the non-linear system by using the so called Nash-Sutcliffe model efficiency coefficient, defined in Equation 2-14 (Moriasi et al., 2007). NSE ranges between 0 and 1 , 1 being the optimal value that indicates a good level of performance of the model under evaluation.

$$NSE = 1 - \frac{\sum \left(y_{measured} - y_{estimated}\right)^2}{\sum \left(y_{measured} - y_{average}\right)^2}$$ Equation 2-14

A second evaluation was done in the linear system. In this case the inverse of the normal law function was calculated for each $y_{measured}$ and the linearity of the plot ln x vs NORMINV ($y_{measured}$) assessed. The perfect line corresponds to an ideal normal distribution. The slope and the intercept of such line were calculated minimising the square of the differences between NORMINV ($y_{measured}$) and the NORMINV ($y_{estimated}$) from the model. The coefficient of determination R^2 defined in Equation 2-15 , with values close to 1 indicating good model performance.

$$R^2 = \frac{\Sigma\left(y_{estimated} - y_{average}\right)^2}{\Sigma\left(y_{measured} - y_{average}\right)^2}$$ Equation 2-15

2.3.3.2. Rosin-Rammler distribution

The Rosin-Rammler (RR) distribution originally developed to describe the particle size of broken coal, was later proved valid for a great variety of materials such as cement, gypsum, clay, glass, etc. produced by grinding, milling and crushing operations (Herdan, 1960, BS ISO 9276-3, 2008). Equation 2-16 and Equation 2-17 illustrate the distribution equation in its original form and after linearization following the application of the logarithmic function.

$$y_{passing} = 1 - \exp\left[-\left(\frac{x}{d'}\right)^{v}\right]$$ Equation 2-16

$$Y = \upsilon X - \upsilon \ln d' \qquad \text{Equation 2-17}$$

where:

$$Y = ln\left[-ln\left(1 - y_{passing}\right)\right] \text{ and } X = ln\, x$$

Where x is the sieve size, d' is a specific size of the particles where 63.2% by mass are smaller and υ is a model parameter that corresponds to the slope of the linear representation Y vs X. The RR model is therefore characterised with the two parameters d' and υ.

2.3.3.3. Fractal model

Fractal geometry concepts were introduced by Mandelbrot (1982) to quantify a variety of scale invariant processes in nature through power law relationships. One of such processes is the fragmentation of rocks and soils which plays an important role in a range of geological phenomena and controls the size-frequency relation (Turcotte, 1986). The power law relationship for fragmentation processes, first suggested by Mandelbrot (1982) , relates the number of particles to their size. The equation was later adjusted by Tyler and Wheatcraft (1992) to relate the size with the mass of material, using the mass fraction of material with a size less than the sieve size R , given by Equation 2-18. The derivation of Equation 2-18 starts from a fractal relationship based on the number of particles within a range of particle size and the assumption that the particles are spheres and have an average particle density. The number of particles within a range of sizes equals the ratio between the mass of particles within such range and the mass of one particle. The mass of one particle is the product between its volume and its particle density. When particle density and shape are available, Equation 2-18 can be corrected accordingly. Yet, this is beyond the scope of this research and Equation 2-18 was applied without particle shape and density corrections.

$$\frac{M(x < \boldsymbol{x_{max}})}{M_T} = \left(\frac{x}{\boldsymbol{x_{max}}}\right)^{3-D} \qquad \text{Equation 2-18}$$

Applying logarithms at both sides and using the symbols from earlier sections, Equation 2-18 is transformed into Equation 2-19 where D is the fractal dimension.

$$log_{10}\, y_{passing} = (3 - D) log_{10}\left(\frac{x}{x_{max}}\right) \qquad \text{Equation 2-19}$$

According to Equation 2-19, a PSD that follows the power relationship for fractal geometry should be a straight line when is plotted on a log-log scale. In this research, experimental data was used to produce the graph and a least squares linear regression performed to calculate the fractal dimension D from the slope of the best fitted line. The performance of the fractal model was evaluated using the Nash-Sutcliffe model efficiency coefficient defined in Equation 2-14 and the coefficient of determination R^2 defined in Equation 2-15.

2.4. Results: graphical representations

Annexes 2-5, 2-6 and 2-7 summarise the PSDs before and after degradation for the specimens investigated. The error bars were calculates with the $STDEV$ according to Equation 2-5 and represent the variability between the replicates of each sample, i.e. 3 for UK MBT and 5 for German MBT and MSW. Results for the samples after degradation are presented as they were originally gathered and, corrected to account for the loss of mass. Siddiqui (2011) reported the dry mass of UK MBT and German MBT before and after degradation. The difference corresponds to the fraction of material transformed to gas and leachate phases during the degradation. Expressed as a percentage of the initial dry mass, the loss of mass was 6.45% and 2.73% for UK MBT and German MBT respectively. In a similar fashion (Ivanova, 2007) reported 24.52% as the mass lost for MSW during degradation.

The correction was done as follows. The mass lost was considered as a new size category referred as to fraction lost. Materials retained in all the other size categories (e.g. 0.03 to 75 mm) were recalculated to add up 100 % mass. For example, the material retained in the

20mm sieve in German MBT-AF was 18.05%. 97.27 % of mass remained after degradation, which gives 17.56% of material when the mass lost is accounted for.

Visual assessment of Annex 2-5 suggests changes with degradation in the PSD of UK MBT. The plot is shifted to the right suggesting a general increase in the particle size. The magnitude of such changes was statistically confirmed as significant as explained in section 2.3.2. The D_{50} for example shows an increase from approximately 4.04 to 6.22 mm. There is a decrease in the content of fines < 1.18 mm together, with an increase in the content of coarse materials > 3.35 mm.

Visual assessment of Annex 2-6 suggests negligible changes with degradation in the PSD of German MBT, this was confirmed statistically. The slight shift of the curve towards the left is experimental errors. D_{50}, for example, does not show any change with degradation. The range of differences between the samples before and after degradation in Annex 2-6-b are less than the magnitude of errors, so they can be explained as a result of experimental variations. When compared with UK MBT, German MBT showed lower gas production and mass losses consistent with its more stabilised nature. The insignificant changes in the PSD could be an indication of a link between the magnitude of changes in the structure of waste during degradation and the magnitude of the mass being transformed to gas and leachate phases.

Similarly, visual assessment of Annex 2-7 suggests important changes with degradation in the PSD of MSW. This was confirmed statistically and is explained in section 2.3.2. The curve after degradation shows a shift towards the right, indicating a general increase in the particle size. For example D_{50} shows an increase from approximately 13 to 23 mm and the content of materials with sizes $\geq$ 10 mm increases from 58.7 to 62.9%. For the PSD analysis after degradation the maximum particle size was corrected to 37.5mm to match the maximum value reported before degradation.

2.5. Results: significance in differences between PSD

The significance in the differences observed between PSDs of the samples before and after degradation was evaluated statistically using the t-test explained in section 2.3.2. Two methods were used for the calculation of x_{mean} (as arithmetic mean and using the formulations for the log-normal distribution).

A summary of results is presented in Table 1-1, Table 2-2 and Table 2-3. For the case of UK MBT and MSW the changes in PSD caused by degradation processes can be regarded as significant given that t was >2. For German MBT, the differences can be regarded as not-significant given that t was < 2. This evaluation strengthens earlier visual judgements discussed in section 2.4.

Table 2-1 Evaluation of significance in changes in PSDs of UK MBT: t-test results

	Method 1		**Method 2**	
	Mean calculated as arithmetic, standard deviation as the root mean square deviation (Equations 2 8 and 2 9)		PSD considered to follow the log-normal law. Use of Ecuations 2-10 to 2-13	
	UK MBT B4	**UK MBT AF**	**UK MBT B4**	**UK MBT AF**
X_{mean}	2.0410	3.0880	3.1987	5.0843
S	0.4298	0.2604	0.4861	0.0799
Delta X_{mean}	1.0470		1.8856	
S_{diff}^2	0.2525		0.2427	
S_{diff}	0.5025		0.4926	
t	**2.0835**		**3.8277**	
Observations	2.0835>2 : differences between samples are significant		3.8277>2 : differences between samples are significant	

Table 2-2 Evaluation of significance in changes in PSDs of German MBT: t-test results

	Method 1		Method 2	
	Mean calculated as arithmetic, standard deviation as the root mean square deviation (Equations 2 8 and 2 9)		PSD considered to follow the log-normal law. Use of Ecuations 2-10 to 2-13	
	German MBT B4	**German MBT AF**	**German MBT B4**	**German MBT AF**
X_{mean}	4.7600	4.4050	7.3085	7.0113
S	0.2539	0.4239	0.1618	0.3193
Delta X_{mean}	0.3550		0.2972	
S_{diff}^2	0.2442		0.1281	
S_{diff}	0.4941		0.3580	
t	**0.7184**		**0.8303**	
Observations	0.7184<2 : differences between samples are non-significant		0.8303<2 : differences between samples are non-significant	

Table 2-3 Evaluation of significance in changes in PSDs of MSW : t-test results

	Method 1		Method 2	
	Mean calculated as arithmetic, standard deviation as the root mean square deviation (Equations 2 8 and 2 9)		PSD considered to follow the log-normal law. Use of Ecuations 2-10 to 2-13	
	MSW B4	**MSW AF**	**MSW B4**	**MSW AF**
X_{mean}	5.0380	6.8820	9.0028	12.0311
S	0.5315	0.7084	0.3516	0.6578
Delta X_{mean}	1.8440		3.0283	
S_{diff}^2	0.7843		0.5563	
S_{diff}	0.8856		0.7459	
t	**2.0822**		**4.0601**	
Observations	2.0822>2 : differences between samples are significant		4.0601>2 : differences between samples are significant	

2.6. Results: lognormal law model

2.6.1. Graphical method

Graphical evaluation of the normal law model followed the method explained in section 2.3.3.1. Annex 2-8 shows the PSD of UK MBT plotted using different scales: linear-linear (a), log-linear (b), log-probabilistic (c) and linear-probabilistic (d). Comparison of the different plots evidences the advantages in representing the distribution in log-probabilistic scale as it allows the identification of regions within the distribution that are most likely to follow the normal law. These regions are identified as those with nearly linear behaviour in the log-probabilistic scale. For UK MBT (Annex 2-8, c) and German MBT (Annex 2-9, a) the region between 6.3 and 0.063 mm sieve size exhibits linear behaviour. Similarly for MSW the range is from 20 to 0.063 mm (Annex 2-9, b). This initial assessment was confirmed with linear regressions and model evaluation explained in section 2.6.2.

2.6.2. Linear regressions and normal law model evaluation

2.6.2.1. UK MBT

Table 2-4 and Annex 2-10 summarize the results obtained from the evaluation of the log-normal law for UK MBT. The outcomes suggest the log-normal law model performs well in the range of sieve size between 6.3 and 0.063 mm and represents better the PSD of the sample before degradation. The coefficient of determinations R^2 (using Equation 2-15) were of 0.9899 and 0.9803 for the sample before and after degradation respectively, whereas NSE (using Equation 2-14) were of 0.9959 and 0.9821 respectively.

Table 2-4 Statistical results from evaluation of Normal law model to PSDs of UK MBT before and after degradation

	UK MBT B4				
Sieve size range (mm) Normal law model evaluation	20-0.032				6.3-0.063
Sieve size range (mm) Linear regression	20-0.032	20-0.063	10-0.063	6.3-0.063	6.3-0.063
Z_{mean}	1,1627				1,3390
Sg	1,6259				2,0000
X_{mean}	3,1987				3,8151
S	0,4861				0,6932
SumSq	0,0180				0,0013
NSE	0,9832				**0,9959**
R^2	0,7454	0,9701	0,9891	0,9899	**0,9899**
	UK MBT AF				
Sieve size range (mm) Normal law model evaluation	20-0.032				6.3-0.063
Sieve size range (mm) Linear regression	20-0.032	20-0.063	10-0.063	6.3-0.063	6.3-0.063
Z_{mean}	1,6262				1,9179
Sg	1,0832				1,6768
X_{mean}	5,0843				6,8070
S	0,0799				0,5169
SumSq	0,0280				0,0036
NSE	0,9746				**0,9821**
R^2	0,7178	0,8483	0,9493	0,9803	**0,9803**

2.6.2.2. German MBT

Table 2-5 and Annex 2-11 summarize the results obtained from the evaluation of the normal law in German MBT. These outcomes suggest that the normal law model performs better than for UK MBT with the highest fit observed in the range of sieve size between 6.3 and 0.063 mm. In the linear scale (Annex 2-11-d), the proximity between the straight lines corroborates the negligible changes in the PSD with degradation.

Table 2-5 Statistical results from evaluation of Normal law model to PSDs of German MBT before and after degradation

	German MBT B4				
Sieve size range (mm) Normal law model evaluation	75-0.032				6.3-0.063
Sieve size range (mm) Linear regression	75-0.032	75-0.063	10-0.063	6.3-0.063	6.3-0.063
Z_{mean}	1,9890				2,2767
Sg	1,1757				1,6946
X_{mean}	7,3085				9,7449
S	0,1618				0,5275
SumSq	0,0154				0,0002
NSE	0,9928				**0,9987**
R^2	0,8280	0,9110	0,9899	0,9942	**0,9942**
	German MBT AF				
Sieve size range (mm) Normal law model evaluation	75-0.032				6.3-0.063
Sieve size range (mm) Linear regression	75-0.032	75-0.063	10-0.063	6.3-0.063	6.3-0.063
Z_{mean}	1,9475				2,4400
Sg	1,3761				2,2126
X_{mean}	7,0113				11,4731
S	0,3193				0,7942
SumSq	0,0235				0,0001
NSE	0,9880				**0,9987**
R^2	0,8380	0,9363	0,9914	0,9988	**0,9988**

2.6.2.3. MSW

Table 2-6 and Annex 2-12 summarize the results obtained from the evaluation of the normal law in MSW. The outcomes suggest that the normal law model performs reasonably well in the range of sieve size between 6.3 and 0.063 mm and even in the range 20 to 0.063 mm and it is generally better after degradation.

Table 2-6 Statistical results from evaluation of Normal law model to PSDs of MSW before and after degradation

	MSW B4						
Sieve size range (mm) Normal law model evaluation	75-0.032					6.3-0.063	20-0.063
Sieve size range (mm) Linear regression	75-0.032	75-0.063	20-0.063	10-0.063	6.3-0.063	6.3-0.063	20-0.063
Z_{mean}	2.1975					3.1721	2.5459
Sg	1.4213					3.0734	2.3039
X_{mean}	9.0028					23.8600	12.7545
S	0.3516					1.1228	0.8346
SumSq	0.0782					0.0005	0.0139
NSE	0.9572					**0.9938**	**0.9600**
R^2	0.8161	0.8112	0.9645	0.9638	0.9540	**0.9540**	**0.9646**
	MSW AF						
Sieve size range (mm) Normal law model evaluation	75-0.032					6.3-0.063	20-0.063
Sieve size range (mm) Linear regression	75-0.032	75-0.063	20-0.063	10-0.063	6.3-0.063	6.3-0.063	20-0.063
Z_{mean}	2.4875					3.4713	3.3092
Sg	1.9306					3.5469	3.3650
X_{mean}	12.0311					32.1803	27.3621
S	0.6578					1.2661	1.2134
SumSq	0.0877					0.0013	0.0019
NSE	0.9346					**0.9824**	**0.9902**
R^2	0.6533	0.8812	0.9816	0.9756	0.9717	**0.9717**	**0.9816**

2.7. Results: fractal model

2.7.1. UK MBT

PSDs were analysed using the fractal model explained in section 2.3.3.3. Figure 2-1 and Table 2-7 summarize the results obtained for UK MBT. The model performs well in the sample after degradation in the range 20 to 0.063 mm sieve size with coefficients of determinations R^2 always greater than 0.99. For the sample before degradation, the fractal model explains better the PSD of the coarse fraction (20-2mm) whereas the normal law shows better fitting in the range of fines (<2mm) which corresponds to the soil like fraction.

2.7.2. German MBT

Figure 2-2 and Table 2-8 summarize the results obtained from the evaluation of the fractal model in German MBT. This model does not represent well the PSD of the sample either before nor after degradation.

2.7.3. MSW

Figure 2-3 and Table 2-9 summarize the results obtained from the evaluation of the fractal model in MSW. The model performs very well in the samples before and after degradation in the range 75 to 0.015 mm sieve size with coefficients of determinations R^2 always greater than 0.99 and NSE of 0.9625 and 0.9843 for the sample before and after degradation respectively.

Table 2-7 Statistical results from evaluation of Fractal model to PSDs of MBT UK before and after degradation

	UK MBT B4				
Sieve size range (mm) Fractal model fitting (linear regression)	-	20-0.032	20-0.063	20-0.15	20-0.3
Sieve size range (mm) Fractal model fitting (non-linear scale)	20-0.032	-	-	-	-
Slope	-	2.0425	0.6305	0.5411	0.4857
$D_{\text{linear regression}}$	-	-	2.3695	2.4589	**2.5143**
R^2	-	0.4506	0.9455	0.9732	**0.9882**
SumSq	0.0197	-	-	-	-
$D_{\text{non linear regression}}$	**2.5354**	-	-	-	-
NSE	**0.9816**	0.9799			
	UK MBT AF				
Sieve size range (mm) Fractal model fitting (linear regression)	-	20-0.032	20-0.063	20-0.15	20-0.3
Sieve size range (mm) Fractal model fitting (non-linear scale)	20-0.032	-	-	-	-
Slope	-	2.1758	0.7049	0.6844	0.6731
$D_{\text{linear regression}}$	-	-	2.2951	2.3156	**2.3269**
R^2	-	0.7418	0.9969	0.9980	**0.9978**
SumSq	0.0143	-	-	-	-
$D_{\text{non linear regression}}$	**2.3771**	-	-	-	-
NSE	**0.9871**	0.9832			

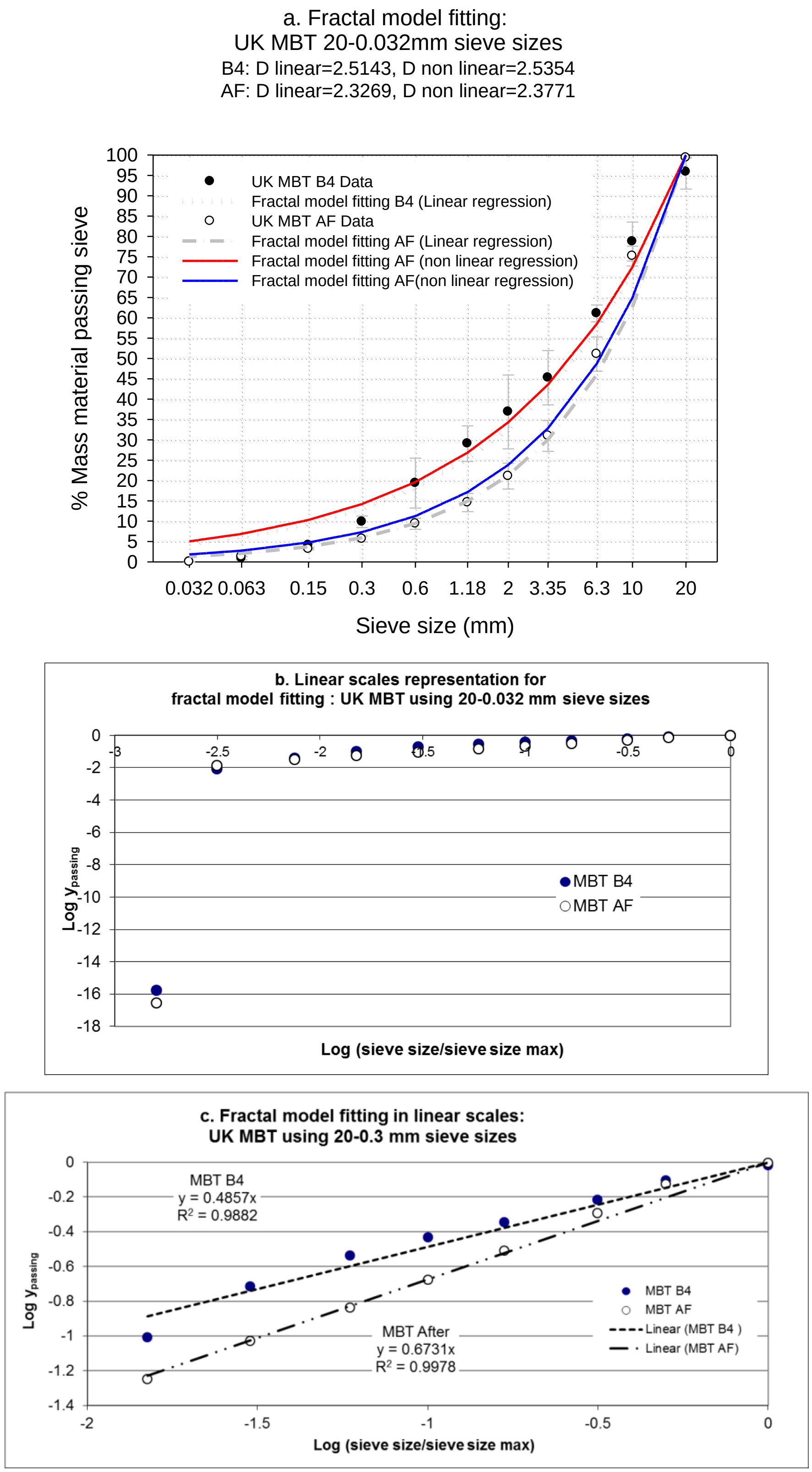

Figure 2-1 Fractal model fitting to PSDs of UK MBT before and after degradation. a. log-linear scale, b. linear scale 20-0.032 mm, c. linear scale 20-0.3 mm.

Table 2-8 Statistical results from evaluation of Fractal model to PSDs of German MBT before and after degradation

	German MBT B4				
Sieve size range (mm) Fractal model fitting (linear regression)	75-0.032	-	-	-	-
Sieve size range (mm) Fractal model fitting (non-linear scale)	-	75-0.032	75-0.063	75-0.15	75-0.30
Slope	-	1.6266	0.6286	0.5824	0.5419
$D_{\text{linear regression}}$	-	-	2.3714	2.4176	**2.4581**
r^2	-	0.4993	0.9586	0.9585	**0.9550**
SumSq	0.1589	-	-	-	-
$D_{\text{non linear regression}}$	**2.6140**	-	-	-	-
NSE	**0.9256**	0.8659			
	German MBT AF				
Sieve size range (mm) Fractal model fitting (linear regression)	75-0.032	-	-	-	-
Sieve size range (mm) Fractal model fitting (non-linear scale)	-	75-0.032	75-0.063	75-0.15	75-0.30
Slope	-	1.0379	0.5339	0.4894	0.4575
$D_{\text{linear regression}}$	-	-	2.4661	2.5106	**2.5425**
r^2	-	0.5644	0.9636	0.9723	**0.9746**
SumSq	0.1027	-	-	-	-
$D_{\text{non linear regression}}$	**2.6271**	-	-	-	-
NSE	**0.9476**	0.9233			

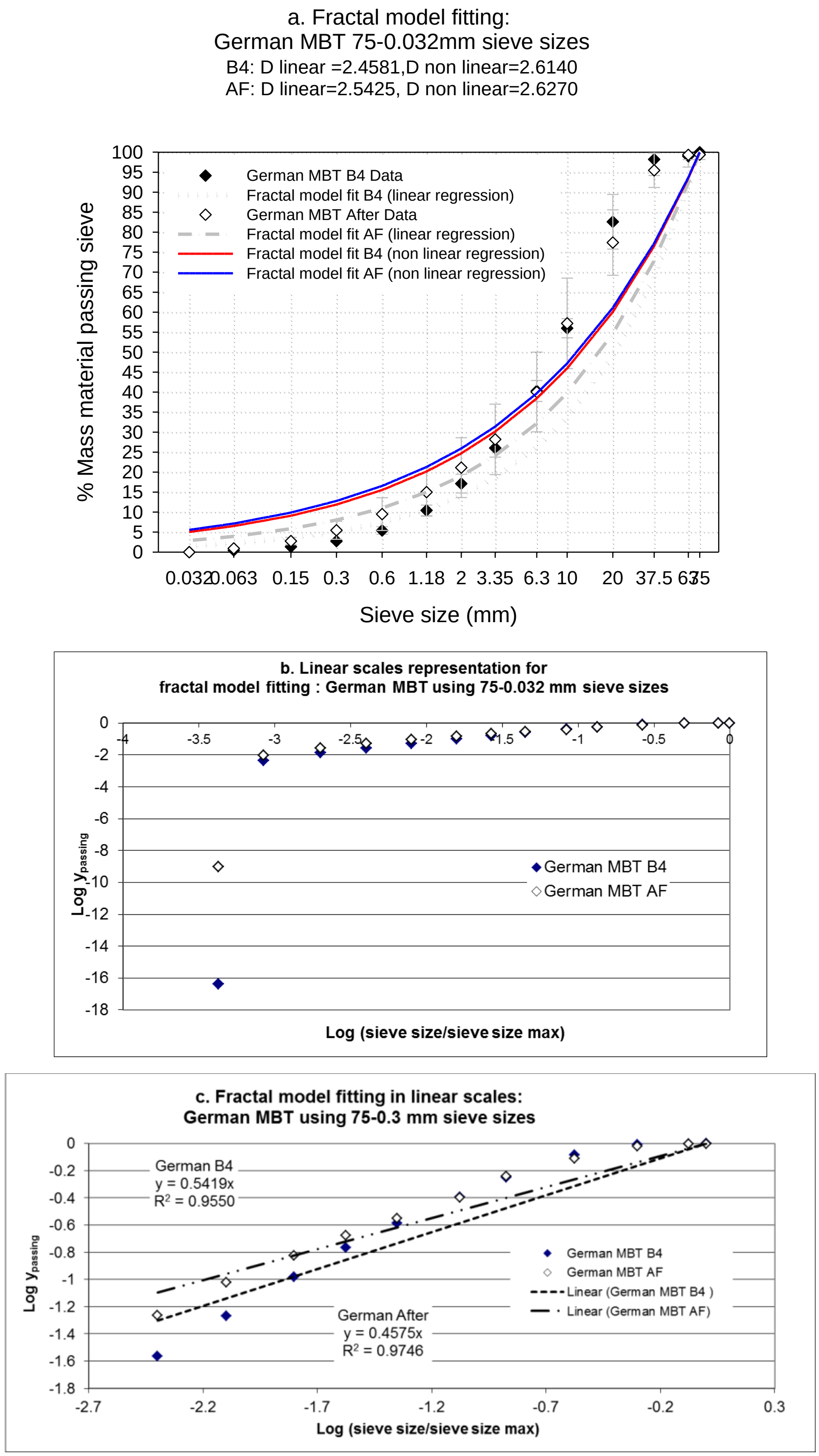

Figure 2-2 Fractal model fitting to PSDs of German MBT before and after degradation a. log-linear scale, b. linear scale 75-0.032 mm, c. linear scale 75-0.3 mm.

Table 2-9 Statistical results from evaluation of Fractal model to PSDs of MSW before and after degradation

	MSW B4				
Sieve size range (mm) Fractal model fitting (linear regression)	75-0.032	-	-	-	-
Sieve size range (mm) Fractal model fitting (non-linear scale)	-	75-0.032	75-0.063	75-0.015	75-0.30
Slope	-	1.0204	0.5111	0.4518	0.4352
$D_{\text{linear regression}}$	-	-	2.4889	2.5482	**2.5648**
r^2	-	0.5508	0.9585	0.9925	**0.9944**
SumSq	0.0641	-	-	-	-
$D_{\text{non linear regression}}$	**2.5927**	-	-	-	-
NSE	**0.9650**	0.9625			
	MSW AF				
Sieve size range (mm) Fractal model fitting (linear regression)	75-0.032	-	-	-	-
Sieve size range (mm) Fractal model fitting (non-linear scale)	-	75-0.032	75-0.063	75-0.015	75-0.30
Slope	-	1.5147	0.4695	0.4412	0.4231
$D_{\text{linear regression}}$	-	-	2.5304	2.5588	**2.5769**
r^2	-	0.3931	0.9845	0.9920	**0.9950**
SumSq	0.0137	-	-	-	-
$D_{\text{non linear regression}}$	**2.5361**	-	-	-	-
NSE	**0.9898**	0.9843			

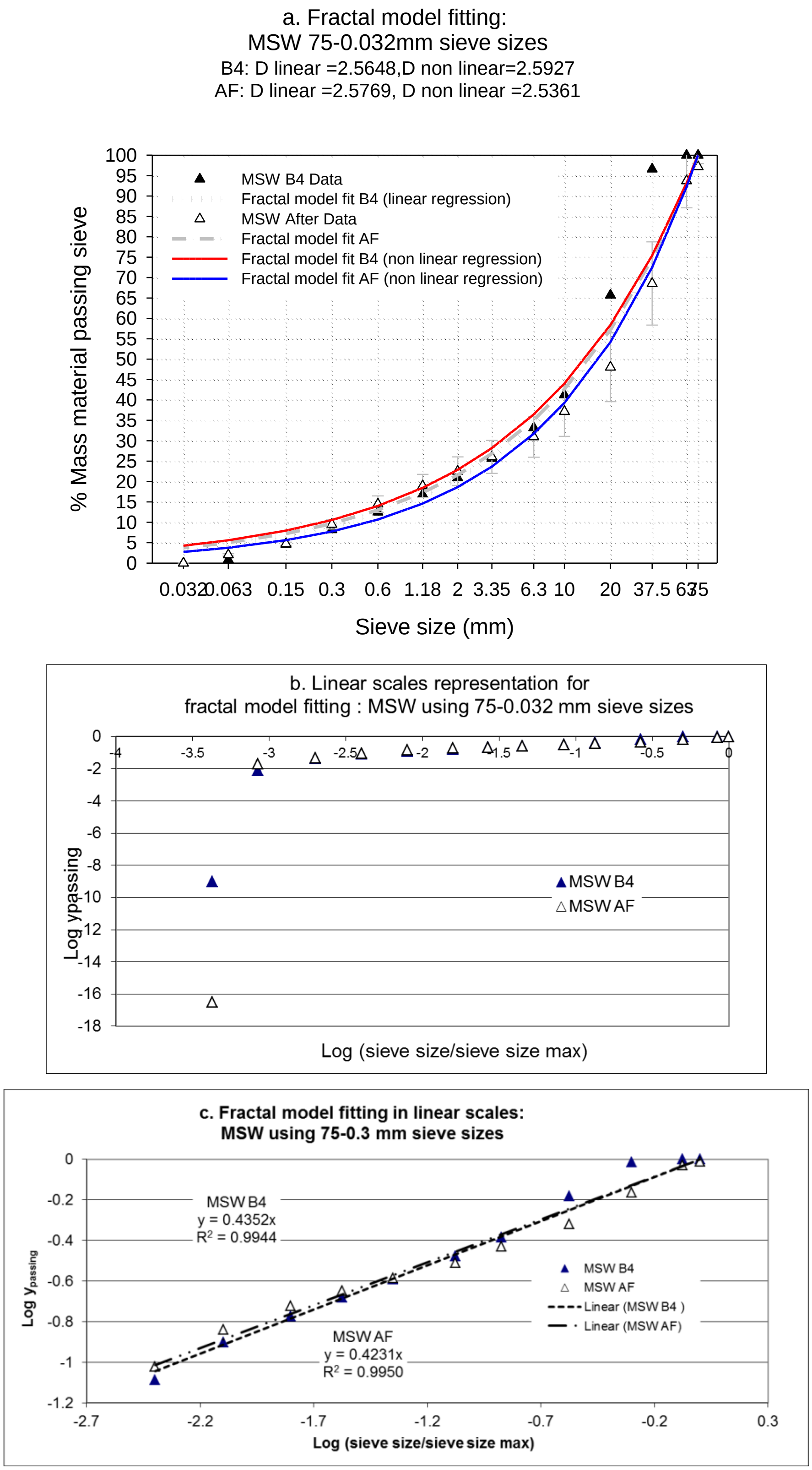

Figure 2-3 Fractal model fitting to PSDs of MSW before and after degradation. a. log-linear scale, b. linear scale 75-0.032 mm, c. linear scale 75-0.3 mm.

2.8. Results: Rosin-Rammler model

A third model was investigated. Results are summarised in Figure 2-4, Figure 2-5 and Figure 2-6 and in Table 2-10, Table 2-11 and Table 2-12. They show the best performance for the entire range of particle size in German MBT.

Table 2-10 Statistical results from evaluation of Rosin-Rammler model to PSDs of UK MBT before and after degradation

	UK MBT B4			
Sieve size range (mm) Rosin-Rammler fitting (linear regression)	20-0.032	20-0.063	20-0.15	20-0.3
Slope	3.3122	0.9201	0.8113	0.7593
Intercept	-4.2322	-1.5142	-1.3700	**-1.2883**
R^2	0.4317	0.9639	0.9843	**0.9870**
NSE	-	-	-	0.9913
	UK MBT AF			
Sieve size range (mm) Rosin-Rammler fitting (linear regression)	20-0.032	20-0.063	20-0.15	20-0.3
Slope	2.1360	0.9420	0.9608	1.0063
Intercept	-3.1828	**-1.8260**	-1.8510	-1.9224
R^2	0.5584	**0.9761**	0.9675	0.9617
NSE		0.9797		

Table 2-11 Statistical results from evaluation of Rosin-Rammler model to PSDs of German UK before and after degradation

	German MBT B4			German MBT AF		
Sieve size range (mm) Rosin Ramler fitting (linear regression)	75-0.032	75-0.063	75-0.15	75-0.032	75-0.063	75-0.15
Slope	1.9035	1.0395	1.0311	1.6531	0.8546	0.8301
Intercept	-4.3480	-2.4240	-2.4036	-3.8255	-2.0472	-1.9882
R^2	0.5951	**0.9922**	0.9896	0.5651	**0.9946**	0.9957
NSE	-	**0.9964**	-	-	**0.9961**	-

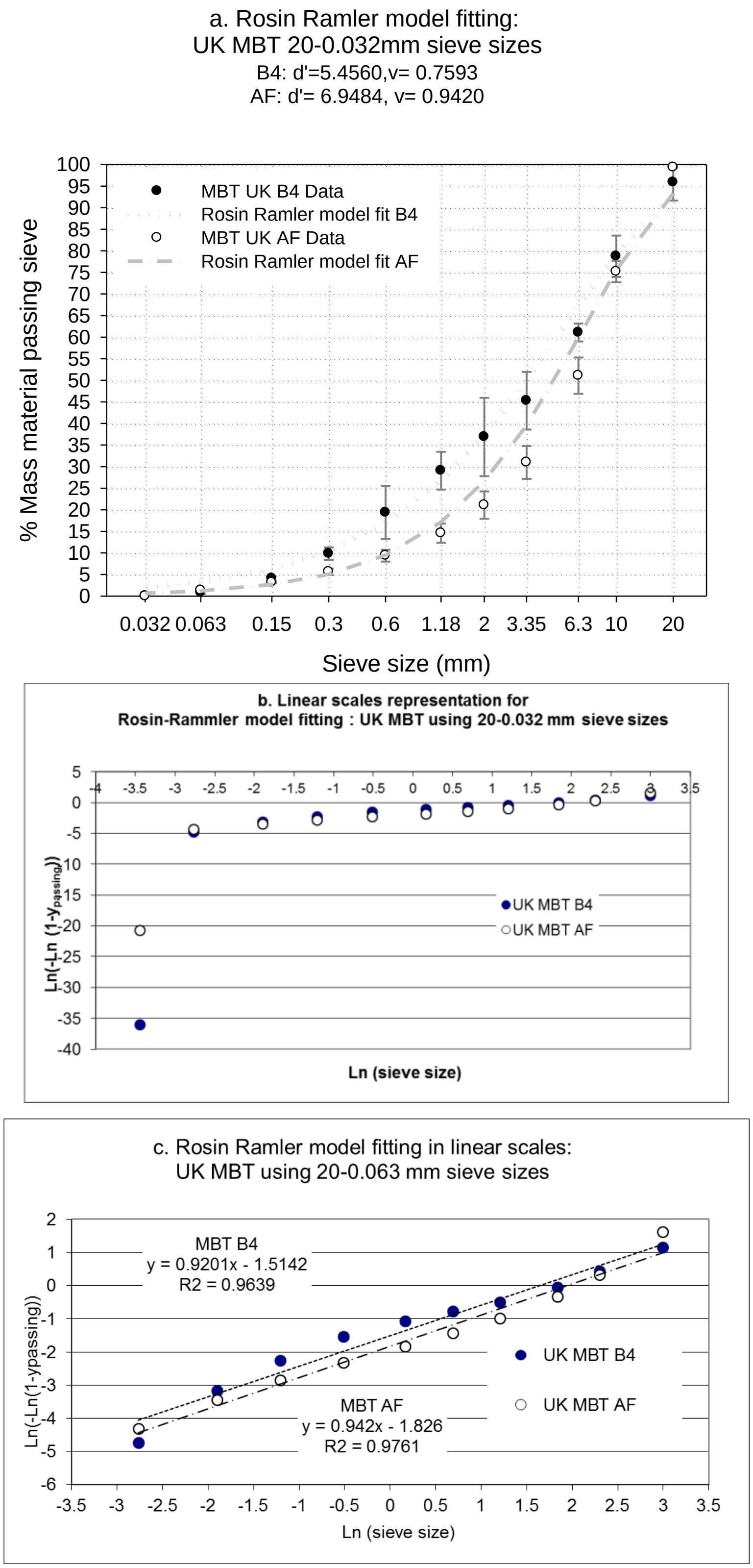

Figure 2-4 RR model fitting to PSDs of UK MBT B4 and AF degradation for different sieve size ranges. a. log-linear scale, b. linear scale 20-0.032 mm, c. linear scale 20-0.063 mm.

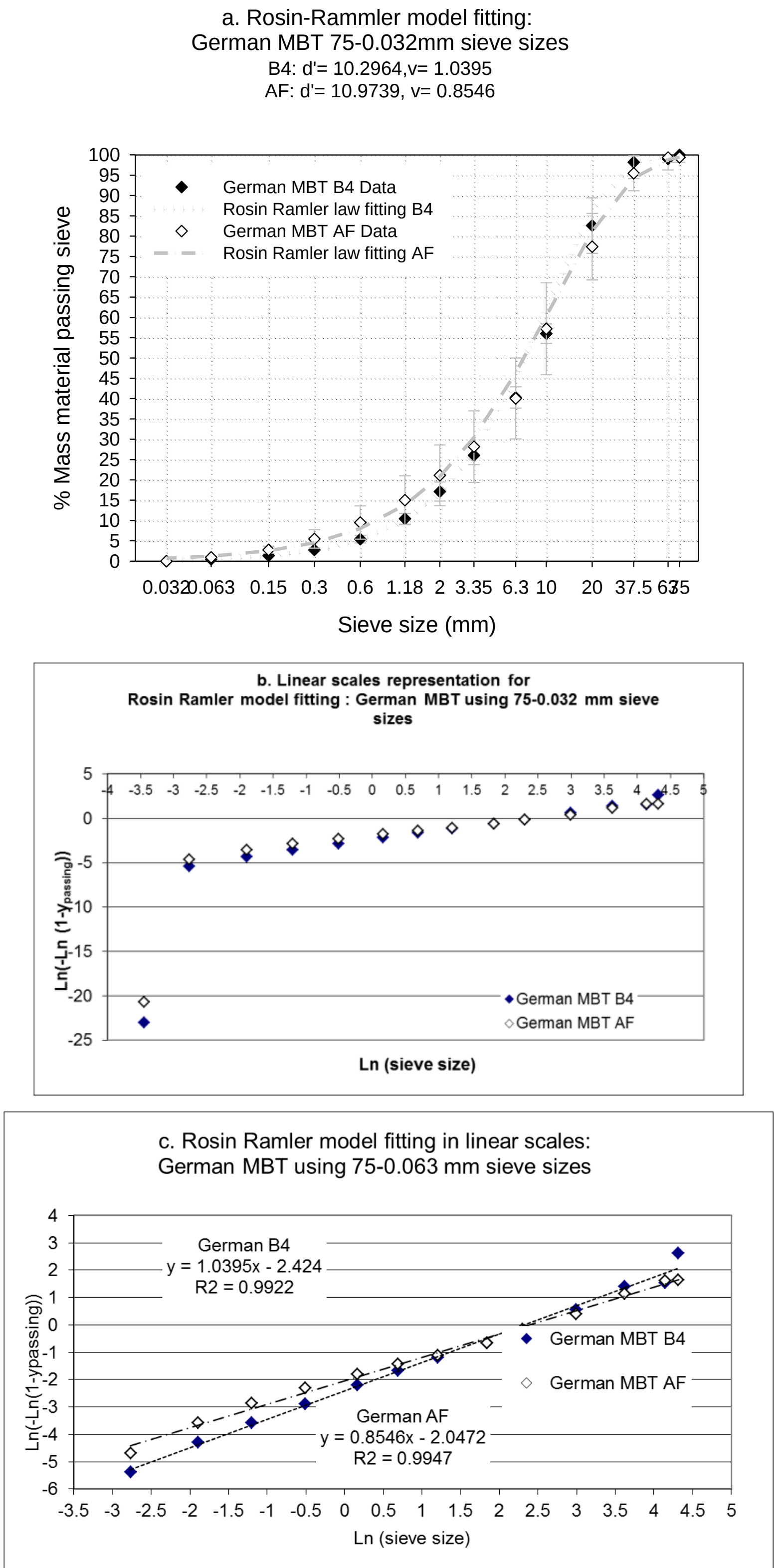

Figure 2-5 RR model fitting to PSDs of German MBT B4 & AF degradat.for different sieve size ranges. a. log-linear scale, b. linear scale 75-0.032 mm, c. linear scale 75-0.063 mm.

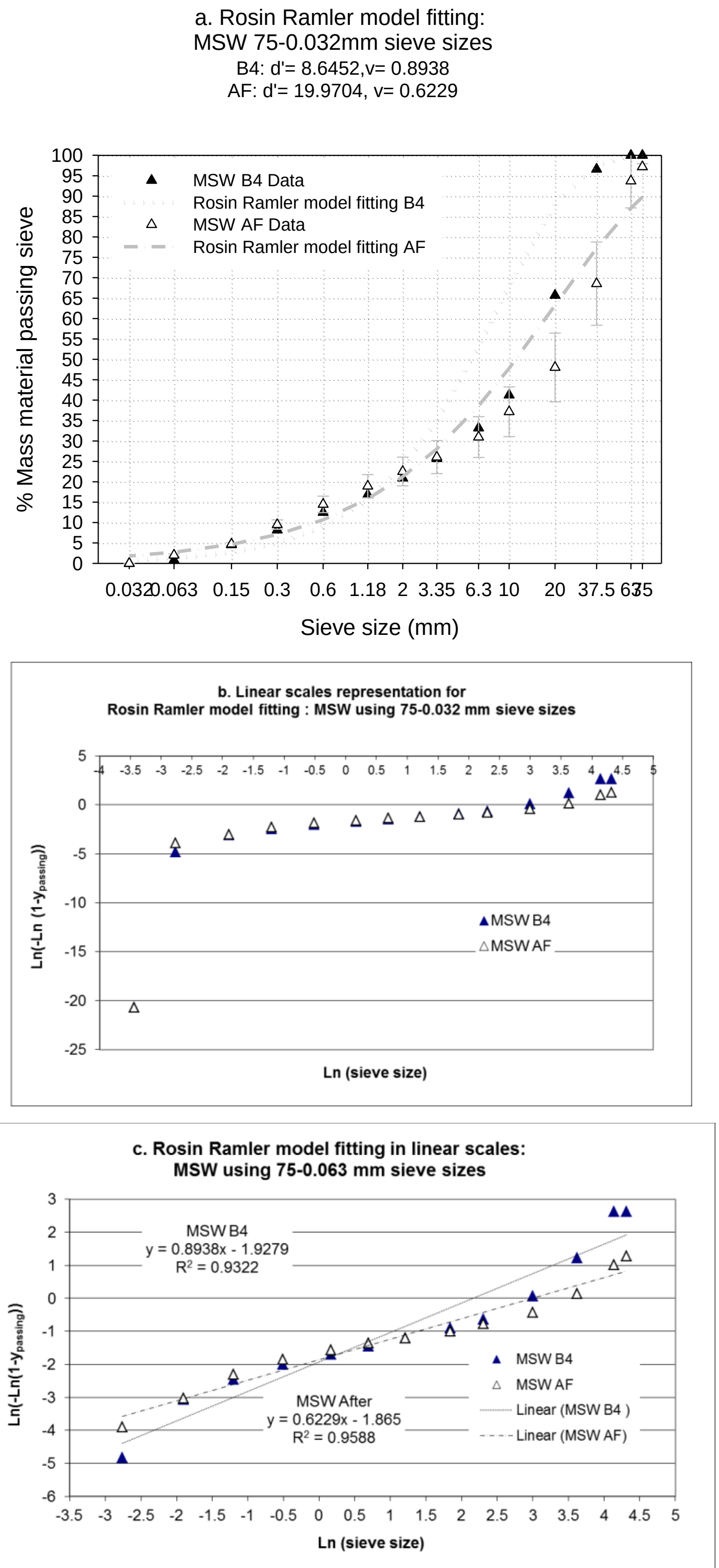

Figure 2-6 RR model fitting to PSDs of MSW B4 & AF for different sieve size ranges. a. log-linear scale, b. linear scale 20-0.032 mm, c. linear scale 20-0.063 mm.

Table 2-12 Statistical results from evaluation of Rosin Rammler model to PSDs of MSW before and after degradation

	MSW B4			MSW AF		
Sieve size range (mm) Rosin Ramler fitting (linear regression)	75-0.032	75-0.063	75-0.15	75-0.032	75-0.063	75-0.15
Slope	1.6915	0.8938	0.8556	1.4711	0.6229	0.5956
Intercept	-3.7044	-1.9280	-1.8358	-3.7540	-1.8650	-1.7992
r^2	0.5720	**0.9322**	0.9098	0.476	**0.9588**	0.9477
NSE	-	**0.9058**	-	-	**0.9539**	-

2.9. Discussion

A graphical comparison between the different models is summarised in Figure 2-7, Figure 2-8 and Figure 2-9. In Table 2-14 a summary of the model parameters and R^2 is presented.

Table 2-13 Summary of the model parameters for the samples of solid waste investigated

	Normal		Rosin-Rammler		Fractal	
Model Parameters	x_{mean}	S	d'	υ	D linear	D non-linear
UK MBT B4	3,1987	0,4861	5,4560	0,7593	2,5143	2,5354
UK MBT AF	5,0843	0,0799	6,9484	0,9420	2,3269	2,3771
German MBT B4	7,3085	0,1618	10,2964	1,0395	2,4581	2,6140
German MBT AF	7,0113	0,3193	10,9739	0,8546	2,5425	2,6270
MSW B4	9,0028	0,3516	8,6452	0,8938	2,5648	2,5927
MSW AF	12,0311	0,6578	19,9704	0,6229	2,5769	2,5361

Table 2-13 illustrates the model parameters obtained for the samples of solid waste examined during this research. The table evidences the reduced number of parameters required to describe each of the models. For example, the normal and RR models require only two parameters for a full description, i.e. x_{mean} , S and d', υ respectively. The fractal model requires only one parameter, the fractal dimension D. Notice that although Table 2-13 reports two parameters for the fractal model (i.e. D linear and D non-linear) the difference only refers to the two methods followed during the calculation (i.e. using the linear and the non-linear

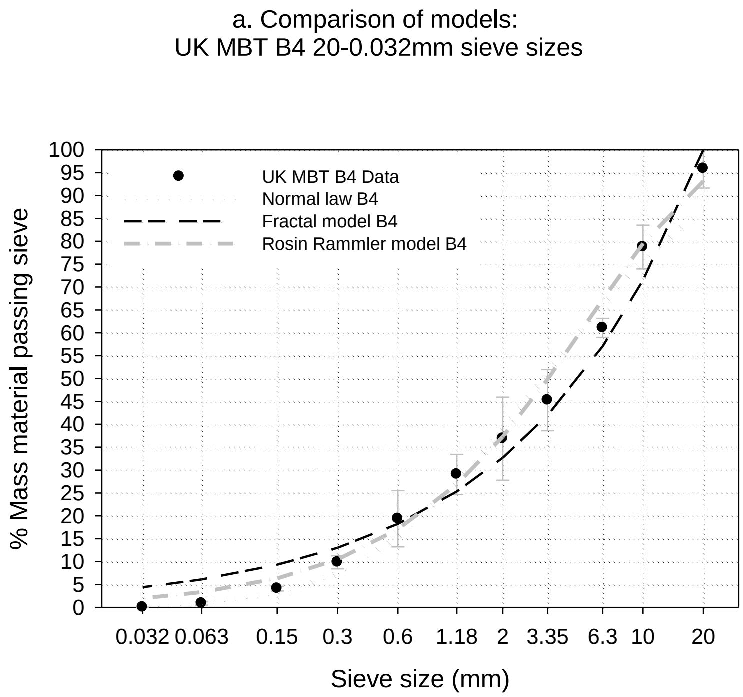

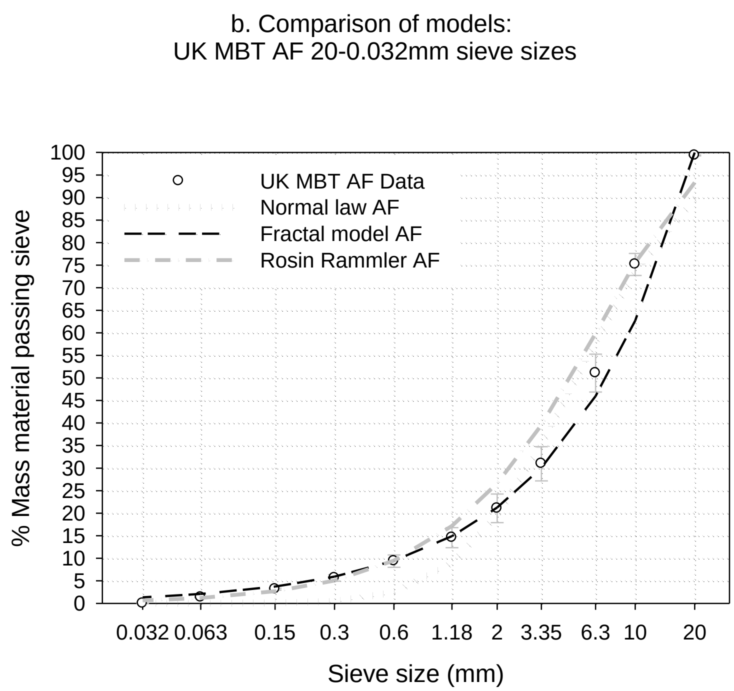

Figure 2-7 Comparison between different models to describe PSD in UK MBT. a. UK MBT before degradation, b. UK MBT after degradation.

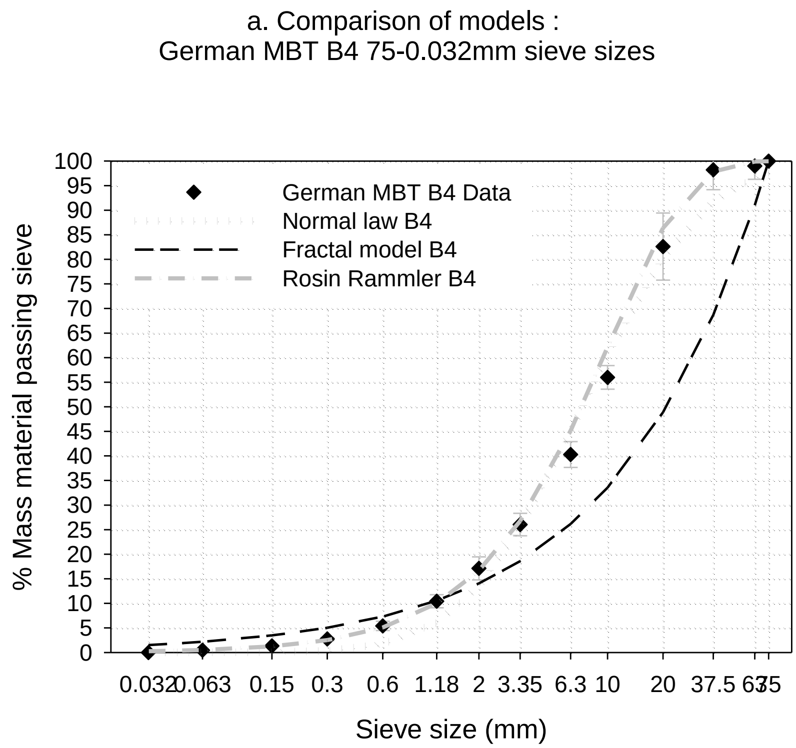

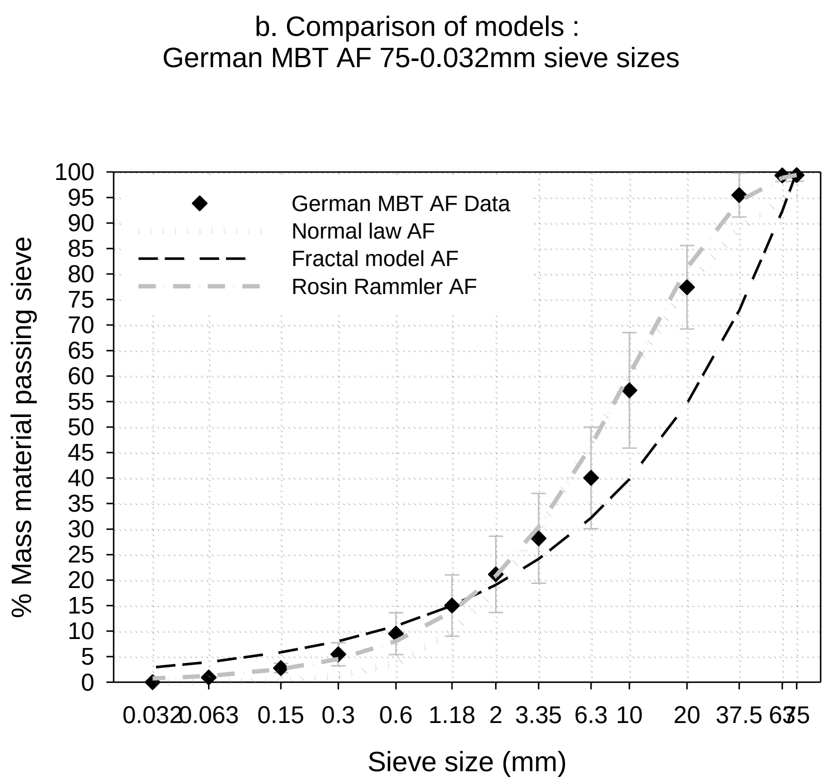

Figure 2-8 Comparison between different models to describe PSD in German MBT. a. German MBT before degradation, b. German MBT after degradation.

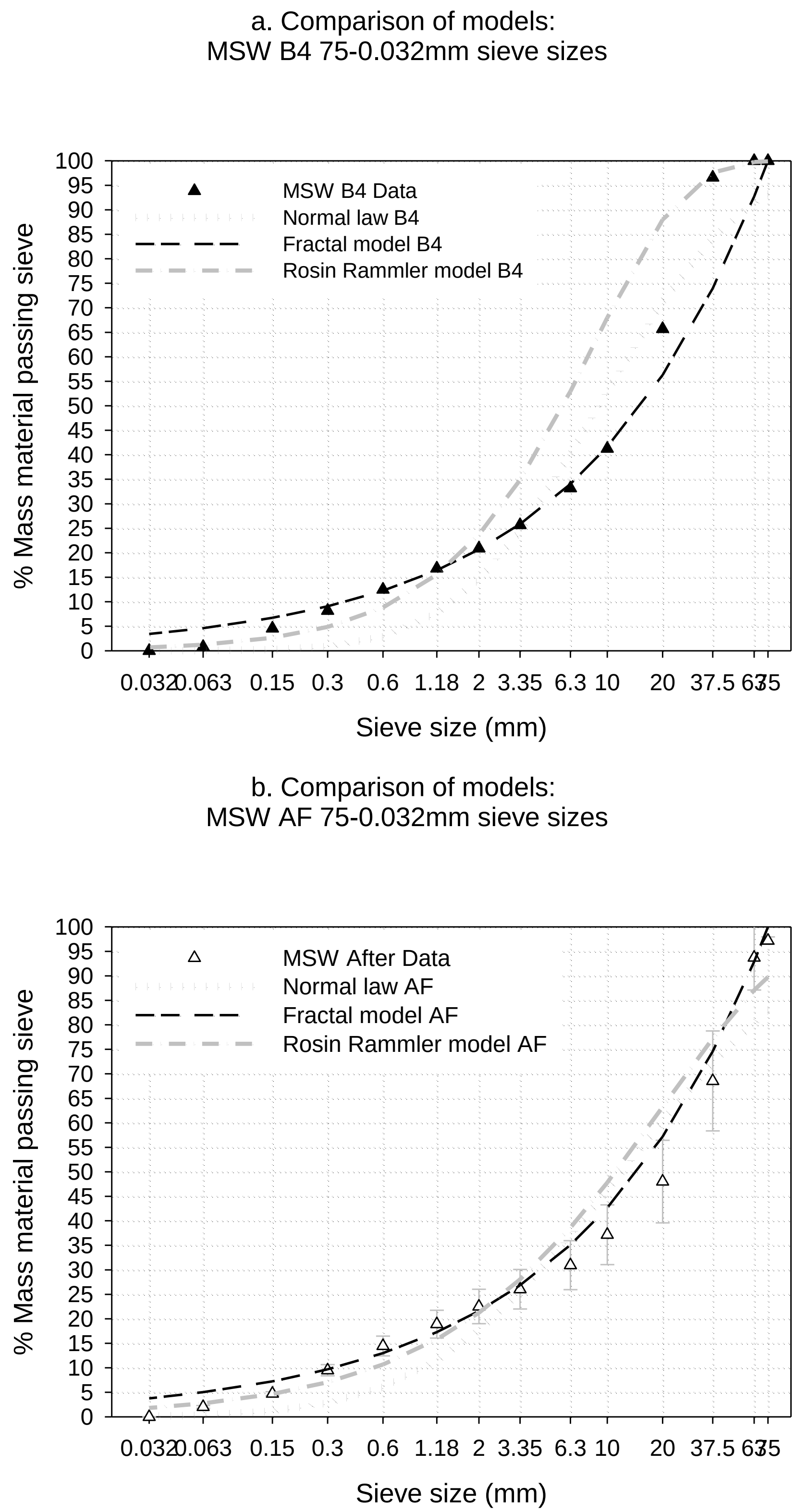

Figure 2-9 Comparison between different models to describe PSD in MSW. a. MSW before degradation, b. MSW after degradation.

model representation) but not to a different parameter. Some of the advantages of having a model are discussed. First, a full PSD (i.e. $y_{passing}$ or $y_{retained}$) can be generated having only the parameter (e.g. fractal) or parameters (e.g. normal or RR) and a relevant range of particle sizes (i.e. the x axis). Furthermore, as the model provides an analytical expression for the PSD, there is not limitation to the amount of data generated and the spacing between the data selected in the x axis. With less spacing between points, calculations that use the PSD information (e.g. pore size distribution) could experience an increased accuracy resulting from having a more detailed system description. An example on the potential use of PSD mathematical models for the estimation of the pore geometry and K is presented in Chapter 6, where the methodology proposed by White and Beaven (2008) was applied. Data presented in Table 2-13 include the results obtained for all the models evaluated, but it does not indicate what the most appropriate model is for each of the samples investigated. This is information that can be deduced from the comparison between the coefficients of the determination R^2 presented in Table 2-14.

Table 2-14 Summary of the coefficients of determination R^2 from linear regressions in the entire sieve size range

	Normal	Rosin-Rammler	Fractal
UK MBT B4	**0,9701**	0,9639	0,9455
UK MBT AF	0,8483	0,9761	**0,9969**
German MBT B4	0,9110	**0,9922**	0,9586
German MBT AF	0,9363	**0,9946**	0,9636
MSW B4	0,8112	0,9322	**0,9585**
MSW AF	0,8812	0,9588	**0,9845**

Table 2-14 shows how well the PSD of the samples of waste studied fit to each of the three mathematical models examined. The R^2 reported correspond to data obtained when the model was plotted in the linear form. The higher the R^2 , the better the fit and the better the model represents the PSD.

The highest R^2 for the sample of German MBT found with the Rosin-Rammler model was 0.9922 and 0.9946 for the sample before and after degradation respectively. The R^2 for the sample of German MBT using the log-normal and fractal models were lower than those with RR model, suggesting that the PSD of the sample of German MBT is better represented with the RR model.

The highest R^2 for the UK MBT sample, 0.9701 and 0.9969, were found with the log-normal and fractal models for the specimens before and after degradation respectively. These results indicate that the PSD of the sample of UK MBT is well described with a log-normal distribution when the material it is just received from the facility, and with a fractal model once it goes through a further process of anaerobic degradation. Unlike for the German MBT, data for R^2 with the RR model were comparatively smaller which indicates that RR is a less appropriated model to describe the PSD of the UK MBT sample.

In the case of the sample of MSW, the highest results of R^2 of 0.9585 and 0.9845 for the sample before and after degradation respectively, were found with the fractal model. Results of R^2 with the other two models, i.e. log normal and RR, were smaller. This indicates that the fractal model is an appropriated model to describe the PSD of the sample of MSW.

A compilation of Table 2-13 and Table 2-14 is presented in Table 2-15 were the parameters for the model with the best fit and the coefficients of determination are presented. The RR was shown as the best option to represent the PSD of the sample of German MBT whilst the fractal model for the UK MBT and MSW. It is worthy to emphasise the convenience of using one single type of model to describe the changes in the PSD with degradation of one sample. This simplifies the calculations: the mathematical expressions that describe the model can be kept intact and only variation in the numerical value(s) of the model parameter(s) is required. This was considered in the construction of Table 2-15, especially for the UK MBT B4. Although the R^2 found with the normal model was the highest, the R^2 with the fractal model was still reasonable high and >0.94 to suggest the fractal model as a rational alternative to represent the PSD of the UK MBT B4. For unification purposes, for those samples where the fractal model had the best fit, the fractal dimension *D* reported in Table 2-15 was the value found with the regression using for the non-linear system. The coefficient *NSE* was in all cases slightly higher than that found with the regression in the linear system.

Table 2-15 Summary of the coefficients of determination R2 from linear regressions in the entire sieve size range

	Rosin-Rammler			Fractal	
Model Parameters	R^2	d'	υ	R^2	D
UK MBT B4				0,9455	2,5354
UK MBT AF				0,9969	2,3771
German MBT B4	0,9922	10,2964	1,0395		
German MBT AF	0,9946	10,9739	0,8546		
MSW B4				0,9585	2,5927
MSW AF				0,9845	2,5361

The results reported along sections 2.4 to 2.9 suggest that the PSD of the waste samples studied can be described using standard mathematical models. The type of model that best suits a data set would depend on the waste nature. For example, during this research the log-normal law described reasonably well the PSD of all the samples but only over a restricted particle size range (<6.3 mm) which corresponds to the soil like fraction. This is consistent with what is seen in many soils and sediments with their PSDs following the log-normal law. This has been explained as the result of natural processes working over long periods of time, e.g. weathering, transportation and deposition (Krumbein, 1938a). Hence, it is not surprising to find that the PSD of the soil like fraction of waste samples can be well described with the log-normal equation.

The Rosin-Rammler model performed well over the entire range of PSD of the German MBT sample both before and after degradation. The German MBT sample corresponds to a highly pre-treated waste produced by a multistep process of mechanical, aerobic and anaerobic degradation. In experiments carried out by Siddiqui (2011), the German MBT sample showed a comparatively low gas production level during the anaerobic degradation in the CAR, which is consistent with its stable nature. In the industry of particulate materials, the RR model is frequently used to describe the PSD of processed materials such as coal, powder, and particulate substances (Herdan, 1960, BS ISO 9276-3, 2008). As the nature of the German MBT sample is consistent with a well processed material, it is reasonable to have its PSD well described with the RR model.

The fractal model worked well describing the PSD of UK MBT and MSW samples before and after degradation. These results could have some important implications in our understanding of the structure of waste and in the kinetics followed during the biodegradation process. Firstly, a successful representation of the PSD of a waste material using a fractal model indicates that the property of particle size is fractal, the material has a fractal dimension and can be therefore described as a fractal (Mandelbrot, 1982, Turcotte 1986). The results here presented suggest that the PSDs of the samples of UK MBT and MSW can be described with the fractal model and consequently the samples can be described as fractals.

Klymko and Kopelman (1982) and Kopelman (1988) experimentally studied diffusion limited reactions in fractal objects and concluded that reaction in such media are likely to follow a fractal like reaction kinetics. That may be the case during the degradation experienced in the CARs by UK MBT and MSW samples and would imply a reaction rate coefficient that varies with time. Further support for this argument is provided by the inclusion in many LFG generation models (Landfill Gas Generation Models), including GasSIM, of more than one first order decay constant. GasSIM includes three organic fractions, considered to degrade rapidly, moderately and slowly, each with its own degradation constant. In other words many existing first order models already include the central assumption of fractal kinetics of some variation in reaction rate coefficient with time.

The nature of both UK MBT and MSW samples corresponds with a heterogeneous fractal material, i.e. diverse materials and sizes, that undergoes a heterogeneous reaction, i.e. intensive anaerobic degradation in the CARs with comparatively significant gas production (Siddiqui, 2011, Ivanova, 2007). As the focus of this research was not the study of the biodegradation kinetics, data on this matter was not collected to test the hypothesis. However, previous experiences with fractal kinetics from Meraz (2004) in solid wastes, and from Xu and Ding (2007), Wang and Feng (2010) and Wang et al. (2011) in the bioenzymatic saccharification of cellulose give a good indication that the hypothesis of fractal kinetics in solid wastes is reasonable. Future research on fractal kinetics in solid wastes could include data from the investigations by Siddiqui (2011) and Ivanova (2007) on the biodegradation and settlement of UK MBT and MSW respectively.

The case for German MBT may be different as the specimen cannot be considered as a fractal. Experimental studies on fractal like degradation kinetics in non-fractal objects are scarce. Kopelman (1988) hypothesises that diffusion limited reactions in non fractal heterogeneous objects could follow a fractal like kinetics. However, in the absence of experiments on fractal like kinetics using heterogeneous non-fractal objects, it is still uncertain whether they will follow a fractal like kinetics. Data collected during this research is limited to the changes experienced by the specimens studied whilst in the CAR. During the time in the CAR, the specimen of German MBT did not experience much degradation as it was received as a highly degraded waste type. This is backed up by the low mass lost and methane production observed (Siddiqui, 2011). The PSDs of the specimens of German MBT B4 and AF are in essence the same and possibly reflect the nature of the treatment process (i.e. mechanical, anaerobic and aerobic) experienced by the residue before being received. The model that best fitted the data was the RR which was developed to describe mechanically processed materials. There are no data on the PSD of the waste prior to being subjected to the German MBT process, but it is possible to speculate that it may also have fitted a fractal distribution. The German MBT treatment process would have contained both mechanical and degradation processes, and it is possible that the degradation, if studied in isolation, may also have exhibited tendencies towards fractal degradation. However, this is rather speculative, but what can be said is that it appears that the mechanical process may have been the step having the major impact on the distribution of particles size and, the other two stages (i.e. anaerobic and aerobic degradation) may have been steps having only a secondary impact on the PSD.

The results presented along the chapter also indicate that the UK MBT and MSW samples once degraded showed a general increase in the size of the particles. This was evidenced by the right shift of the PSDs and by the statistical analyses. An increase in the size of the particles might be an indication of a degradation mechanism where the readily degradable and smaller particles were preferred over the inert coarser materials. This is consistent with a fractal-like degradation. The molecules of readily degradable materials are favoured for solubilisation and transportation to the liquid phase where degradation occurs. The inert coarse materials have a tendency to remain in the sample as the solubilisation and transportation to the liquid phase of their organic matter is more difficult. The presence of coarse inert materials (e.g. plastics) increases the heterogeneity of the medium and promotes the presence of heterogeneous reactions. With the smaller readily degradable particles degraded and the inert coarse particles intact, an overall increase in particle size could be expected. Further evidence to stress this hypothesis is presented in Chapter 3 where the material characterisation shows a general increase of the inert materials with degradation. Analysis of alternative mechanisms to explain the overall increase in particle size follows. During degradation wet conditions could promote bio-film growth, favour particles binding and clustering and therefore agglomeration. Two conditions would be an indication of agglomeration. Change in the appearance of waste particles yet negligible modification in the material composition. If only agglomeration causes the increase in particle size, degradation would take place uniformly across the waste body and independently of the particle composition. In these conditions the overall composition should not see important changes. The evidence gathered during the material characterisation discussed in Chapter 3 does not favour agglomeration. Particle appearance was visually assessed without finding evidence of bio-film growth or particle binding. Material composition showed that inert and slowly degradable materials (e.g. plastics, glass, textiles and paper according to Meraz et al. (2004)) constitute the coarser fractions whereas soil like components the finer. After degradation, composition was found richer in inert and slowly degradable materials. This indicates that soil like components with high content of readily biodegradable organic matter were easier to solubilise than synthetic materials composed by longer organic chains less accessible to anaerobic microorganisms.

Movement of fine particles is another option that could explain the overall increase in particle size with degradation. Degradation in CARs was carried out under continuous leachate recirculation. Liquid transportation could favour mobilisation of the finer particles in the bottom to the top direction. This would create an overall increase in the particle size at the bottom with a complementary decrease in the overall particle size at the top. UK MBT after degradation sampled from the bottom of the waste body showed an increase in the particle size which agrees with the possibility of fines mobilisation. However, German MBT sampled from the top did not show any changes in the particle size indicating un-significant fines re-location. This evidence does not suggest the re-location as the mechanism producing the increase in particle size.

2.10. Summary

The use of standard models to simplify the description of particle size in solid waste was proved feasible.

The application of three different models, i.e. Normal, Rosin-Rammler and Fractal, of relevance for particulate materials was explored during this study. The method followed for the selection of a PSD was based on the mathematical comparison between the experimental and modelled data. Modelled data was obtained once the model parameters were calculated following the minimal square root method. The data sets were represented graphically in both the linear and non-linear representations. The goodness of fit of each model was evaluated using two types of coefficients, i.e. R^2 and NSE for the linear and non-linear representations respectively. The model with the best fit was that with the coefficients closer to the unit.

Some of the advantages of having a model to describe the PSD of a sample of waste were discussed. A full PSD can be generated with only the model parameter (e.g. fractal) or parameters (e.g. normal or RR). As a model provides an analytical expression to describe the PSD, there is not limitation to the amount of data generated and the spacing. The calculations that use the PSD information (e.g. pore size distribution, permeability) can be performed with an increased accuracy. This could result in a better estimation of properties such as the hydraulic conductivity and have therefore a positive impact in the existing landfill macro scale models. A further advantage is the possibility to model the changes with biodegradation in the PSD and in properties such as permeability with only adjusting the numerical value(s) of the model parameter(s).

During this study it was also shown that the nature and story of the waste investigated has an influence on the type of model that best describes its PSD. For example, the Rosin-Rammler model described well the PSD of the German MBT sample, which is a stable material produced in a controlled treatment process of sequential mechanical, aerobic and anaerobic degradation. This could be an indication that in terms of particle size, the pre-treatment process experienced for the German MBT sample followed a mechanism similar to those during grinding and crushing of powders and particulate materials which PSDs are traditionally well described with the RR model.

The three specimens of solid waste studied have a heterogeneous nature. According to theory on fractal reaction kinetics, a heterogeneous system will experience a fractal like kinetics mechanism during a diffusion controlling reaction. Therefore, degradation of any of the specimens is expected to follow a fractal like kinetics mechanism. However, experiments on fractal kinetics have been mainly carried out on fractal objects whilst the behavior of non-fractal objects during diffusion controlled reactions is a subject of investigation. Only two of the specimens (i.e. UK MBT and MSW) can be considered as fractals as their PSDs were well explained with the fractal model. UK MBT and MSW were received in less degraded conditions than the German MBT specimen, experienced significant degradation during their time inside the CAR as well as changes in their PSDs with an overall increase in the particle size. Degradation in UK MBT and MSW specimens is therefore expected to have followed fractal reaction kinetics.

The German MBT was received as a more stable specimen and did not experience any significant degradation during the time in the CAR, therefore it is not possible to speak about fractal reaction kinetics for this specimen during that period. However, as the specimen underwent pretreatment which included mechanical, aerobic and anaerobic degradation, the degradation could have followed a fractal like kinetics. Yet, the degradation was possibly not the step controlling the final particle size distribution. The general appearance of the PSD fitted by the RR model suggests that the mechanical treatment could have been the step during treatment having the highest influence on the particle size.

Fractal kinetics was developed (Kopelman, 1988) and has been successfully applied during the last decades to explain reactions in heterogeneous media (Kopelman, 1988, Meraz et al., 2004, Wang and Feng, 2010, Wang et al., 2011, Xu and Ding, 2007) that includes the biodegradation of solid wastes (Meraz et al., 2004). The heterogeneous nature in solid wastes could be indicating that the anaerobic degradation processes will follow a fractal like mechanism. This is a hypothesis that needs more research but that is backed up by theory and evidence in other biodegradable systems. A scale up of the applicability of fractal kinetics in solid wastes to more types of solid wastes could offer a rational alternative to incorporate the heterogeneous structure of solid wastes into landfill modelling.

The study presented along this chapter indicates a tendency towards the increase in particle size with degradation. This is in opposition to results from investigations by White and Beaven (2008) and Rezanezhad et al. (2010). White and Beaven (2008) indicated that during solid waste landfilling and as the result of biodegradation and crushing, coarser particles break into smaller fragments and consequently the overall particle size is decreased. Similar arguments had been drawn for decomposing peat by Rezanezhad et al. (2010). The results obtained during this study suggest that landfilled solid wastes could experience structural changes with degradation and an overall increase in particle size. The magnitude of such changes would depend on the material initial state of degradation and treatment history. Well degraded MBTs residues could face smaller changes than those in raw MSW and low or intermediated degraded MBTs.

3. The nature of particle shape in solid waste

Chapter 1 discussed the need to study the structure of a porous material from the particle to the packed bed level. Particle size and particle shape were selected as the properties at the particle level for investigation during the research presented in this thesis. Chapter 2 focused in the study of particle size and examined the important role that particle size and particle shape play in the flow of fluids through porous media. The following chapter discusses a method to describe waste particle shape and applies this methodology to the samples of UK MBT, German MBT and MSW described in Chapter 2.

Some aspects of the results obtained during this research have previously been presented as a framework to describe solid waste using particle shape and applying it to the samples of UK MBT and German MBT prior to degradation (Velkushanova et al., 2009). This chapter extends this framework to samples of MBT and MSW waste after degradation. Research highlighting the relevance and importance of particle shape in influencing the flow of fluids through landfilled waste is also presented.

Providing a description of particle shape in waste is not a straight forward task. Heterogeneity of the particles in solid waste creates difficulties in describing particle shape using the conventional descriptors used for spherical particles in soils, i.e. sphericity, roundness and smoothness (Santamarina and Cho, 2004). Acknowledging this, Kölsch (1995) proposed an alternative system to describe particle shape in solid waste based on the particle's dimensionality as:

- Dimension 0 (0D) - grains
- Dimension 1 (1D) – fibres, sticks or strings
- Dimension 2 (2D) – foils and sheets , and
- Dimension 3 (3D) – boxes

Dixon and Langer (2006) used the dimensionality defined by Kölsch (1995) and developed a comprehensive characterisation framework for solid wastes. Particle shape is used to classify materials according to their mechanical behaviour into:

- Reinforcing- 1D and 2D particles, e.g. plastic bags, sheets of paper, etc
- Compressible- 3D particles, e.g. putrescibles, plastic packing, beverage cans, etc
- Incompressible – bulky 3D particles, e.g. bricks

Velkushanova et al. (2009) employed dimensionality definitions and particle classifications according to their potential to alter flow paths and fluid flow. A conceptual model proposed by Xie et al. (2006) and referred as to the thin sheet model was applied. Xie et al. (2006) model argues that horizontally or semi-horizontally aligned impermeable plastic fragments embedded in waste materials, may either impede fluid flow or allow pooling of water. The greater the number and size of the plastic fragments, the greater their influence on hydraulic conductivity. Accordingly, Velkushanova et al. (2009) defined four types of particles (represented in Figure 3-1):

- Matrix comprising grains which are 0D particles with each dimension less than a certain minimum significant length. Solid waste may be considered to be a general matrix of particles into which other particles are embedded that can change its flow properties. For raw MSW, Kölsch (1995) chose the minimum significant dimension such that particles smaller than 8 mm are considered as 0D.
- One-dimensional 1D: fibres, sticks or strings. One dimension is long relative to the typical particle dimension. These particles do not influence fluid flow and are neutral in terms of flow.
- Two-dimensional 2D: sheets or foils. These particles are flat, with two long dimensions and one short. They may act as elements that divert or impede fluid flow depending on the material from which they are formed. Impermeable materials such as plastics and metals will tend to divert flow across their area, whereas more

permeable materials such as textiles and perhaps paper and card may impede rather than divert the flow.

- Three-dimensional 3D: bulky materials. These particles are rotund, with all three dimensions greater than the minimum significant value. They may act to impede fluid flow, or they may enable preferential flow, depending on the material from which they are made, their size relative to the matrix, shape and their packing geometry (Bouwer and Rice, 1984). These two effects are contradictory, and probably compensatory. Therefore, it was argued that they can be considered to have a neutral effect on fluid flow.

The model proposed by Xie et al. (2006) was tested in clay modified with 1% by mass of horizontally placed PVC garbage bags of 4x4 and 8x8 cm size. They found the hydraulic conductivity halved with the intrusion of 4 cm pieces and reduced to one third with the addition of 8 cm pieces. Xie et al. (2006) also measured the hydraulic conductivity of MBT waste samples and sieved fractions and compared the experimental results with estimations using the Hazen (1911) equation (Equation 2-3 with $d = d_{10}$). The comparison showed that the experimental hydraulic conductivities were at least four orders of magnitude smaller than the estimations, suggesting that not only the fine fraction plays a role in the hydraulic conductivity but also the presence of plastic fragments. The coarser sieved fractions for example, rendered in some cases, lower hydraulic conductivities than those composed of finer material. This may be explained by the fact that thin plastic sheets are difficult to tear into small pieces, and that coarser fractions are likely to contain higher quantities of plastics that can prolong flow paths and decrease the hydraulic conductivity.

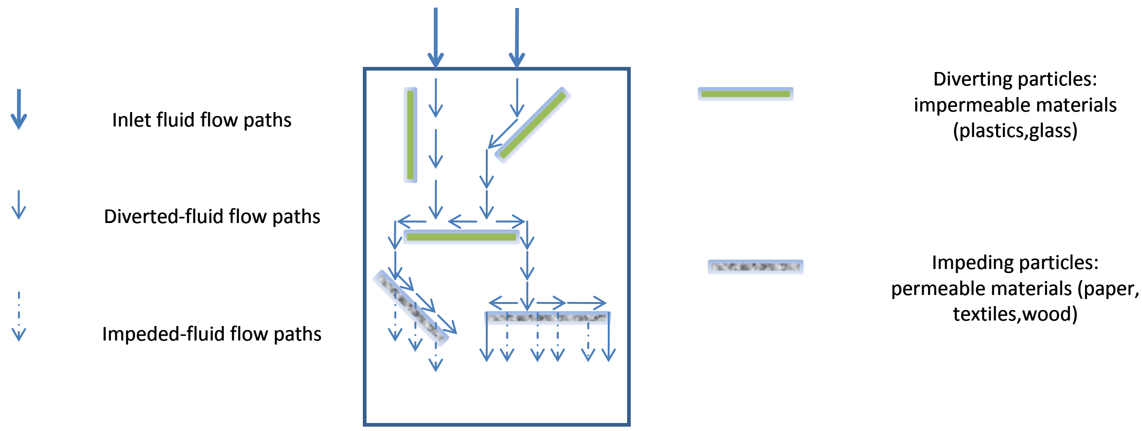

Figure 3-1 Conceptual model to explain flow through landfilled waste (Adapted from thin sheet model –Xie et al., 2006)

3.1. Methods

Material characterisation was performed in the specimens of UK MBT, German MBT and MSW before and after degradation which were described in Chapter 2. The characterisation was carried out through visual assessment of each of the sieved fractions and was therefore a highly time consuming task. The stack of 200 mm diameter sieves (BS 1377-2, 1990) used and described in Chapter 2 imposed a limitation in the maximum amount of material to be sieved in each one batch to 915g. An alternative sieving method was considered to speed up the separation process of larger quantities of materials and reduce the number of sieved fractions. A stack of sieves >20 mm, 20-12 mm, 12-7 mm, 7-5 mm and <5 mm with 450mm diameter able to sieve up to 35.5 kg was selected for this purpose.

Each size fraction was manually sorted into the following material categories: flexible plastics, stiff plastics, textiles, glass, ceramics, stones, metals, paper, wood, bones, rubber, and unidentified. Materials were classified as unidentified when it was not possible to visually decide its composition, either because of their size (i.e. the case for 0D < 5 mm particles) or because they were composed of agglomerates. Additional categories of yard waste, combustible and food were included for the MSW specimen. These categories are similar to those suggested by some authors , e.g. Dixon and Langer (2006) but differ from the groups described by others, e.g. Landva and Clark (1990), Grisolia (1995) and Kölsch (1995). They were partly selected because of the need for categories to be amenable to identification by visual inspection, although the smaller particle size inherent to MBT wastes makes this more difficult than for raw MSW. This is evident as over 50% of the material (by mass) was placed in the 'unidentified' categories for both the UK and the German MBT waste samples.

MSW AF was sieved through a 200 mm diameter stack of sieves (in the range 75-10 mm) since the amount of sample available was limited to 2 kg; whilst UK MBT AF was sieved only through a 5mm sieve. The information gathered in both cases was sufficient to examine the changes occurring in material composition with degradation.

It was considered relevant to assess the significance of the differences in material composition between the samples before and after degradation. For that, it was necessary to understand the magnitude of the experimental errors associated with material classification in solid wastes. Then, variations in material composition of greater magnitude could be explained as differences in nature between samples. Ideally, each specimen should be studied by duplicate and the variations between the two analyses calculated and reported as experimental errors. However, there were restrictions imposed by the time scale and by the quantity of the samples of waste available for this research which made not possible to run a duplicate material classification. Alternatively, literature sources were searched to identify studies that had quantified the magnitude of the experimental errors expected during material classification in waste materials. It was not possible to identify studies where a specimen had been analysed several times and results reported. However, the results of a comprehensive waste sampling programme across the US, reported in ASTM D 5231-92 9 (2008)-Table 3, give an indication of the magnitude of the variations in material composition expected when sampling, sorting and visually assessing solid wastes. Those variances however could also include seasonal differences, although this was not clearly stated in the standard. Nevertheless, the data reported in the ASTM standard was the most appropriate information available for the analysis of significance required. The information was used as an estimation of the experimental variations during the material characterisation of solid wastes and variations of greater magnitude than those reported in ASTM D 5231-92 9 (2008)-Table 3 indicate that they exceeded the magnitude of seasonal and experimental variations and could be therefore explained by differences in the nature between samples.

Table 3-1 summarises the standard deviations (SDs) reported in ASTM D 5231-92 9 (2008)-Table 3. The magnitude of the SDs corresponds to the error bars in Figures 3-2, 3-3 and 3-4. They were used for graphic comparisons of the material content in the specimens before and after degradation. The experimental material content measured in the specimen before and after degradation is represented as the mean values. Then, when the composition after degradation lies inside the error bar, the difference can be regarded as insignificant as it can be explained by the experimental errors. Whereas when it lies inside the error bar, the difference can be regarded as significant and can be explained by differences in the nature between the specimens.

Data gathered during material characterisation was used to classify the particle shape of the specimens investigated according to their dimensionality and their potential to affect flow following the criteria developed by Velkushanova et al. (2009). Criteria for the classification of particle shape are summarised in Tables 3-2, 3-3 and 3-5. In all cases, the dimensionality was assessed by visual inspection of each material fraction.

Table 3-1 Values of Standard Deviation(s) estimated from field data during solid waste sampling programme at several locations around the United States (Adapted from ASTM D 5231-92,2008-Table 3)

Materials	Standard deviation (%)	Category in ASTM D 5231-92, 2008 -Table 3
Flexible Plastic	3.0%	Plastic
Rigid Plastic	3.0%	Plastic
Textiles	6.0%	Other organics: textiles, diapers, rubber
Glass	5.0%	Glass
Ceramics	3.0%	Other inorganics
Stones	3.0%	Other inorganics
Metals	0.4%	Aluminum
Paper/Cardboard	6.5%	Average between newsprint (0.07) and corrugated (0.06)
Wood	6.0%	Wood
Bones	3.0%	Other inorganics
Rubber	6.0%	Other organics: textiles, diapers, rubber
Yard waste	14.0%	Yard waste
Combustible	6.0%	Other organics
Food	3.0%	Food waste
Unidentified	14.0%	Yard waste

Table 3-2 Breakdown by the dominant dimensions of the materials found in the UK MBT sample

	Sieve size (mm)									
	>20		20-12		12-7		7-5		<5	
Materials	*Dim.*	*Potential to block flow*	*Dim.*	*Potential to block flow*	*Dim.*	*Potential to block flow*	*Dim.*	*Potential to block flow*	*Dim.*	*Potential to block flow*
Flexible Plastic	2D	Diverting	2D	Diverting	2D	Diverting	2D	Diverting		
Rigid Plastic	3D	neutral	2D	Diverting	2D	Diverting	2D	Diverting		
Textiles	2D	Impeding	2D	Impeding	2D	Impeding	2D	Impeding		
Glass	2D	Diverting	2D	Diverting	2D	Diverting	2D	Diverting		
Ceramics	3D	neutral	3D	neutral	3D	neutral	3D	neutral		
Stones	3D	neutral	3D	neutral	3D	neutral	3D	neutral		
Metals	2D	Diverting	2D	Diverting	2D	Diverting	2D	Diverting		
Paper/Cardboard	2D	Impeding	2D	Impeding	2D	Impeding	2D	Impeding		
Wood			1D	neutral	1D	neutral	1D	neutral		
Bones			3D	neutral	3D	neutral	3D	neutral		
Rubber			3D	neutral	3D	neutral	3D	neutral		
Unidentified	3D	neutral	3D	neutral	3D	neutral	3D	neutral	OD	Matrix

Table 3-3 Breakdown by the dominant dimensions of the materials found in the German MBT sample

	Sieve size (mm)									
	>20		20-12		12-7		7-5		<5	
Materials	*Dim.*	*Potential to block flow*	*Dim.*	*Potential to block flow*	*Dim.*	*Potential to block flow*	*Dim.*	*Potential to block flow*	*Dim.*	*Potential to block flow*
Flexible Plastic	2D	Diverting	2D	Diverting	2D	Diverting	1D	neutral		
Rigid Plastic	3D	neutral	2D	Diverting	2D	Diverting	2D	Diverting		
Textiles	2D	Impeding	1D	neutral	1D	neutral	1D	neutral		
Glass	2D	Diverting	2D	Diverting	2D	Diverting	2D	Diverting		
Ceramics	3D	neutral	3D	neutral	3D	neutral	3D	neutral		
Stones	3D	neutral	3D	neutral	3D	neutral	3D	neutral		
Metals	2D	Diverting	2D	Diverting	2D	Diverting	2D	Diverting		
Paper/Cardboard	2D	Impeding	2D	Impeding	2D	Impeding	2D	Impeding		
Wood	3D	neutral	1D	neutral	1D	neutral	1D	neutral		
Bones	3D	neutral	3D	neutral	3D	neutral	3D	neutral		
Rubber	3D	neutral	3D	neutral	3D	neutral	3D	neutral		
Unidentified	3D	neutral	3D	neutral	3D	neutral	3D	neutral	OD	Matrix

3.2. Results

3.2.1. Material characterisation

Results from the material characterisation are summarised in Table 3-4 and Figure 3-2 for UK MBT, Table 3-6 and Figure 3-3 for MSW, and Table 3-7 and Figure 3-4 for German MBT. The results were also corrected to account for the mass losses during the degradation process as reported by Ivanova (2007) and Siddiqui (2011) for the MSW and MBT specimens respectively. A material category labelled as fraction lost represents the change in mass with degradation, and the sum of the remaining components (e.g. 0.03 to 75 mm) the mass staying after the degradation. This calculation gives a further indication of the material composition of the specimen after degradation just before the degraded fraction is released.

Table 3-4 Composition of UK MBT waste specimen by material type. For comparative purposes results obtained before and after degradation are presented. The column After with Lost considers a mass loss of 6.45% reported by Siddiqui (2011)

Materials	Sieve size							
	> 20 mm	20-12 mm	12-7 mm	7-5 mm	<5 mm	Total		
	B4	B4	B4	B4	B4	B4	After no lost	After with lost
Flexible Plastic	0.14%	2.87%	1.18%	0.38%	0.00%	4.57%	9.00%	8.42%
Rigid Plastic	0.16%	2.69%	2.67%	0.75%	0.00%	6.27%	11.00%	10.29%
Textiles	0.07%	0.89%	0.22%	0.15%	0.00%	1.33%	1.40%	1.31%
Glass	0.01%	7.70%	12.03%	3.02%	0.00%	22.77%	23.50%	21.98%
Ceramics	0.00%	1.07%	1.23%	0.00%	0.00%	2.29%	2.40%	2.25%
Stones	0.00%	0.81%	0.78%	0.15%	0.00%	1.73%	0.50%	0.47%
Metals	0.00%	0.19%	0.23%	0.07%	0.00%	0.49%	0.04%	0.04%
Paper/Cardboard	0.01%	0.16%	0.22%	0.04%	0.00%	0.43%	0.39%	0.36%
Wood	0.00%	0.49%	0.74%	0.34%	0.00%	1.57%	1.50%	1.40%
Bones	0.00%	0.12%	0.12%	0.00%	0.00%	0.25%	0.02%	0.02%
Rubber	0.00%	0.10%	0.08%	0.01%	0.00%	0.18%	0.09%	0.08%
Unidentified	0.39%	8.01%	8.80%	11.74%	29.15%	58.10%	50.16%	46.92%
Fraction lost	-	-	-	-	-	-	-	6.45%
Total	0.80%	25.10%	28.30%	16.66%	29.15%	100.00%	100.00%	100.00%

Unidentified material after degradation corresponds to 35.15% < 5mm and 15.01% > 5mm

Table 3-5 Breakdown by the dominant dimensions of the materials found in the MSW sample

	Sieve size (mm)											
	>75		75-63		63-37.5		37.5-20		20-10		<10	
Materials	*Dim.*	*Potential to block flow*	*Dim.*	*Potential to block flow*	*Dim.*	*Potential to block flow*	*Dim.*	*Potential to block flow*	*Dim.*	*Potential to block flow*	*Dim.*	*Potenti al to block flow*
Flexible Plastic	2D	Diverting	2D	Diverting	2D	Diverting	2D	Diverting	2D	Diverting		
Rigid Plastic	3D	neutral	2D	Diverting	2D	Diverting	2D	Diverting	2D	Diverting		
Textiles	2D	Diverting	1D	neutral	1D	neutral	1D	neutral	1D	neutral		
Glass	2D	Diverting	2D	Diverting	2D	Diverting	2D	Diverting	2D	Diverting		
Metals	2D	Diverting	2D	Diverting	2D	Diverting	2D	Diverting	2D	Diverting		
Paper/Cardboard	2D	Impeding	2D	Impeding	2D	Impeding	2D	Impeding	2D	Impeding		
Wood	3D	neutral	1D	neutral	1D	neutral	1D	neutral	1D	neutral		
Yard waste	3D	neutral	3D	neutral	3D	neutral	3D	neutral	3D	neutral		
Combustible	3D	neutral	3D	neutral	3D	neutral	3D	neutral	3D	neutral		
Food	3D	neutral	3D	neutral	3D	neutral	3D	neutral	3D	neutral		
Unidentified	3D	neutral	3D	neutral	3D	neutral	3D	neutral	3D	neutral	OD	Matrix

Table 3-6 Composition of MSW waste specimen by material type. For comparative purposes results obtained before and after degradation are presented. The column After with Lost considers a mass loss of 24.52% reported by (Ivanova)(2007)

Materials	B4	After no lost	After with lost
Paper	27.34%	21.46%	16.20%
Yard waste	18.40%	3.38%	2.55%
Unidentified	13.32%	28.82%	21.75%
Flexible Plastics	10.16%	13.44%	10.15%
Rigid Plastics	9.87%	14.91%	11.25%
Metals	6.78%	0.15%	0.12%
Wood	3.19%	3.81%	2.87%
Textiles	3.08%	6.62%	5.00%
Combustible	2.96%	0.83%	0.63%
Glass	2.63%	6.42%	4.84%
Food	2.27%	0.16%	0.12%
Fraction Lost	0.00%	0.00%	24.52%
TOTAL	100.00%	100.00%	100.00%

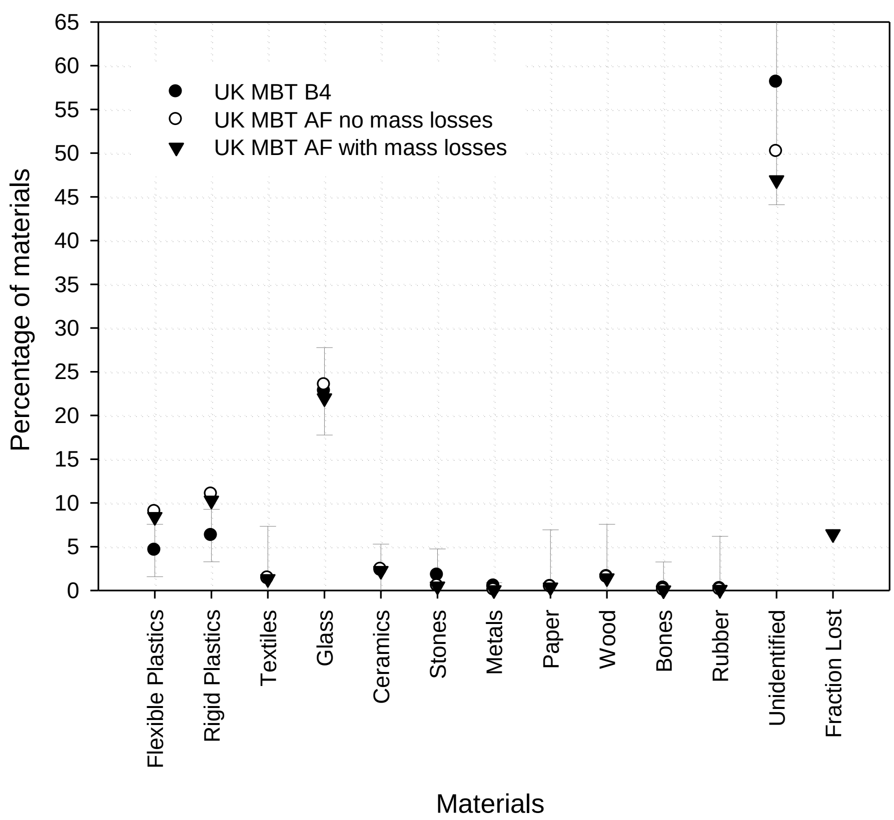

Figure 3-2 Composition of UK MBT waste sample by material type

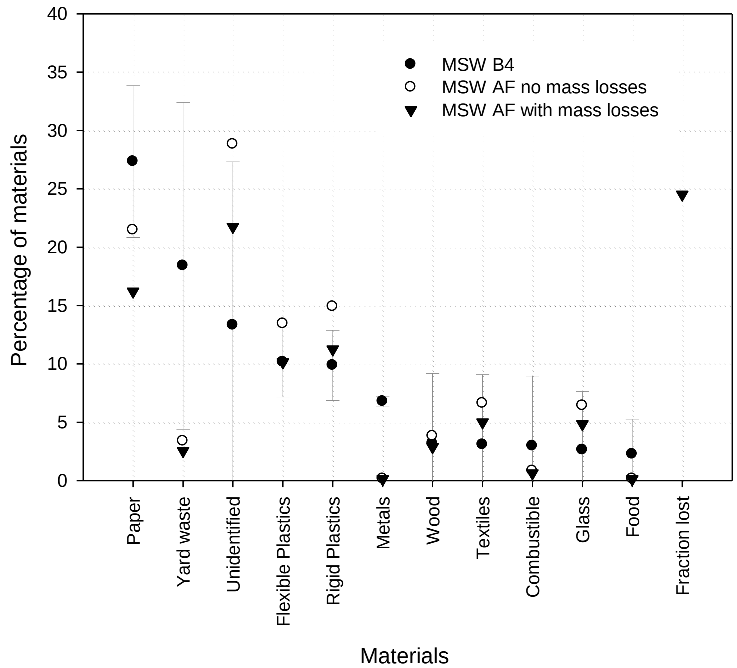

Figure 3-3 Composition of MSW waste sample by material type

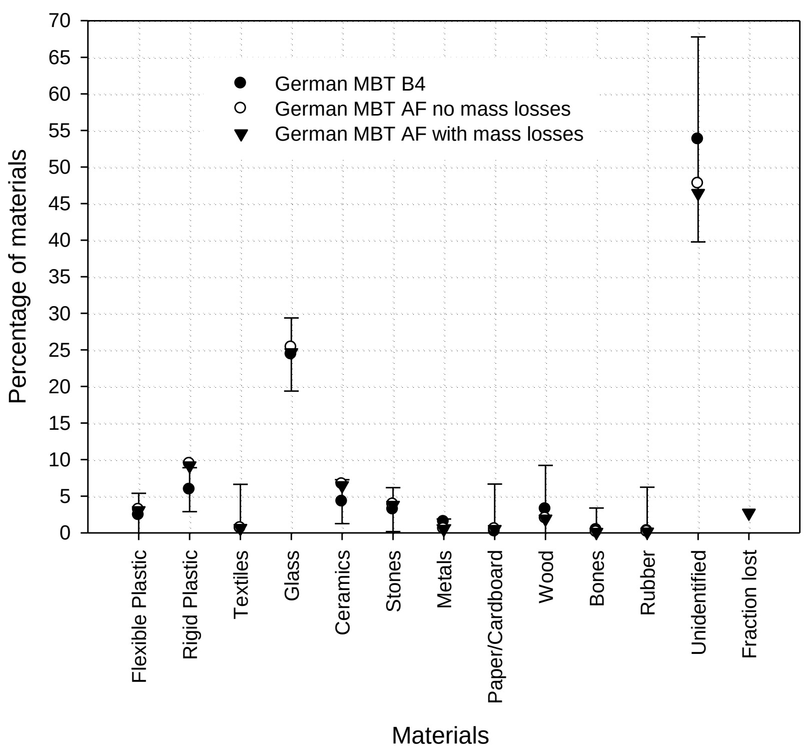

Figure 3-4 Composition of German MBT waste sample by material type

A graphical comparison of the materials composition between specimens before degradation is presented in Figure 3-7.

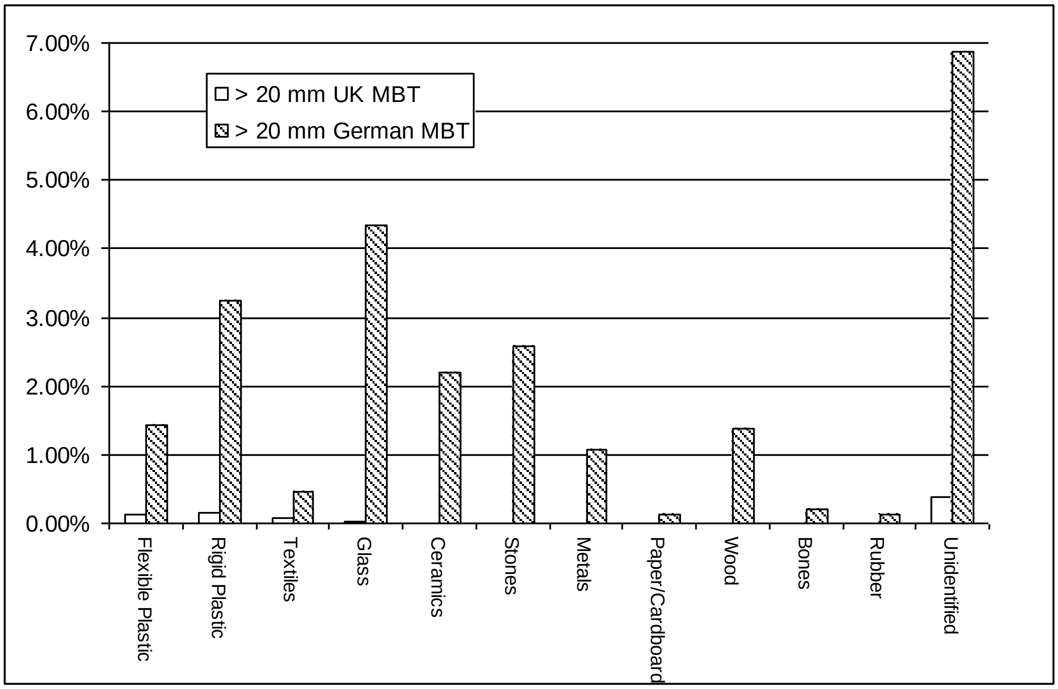

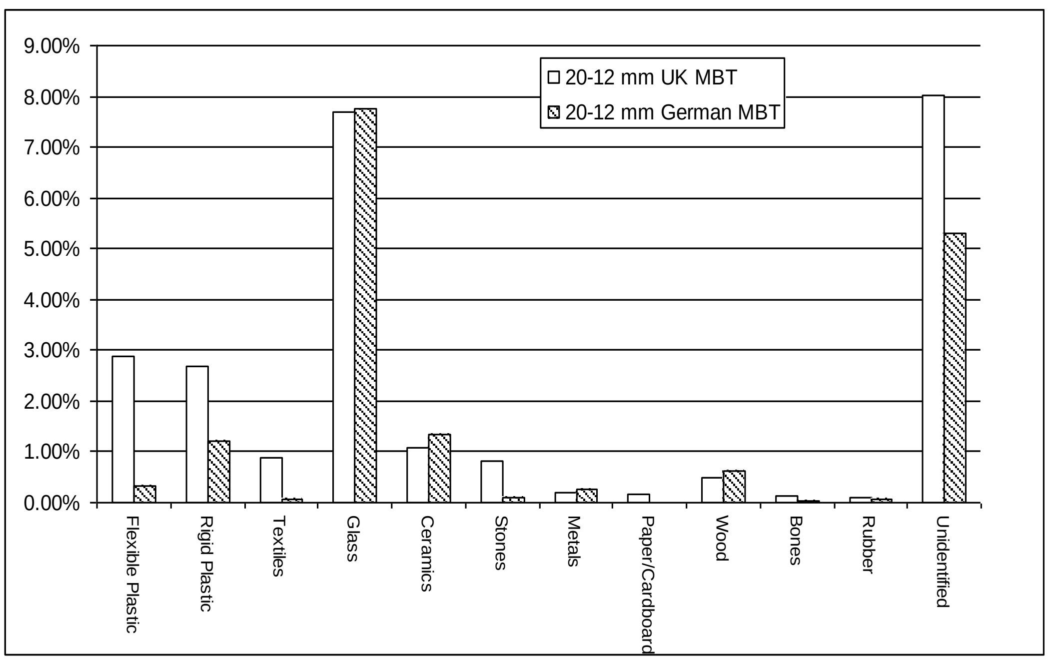

Figure 3-5 Comparison of materials composition in UK MBT and German MBT in the >20 mm and 20-12 mm fractions

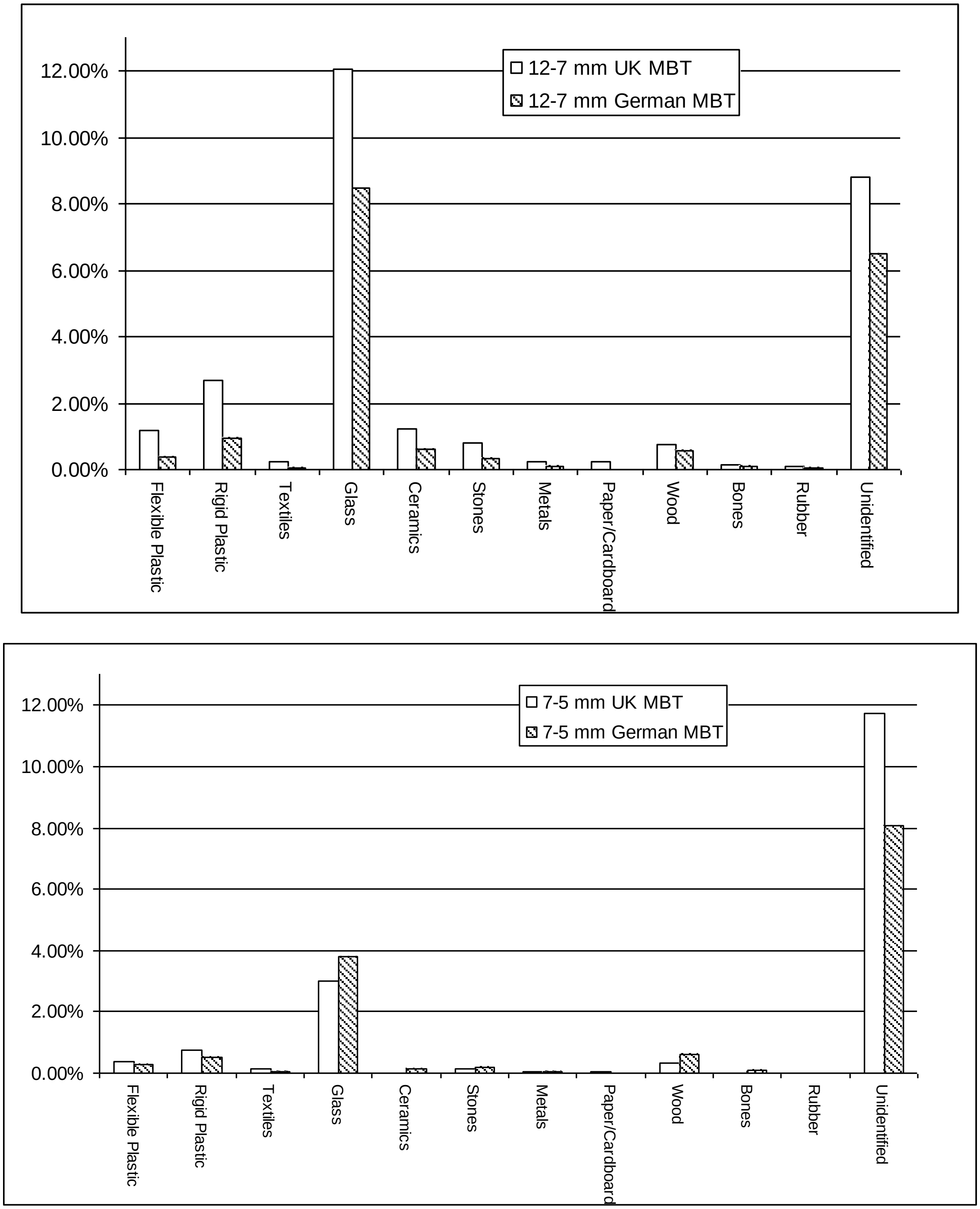

Figure 3-6 Comparison of materials composition in UK MBT and German MBT in the 12-7 mm and 7-5 mm fractions

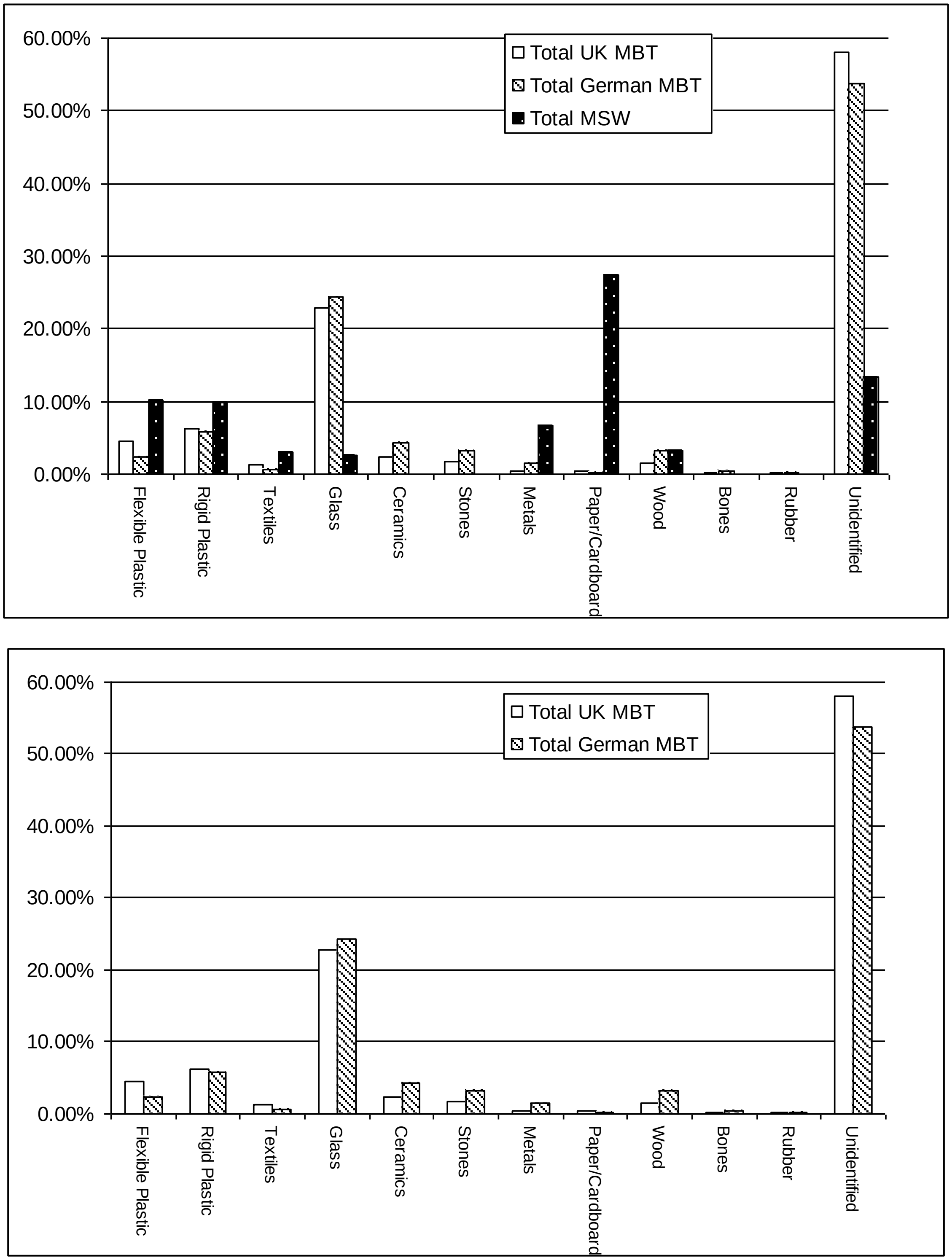

Figure 3-7 Comparison of the total materials composition in UK MBT, German MBT and MSW

Table 3-7 Composition of German MBT waste sample by material type. For comparative purposes results obtained before and after degradation are presented. The column After with Lost considers a mass loss of 2.73% reported by Siddiqui (2011)

	>20 mm			20-12 mm			12-7 mm			7-5 mm			<5mm			Total		
Materials	**B4**	**After-no lost**	**After with lost**	**B4**	**After no lost**	**After with lost**	**B4**	**After no lost**	**After with lost**	**B4**	**After no lost**	**After with lost**	**B4**	**After no lost**	**After with lost**	**B4**	**After no lost**	**After with lost**
Flexible Plastic	1.42%	1.68%	1.63%	0.32%	0.50%	0.49%	0.37%	0.73%	0.71%	0.29%	0.24%	0.23%	0.00%	0.00%	0.00%	2.41%	3.14%	3.06%
Rigid Plastic	3.26%	4.42%	4.30%	1.20%	1.20%	1.17%	0.94%	3.02%	2.94%	0.51%	0.78%	0.76%	0.00%	0.00%	0.00%	5.90%	9.43%	9.17%
Textiles	0.47%	0.37%	0.36%	0.05%	0.14%	0.14%	0.07%	0.10%	0.10%	0.03%	0.03%	0.02%	0.00%	0.00%	0.00%	0.62%	0.64%	0.62%
Glass	4.33%	4.91%	4.78%	7.76%	3.18%	3.09%	8.49%	11.84%	11.52%	3.78%	5.40%	5.26%	0.00%	0.00%	0.00%	24.36%	25.33%	24.64%
Ceramics	2.19%	4.36%	4.24%	1.34%	1.15%	1.12%	0.60%	1.06%	1.03%	0.12%	0.08%	0.08%	0.00%	0.00%	0.00%	4.26%	6.65%	6.47%
Stones	2.58%	1.54%	1.50%	0.08%	0.17%	0.17%	0.31%	1.83%	1.78%	0.20%	0.35%	0.34%	0.00%	0.00%	0.00%	3.17%	3.89%	3.79%
Metals	1.07%	0.30%	0.29%	0.25%	0.14%	0.13%	0.11%	0.03%	0.03%	0.06%	0.05%	0.05%	0.00%	0.00%	0.00%	1.48%	0.52%	0.50%
Paper/Cardboard	0.13%	0.10%	0.10%	0.01%	0.10%	0.10%	0.02%	0.20%	0.19%	0.02%	0.09%	0.09%	0.00%	0.00%	0.00%	0.17%	0.49%	0.48%
Wood	1.38%	0.67%	0.65%	0.64%	0.26%	0.25%	0.57%	0.73%	0.71%	0.63%	0.30%	0.29%	0.00%	0.00%	0.00%	3.22%	1.96%	1.91%
Bones	0.19%	0.00%	0.00%	0.02%	0.08%	0.08%	0.09%	0.00%	0.00%	0.07%	0.01%	0.01%	0.00%	0.00%	0.00%	0.38%	0.09%	0.09%
Rubber	0.12%	0.00%	0.00%	0.08%	0.04%	0.04%	0.03%	0.08%	0.07%	0.02%	0.01%	0.01%	0.00%	0.00%	0.00%	0.24%	0.13%	0.13%
Unidentified	6.87%	3.58%	3.49%	5.30%	2.51%	2.44%	6.52%	4.50%	4.38%	8.06%	3.15%	3.07%	27.02%	33.97%	33.05%	53.77%	47.72%	46.42%
Fraction Lost	-	-	-	-	-	-	-	-	-	-	-	-	-	-	-	-	-	2.72%
TOTAL	24.00%	21.94%	21.34%	17.06%	9.48%	9.22%	18.12%	24.12%	23.46%	13.79%	10.49%	10.21%	27.02%	33.97%	33.05%	100.00%	100.00%	100.00%

3.2.2. Particle shape

Using the materials classification in Tables 3-2 to 3-4, the specimens of waste were described in terms of the dimensionality of the particles and their potential to alter flow behaviour. Results for UK MBT are presented in

Table 3-8 and Table 3-9, Table 3-10 and Table 3-11 correspond to German MBT whilst Table 3-12 and Table 3-13 to MSW.

Table 3-8 Classification of materials according to their dimensionality and potential to alter flow in UK MBT-B4

			Size (mm)						
Flow Behaviour	**Materials**	**Dim**	**>20**	**20-12**	**12-7**	**7-5**	**<5**	**Total**	
Diverting	Flexible Plastic	2D	0.14%	2.87%	1.18%	0.38%		4.57%	33.94%
	Glass	2D	0.01%	7.70%	12.03%	3.02%		22.77%	
	Metals	2D	0.00%	0.19%	0.23%	0.07%		0.49%	
	Rigid Plastic	2D		2.69%	2.67%	0.75%		6.11%	
Impeding	Paper	2D	0.01%	0.16%	0.22%	0.04%		0.43%	1.76%
	Textiles	2D	0.07%	0.89%	0.22%	0.15%		1.33%	
Neutral	Bones	3D		0.12%	0.12%	0.00%		0.25%	35.14%
	Ceramics	3D	0.00%	1.07%	1.23%	0.00%		2.29%	
	Rigid Plastic	3D	0.16%					0.16%	
	Rubber	3D		0.10%	0.08%	0.01%		0.18%	
	Stones	3D	0.00%	0.81%	0.78%	0.15%		1.73%	
	Unidentified	3D	0.39%	8.01%	8.80%	11.74%		28.95%	
	Wood	1D		0.49%	0.74%	0.34%		1.57%	
Matrix	Unidentified	OD					29.15%	29.15%	29.15%
Total			0.80%	25.10%	28.30%	16.66%	29.15%	100.00%	100.00%

Table 3-9 Classification of materials according to their dimensionality and potential to alter flow in UK MBT AF

			Size (mm)			
Flow Behaviour	**Materials**	**Dim**	**5-20 mm**	**<5 mm**	**Total**	
Diverting	Flexible Plastic	2D	9.00%		9.00%	43.54%
	Glass	2D	23.50%		23.50%	
	Metals	2D	0.04%		0.04%	
	Rigid Plastic	2D	11.00%		11.00%	
Impeding	Paper	2D	0.39%		0.39%	1.79%
	Textiles	2D	1.40%		1.40%	
Neutral	Bones	3D	0.02%		0.02%	19.52%
	Ceramics	3D	2.40%		2.40%	
	Rubber	3D	0.09%		0.09%	
	Stones	3D	0.50%		0.50%	
	Unidentified	3D	15.01%		15.01%	
	Wood	1D	1.50%		1.50%	
Matrix	Unidentified	0D		35.15%	35.15%	35.15%
Total			64.85%	35.15%	100.00%	100.00%

Table 3-10 Classification of materials according to their dimensionality and potential to alter flow in German MBT B4

			Size (mm)						
Flow Behaviour	**Materials**	**Dim**	**>20**	**20-12**	**12-7**	**7-5**	**<5**	**Total**	
Diverting	Flexible Plastic	2D	1.42%	0.32%	0.37%			2.12%	30.62%
	Glass	2D	4.33%	7.76%	8.49%	3.78%		24.36%	
	Metals	2D	1.07%	0.25%	0.11%	0.06%		1.48%	
	Rigid Plastic	2D		1.20%	0.94%	0.51%		2.65%	
Impeding	Paper	2D	0.13%	0.01%	0.02%	0.02%		0.17%	0.64%
	Textiles	2D	0.47%					0.47%	
Neutral	Bones	3D	0.19%	0.02%	0.09%	0.07%		0.38%	41.72%
	Ceramics	3D	2.19%	1.34%	0.60%	0.12%		4.26%	
	Flexible Plastic	1D				0.29%		0.29%	
	Rigid Plastic	3D	3.26%					3.26%	
	Rubber	3D	0.12%	0.08%	0.03%	0.02%		0.24%	
	Stones	3D	2.58%	0.08%	0.31%	0.20%		3.17%	
	Textiles	1D		0.05%	0.07%	0.03%		0.15%	
	Unidentified	3D	6.87%	5.30%	6.52%	8.06%		26.75%	
	Wood	1D		0.64%	0.57%	0.63%		1.84%	
		3D	1.38%					1.38%	
Matrix	Unidentified	OD					27.02%	27.02%	27.02%
Total			24.00%	17.06%	18.12%	13.79%	27.02%	100.00%	100.00%

Table 3-11 Classification of materials according to their dimensionality and potential to alter flow in German MBT AF

Flow Behaviour	Materials	Dim	Size (mm) >20	20-12	12-7	7-5	<5	Total	
Diverting	Flexible Plastic	2D	1.68%	0.50%	0.73%			2.91%	33.77%
	Glass	2D	4.91%	3.18%	11.84%	5.40%		25.33%	
	Metals	2D	0.30%	0.14%	0.03%	0.05%		0.52%	
	Rigid Plastic	2D		1.20%	3.02%	0.78%		5.01%	
Impeding	Paper	2D	0.10%	0.10%	0.20%	0.09%		0.49%	0.86%
	Textiles	2D	0.37%					0.37%	
Neutral	Bones	3D	0.00%	0.08%	0.00%	0.01%		0.09%	31.40%
	Ceramics	3D	4.36%	1.15%	1.06%	0.08%		6.65%	
	Flexible Plastic	1D				0.24%		0.24%	
	Rigid Plastic	3D	4.42%					4.42%	
	Rubber	3D	0.00%	0.04%	0.08%	0.01%		0.13%	
	Stones	3D	1.54%	0.17%	1.83%	0.35%		3.89%	
	Textiles	1D		0.14%	0.10%	0.03%		0.27%	
	Unidentified	3D	3.58%	2.51%	4.50%	3.15%		13.74%	
	Wood	1D		0.26%	0.73%	0.30%		1.29%	
		3D	0.67%					0.67%	
Matrix	Unidentified	OD					33.97%	33.97%	33.97%
Total			21.94%	9.48%	24.12%	10.49%	33.97%	100.00%	100.00%

Table 3-12 Classification of materials according to their dimensionality and potential to alter flow in MSW B4

Flow Behaviour	Materials	Dim	Size (mm) 37.5-10	<10	Total	
Diverting	Flexible Plastics	2D	10.16%		10.16%	19.57%
	Glass	2D	2.63%		2.63%	
	Metals	2D	6.78%		6.78%	
Impeding	Paper	2D	27.34%		27.34%	30.42%
	Textiles	2D	3.08%		3.08%	
Neutral	Combustible	3D	2.96%		2.96%	36.69%
	Food	3D	2.27%		2.27%	
	Rigid Plastics	3D	9.87%		9.87%	
	Wood	3D	3.19%		3.19%	
	Yard waste	3D	18.40%		18.40%	
Matrix	Unidentified	0D		13.32%	13.32%	13.32%
Total			86.68%	13.32%	100.00%	100.00%

Table 3-13 Classification of materials according to their dimensionality and potential to alter flow in MSW AF

			Size (mm)							
Flow	**Materials**	**Dim**	**>75**	**75-63**	**63-37.5**	**37.5-20**	**20-10**	**<10**	**Total**	
Diverting	Flexible Plastics	2D	0.88%	0.93%	6.36%	4.47%	0.80%		13.44%	34.82%
	Glass	2D	0.00%	0.00%	0.00%	1.21%	5.21%		6.42%	
	Metals	2D	0.00%	0.00%	0.15%	0.00%	0.00%		0.15%	
	Rigid Plastics	2D		2.15%	8.65%	3.49%	0.53%		14.81%	
Impeding	Paper	2D	0.00%	0.80%	8.23%	8.49%	3.94%		21.46%	21.50%
	Textiles	2D	0.03%						0.03%	
Neutral	Combustible	3D	0.00%	0.00%	0.15%	0.65%	0.03%		0.83%	14.86%
	Food	3D	0.00%	0.00%	0.00%	0.00%	0.16%		0.16%	
	Rigid Plastics	3D	0.10%						0.10%	
	Textiles	1D		0.00%	2.87%	3.34%	0.38%		6.59%	
	Unidentified	3D	0.00%	0.00%	0.00%	0.00%	0.00%		0.00%	
		1D		0.00%	1.82%	1.27%	0.73%		3.81%	
	Wood	3D	0.00%						0.00%	
	Yard waste	3D	2.19%	0.00%	0.30%	0.34%	0.56%		3.38%	
Matrix	Unidentified	0D						28.82%	28.82%	28.82%
Total			3.20%	3.88%	28.52%	23.26%	12.33%	0.00%	100.00%	100.00%

A graphical comparison of the six specimens is presented in a ternary plot in Figure 3-8.

3.3. Discussion

A comparison between UK MBT and German MBT before degradation shows that their composition is similar, with a slightly higher content of plastics in UK MBT than in German MBT (10.84% vs 8.31%) and unidentified material (58.10% vs 53.77%). However, the size of the materials differs with the coarser components found in German MBT (e.g. 24% for particles >20mm vs only 0.80% in UK MBT). MSW has a higher plastics and paper content (i.e. 20.03% and 27.34% respectively) than both MBT waste (less than 1% paper).

Changes in material composition due to degradation were assessed and only those materials with a final content outside the error bars were regarded as significant. In MSW, flexible and rigid plastics increased from 10.16% to 13.44% and 9.87% to 14.91% respectively. Similarly, in UK MBT the content of flexible and rigid plastics increased from 4.57% to 9.00% and 6.27% to 11.00% respectively. In German MBT, the composition did not change significantly with degradation (see Figure 3-4). This was expected given the negligible changes in PSD and in mass (i.e. mass losses of only 2.73%).

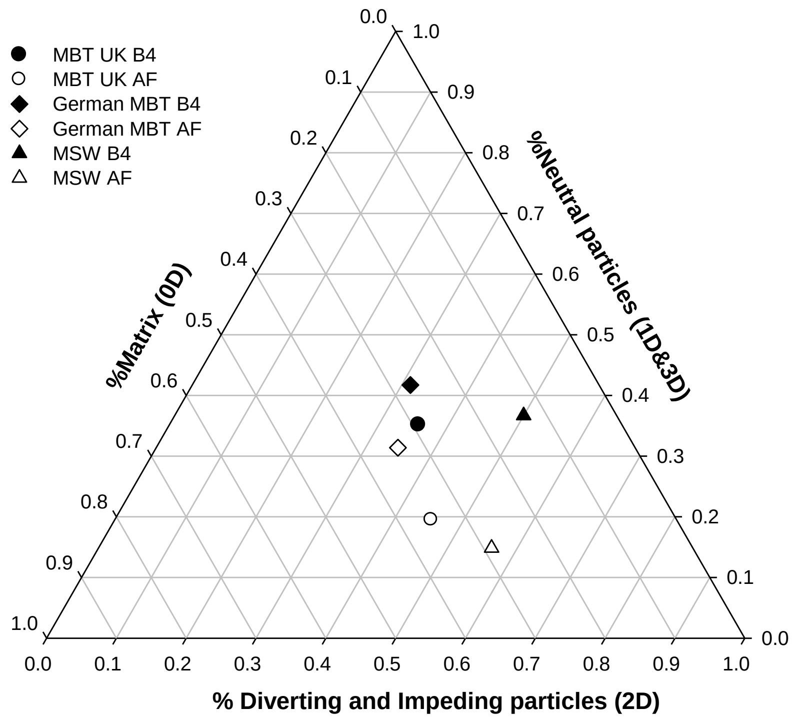

	Diverting & Impeding	Neutral	Matrix
MBT UK B4	35.71%	35.14%	29.15%
MBT UK AF	45.33%	19.52%	35.15%
German MBT B4	31.26%	41.72%	27.02%
German MBT AF	34.63%	31.40%	33.97%
MSW B4	49.99%	36.69%	13.32%
MSW AF	56.32%	14.86%	28.82%

Figure 3-8 Comparative Ternary Plot of waste samples classified according to their particle dimensionality and potential to alter flow behaviour

In UK MBT and MSW, the two specimens of waste with higher mass losses and changes in particle size, the relative content of diverting particles (i.e. 2D flexible & rigid plastics, glass and metals) increased with degradation from 33.94% to 43.54% and from 19.57% to 34.82% respectively. The content of unidentified 0D components increased from 29.15% to 35.15% and from 13.32% to 28.82% respectively. These changes were balanced with the decrease in neutral 3D materials whose unidentified fraction may comprise easily degradable constituents.

Figure 3-8 summarises the information in a ternary plot. The graph was constituted such that 0D, 2D and 1D/3D particles are represented in each of the three axes. This type of graph was suggested by Dixon and Langer (2006) to evaluate the changes in mechanical behaviour of waste resulting from emplacement and long term degradation. Here, it was extended to evaluate the potential alterations in flow behaviour arising from changes in particle size and shape with degradation. All the samples studied showed an increase in the content of 2D-diverting and impeding particles after degradation , which was more pronounced in the UK MBT and MSW specimens than in the German MBT. Before degradation the content of 2D particles ranged from 30% in German MBT to 50% in MSW; after degradation this had increased to 34% in German MBT and 56% in MSW. This suggests that 2D particles constitute at least 30% by dry mass in solid wastes, even in pre-treated wastes where recyclables are previously removed. After degradation, the proportion of 2D particles is even higher. As a result of the conversion to gas and liquid phases of readily and moderately degradable materials (i.e. food, yard waste, and unidentified fraction in MBT wastes) the dry mass of waste is reduced as well as the percentage of neutral 3D materials. The inert (i.e.plastics & glass) and slowly degradable materials (paper, textile and wood) remain virtually intact and form a higher percentage in the resulting waste. In Chapter 2, the particle size was found to increase with degradation. 2D particles are preferentially located in the coarsest waste fractions (e.g. plastics and glass are not easily cut during the mechanical pre-treatment processes). An increase in their content is therefore consistent with the increase in particle size.

The characterisation of waste based on particle shape and flow behaviour has advantages as it offers the possibility of simplifying the description of heterogeneous solid waste into only three groups of materials. However, some limitations are acknowledged. For example, the ternary graph does not consider the changes that arise from waste compaction, which is recognised as the single most important factor that controls fluid flow (Beaven, 2000). Therefore, the method allows a qualitative assessment of the nature of changes to waste structure arising only from degradation that could be linked to changes in fluid flow.

The high content of 2D particles in solid waste suggests that they should play a significant role in fluid flow processes through landfilled wastes and that the thin-sheet conceptual model proposed by Xie et al. (2006) is a relevant framework for the study of flow phenomena. According to the thin-sheet model, 2D particles may impede flow or allow pooling of water. At least two effects on fluid flow properties are expected:

- Reduction in the saturated hydraulic conductivity, and
- the creation of more tortuous flow paths and enhancement of preferential flow phenomena

A study of the changes in the saturated hydraulic conductivity produced by 2D particles is the focus of Chapter 4, whilst the development of preferential flow phenomena is studied in Chapter 5. In Chapter 4 the hydraulic conductivity of laboratory controlled specimens produced at different levels of 2D particles was measured. These two chapters add information to develop further the classification system by understanding the role that 2D particles play during fluids flow through landfilled waste.

4. The role of 2D particles on permeability

In Chapter 3, a classification framework based on particle shape was applied to samples of MBT and MSW. The system is based on the assumption that due to their shape some materials in waste, e.g. plastic sheets, have the potential to alter fluid flow properties (Velkushanova et al., 2009). According to that framework, materials are grouped according to their dimensionality as 0D, 1D, 2D and 3D following Kölsch (1995). Components under 5 mm size are considered as 0D. They are sufficiently small and possibly composed by organic particles, to be considered as matrix components. Materials larger than 5mm, i.e. 5 times larger than the matrix, are classified as either 1D, 2D or 3D. In particular, 2D particles are considered to be flow diverting or impeding depending on whether they are made of impermeable or semipermeable materials, i.e. plastics or textiles, respectively. The criteria for classifying materials according to their flow altering properties requires further investigation. That is the main aim of this chapter.

Research in granular soils has shown the considerable effect that particle shape has on the permeability, void ratio and porosity characteristics. Researchers however differ on whether particle irregularity increases or decreases the porosity of the medium. Whilst some studies suggest that round particles can mobilize more easily against each other and form denser structures (Cho et al., 2006, Cubrinovski and Ishihara, 2002), others argue that angular particles have increased void filling capacities and form highly packed media (Goktepe and Sezer, 2010).

The geometrical characteristics required to build arrangements at diverse void ratios have been investigated intensively in the powder industry. Research by Deresiewicz (1958) showed that in a system consisting of uniform spheres, the minimal density and maximal porosity are obtained in cubic packing. In this mode of packing, each grain touches six neighbours and the porosity is 47.6%, regardless of the diameter of the spheres. The densest packing is obtained with either tetrahedral or octahedral arrangements where each grain touches 12 neighbours and the porosity is 25.9%. Figure 4-1 illustrates the different packing models.

The area of packing of non-spherical particles has been predominantly empirical and limited to a number of studies (Lee et al., 2007, Santamarina and Cho, 2004, White and Walton, 1937). Lee et al. (2007) investigated the effect that flat surfaces have on packing spherical particles and proposed a conceptual model illustrated in Figure 4-2 based on a mixed effect between ordering and bridging. Flat particles enforce ordering of the spheres that fall on their surface which results in denser arrangements. At the same time they form bridges over the spheres leaving a high local porosity underneath. The two mechanisms combine to control the packing density. White & Walton (1937) showed that the introduction of properly arranged cylindrical particles into assemblages of spherical particles reduces the void ratio below that possible with the consecutive introduction of smaller spheres.

Studies in soils and powders provide some understanding of the role of particle shape on permeability, however the direct applicability to solid wastes is limited by the differences in the form of the particles. For example, although platy particles can be found in soils, e.g. clay and mica, they are not several times bigger than the surrounding matrix and cannot be considered as 2D. Research specifically addressing the conditions in solid waste is required.

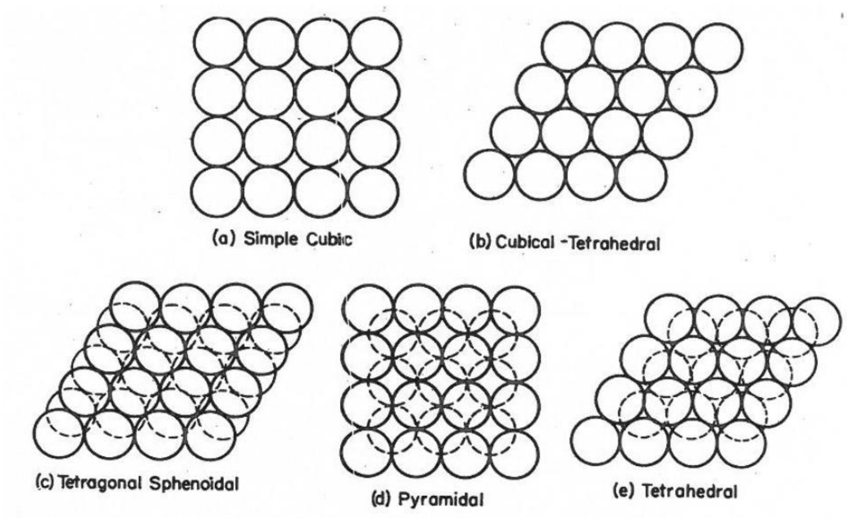

Type of packing	Coordination number	Density		Porosity (%)
Simple cubic	6	π/6	0.5236	47.64
Cubic tetrahedral	8	π/3√3	0.6046	39.54
Tetragonal sphenoidal	10	2π/9	0.6981	30.19
Pyramidal	12	π/3√2	0.7405	25.95
Tetrahedral	12	π/3√2	0.7405	25.95

Figure 4-1 Models of packing of uniform spheres a) simple cubic, b) cubical tetrahedral, c) tetragonal sphenoidal, d) pyramidal, and e) tetrahedral geometry (adapted from Deresiewicz, 1958)

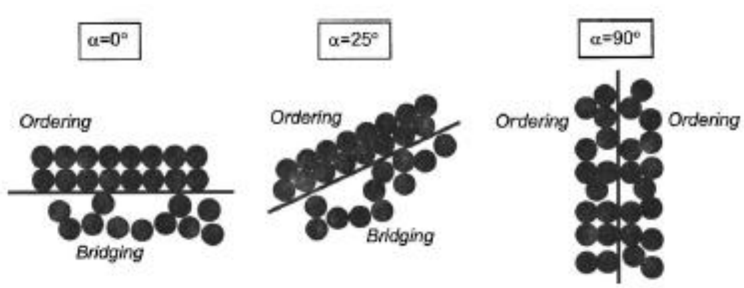

Figure 4-2 Impact of flat surfaces in packing of uniform spheres (adapted from Santamarina and Cho (2004))

A second body of work classified particles of reinforced soils and solid waste according to their mechanical properties (Dixon and Langer, 2006, Michalowski and Zhao, 1996). Dixon and Langer (2006) suggested that 2D particles could be classified as reinforcing, i.e. particles that provide global strength enhancement by their tensile strength (Kölsch, 1995), when they exceed the nominal diameter of the particles around it. Michalowski and Zhao (1996) considered that reinforcing particles should be at least 5 times longer than the typical particle size in the surrounding matrix. The particle size of the matrix, i.e. materials< 5mm, in UK MBT and German MBT was analysed. Results showed that the D_{50} was in the order of 1mm (Figure 10 in Velkushanova et al. (2009)). Considering a representative matrix diameter as 1 mm, materials above 5 mm (e.g. 5-7 mm) would be at least five times longer than the typical particle in the surrounding matrix.

Velkushanova et al. (2009) extended Dixon and Langer (2006) classification of 2D particles as reinforcing components by adding their potential to affect fluid flow. The assumption was that 2D particles can be considered as potentially flow diverting or impeding if they are at least 5 times longer than the typical size of the surrounding matrix. This hypothesis implies that not only the stress level, as reported by Beaven (2000), has an influence on the hydraulic conductivity of solid wastes, but also the characteristics at the particle level (i.e. particle size and shape) of the landfilled residue. In consequence, the estimation of the hydraulic properties in a refuse would require the consideration of the refuse composition, grading and particle shape description. The hypothesis has two components. Firstly, that 2D particles can divert fluid flow, based on the thin sheet conceptual model proposed by Xie et al. (2006) (see Figure 3-1). Secondly, that 2D particles need to be larger than the surrounding matrix for the length of the fluids flow paths to be affected. In absence of studies that indicate the size of the 2D particles required to affect flow paths, the size criteria for classifying reinforcing elements was adopted.

Xie et al. (2006) argued that horizontally or semi-horizontally aligned impermeable plastic fragments embedded in waste materials have the potential to impede fluid flow and change the hydraulic conductivity; and that the greater the number and size of the plastic fragments, the greater their influence on the hydraulic conductivity. They tested the hydraulic conductivity of clay modified with 1% by mass of 4x4 and 8x8 cm size PVC pieces from garbage bags and found that the hydraulic conductivity was halved and reduced to one third by the addition of 4 and 8 cm pieces respectively.

The impact of particles inclusion on conduction phenomena has been subject of investigation in areas such as electric and thermal conduction. Like fluid conduction in porous media, electric and thermal conduction are processes governed by a linear relationship between the flux and the driving force. As part of the research discussed in this chapter, an approach based on the application of the Maxwell model, originally developed to study the effect of spherical particles embedded in a matrix on the electric and thermal conduction, was suggested and guided by Prof. John Barker. The methodology and results are presented in sections 4.1.4 and 4.4. Some discussion on the nature of the model follows.

The coefficients that relate the fluxes to the driving forces are the conductivities, electrical, thermal, or hydraulic, as the case may be (Zimmerman, 1996). Thus, electric and thermal conduction processes can be reasonably used as analogues when studying fluid flow processes. In the context of electrical conduction, Maxwell (1954) derived an equation (see Equation 4-12) for the conductivity of a medium comprising a matrix in which spheres, with different resistivity, are embedded. The equation that relates the hydraulic conductivity of the medium to the proportion by volume of the embedded spheres is particularly relevant in the context of the current research. Further details are given in Section 4.1.4. Using Maxwell's (1954) equations, Zimmerman (1996) and Pozdniakov and Tsang (2004) studied heterogeneous materials consisting of a matrix material in which there were dispersed inclusions. They concluded that the effective conductivity of such media will depend on the conductivities of the matrix and inclusion phases, the volume fraction and the shape of the inclusions.

In this Chapter, a study designed to provide further information to develop the criteria to classify materials according to their potential to influence fluid flow is discussed. The study addresses the following questions:

- What is the critical content (mass or volume) of 2D particles above which a significant reduction in the hydraulic conductivity is evidenced?. Volume and mass contents can be related using the particle density given by the material from which the particle is made.
- What is the critical size of 2D particles above which a significant reduction in the hydraulic conductivity is evidenced?

Solid waste is a highly heterogeneous material. Isolation of the effect that individual parameters play on the hydraulic conductivity, e.g. particle shape, is therefore not an easy task. Other factors that modify the structure of waste and therefore have an impact on the hydraulic conductivity, i.e. degradation, compression and gas build up, are experimentally difficult to control. For this reason, analogues of waste were preferred.

The design of the analogue specimens considered the need to represent a simplified porous medium where the effect of particle shape on hydraulic conduct was easily isolated from other factors. The use of an inert and incompressible matrix material mixed with 2D particles was considered appropriate for this purpose. Mixtures of sand systematically modified with 2D plastic discs were used. The hydraulic conductivity of each mixture was determined experimentally by application of Darcy's law and compared with that for unmodified specimens. This provided a method to assess the magnitude of the effect of 2D particles on permeability. Two parameters were investigated: 2D/matrix relative size and the relative content of 2D particles. Two further factors were considered during the study: the angle formed between 2D particles and the plane normal to the flow direction and the porosity. Some of the specimens were investigated using a non-destructive technique, i.e. Micro-focus Computed Tomography (μCT). The use of μCT provided a method to inspect the internal structure of the specimens and qualitatively assess the orientation of 2D particles. The porosity was measured in each case.

4.1. Background

Section 4.1.1 provides a theoretical background on Darcy's law required for the hydraulic conductivity calculations. In Section 4.1.2, work by Hubbert (1940) on understanding the parameters that influence K is briefly explained, where the relevance of factors such particle shape and size is emphasised. Description of the correction required to account for differences in temperature is included in Section 4.1.3. Analogue models for conduction through heterogeneous media are introduced in Section 4.1.4. The specimens tested were described using the traditional phase relationships from soil mechanics which are briefly described in Section 4.1.5.

4.1.1. Darcy's Law

Darcy's law is an empirical equation proposed by Henry Darcy from the results of his experiments on water flow through a packed sand column (Darcy, 1856). Research over years has shown that Darcy's law describes fluids flow in very diverse porous media such as moisture in soils, oil and gas in geological formations and flow through filters.

The equation proposed by Darcy can be understood considering Figure 4-3; which shows a circular cylinder of cross section A [L^2] filled with a porous medium connected to inflow and outflow tubes as well to a pair of manometers.

Water is introduced into the cylinder and allowed to flow until all pores are filled with water and the inflow rate Q [L^3T^{-1}] equals the outflow rate and the steady state is reached. An arbitrary datum is selected as the elevation z=0. The elevations of the manometer intakes are z_1 and z_2, and the elevations of the fluid levels in each manometer are h_1 and h_2. The distance between the manometer intakes is Δl.

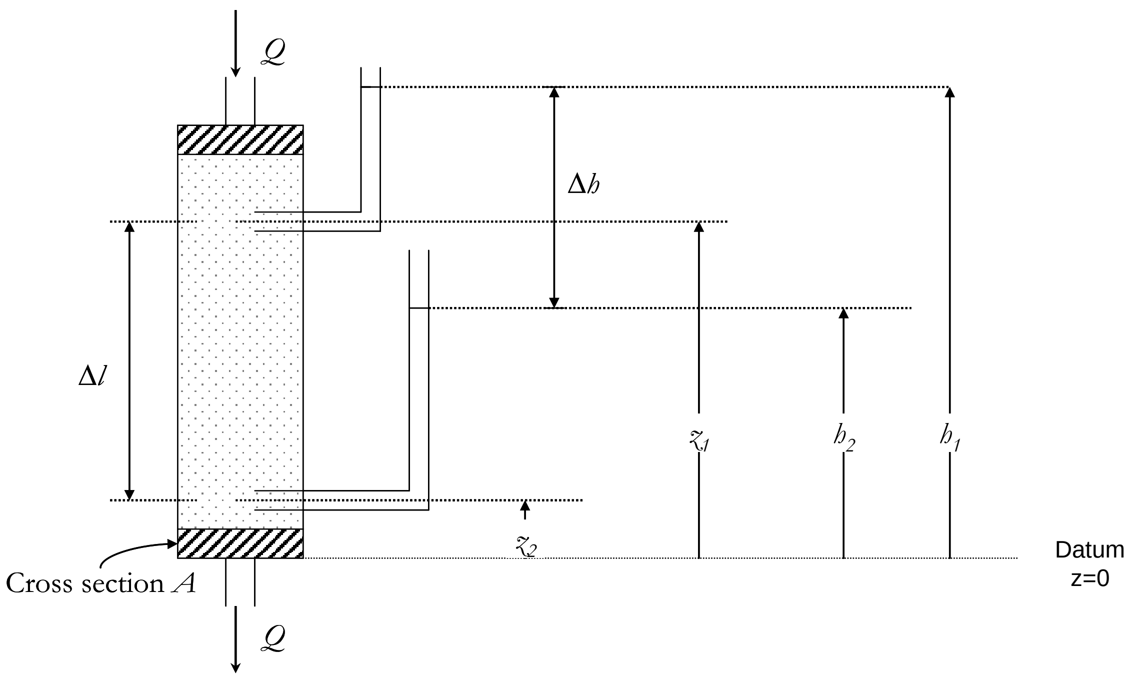

Figure 4-3 Experimental Apparatus for the illustration of Darcy's law

Experiments carried out by Darcy showed that the specific discharge ν is directly proportional to h_1 - h_2 when Δl is held constant, and inversely proportional to Δl when h_1 - h_2 is held constant (Equation 4-1):

$$\nu = \frac{Q}{A} = -K\frac{\Delta h}{\Delta l} \qquad \text{Equation 4-1}$$

K [LT^{-1}] is a constant of proportionality that Henry Darcy called "un coefficient dépendant de la pérmeabilité" (Daniel, 1993), and it is known as the hydraulic conductivity. h is the hydraulic head and $\Delta h/\Delta l$ is the hydraulic gradient which is also named as the dimensionless i [L^0]:

$$\mathrm{i} = \frac{\Delta h}{\Delta l} \qquad \text{Equation 4-2}$$

Combining Equation 2-1 and Equation 4-2 gives:

$$Q = -KA\mathrm{i} \qquad \text{Equation 4-3}$$

Equation 4-3 implies that when:

$Q = 0$,	$h_2 = h_1$	or	$h_2 - h_1 = 0$,
$Q > 0$,	$h_2 < h_1$	or	$h_2 - h_1 < 0$,
$Q < 0$,	$h_2 > h_1$	or	$h_2 - h_1 > 0$,

The first condition implies that a graph of Q vs i with K and A constants is a straight line with an intercept in (0,0). The second condition implies that flow occurs from point 1 with higher h to point 2 with a smaller h. Although, K is the constant of proportionality, it actually depends on the properties of the solid material. Hubbert (1940) showed that Darcy kept some factors arbitrarily constant, and that consequently a number of factors are lumped in K. An explanation of the work by Hubbert (1940) follows in Section 4.1.2.

4.1.2. Analysis of the parameter *K*

Hubbert (1940) focused on the identification of the factors lumped in K. First, he considered the relationship between driving and resisting forces on a microscopic fluid element, which were then scaled up to a macroscopic level. A brief outline of the results follows, whilst the complete deduction can be found in Hubbert (1940). Equation 4-4 is the expression found by Hubbert (1940), which relates K with five factors:

$$K = Cd^2\rho\frac{1}{\mu}g \qquad \text{Equation 4-4}$$

Where ρ is the fluid density, μ the fluid dynamic viscosity and g the acceleration due to gravity. Whilst d is the characteristic length of the system, which could be represented by a characteristic diameter of the solid grains, any other suitable length scale related to the coarseness of the solid matrix, or a representative dimension of the pore space. And C is a dimensionless coefficient that depends upon the geometrical characteristics of the solid medium and may include aspects such as the porosity, grains sphericity and roundness, packing characteristics and parameters that describe the particle size distribution (Freeze and Cherry, 1979).

A dimensional analysis by Hubbert (1940) confirmed that the factors and powers included in Equation 4-4 were the correct ones and that no other essential quantities were omitted. This analysis is briefly described in Annex 4-1. Combining Equation 4-3 and Equation 4-4 gives Equation 4-5:

$$\frac{Q}{A\mathrm{i}} = -Cd^2\rho\frac{1}{\mu}g \qquad \text{Equation 4-5}$$

Equation 4-5 shows that Q varies with the size and shape characteristics of the solid media. In order to separate the contribution of the two groups of factors, i.e. fluid and solid media, k a parameter referred as to the specific or intrinsic permeability is defined according to Equation 4-6:

$$k = Cd^2 \qquad \text{Equation 4-6}$$

K can then be expressed in terms of k according to Equation 4-7:

$$K = \frac{k\rho g}{\mu} \qquad \text{Equation 4-7}$$

Experimental evidence supports the form of Equation 4-6. For example, Hazen (1911) obtained an expression for clean sands (Equation 4-8) where D_{10}, is the size of the 10% finer fraction:

$$k = C\mathrm{D}_{10}^2 \qquad \text{Equation 4-8}$$

k is controlled by the fraction of fines represented as D_{10}. Powrie (1997) explains that in clean sands, the smaller D_{10} particles fit into the voids between the larger particles and exert a strong control over fluids flow. *C* in this case is a coefficient of proportionality that varies with sand cleanliness, uniformity, particles shape and packing (Hazen, 1911). Other equations similar to Equation 4-8 have been obtained experimentally where k is a function of some grain size descriptor at a power close to 2 (Dullien, 1992, Cronican and Gribb, 2007). Although the equations had been obtained for clean sands and the direct application to other media is not straightforward, they give extra support to validate the form of Equation 4-6.

4.1.3. Influence of temperature in the parameter *K*

When the solid medium is kept constant *K* is a function of only the fluid properties (Equation 4-4). If the temperature changes so does ρ , μ and hence *K*. *K* of two experiments run at temperature T and 20°C can be written as:

$$K_T = \frac{k\rho_T g}{\mu_T}$$

$$K_{20} = \frac{k\rho_{20} g}{\mu_{20}}$$

Then, K_{20}/K_T is:

$$\frac{K_{20}}{K_T} = \frac{\rho_{20}}{\mu_{20}} \frac{\mu_T}{\rho_T}$$

And K_{20} can be expressed as :

$$K_{20} = K_T \frac{\mu_T}{\mu_{20}} \frac{\rho_{20}}{\rho_T}$$ Equation 4-9

Equation 4-9 is used to correct measurements of K made at temperatures that differ from 20°C (BS 1377-5, 1990). In terms of flow rate Q can be written as Equation 4-10.

$$Q_{20} = Q_T \frac{\mu_T}{\mu_{20}} \frac{\rho_{20}}{\rho_T}$$ Equation 4-10

Lambe (1951) provided a graphical method to calculate the correction factor. Variations in viscosity with temperature are more significant than those in density. Hydraulic conductivity tests during this research took place between 16.4 to 23.6°C. The correction factor was obtained using data from Lambe (1951) in the range 10 to 30ºC. The plot of T vs μ_T/μ_{20} produced follows the exponential curve in Equation 4-11, with a correlation coefficient of 0.999 (see Annex 4-7).

$$\frac{\mu_T}{\mu_{20}} = 1.644\ exp^{-0.0246T}$$ Equation 4-11

4.1.4. Conduction in heterogeneous media

Electrical conduction and fluid flow in porous media are both processes governed by a linear relationship between a flux and a driving force. The relating coefficient corresponds to the electrical or hydraulic conductivity respectively. Electric conduction thus can be used as a reasonable analogue for fluid flow processes. The work by Maxwell (1954) and later applications by Zimmerman (1996) and Pozdniakov and Tsang (2004) on conduction through heterogeneous media comprising a matrix in which spheres of a different material are embedded, provides a rational framework for the analysis of the matrix of sand modified with 2D particles used during this research.

The equation derived by Maxwell (1954) and applied by Zimmerman (1996) and Pozdniakov and Tsang (2004) among others, considers the effective specific resistance r of a medium comprised of *N* spheres with radius α_1 and resistance $r_1$and a matrix of particles with radius α_2 and resistance r_2 (Equation 4-12). The equation assumes that distances between intrusions are such that their effects in disturbing the conduction may be taken as independent of each other, i.e. low to moderate concentrations. It also assumes that the intrusions are randomly distributed along the specimen. Further details can be found in Maxwell (1954) (Equation 17, Volume 1 page 440).

Equation 4-12 expresses r in terms of r_1, r_2 and the proportion by volume of the spheres *p*, defined according to Equation 4-13:

$$\frac{r}{r_2} = \frac{2r_1 + r_2 + p(r_1 - r_2)}{2r_1 + r_2 - 2p(r_1 - r_2)}$$ Equation 4-12

$$p = \frac{N\alpha_1^3}{\alpha_2^3}$$ Equation 4-13

Maxwell (1954) transformed Equation 4-12 into an expression of the media conductivity by taking the reciprocals of the resistances r , r_1, r_2 as *K*, K_1 and K_2. The result is Equation 4-14, which can be expressed as Equation 4-15 where *K* , *Ko* and *Kdiscs* are the hydraulic conductivities of the mixture, matrix and discs respectively.

$$\frac{K}{K_2} = \frac{2K_2 + K_1 - 2p(K_1 - K_2)}{2K_2 + K_1 + p(K_1 - K_2)}$$ Equation 4-14

$$\frac{K}{K_2} = \frac{2K_0 + K_{discs} - 2p(K_{discs} - K_0)}{2K_0 + K_{discs} + p(K_{discs} - K_0)}$$ Equation 4-15

Given that the discs used during this research are impermeable, i.e. made of polystyrene, *Kdiscs* is 0 and Equation 4-15 is transformed into Equation 4-16. The equation relates *K*/ *Ko* to the proportion by volume of the 2D particles, which is calculated using Equation 4-13 as a function of the particles size.

$$\frac{K}{K_0} = \frac{2(1-p)}{2+p}$$ Equation 4-16

Equation 4-16 can be expressed in terms of the inverse *Ko*/*K* expanding the Taylor series for (1-p) -1 and be transformed to Equation 4-17 (if p is small).

Equation 4-17

$$\frac{K_0}{K} = \frac{2+p}{2(1-p)} = 1 + \frac{3}{2}p + \frac{3}{2}p^2 + \cdots \approx 1 + \frac{3}{2}p$$

Mathematical models have been also developed in the context of composites materials, i.e. materials that consist of a matrix filled with plate-like fillers of high aspect ratio, to estimate transport, mechanical and thermal properties (Nielsen, 1967, Fredrickson and Bicerano, 1999). Those expressions usually relate the conductivity of the modified system (e.g. diffusivity, hydraulic conductivity, etc.) to the conductivity of the matrix and parameters of the composite such as the aspect ratio and the volumetric content of the filler particles. Different equations have been developed for specific conditions, e.g. low and high discs content (Fredrickson and Bicerano, 1999), geomaterials (Yamada et al., 2011), food packaging (Duncan, 2011) and nanomaterials (Choudalakis and Gotsis, 2009). Time constraints meant that consideration of these types of models to flow through waste like materials was not possible and only the Maxwell´s simplified approach was investigated in Section 4.4.. However, further research in this area is strongly recommended.

4.1.5. Phase relationships

The specimens tested during this research can be described using the conventional relationships from soil mechanics that link the relative volumes of solid, liquid and gas phases (Powrie, 1997).

Void ratio e, is the ratio of the volume of the voids to the volume of solids. In a dry soil it is defined in terms of the soil dry mass density ρ_{dry}:

Equation 4-18

$$e = \frac{G_S}{\rho_{dry}} - 1$$

G_S is the relative density of the soil grains. Annex 4-5 presents the derivation for a soil element composed by two types of solid particles, i.e. sand and plastics. G_s is replaced by $\bar{G}_S$, the relative density of the mixture to give:

Equation 4-19

$$e = \frac{\bar{G}_S}{\rho_{dry}} - 1$$

Porosity n is defined as the volume of voids per unit total volume which in terms of e can be expressed as:

$$n = \frac{e}{1+e}$$ Equation 4-20

4.2. Materials and Methods

At the laboratory scale the saturated hydraulic conductivity *K* is measured using a permeameter and calculations are performed according to Equation 4-3. Permeameters can have either rigid or flexible walls. Rigid wall cells are preferred for granular materials such as sands where either constant or variable head tests are performed (Daniel, 1993). In this study the constant head method was followed. A detailed description can be found in BS 1377-5 (1990)- Part 5 and in ASTM D 2434 (1968). The constant head method is suitable for materials with hydraulic conductivities in the range between 10^{-2} to 10^{-5} m/s. All the specimens tested during this study were within this range. In materials with permeabilities below 10^{-5} m/s flow rates are so small that evaporation could lead to significant errors and the falling head test is preferred.

Some of the specimens were further examined using μCT, a radiographic technique that allows the non invasive investigation of internal structures by detecting the proportion of the x-rays that reach an object and are then attenuated through their journey along the structure. X-ray attenuation depends on material properties such as density and chemical composition. This means that x-ray attenuation varies across the specimen as a function of the components found, which allows the discrimination between materials. μCT produces a sequence of images that are computationally manipulated and used to make a 3D reconstruction of the object under study. Several steps, further explained in section 4.2.2. were taken during the use of μCT during this research to obtain images with good contrast and facilitate the discrimination between materials.

4.2.1. Hydraulic Conductivity

4.2.1.1. Experimental setup

Figure 4-4 shows the permeameter configuration. The Perspex cylinder has 3 take off points and anodised aluminium end plates. The internal diameter, D, is 75 mm which gives a cross sectional area, A, of 4.418×10^{-3} m^2. The equipment total length, L, is 238 mm, and the distance between the standpoints, Δl, 70 mm.

The permeameter is connected to a 7.7 litres capacity main tank which provides water to a 200 ml constant head reservoir equipped with an overflow. The elevation of the constant head reservoir can be adjusted by a pulley system. The main tank is filled with de-aired water prepared in an external Geokon nold De-aerator then pumped into the 7.7 l tank. Annex 4-2 shows further details of the experimental set up.

The use of de-aired water was essential. In the main water supply line, water is at high pressure and contains large amounts of dissolved air. Once water is depressurised, air comes out of the solution and bubbles accumulate progressively. This produces a decrease in the hydraulic conductivity. In many cases, knowing the order of magnitude of the hydraulic conductivity satisfies the application requirements and air accumulation does not represent a serious problem (Daniel, 1993). This was not the case for the experiments during this research. Xie et al. (2006) showed that 2D particles produced changes in the hydraulic conductivities within one order of magnitude. Therefore the determination of the hydraulic conductivity required higher accuracy and a better water control.

The de-aeration system is equipped with a vacuum pump and an impeller to remove and extract air bubbles. For each water batch, the de-aeration system was operated for about 15 minutes. Initial trials were run to test the quality of the de-aeration process. The content of dissolved oxygen (DO) was measured using a Lab BOD Dissolved Oxygen instrument YSI model 5100. The readings confirmed that DO decreased from above 8 mg/l in tap water to below 2 mg/l. The impact in the hydraulic conductivity with the use of de-aired water was evaluated in a sand specimen and results are summarised in Annex 4-3.

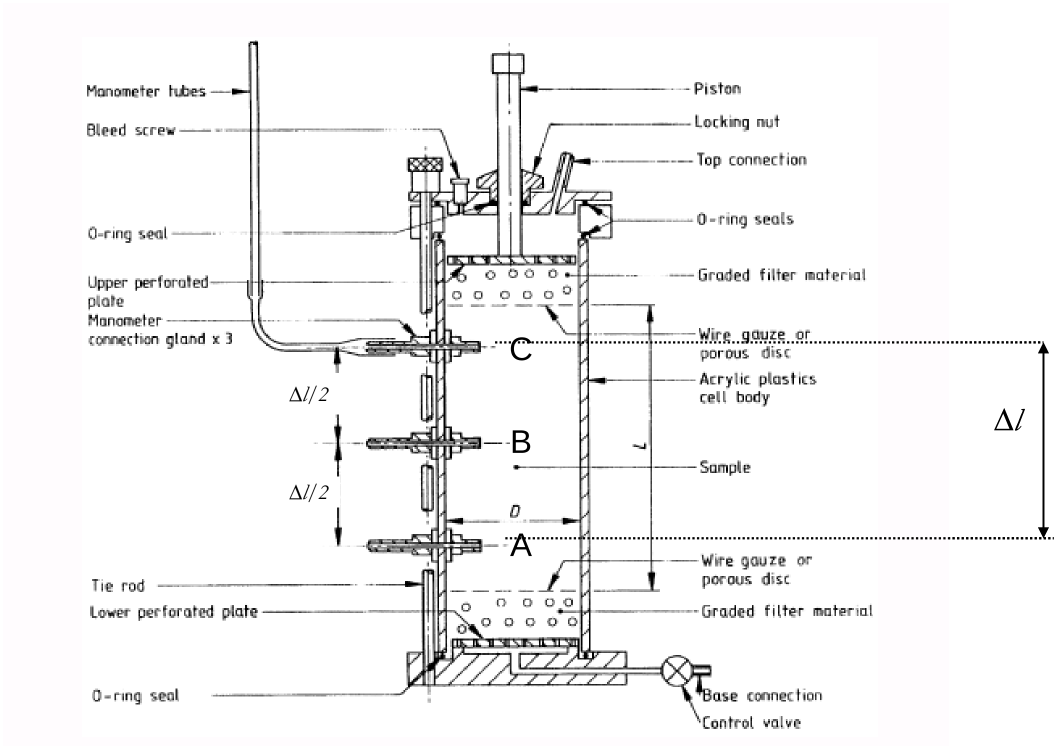

Figure 4-4 Section of the constant head permeability cell (adapted from BS 1377-5 (1990))

4.2.1.2. Test description

Hydraulic conductivity tests were done according to BS 1377-5 (1990)- Part 5 and followed these steps:

- Initially, a 3 cm layer of filter material was placed in the permeameter following the recommendations in BS 1377-5 (1990)
- The permeameter filled with the filter material was weighted to a precision of 0.01 g
- Sand and plastic discs were weighted to a precision of 0.01 g in the proportions required for the specimen, thoroughly mixed in a tray and placed by pluviation (see Section 0)
- The permeameter filled with the specimen was weighted to a precision of 0.01 g and the mass of the mixture added was calculated

- The height of the mixture inside the permeameter was measured with a levelled ruler to a precision of 1 mm

- ρ_{dry} , e , n were calculated using Equation 4-19 and Equation 4-20

- The specimen was slowly saturated from bottom to top using de-aired water

- The specimen was tested under upward flow conditions, i.e. water flowing from bottom to top, using typically five different flow rates

- The specimen was tested under downward flow conditions, i.e. water flowing from top to bottom, using typically five different flow rates

Further details of the procedure can be summarised as:

- Each specimen was tested under approximately 10 different flow rates to cover i in the range 0 to 1.0 (Equation 4-2). A maximum limit of i equal to 1 was used to minimise deviations from Darcy's law (Freeze and Cherry, 1979)

- Before starting the test, the condition $Q=0$, i=0 was verified by checking that the elevation of the column of water in each of the three standpipes were the same. Any air bubbles were released until the condition was satisfied

- For each flow rate the steady state was reached, i.e. readings were constant over a period of time, before the readings were recorded. Then three to four measurements of Q were taken together with the elevations of water in each manometer, i.e. h_A, h_B and h_C . Equation 4-2 was used for the calculation of i between standpipes A and C (see Figure 4-4). i was also calculated for shorter sections , i.e. A to B and B to C, to assess the specimens homogeneity. All the specimens tested were found to be homogeneous with no significant variations in the hydraulic conductivity identified across the samples

- Each specimen was prepared and tested by duplicate. Data reported corresponds to average values between two tests. As already mentioned, each individual specimen was tested for approximately 10 flow conditions and for each flow condition 3 to 4 readings were taken. The average was taken for the first specimen. The same procedure was followed for the duplicate specimen which was tested under the same flow conditions. Then, each single point in a Q vs i graph is the average between the results for two specimens resulting from six to eight readings.

- Q was measured using a calibrated cylinder with 0.1 ml gradations. The hydraulic head, h, was measured using a fixed scale and a level with a precision of 1 mm. The temperature of the outflow water was frequently monitored. The average of the individual Q and i measurements were used to produce a plot of Q vs i for each specimen. K was obtained from the slope of the linear regression according to Equation 4-3. Q was corrected to 20°C using Equation 4-10 and Equation 4-11. A second plot of Q_{20} vs i was produced with the slope being K_{20}, the hydraulic conductivity at 20°C .
- Further measurement of sample height after each conductivity test confirmed that no volume change occurred.

4.2.1.3. Materials

Two types of materials were required during this research:

- 0D or matrix, which according to Kölsch (1995) comprises grains of uniform size and shape
- 2D particles, with uniform shape but substantially larger than the matrix particles

The selection of the materials was limited by two aspects:

- According to BS 1377-5 (1990) the diameter of the permeameter should be at least 12 times the maximum particle size of the specimen tested. The permeameter used had an internal diameter of 75 mm implying a maximum particle size of 6.25 mm
- Some of the specimens were further examined using μCT, a radiographic technique that allows non invasive investigation of internal structures by detecting attenuated x-

rays. Images with good contrast are required to discriminate between materials. X-ray attenuation characteristics, which depend on material properties such as density and chemical composition, should be substantially different for the components within a specimen.

By consideration of these requirements, sand and polystyrene pieces were judged to be appropriate. Leighton Buzzard sand (LB), a standard material according to the requirements in BS 1881:Part 131 (1998), was selected as the matrix material. Properties of the material are summarised in Annex 4-4, where fractions B (600 μm-1.18 mm; LB-b) and D (150 μm -300 μm; LB-d) were selected based on the range of relative size to study as discussed in Section 4.2.1.4. Polystyrene discs of 3 and 5 mm diameter and 0.6 mm thickness were used as 2D particles, which were purpose built by an injection moulding process.

4.2.1.4. Parameters to study

This section discusses the parameters studied and justifies the type of materials selected and in general the approach adopted for the study.

Two parameters were selected for investigation:

- The relative size of the 2D particles to the matrix material , referred as *RS*,
- and the content by volume of the 2D particles, referred as *VC.*

The selection of parameters was supported by the results from Xie et al. (2006) where the decrease in the hydraulic conductivity of a matrix resulting from the presence of 2D particles was shown to be controlled by the relative size and volumetric content of the 2D particles. The angle formed between the 2D particles and the plane normal to the flow direction was also shown to be an influential parameter (see Figure 3-1). The selection of the *RS* range was based in the following reasoning. The definition given in Velkushanova et al. (2009), where 2D particles at least 5 times the size of the surrounding grains are considered as potentially flow diverting or impeding, was considered in the first instance. This means a *RS* of 5. Then, an extension of this value was evaluated to cover larger 2D particles. A maximum RS of 25 was judged appropriated and achievable with the materials available for the study (i.e. 3 and 5 mm polystyrene discs with LB sand). This maximum RS could represent the impact of 2D materials as large as 25 mm size in a matrix of particles of 1mm size, a reasonable representation for large 2D (e.g. coarse plastic pieces) particles in MBT residues. A RS of 25 could be also a sensible representation for 2D particles of up to 125 mm size in a matrix of 5 mm particles, as may be the case for raw MSW. Also, a minimum value for RS was analysed. In this case, a RS of 3.8 was selected. 2D particles with an RS below 3.8 were not expected to have a significant impact on the hydraulic conductivity of the matrix. Then, the study of RS below 3.8 was assessed unnecessary for the investigation, an assumption later confirmed experimentally where only particles with RSs above 15 caused significant changes in the hydraulic conductivity. Therefore, the range selected for the study of RS was from 3.8 to 25. This was achieved adjusting the size of the matrix particles (e.g. changing from LB-b to LB-d) the type of sand , the size of the 2D particles or the size of both materials. RS was calculated according to Equation 4-21, where $Ddiscs$ represent the diameter of the 2D particles and d_{min} and d_{max} the minimum and maximum diameters of the sand grains respectively.

$$RS = \frac{\left(\frac{D_{discs}}{d_{min}} + \frac{D_{discs}}{d_{max}}\right)}{2} \qquad \text{Equation 4-21}$$

In the other hand, the relative content of 2D particles (VC) was varied to cover the range 0 to 40%. In mass terms this range is equivalent to 0 to 13.7%. The range was selected considering the actual mass content of flexible and rigid plastics in solid wastes. A reference point was taken from the results of material characterisation obtained during the investigation discussed in this document and presented in Chapter 3, which showed a mass content of plastics in UK MBT and German MBT of 10.68% and 4.77% respectively. A mass content range between 0 to 13.7%, and its equivalent in volumetric terms of 0 to 40%, could be therefore a reasonable representation of the plastic 2D particles contained in MBT wastes. VC

was defined as the ratio between the volumetric content of 2D particles (*Vdiscs*) and sand grains (*Vsand*). Calculations were made considering *Vsand* as a constant equal to 100 and *Vdiscs* being varied in the range 0 to 40. Thus, the relative volumetric content of 2D particles calculated with Equation 4-22 .

$$VC = \frac{V_{discs}}{V_{sand}} \qquad \text{Equation 4-22}$$

4.2.1.5. Control of density and orientation

The hydraulic conductivity K and the intrinsic permeability k are functions of the porosity n (see Equation 2-4). Control of the porosity was thus a requirement during this research. This involved the identification of a repeatable method to preserve the integrity of the particles and produce stable specimens that would experience negligible changes in porosity during testing. Dense specimens were preferred and alternative preparation methods explored. For example, the procedure to determine the maximum density in sands uses an electric vibrating hammer to compact the sample (BS 1377-4, 1990). A comparable method was used in a trial test in a sample of LB-b modified with 5% by volume of 3mm plastic discs. The sample was compacted using an electric vibrating table. It was shown that most plastic discs that were initially horizontally orientated were rearranged against the permeameter wall after the compaction. This suggested that the method in BS 1377-4 (1990) was not a suitable option to prepare the specimens for this research. Moreover, although the method produces dense specimens it does not preserve the integrity of the particles which may crush as the result of the vibratory compaction (Cresswell et al., 1999).

A second method known as pluviation which is based on the deposition of granular materials through a sequence of diffuser meshes was explored. Pluviation produces well compacted samples, i.e. densities $\geq$90% the maximum dry density, whilst preserving the integrity of the particles (Cresswell et al., 1999). A schematic representation of a pluviation apparatus is detailed in Annex 4-6. The diffuser meshes are offset interwoven wires that create an even sand rain. The tube and the collection container have similar diameters whilst the tube is considerable longer than the container length. This depositional mechanism promotes more uniform and horizontally aligned deposition of the plastic discs. This was qualitatively assessed using μCT in some of the specimens. The images obtained for the sand/polystyrene discs had a good contrast that allowed the visual differentiation of each material. Visual assessment of the images confirmed that there was no pronounced segregation of discs and that discs and grains were well mixed and distributed along the sample. There was also no evidence of important variations of the density along the sample as suggested by relatively uniform grey value profiles at several cross sectional areas across different images. All this suggested pluviation as an appropriate preparation method for the purposes of the study described in this chapter. A 75 mm diameter x 800 mm length pluviation tube was purpose built for this research. A selection of the supportive images are available in Caicedo et al. (2011) where details of the methodology to obtain and process the images are fully described.

4.2.1.6. Temperature corrections

Variations in the temperature of water of 1°C can have an impact of up to 3% on the hydraulic conductivity (Daniel, 1993). The temperature (T) of the water coming from the output valve was measured during the test and corrections to 20°C done using Equation 4-9, Equation 4-10 and Equation 4-11.

4.2.2. μCT Scanning

The orientation of the plastic discs was investigated in two of the specimens (#6 and #12) using μCT. The equipment used was an X-Tek XT H 450 (X-Tek Systems Ltd, Tring, Hertfordshire, UK). The machine was equipped with a 2000 × 2000 pixel PerkinElmer 1621 X-ray flat panel detector with pixel size 200 μm x 200 μm with a resolution limit of 100 μm.

The specimens were prepared following the procedure described in section 4.2.1 and placed in the μCT equipment in their dry state, i.e. before being saturated with de-aired water. This was considered sensible to facilitate the discrimination between materials by limiting the number of materials in the specimen to 3 (i.e. sand, plastics and air filled pores) instead of 4 (i.e. sand, plastic, air filled and water filled pores).

Preliminary trial runs were required to find optimal settings to obtain high quality images, this implied high signal to noise ratio and minimimal artefacts. Artefacts are defined by ASTM (2005) as anything in the image that does not accurately reflect true structure in the sample being inspected. Minimization of artefacts was aided using the 'ring compensation' mode during the acquisition. Optimal scanning conditions were found to be a beam voltage of 200 kV and current of 175 μA with the use of a 1mm thick copper filter. The total scanning time was 3.5 hours, and the scan consisted of 3143 radiographic projections with an individual exposure time of about 4s. Further details of data processing techniques are provided in section 4.3.2.

4.3. Results

4.3.1. Hydraulic conductivity

Table 4-1 and Table 4-2 detail the specimens tested. Samples are grouped into those prepared using Leighton Buzzard Sand fraction B (LB-b)-Table 4-1 and those using Leighton Buzzard Sand fraction B (LB-d)-Table 4-2. *RS* was calculated using Equation 4-21 and varied between 3.8 and 25, depending on the size of the 2D particles (3 mm and 5 mm) and the type of sand used. The *VC* was calculated using Equation 4-22 and varied between 4% and 40%. Hydraulic conductivity tests were performed as described in Section 4.2.2. Plots of Q_{20} vs i were produced for each specimen, results are shown in Figure 4-5 to Figure 4-8.

In Figure 4-6 and Figure 4-8, results of the linear regressions were included to assist in the estimation of K, calculated from the slope of the line using Equation 4-3. Table 4-3 and Table

4-4 summarise the results obtained. K/Ko is the ratio between the hydraulic conductivity of the modified specimen and the 100% sand control specimen denoted as Ko. K/Ko was used to assess the magnitude of the changes in the hydraulic conductivity once the 2D particles were added. In Figure 4-9, K/Ko was plotted against the VC whilst in Figure 4-10, K/Ko was plotted against RS. Figure 4-11 shows the variation in void ratio with the VC of 2D particles.

Table 4-1 Description of specimens composed of Leighton Buzzard Sand fraction B (LB-b) and 2D particles

					Solids volumetric content		Solids mass content				
Sample ID	Sand type	Size 2D particles (mm)	RS [a]	VC [b]	%Vol content Sand	%Vol content 2Dparticles	%Mass content Sand	%Mass content 2D particles	Dry Density (Mg/m^3)	Void Ratio (e) [c]	Porosity (n) [d]
1	LB-b	na	0,0	0,00	100,00	0,0	100,00	0,00	1,99	0,33	0,25
2	LB-b	3	3,8	4,00	96,15	3,85	98,44	1,56	1,96	0,32	0,24
3	LB-b	3	3,8	19,21	83,89	16,11	92,91	7,07	1,81	0,32	0,24
4	LB-b	3	3,8	29,99	76,93	23,07	89,37	10,62	1,73	0,32	0,24
5	LB-b	3	3,8	40,01	71,42	28,58	86,32	13,68	1,66	0,32	0,24
6	LB-b	5	6,3	12,78	88,67	11,33	95,18	4,82	1,87	0,32	0,24
7	LB-b	5	6,3	19,99	83,34	16,66	92,65	7,34	1,82	0,31	0,24
8	LB-b	5	6,3	29,99	76,93	23,07	89,37	10,62	1,80	0,27	0,21
9	LB-b	5	6,3	39,73	71,57	28,43	86,40	13,60	1,75	0,25	0,20

a Calculated according to Equation 4-21

b Calculated according to Equation 4-22

c Calculated according to Equation 4-19

d Calculated according to Equation 4-20

Table 4-2 Description of specimens composed of Leighton Buzzard Sand fraction D and 2D particles

					Solids volumetric content		Solids mass content				
Sample ID	Sand type	Size 2D particles (mm)	RS [a]	VC [b]	%Vol content Sand	%Vol content 2Dparticles	%Mass content Sand	%Mass content 2D particles	Dry Density (Mg/m^3)	Void Ratio (e) [c]	Porosity (n) [d]
10	LB-d	na	0,0	0,00	100,00	0,0	100,00	0,00	1,84	0,44	0,30
11	LB-d	3	15,0	10,01	90,90	9,10	96,19	3,81	1,75	0,43	0,30
12	LB-d	3	15,0	20,00	83,33	16,67	92,66	7,34	1,75	0,36	0,26
13	LB-d	3	15,0	29,99	76,93	23,07	89,37	10,62	1,74	0,31	0,24
14	LB-d	3	15,0	40,01	71,42	28,58	86,32	13,68	1,73	0,27	0,21
15	LB-d	5	25,0	10,01	90,90	9,10	96,19	3,81	1,84	0,36	0,26
16	LB-d	5	25,0	19,98	83,35	16,65	92,66	7,34	1,77	0,35	0,26
17	LB-d	5	25,0	29,99	76,93	23,07	89,37	10,62	1,80	0,27	0,21
18	LB-d	5	25,0	40,00	71,43	28,57	86,32	13,68	1,77	0,24	0,19

a Calculated according to Equation 4-21

b Calculated according to Equation 4-22

c Calculated according to Equation 4-19

d Calculated according to Equation 4-20

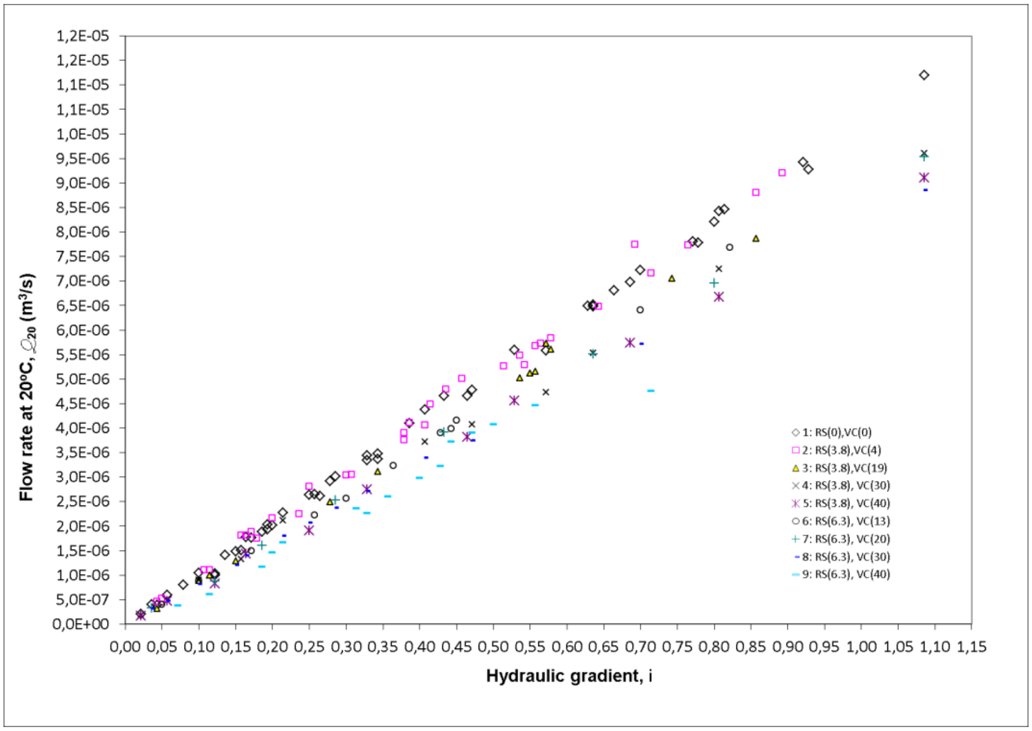

Figure 4-5 Hydraulic conductivity tests specimens with *RS* (3.8-6.3) at different *VCs*

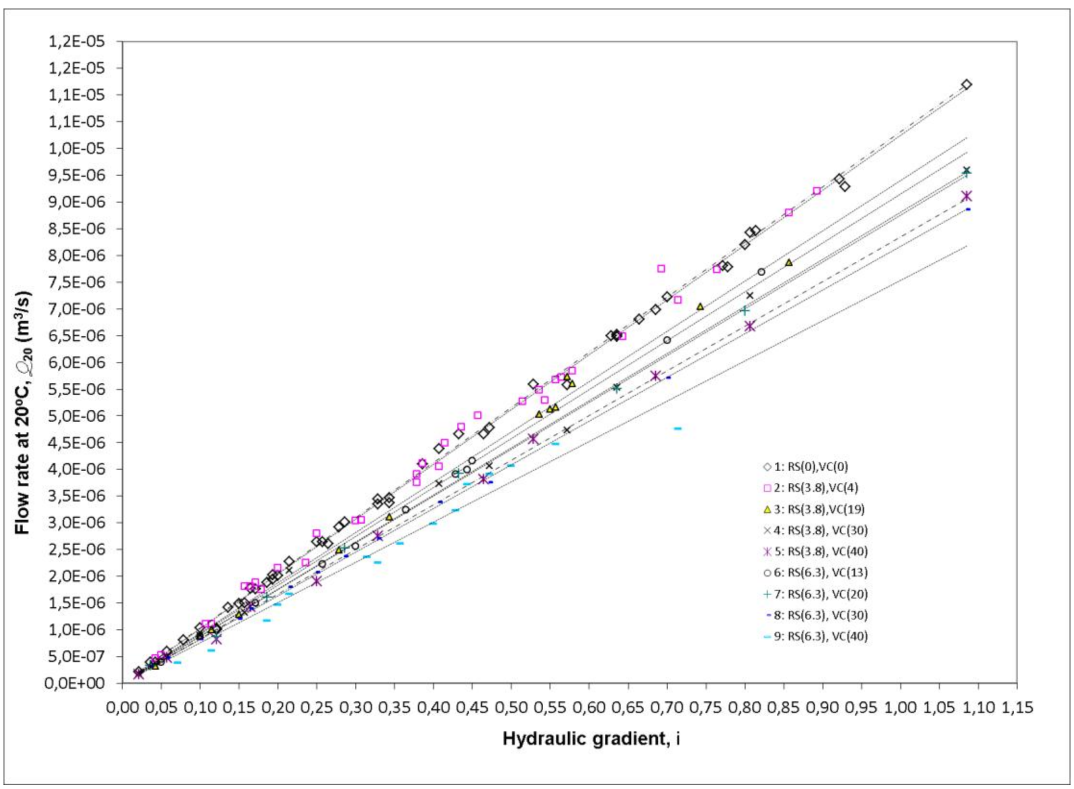

Figure 4-6 Linear regressions of hydraulic conductivity tests specimens with *RS* (3.8-6.3) at different *VCs*

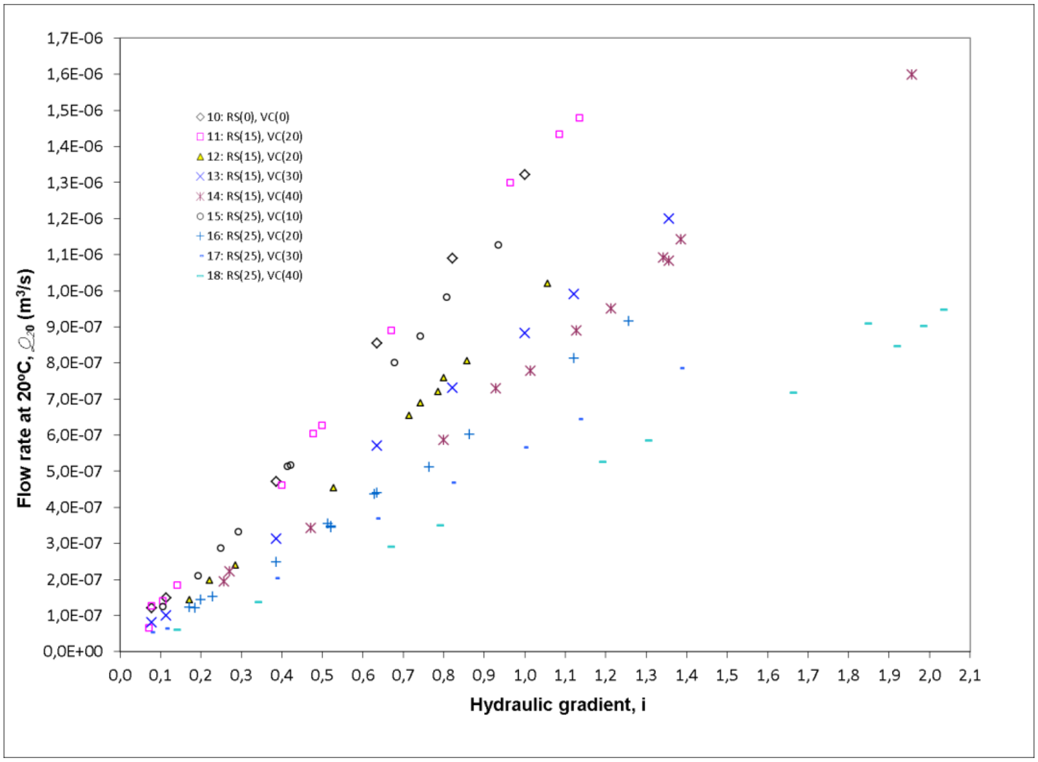

Figure 4-7 Hydraulic conductivity tests specimens with *RS* (15-25) at different *VCs*

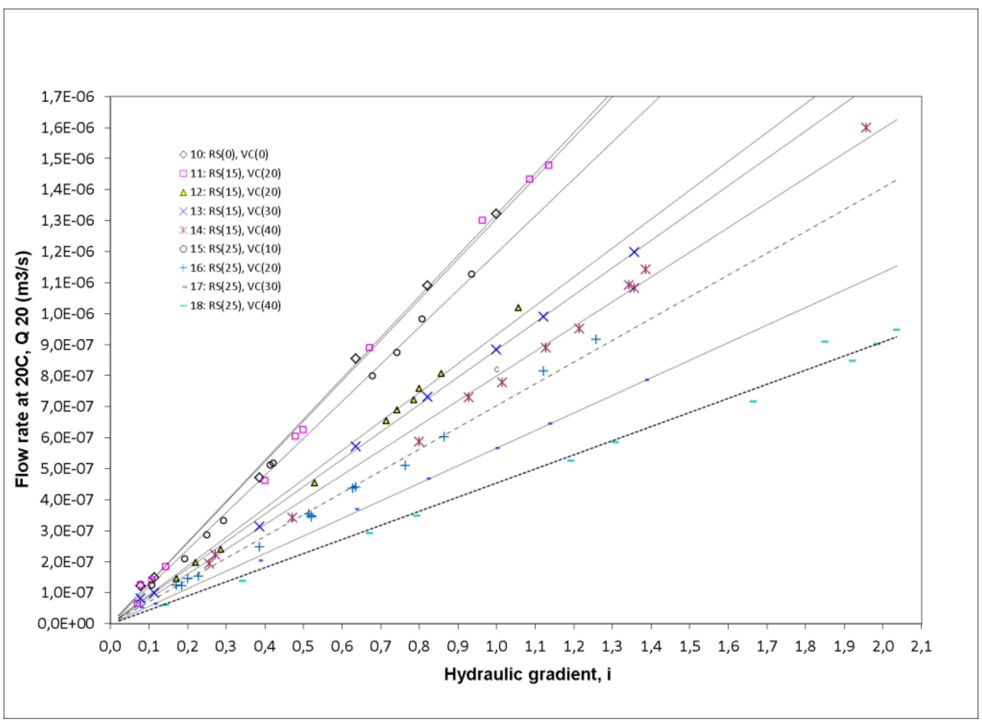

Figure 4-8 Linear regressions of hydraulic conductivity tests specimens with *RS* (15-25) at different *VCs*

Table 4-3 Comparison of the hydraulic conductivity in specimens with relative sizes of 3.8 and 6.3 and different contents of 2D particles

Sample ID	Description	R^2	Slope	*K* (m/s)	*K/Ko*	% Decrease in K
1	100% LB-b	0.9985	1.02E-05	2.32E-03	1.00	-
2	4%2D particles/RS 3.8	0.9942	1.03E-05	2.33E-03	1.01	-
3	19.2%2D particles/RS 3.8	0.9965	9.40E-06	2.13E-03	0.92	-8.21
4	30%2D particles/RS 3.8	0.9976	8.80E-06	1.99E-03	0.86	-14.01
5	40%2D particles/RS 3.8	0.9987	8.34E-06	1.89E-03	0.81	-18.51
6	12.8%2D particles/RS 6.3	0.9980	9.14E-06	2.07E-03	0.89	-10.69
7	20%2D particles/RS 6.3	0.9992	8.75E-06	1.98E-03	0.85	-14.51
8	30%2D particles/RS 6.3	0.9997	8.17E-06	1.85E-03	0.80	-20.24
9	39.7%2D particles/RS 6.3	0.9620	7.53E-06	1.70E-03	0.74	-26.45

Table 4-4 Comparison of the hydraulic conductivity in specimens with relative sizes of 15 and 25 and different contents of 2D particles

Sample ID	Description	R^2	Slope	*K* (m/s)	*K/Ko*	% Decrease in K
10	100% LB-d	0.9984	1.32E-06	2.99E-04	1.00	-
11	10%2D particles/RS 15	0.9971	1.31E-06	2.96E-04	0.99	-1.02
12	20%2D particles/RS 15	0.9945	9.32E-07	2.11E-04	0.71	-29.43
13	30%2D particles/RS 15	0.9992	8.83E-07	2.00E-04	0.67	-33.13
14	40%2D particles/RS 15	0.9954	7.99E-07	1.81E-04	0.60	-39.53
15	10%2D particles/RS 25	0.9981	1.20E-06	2.71E-04	0.91	-9.48
16	20%2D particles/RS 25	0.9949	7.03E-07	1.59E-04	0.53	-46.82
17	30%2D particles/RS 25	0.9993	5.67E-07	1.28E-04	0.43	-57.11
18	40%2D particles/RS 25	0.9919	4.54E-07	1.03E-04	0.34	-65.64

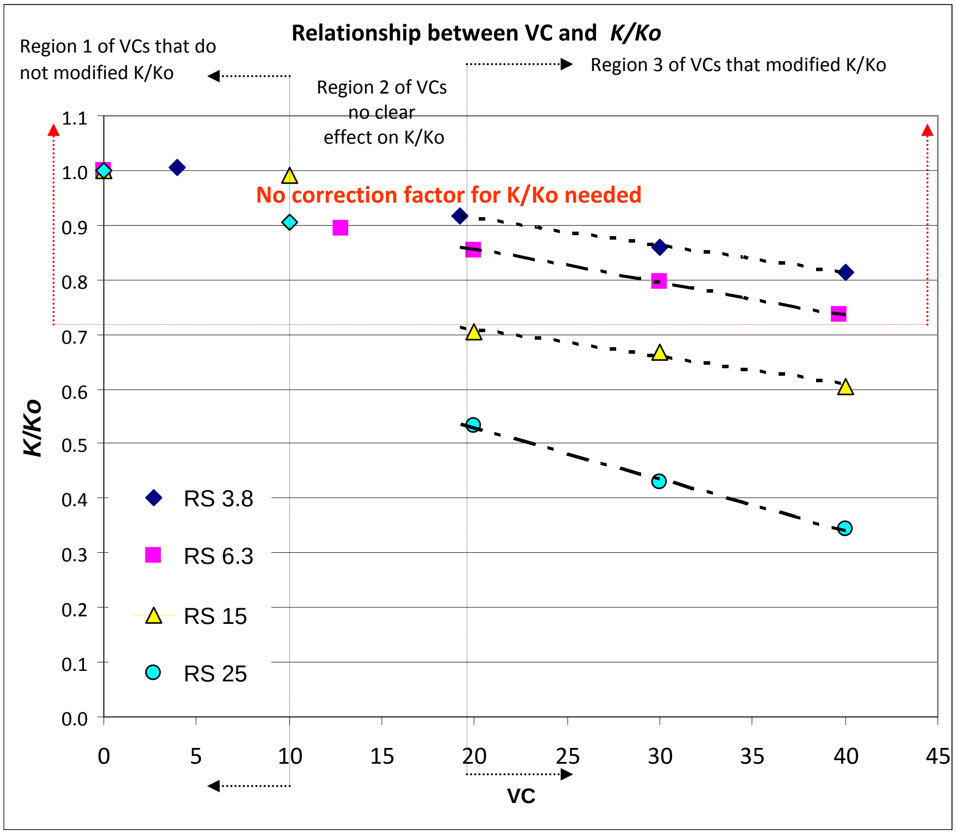

RS	R^2	Slope	Intercept
3.8	0.9974	-5.00E-03	1.01
6.3	0.9990	-6.10E-03	0.98
15	0.9769	-5.00E-03	0.81
25	0.9971	-9.40E-03	0.72

Figure 4-9 Variation in K/Ko with the volumetric content of 2D particles for specimens with different relative sizes

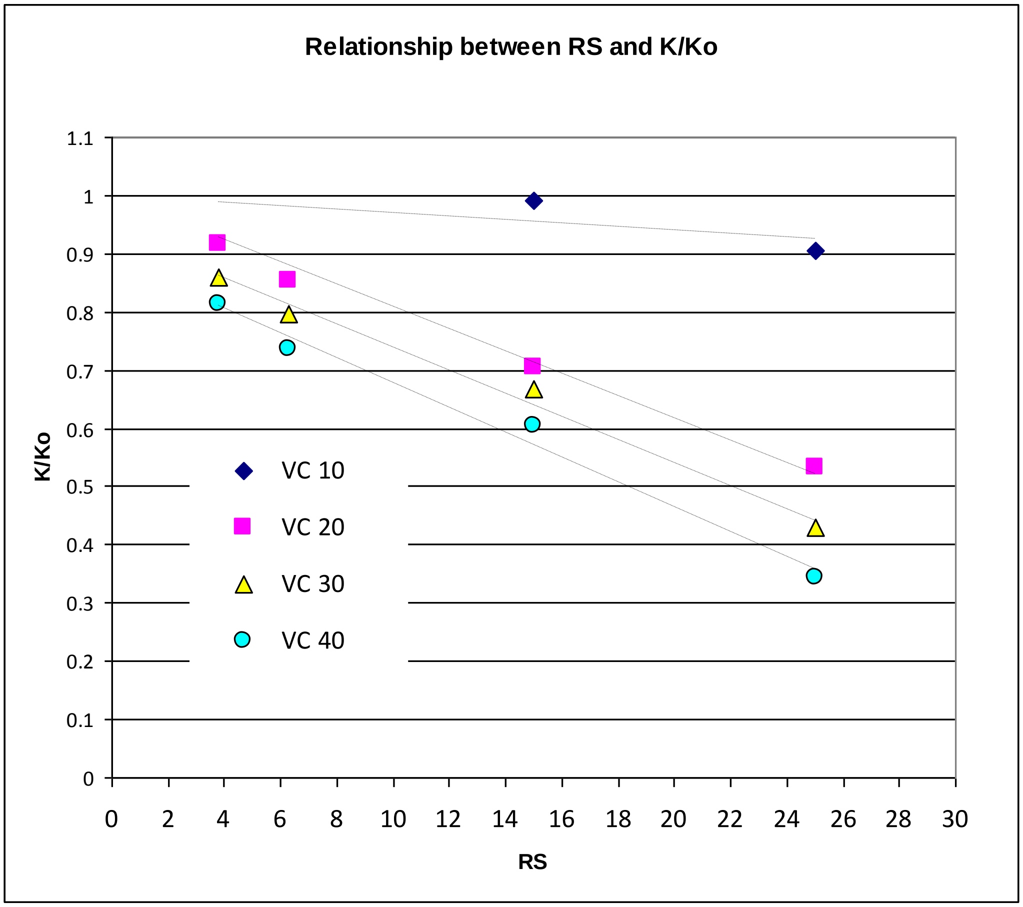

VC	R^2	Slope	Intercept
10	0.5523	-3.00E-03	1.00
20	0.9905	-1.92E-02	1.00
30	0.9889	-1.97E-02	0.94
40	0.9859	-2.13E-02	0.89

Figure 4-10 Variation in K/Ko with RS of 2D particles for specimens with different volumetric content

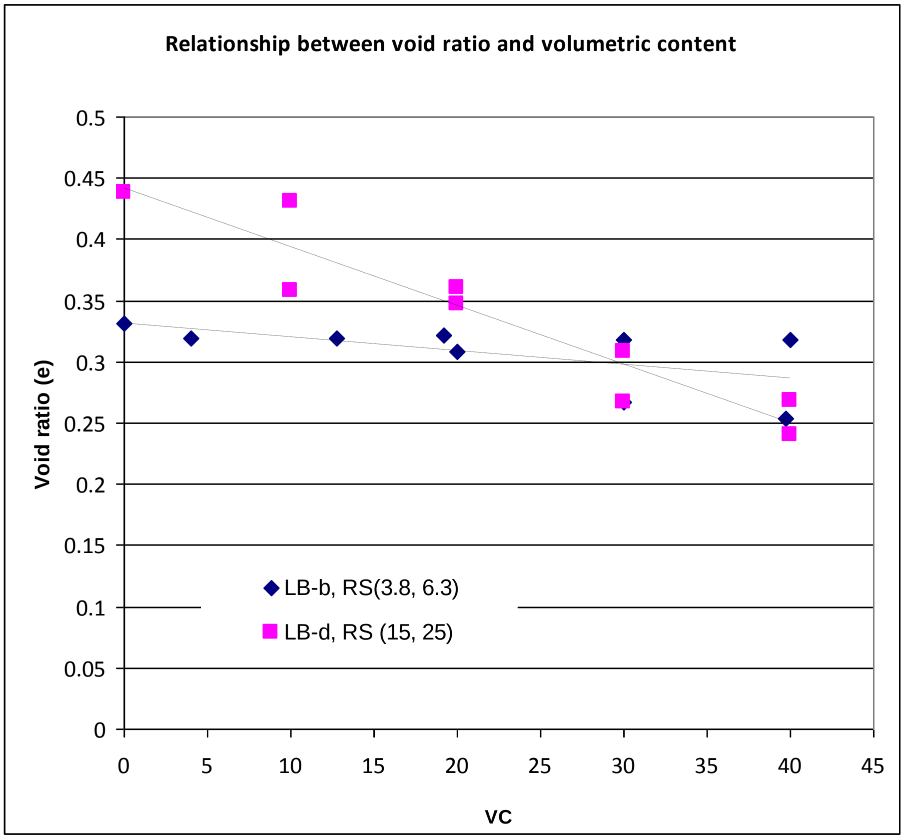

Sand Type	R^2	Slope	Intercept
LB-b	0.3652	-1.10E-03	0.33
LB-d	0.8897	-4.80E-03	0.44

Figure 4-11 Variation in void ratio with the volumetric content of 2D particles for specimens with different relative sizes

4.3.2. μCT Scanning

The orientation of the plastic discs was investigated in two of the specimens using μCT. Selected images are presented in Figure 4-12 and Figure 4-13. In Figure 4-12, images taken in sample # 9, a specimen made with LB-b and 5mm discs and corresponding *RS* of 6.3 and *VC* of 40, show that 2D particles (represented by the darker circles) were preferentially oriented in the x-y plane perpendicular to the flow plane. Also, the images evidenced that the 2D particles were reasonably well distributed along the sample, although a gradual increase in the content of discs from bottom to top was observed.

Similar situation as shown in Figure 4-13, was observed for sample # 16, a specimen made with LB-d and 5mm discs and corresponding *RS* of 25 and *VC* of 20. Images presented in Figure 4-12 and Figure 4-13 were obtained following three basic steps: acquisition, reconstruction and processing. Details about the equipment used and the scanning conditions were described in section 4.2.2.

Reconstruction was carried out using a filter back projection algorithm. Once reconstructed, 3D images were obtained using VG-Studio Max V2 whilst 2D images were obtained using Image J. The reconstruction process produced 1376 horizontal slices separated by 0.059 mm.

Images processing started by reducing the number of slices to 1083 (with a voxel size of 0.000215 mm^3) to cover a subsection (referred as the region of interest, ROI). This was done to reduce the computational demand and accelerate processing. The ROI was located between the piezometer ports in the permeameter. Then, the ROI was divided from bottom to top into four sub-regions: ROI-1, ROI-2, ROI-3 and ROI-4. All images were stored in 8 bit format. The resulting images were grey scale images with grey values in the range between 0 and 255 which were visually and quantitatively assessed. The quantitative assessment was based on the grey value at each voxel or pixel of the 3D or 2D images respectively. The grey value is related to the amount of X-rays that a material can absorb and transmit, which is a function of the material density (Kak and Slaney, 1988). Grey value histograms were obtained for each of the ROIs where the number of voxels for each grey value was plotted (Figure 4-14).

Quantification of the volume content for each grey value using the number of voxels and the size of each voxel followed. Different regions in the histogram (i.e. regions separated by clear peaks) were used for the volumetric quantification of each material in the specimen. For example, in Figure 4-14, two peaks clearly divided at a grey value of around 143 are evident. As images were mapped for brighter materials to be displayed with the higher grey levels, those voxels with grey values above 143 correspond to sand. This was verified during visualisation in 3D by disabling the interval 0-143. The rendered volume showed only sand grains validating that materials in the range 0-143 correspond to plastic discs and pores.

The cumulative distribution of grey values is illustrated in Figure 4-15. The y axis is the percentage of voxels with a grey value < x. Therefore, the graph represents the volumetric content of the components in the specimen. Volumetric concentrations of pores and discs were calculated for each ROI using a threshold equal to 143 and the corresponding quantity in the y axis. They were compared against the percentages used during the specimen preparation (e.g. 54.4% sand, 21.6% discs and 24% pores for sample # 9). Results from the sum of all ROIs showed close agreement with the actual composition (see the sum of all ROIs in Figure 4-15). Differences in the volumetric contents between the four ROIs suggest a gradual increase in the content of plastic discs, from bottom to top, and this is also shown in the horizontal views.

Separation between discs and pores was more difficult given the smaller differences between their grey values. Alternative segmentation methods were explored, i.e. region growing and shape based techniques. These were successfully applied to smaller sub-regions of the specimens, but required a substantial amount of manual input and were therefore highly time consuming. This limited the possibility to complete the segmentation within the time framework of this research. A broad range of fast segmentation algorithms are available in the different commercial image processing applications available and should be explored in future research on the effect of the orientation of the 2D particles. Further details of the steps taken to obtain images is available in Caicedo et al. (2011) (see Annex 4-7).

Differentiation between discs and pores based on grey level was more difficult. Grey value histograms under 143 do not show clear peaks to distinguish between these two materials. Although the distribution for ROI-4 (see Figure 4-14) suggests that the curve is the result of two different distributions: the first with a maximum at around 60 presumably for pores and the second with a maximum at around 118 presumably for plastics, they share a significant region of grey values making any unambiguous differentiation unreliable.

Figure 4-12 Selected images of sample # 9 (LB-b and 5mm discs, RS 6.3, VC 40) obtained by μCT

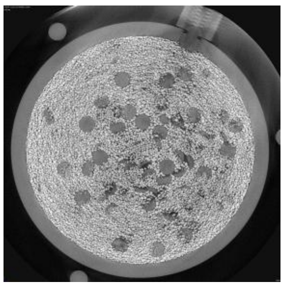	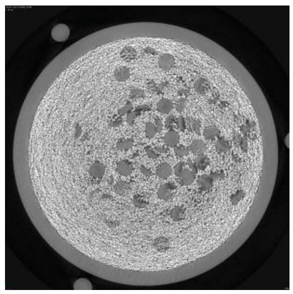	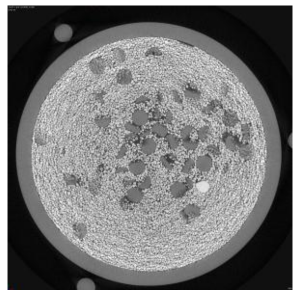	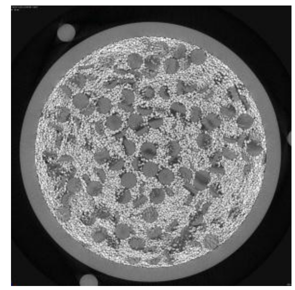
a. Horizontal view at 0 mm	b. Horizontal view at 9.6 mm	c. Horizontal view at 21.4 mm	d. Horizontal view at 33.2 mm
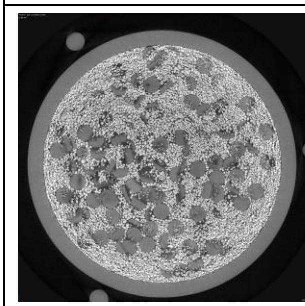	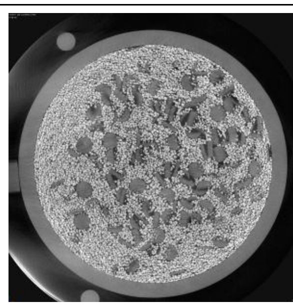	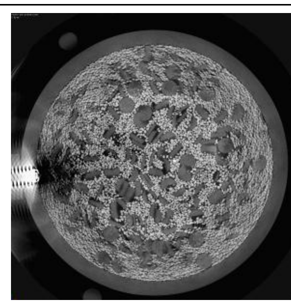	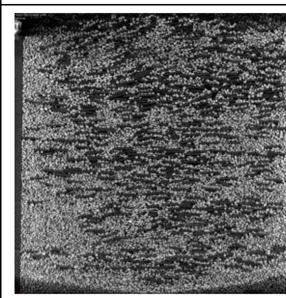
e. Horizontal view at 45.0 mm	f. Horizontal view at 62.7 mm	g. Horizontal view at 70 mm	h. Cross sectional cut at 36 mm

At the time of writing no further attempts have been made to achieve segmentation between plastics and pores. This could have been possible using alternative segmentation algorithms like those based on differences in shape (i.e. Hough transform, template matching) or on the statistical treatment of histogram to obtain two separated normal distributions (Nixon and Aguado, 2008). This will be the subject of further research.

Figure 4-13 Selected images of sample # 16 (LB-d and 5mm discs, RS 25, VC 20) obtained by μCT

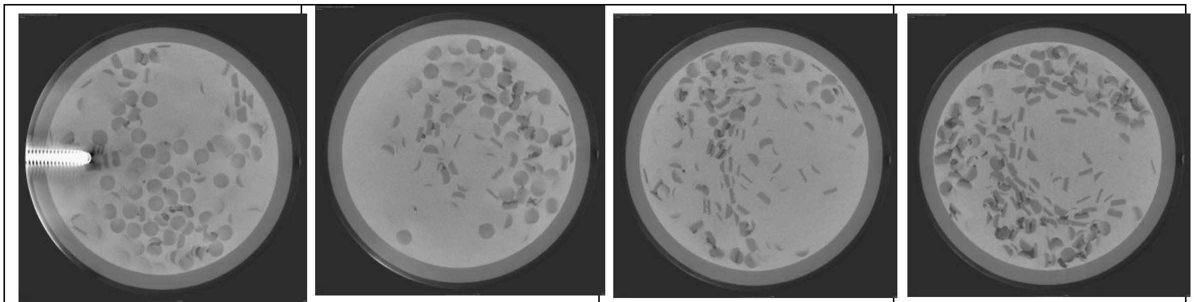

a. Horizontal view at 2.1 mm	b. Horizontal view at 13.3 mm	c. Horizontal view at 24.0 mm	d. Horizontal view at 40.3 mm

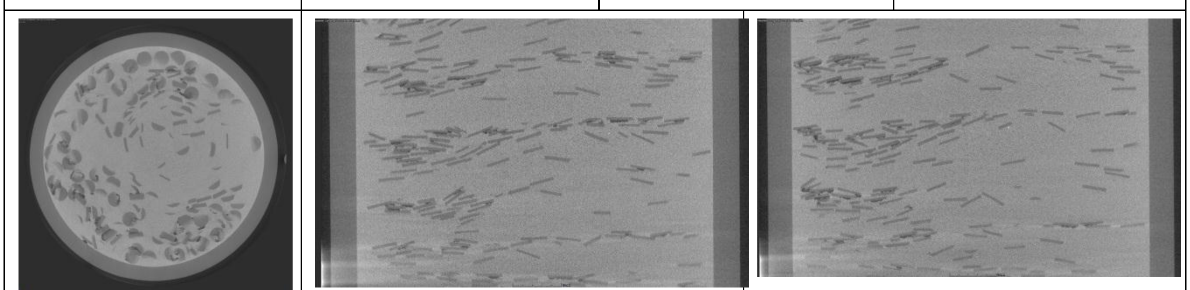

e. Horizontal view at 58.2 mm	f. Cross sectional cuts

Figure 4-14 Grey value distribution for Sample #9. Y axis represents the number of voxels with a grey value equal to X. The grey scale is in the range 0-255 as a result of images being stored in 8 bit format

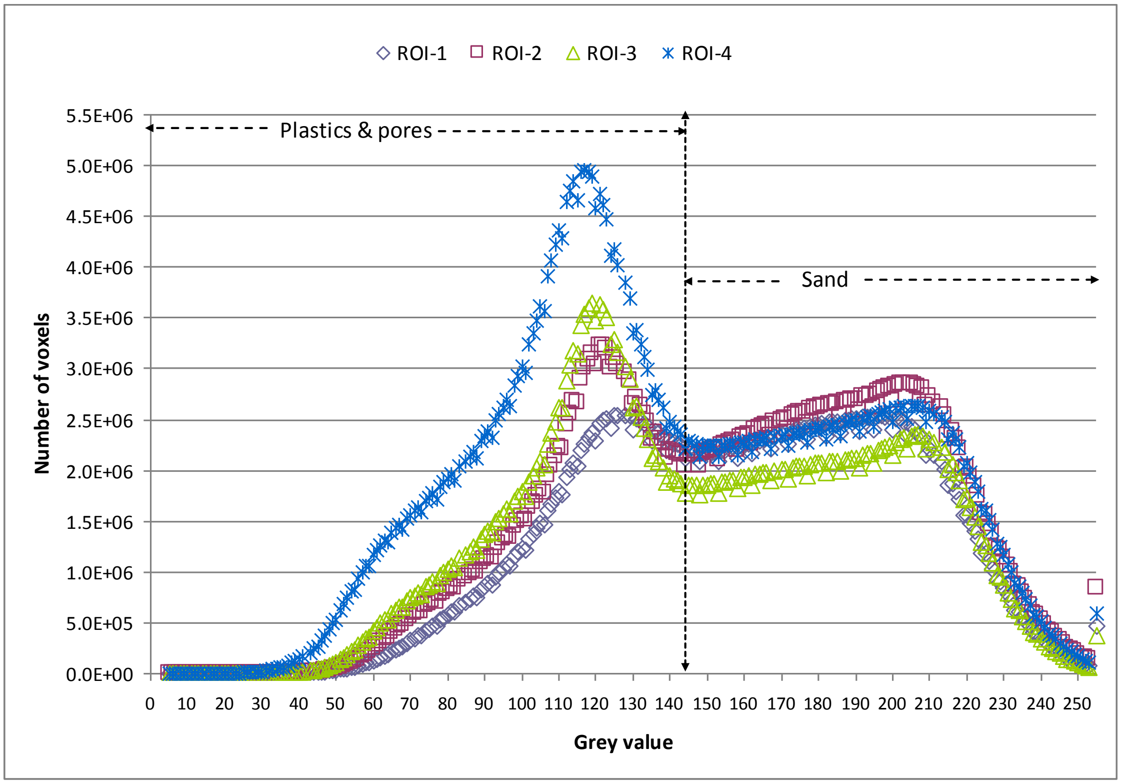

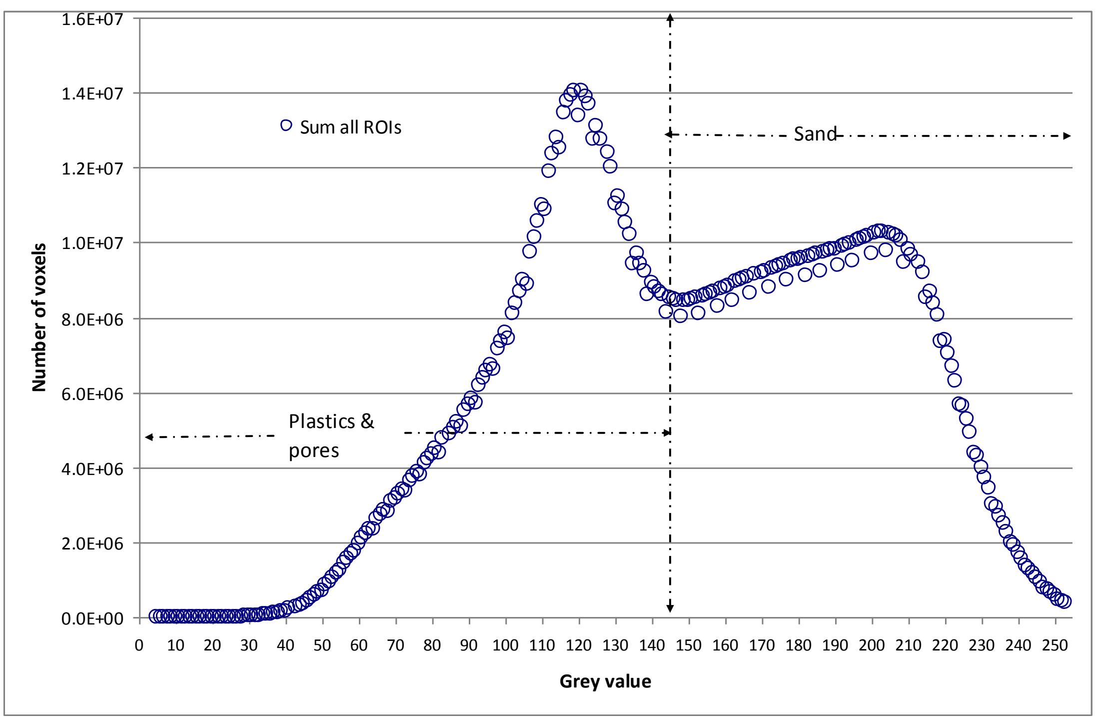

Figure 4-15 Cumulative grey value distribution for Sample #9. Y axis represents the percentage of voxels as the total sample volume with a grey value less than X. The threshold grey value of 143 corresponds to the point dividing the peaks for sand and plastics and pores in Figure 4-14

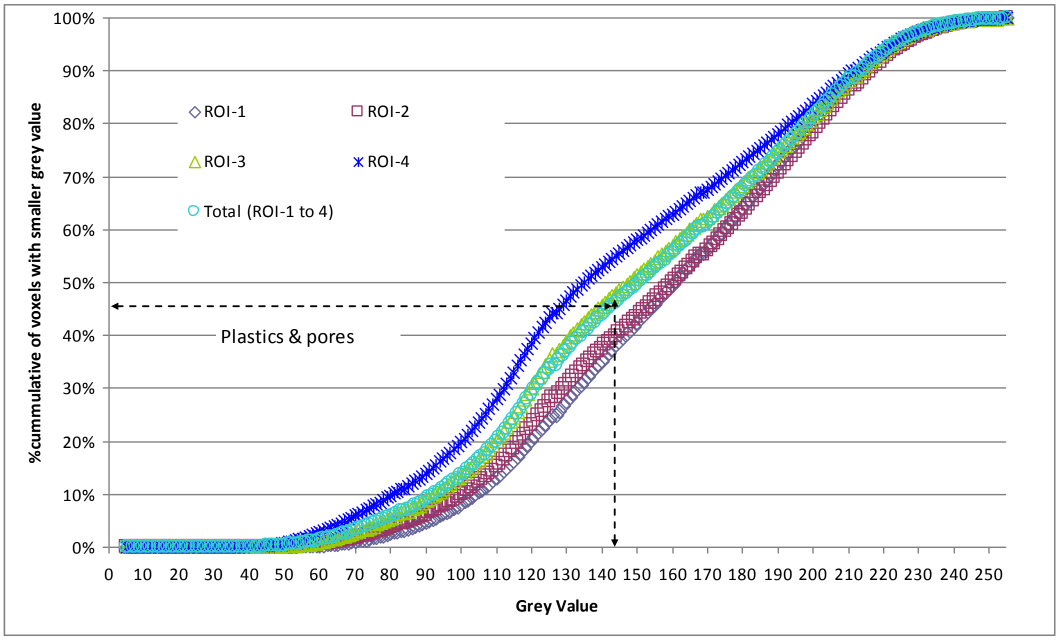

		From voxel information Threshold grey value=143				
Materials	%Vol[a]	ROI-1	ROI-2	ROI-3	ROI-4	Sum all ROIs
Plastic pieces & pores	45.6	37.4	39.3	47.3	54.5	45.5
Sand	54.4	62.6	60.7	52.7	45.5	54.5

a: data from preparation

4.4. Analysis of results using analogous models

Further analyses were carried out using the analogue model proposed by Maxwell (1954) for conduction through heterogeneous porous media (explained in Section 4.1.4). The model relates *K/Ko* to the proportion by volume of 2D particles, p, as indicated in Equation 4-16. Maxwell (1954) defined p as a function of the ratio between the matrix and spheres radius according to Equation 4-13. To account for the differences in the geometry between the media of spheres embedded studied by Maxwell (1954) and the matrix modified with 2D particles used during this research, a generalized definition of p was considered. Equation 4-13 was modified as suggested by Prof. John Barker through a personal communication, and expressed as:

$$p = \alpha N D^{3-\varepsilon} d^{\varepsilon} \qquad \text{Equation 4-23}$$

Where p [L^0] is a non-dimensional parameter , α [L^0] the constant of proportionality, N [L^{-3}] the number of 2D particles per unit volume, D [L] the diameter of the 2D particles and d [L] the diameter of the sand grains. N is defined in terms of N_0, the number of discs in the sample as:

$$N = \frac{N_0}{V} \qquad \text{Equation 4-24}$$

where V is the specimen volume. For Equation 4-23 to be dimensionally correct, the sum of D and d powers must equal 3, therefore the need to use the power coefficient ε. The diameter of the sand grains d, was calculated as the geometric mean between the maximum and minimum particle size according to Equation 4-25:

$$d = \sqrt{d_{min}d_{max}} \qquad \text{Equation 4-25}$$

The geometric mean was preferred over the arithmetic and harmonic means as it is generally accepted that a heterogeneous media is well approximated to a homogeneous media by considering the geometric mean of the property under investigation, in this case the particle size (Gómez-Hernández and Gorelick, 1989).

In Equation 4-23 the effective volume of the 2D particles was considered to be a function of their diameter D and their thickness was not included. The rationale for this follows: consider a hypothetical experiment where the number of discs is kept constant and their thickness is continually halved. Provided the discs remain impermeable there is no reason to imagine that the permeability would change. This suggests that the permeability cannot depend on the discs' thickness.

Values for α and ε were estimated using the solver tool in Excel by an iterative process where the square sum of the differences between *K*/*Ko* calculated with Equation 4-16 and the experimental results was minimized. Results are summarised in Table 4-5. The sum of squares was evaluated < 0.08 which suggests a reasonable agreement with the experimental data. Additionally, plots of *K*/*Ko* model vs *K*/*Ko* experimental were used to evaluate the models performance. These results are presented in Figure 4-16.

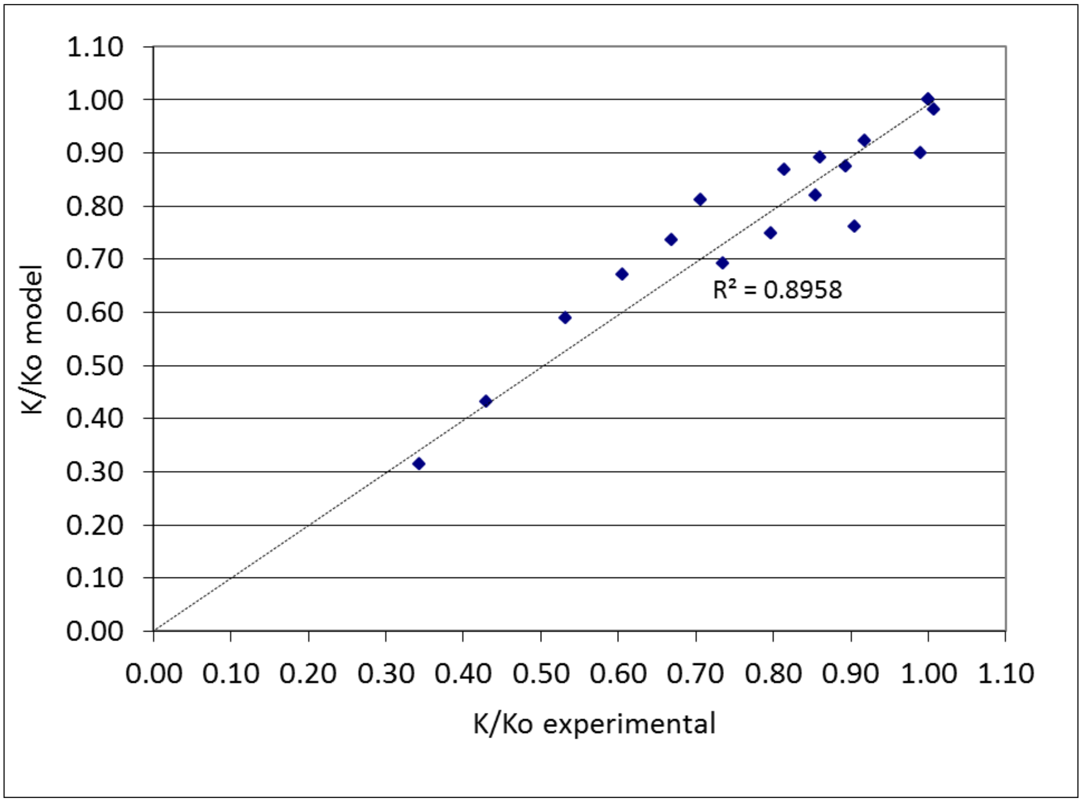

Figure 4-16 Evaluation of analogous models for conduction through heterogeneous media

Combining Equation 4-17 with Equation 4-23 gives the following expressions for *Ko*/*K*:

$$\frac{K_0}{K} = 1 + \alpha_\nu' N \quad D^{3-\varepsilon} d^{\varepsilon}$$ Equation 4-26

Figure 4-17 was produced to evaluate Equation 4-26 and assess the correlation between *Ko*/*K* and p. The trend lines shown was derived excluding data for *Ko*/*K* equal to 1. Table 4-5 summarises the results of this analysis.

Table 4-5 Results from analogous model on conduction through heterogeneous media

Sample ID	K/Ko experiment.	D (mm)	d(mm)	N_o	N (mm^{-3})	p	K/Ko fitted
1	1.0000	0	0.8414	0	0.0000	0.0000	1.0000
2	1.0068	3	0.8414	5344	0.0069	0.0124	0.9816
3	0.9179	3	0.8414	23343	0.0287	0.0517	0.9245
4	0.8599	3	0.8414	23511	0.0413	0.0742	0.8927
5	0.8149	3	0.8414	29125	0.0511	0.0919	0.8683
6	0.8931	5	0.8414	5497	0.0073	0.0861	0.8762
7	0.8549	5	0.8414	6112	0.0108	0.1276	0.8201
8	0.7976	5	0.8414	8464	0.0155	0.1824	0.7493
9	0.7355	5	0.8414	6633	0.0192	0.2272	0.6940
10	1.0000	0	0.2121	0	0.0000	0.0000	1.0000
11	0.9898	3	0.2121	9774	0.0150	0.0691	0.8998
12	0.7057	3	0.2121	20551	0.0289	0.1333	0.8125
13	0.6687	3	0.2121	23511	0.0416	0.1918	0.7375
14	0.6047	3	0.2121	27224	0.0531	0.2451	0.6725
15	0.9052	5	0.2121	4019	0.0058	0.1759	0.7575
16	0.5318	5	0.2121	6923	0.0105	0.3179	0.5886
17	0.4289	5	0.2121	8464	0.0155	0.4680	0.4311
18	0.3436	5	0.2121	12963	0.0196	0.5926	0.3143
SumSq						0.0661	
α						2.79E-02	
ε						-0.6841	

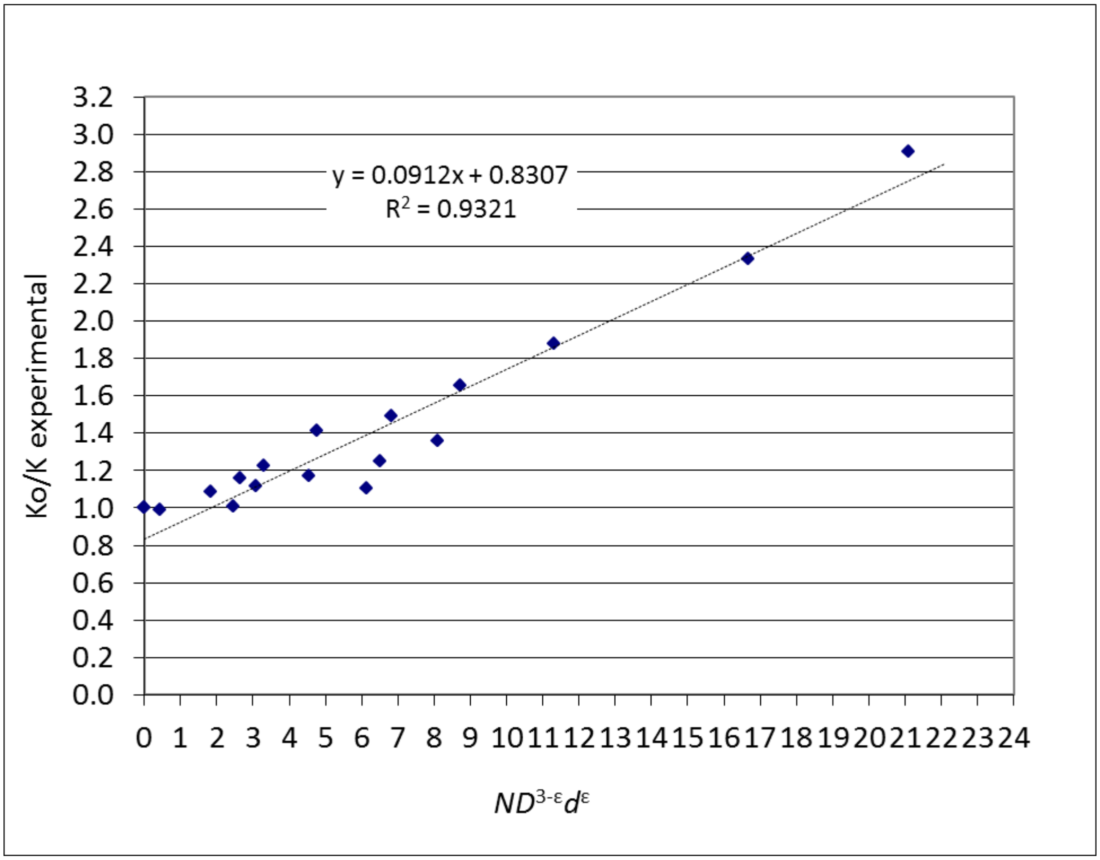

Figure 4-17 Ko/K **vs** $N \quad D^{3-\varepsilon}d^{\varepsilon}$

4.5. Discussion

Plots of Q_{20} vs i presented in Figure 4-5 and Figure 4-7 confirm that the experiments were performed under conditions where Darcy's law is valid, i.e. laminar flow; correlation coefficients $R^2 > 0.99$. Only sample 9 showed a lower R^2 of 0.9620 but still indicates agreement with Darcy's law.

In Figure 4-6 and Figure 4-8 linear regressions of Q_{20} vs i plots were included. The slope of the plots decreases at greater *RS* and *VC*. The reduction in the slope demonstrates a progressive decrease in the hydraulic conductivity which can be further appreciated in the results summarised in Table 4-3 and Table 4-4. The reduction in the hydraulic conductivity with the increase in *RS* and *VC* is clear. For example, specimens at 40%*VC* displayed reductions in the hydraulic conductivity of 18.51, 26.45, 39.53 and 65.64 % for *RS* of 3.8, 6.3, 15 and 25 respectively. Specimens where *RS* was kept constant at 25 exhibited a reduction in the hydraulic conductivity of 9.48, 46.82, 57.11 and 65.64% for VC of 10, 20, 30 and 40% respectively. The maximum reduction in the hydraulic conductivity during this study was 65.64% for the specimen with the highest *VC* and *RS*, i.e. the hydraulic conductivity was reduced to one third with the inclusion of 40%*VC* of 2D particles with a *RS* of 25. These results are comparable in magnitude to those reported by Xie et al. (2006) albeit under the very different conditions used during this study. Xie et al. (2006) used smaller content of larger 2D particles, i.e. 1% by mass of particles approximately 10k the size of the matrix particles.

Reductions in the hydraulic conductivity caused by the intrusion of 2D particles from this study were in all cases of less than one order of magnitude (i.e. a maximum reduction of 65.64%). This contrasts with the results reported by Beaven and Powrie (1995) where decay in the hydraulic conductivity with the increase in the stress level was of several orders of magnitude. These results indicate that although the stress level determines the order of magnitude of the hydraulic conductivity, the content and size of 2D materials play a role in controlling the figure taken by the hydraulic conductivity within the order of magnitude determined by the stress level.

The effect of *VC* and *RS* can be further studied using Figure 4-9. The graph shows three regions according to their percentage of decrease in the hydraulic conductivity. A limit definition to discriminate between conditions (i.e. *VC* and *RS*) that cause significant changes in the hydraulic conductivity from those that do not was necessary. References to back up the limit selection were not available. For example, although Xie et al. (2006) reported reductions in the hydraulic conductivity from the intrusion of 2D particles to a matrix of solid waste, their experiments were not systematically performed to report changes in *K* over a range of conditions and identify those that caused significant changes. Thus, the limit was defined using the experience gained during this research. First, the results during this research showed changes in the hydraulic conductivity within one order of magnitude.

Therefore, the definition of significance in the decrease of *K* needed to be placed in the range between 0 and 100%. A division of the range in thirds was judged appropriated. The first third, i.e. decrease from 0 to approximately 30%, could probably be considered as insignificant and be explained through experimental errors arisen during measuring the hydraulic conductivity, e.g. temperature, piezometer level variations, air accumulation, etc. (Daniel, 1993). However, a decrease in the hydraulic conductivity over 30% could probably not be explained from experimental errors and rather result from differences in the structure of the specimen tested. Then, a decrease in the hydraulic conductivity of more than 30% was selected as the limit.

Region 1, for $VC \leq 10$ or 3.8% dry mass, where regardless the *RS* there is not effect on the hydraulic conductivity, i.e. reduction always < 10%. Region 2, 10< *VC*< 20 or 3.8-7.3% dry mass, where the effect on *K*/*Ko* is not clear as specimens with intermediate *VC*s were not tested. And region 3 for $20 \leq VC \leq 40$, where *K*/*Ko* decreases with *VC* following linear relationships with $R^2 > 0.98$. In region 3, if a reduction of 30% in *K*/*Ko* is considered significant, i.e. 0.7, then the conditions where significant changes in the hydraulic conductivity begin can be identified. The maximum reduction in hydraulic conductivity observed in specimens with $RS \leq 6.3$ was 26.45% which may be regarded as insignificant. For the group of specimens with *RS* equal to 15, the hydraulic conductivity was reduced to approximately 30% at a *VC* of 20%. These conditions can be regarded as the critical point where significant reduction in the hydraulic conductivity occurred. These results suggest that additions of less than 7.3% dry mass of 2D particles with *RS* < 15 will not affect the hydraulic conductivity. Whilst, additions of more than 7.3% dry mass of 2D particles with $RS \geq 15$ will cause a reduction in the hydraulic conductivity greater than 30%. This information can be used as an indication of the expected reduction in the hydraulic conductivity for waste materials knowing the mass content of 2D components, i.e. plastics, textiles and paper, and their size relative to the matrix particles.

Figure 4-10 shows the linear relationship between RS and K/Ko when VC is kept constant. For VC equal to 10, K/Ko remains constant regardless RS. For $20 \leq VC \leq 40$, $R^2 > 0.99$ and the slope experienced a smooth but progressive increase with VC. For 20%VC, the slope of the plot was -0.0192 which indicates that one unit increase in RS would cause a decrease of 1.92% in the hydraulic conductivity. For 40%VC the slope of -0.0213 indicates a decrease of 2.13% in the hydraulic conductivity with every unit of increase in RS.

The impact of VC on the void ratio was investigated in Figure 4-11. The plot evidences a general decrease in void ratio at higher VC. The magnitude of the reduction is more market at higher RS. Specimens with RS of 3.8 and 6.3 showed a constant void ratio over the investigated VC range. Specimens with RS 15 and 25 had their void ratios reduced by 38 and 45% respectively when VC was increased from 0 to 40%. These results suggest that the intrusion of 2D particles creates a medium with better packing properties, denser structures and smaller void ratios. This agrees with the results of Lee et al. (2007), who found that 2D particles enforce ordering of the grains that fall on their surface and hence result in denser arrangements. In the current research, as 2D particles were distributed in the specimen, a large number of flat surfaces were available to order sand grains. At higher VC, more particles were available which increased the effect. Also, with more 2D particles the effect of bridging in the underneath particles could have been also minimised.

This shows that the reduction in the hydraulic conductivity caused by large 2D particles ($RS \geq 15$) at contents over 7.3% dry mass ($VC \geq 20$) is the result of two factors. Modification of flow paths: permeable and impermeable materials divert and impede flow respectively (see Figure 3-1). Decrease in the void ratio: order enforced by the presence of flat surfaces (see Figure 4-2). During this research, the two factors acted in a complementary fashion to affect the hydraulic conductivity and although efforts were made to isolate one from the other, this proved to be experimentally unachievable given the inherent physical ordering enforced by the flat surfaces. The decrease in K/Ko with VC and RS follows clear linear relationships, i.e. $R^2 > 0.98$ and 0.99 respectively, which indicate the linear influence of VC and RS on K/Ko. The relationship between K/Ko and void ratio is less clear, i.e. $R^2 < 0.89$ for linear fitting, and needs further research.

The evaluation of the analogous model proposed by Maxwell (1954) showed good agreement with experimental data (see Figure 4-16). This suggests that the use of the Maxwell (1954) model and its simplified version for impermeable intruded spheres (Equation 4-16), originally developed for a system of embedded spheres, adequately captures the impact on the permeability of a granular media with embedded 2D particles.

In the Maxwell (1954) model, K/Ko depends on a single parameter p that measures the proportion by volume of the embedded particles. The model was evaluated by means of the sum of the square differences between the experimental and modelling results ($SumSq$ in Table 4-5) and by linear regression of a plot K/Ko experimental vs K/Ko model (Figure 4-16). The p model showed agreement with the experimental results with a $SumSq$ 0.0661 and R^2 0.8917. Further information can be obtained from Figure 4-17 where K/Ko experimental was plotted against $ND^{3-\varepsilon}d^{\varepsilon}$. A linear regression of the data set excluding points where K/Ko equal 1 gave a regression coefficient R^2 of 0.9321. This suggests that K/Ko can be expressed as a linear function of $ND^{3-\varepsilon}d^{\varepsilon}$ according to Equation 4-26:

$$\frac{K_0}{K} = \begin{cases} 1 & N = 0 \\ 1 + \alpha\cdot(ND^{3-\varepsilon}d^{\varepsilon} + \beta) & N > 0 \end{cases} \qquad \text{Equation 4-27}$$

Equation 4-26 agrees with Equation 4-26, which resulted from expanding the Taylor series of the simplified Maxwell (1954) model for impermeable spheres. A recommended area for future research is the application to solid waste of the mathematical equations developed in the context of composites (Fredrickson and Bicerano, 1999, Nielsen, 1967). This could enhance further our understanding of the parameters that control the decrease in the hydraulic conductivity evidenced during the research described along this chapter and that results from the presence of flat particles in solid residues.

4.6. Summary

In solid wastes, materials such as flexible and rigid plastics, paper, textiles, metals and glass can be classified as 2D. Overall 2D materials constitute a significant percentage in solid wastes, i.e. up to 30% dry mass, as discussed in Chapter 3. Although some researchers have argued that 2D particles can affect fluid flow properties of landfill waste (Xie et al., 2006, Velkushanova et al., 2009), characterisation of the geometry of the particles in solid waste and the impact on fluid flow remains an unexplored area of research.

Analysis of the permeameter tests discussed in this chapter provide a systematic study on the impact of 2D particles on hydraulic conductivity. Specimens comprising Leighton Buzzard sand (matrix) and plastic discs (2D particles) were used as analogues to investigate changes in the hydraulic conductivity of a media systematically altered by plastic 2D particles. The study evidenced the effect of the inclusion of 2D particles in reducing hydraulic conductivity by a factor that depends on the relative content and size of the particles, but that is always within one order of magnitude. Two parameters were examined over ranges that are representative of solid wastes: the relative size (*RS*, 0-25) and relative volumetric content (*VC*, 0-40%). The results showed that:

- Low content of 2D particles, i.e. *VC* < 20% = 7.34% dry mass, even with a *RS* several times the surrounding matrix, did not have a significant effect on the hydraulic conductivity, i.e. reduction < 30% was observed.
- Reductions in the hydraulic conductivity of more than 30% started at *RS* 15 and *VC* 20%, conditions that were considered as the critical point where significant changes in the hydraulic conductivity started to be evident.

- The maximum reduction in K of ≈ 65% was observed in the specimen with the highest content of the largest 2D particles, i.e. *RS* 25 and *VC* 40%.
- For $VC \geq 20\%$, the hydraulic conductivity decreased by approximately 2% for each unit of increase in the *RS*. This suggests that the intrusion of 2D particles with dimensions 5 times greater than the surrounding matrix will produce a decrease of approximate 10% in the hydraulic conductivity. Consequently, a reduction in $K \geq 30\%$ would be caused by particles at least 15 times larger than the size of the particles of the surrounding matrix.
- The void ratio was progressively reduced with the increase in *RS* and *VC* of the 2D particles. The net effect of 2D particles on the hydraulic conductivity is the result of their simultaneous potential to divert flow and change the packing/structure properties of the system.
- The behaviour of K/Ko was well explained by an analogous model proposed by Maxwell (1954) for conduction through an heterogeneous media modified with embedded spheres. For impermeable spheres, the model expresses K/Ko as a simple linear function of the non-dimensional parameter p which measures the content per volume and the relative size of 2D particles in a single term. The use of this simplified model allowed the characterisation of the geometrical properties of the media using the variable under investigation.

Velkushanova et al. (2009), described a framework in which 2D particles are classified as potentially flow diverting or impeding if they are at least 5 times larger than the size of the particles in the matrix. This framework does not consider the relative content as criterion for classification. Based on the results discussed in this chapter this definition needs adjustment as 2D materials may be considered as flow diverting if they are 15 times larger the surrounding matrix and constitute at least 7.3% (by dry mass) of the solid waste. eExperiments were not carried on semi-permeable materials and thus do not provide the necessary criteria to classify 2D materials as flow impeding.

The results highlight the important role 2D particles have in fluid flow processes and give a reasonable indication of the magnitude of changes expected in the hydraulic conductivity arising from the presence of 2D materials in landfilled waste. Similar experiments using solid waste are required to validate these findings and gain further understanding in a more heterogeneous and highly degradable porous media.

5. The study of preferential flow paths and the structure of MSW

The study discussed in Chapter 4 showed that the inclusion of 2D particles reduces the hydraulic conductivity by a factor that depends on the relative content and size of the particles. This is probably not the only effect that 2D particles have on fluid flow processes. Research in columns packed with elongated particles suggest the formation of longer flow paths than those formed in columns with spherical particles (Donohue and Wensrich, 2008, Donohue and Wensrich, 2009). Research by Xie et al. (2006) indicates that 2D particles can divert flow paths and increase flow tortuosity. Investigations at laboratory scale in columns filled with solid waste indicate the presence of preferential flow paths (Korfiatis, 1984, Zeiss and Major, 1992, Bendz and Singh, 1999, Johnson et al., 2001) and anisotropy in the hydraulic conductivity (Hudson, 2007). These studies taken together suggest that 2D particles can change the structure of the solid waste leading to favoured flow through some paths.

This chapter discusses:

1. the presence of preferential flow paths in solid wastes
2. the role played by 2D particles in preferential flow and
3. the characteristics of the structure created in solid wastes as the result of the presence of 2D particles

based on a case of study in which dye-tracing, invasive (thin sectioning) and non–invasive methods (μCT) were explored to visualize flow routes and investigate the structure developed in an undisturbed specimen of MSW.

A review of the background in structure of porous media and methods for the study of structure is the subject of Section 5.1. Research of the structure developed in porous media in the presence of modifying materials and the theoretical concepts developed around them is discussed in Section 5.1.1. Section 5.1.1 also discusses the characteristics of the structure in solid wastes. Methods for the investigation of the structure and preferential flow phenomena in porous media are covered in Sections 5.1.2 and 5.1.3.

Section 5.2 describes materials and methods with special emphasis on the procedure designed to preserve the structure of the specimen during the study. The specimen under investigation was obtained from a core sample of degraded MSW which was previously characterised and results examined in Chapters 2 and 3. Sections 5.3 and 5.4 present the results from this study and their implications.

5.1. Background

5.1.1. The structure of solid wastes and analogue porous media

Little research has been done on the structure that develops once solid waste is landfilled. Yet, it is recognized that like geological materials and as a result of the deposition in progressive layers, compaction and heterogeneity, MSW develops a strong (Dixon and Jones, 2005), layered (Rees-White, 2004) and anisotropic structure (Hudson, 2007). It is also accepted that plastics and textiles, due to their flat shape, tensile strength and orientation, can enhance the strength (Kölsch, 1995, Dixon et al., 2008, Fernando et al., 2009), and has been argued that they could also influence flow behavior by diverting fluid flow (Xie et al., 2006, Velkushanova et al., 2009). Additionally, as degradation progresses and in common with other organic materials, e.g. organic soils and peat (Rezanezhad et al., 2010, Kettridge and Binley, 2011), changes in the waste structure can be expected (White and Beaven, 2008). Another aspect to consider is that the introduction of the European Landfill Directive has produced a new type of MBT wastes that will develop a different structure in landfills (Powrie et al., 2007)

Our detailed understanding of the structure that develops once solid waste is placed into landfills, and how the structure affects fluid flow is very limited. An insight into the characteristics of the structure that develops in porous media and in the theoretical concepts developed around them can assist increasing this understanding. For this purpose, the Carman-Kozeny model is discussed in Section 5.1.1.1 which introduces the tortousity factor to describe the increase in flow path lengths in porous media. In Section 5.1.1.2, a study in columns packed with fibrous particles illustrates the impact in the tortuosity factor with the inclusion of fibrous materials. Section 5.1.1.3 examines the structure of solid wastes and some implications on the light of previous sections. Section 5.1.2 reviews the invasive methods (e.g. dye tracing, thin section) for the study of structure in porous media whilst Section 5.1.3 the non-invasive technologies (e.g. μCT).

5.1.1.1. Carman-Kozeny model

The Carman-Kozeny model conceptualises porous media as a network of interconnected conduits. The model assumes that a hypothetical fluid particle, flowing with a velocity v covers a path length *L* in the same time as an actual fluid particle, flowing with velocity v_P, covers an average effective path length *Le* (see Figure 5-1).

Inflow rate *Q* can be expressed in terms of both ν and ν_p as expressed in Equation 5-1. ν is the velocity of an hypothetical particle moving through a straight path and ν_p is the velocity of an actual particle moving through a tortuous path as:

$$Q = vA = v_p a \qquad \text{Equation 5-1}$$

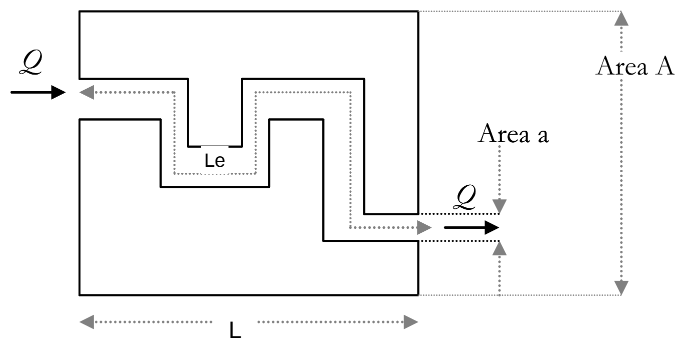

Le= effective path length

Figure 5-1 Illustration of the conceptualised porous media in Carman- Kozeny model (adapted from Dullien, 1992)

The porosity of the medium *n* can be expressed according to Equation 5-2 where *Le* is the tortuous path and *L* is the shortest distance or straight flow path. Replacing Equation 5-2 in Equation 5-1 gives an expression for v_p in terms of the ratio *Le/L* , the tortuosity factor, a concept that describes the structure of the pore space (see Equation 5 3).

$$n = \frac{aLe}{AL}$$ Equation 5-2

$$v_p = \frac{v}{n}\left(\frac{Le}{L}\right)$$ Equation 5-3

Le is larger than *L* and the difference depends on the structure of the media. For example, flow paths across uniform materials tend to be shorter and have lower tortuosity factors than those for well graded materials, where smaller grains can fill the larger voids (Fetter, 1999, Dullien, 1992). This suggests that heterogeneity increases the tortuosity of the flow paths.

The Carman-Kozeny model developed an expression for *K*. In the derivation ν_p is calculated according to the Hagen-Poiseuille equation for flow through small pipes. The derivation resulted in Equation 5-4 where k_0 is a shape factor and *So* the specific area. The sub-index CK refers to the Carman-Kozeny model. A full explanation of the equation can be found in Dullien (1992).

$$K_{CK} = \frac{n^3}{k_0 \mu S_o{}^2 (1-n)^2} \left(\frac{L}{Le} \right)^2 \qquad \text{Equation 5-4}$$

5.1.1.2. Implications of Carman-Kozeny model

After the definition of the tortuosity factor in the Carman-Kozeny model, a porous medium is referred as tortuous to express the fact that fluid paths differ from straight lines. Evidence suggests that heterogeneity increases the tortuosity (Fetter, 1999, Dullien, 1992). It is recognised that the presence of 1D, 2D and 3D particles increases the heterogeneity of the medium (White and Walton, 1937, Santamarina and Cho, 2004). Thus, changes in the pore space structure, increase of flow paths length and of the tortuosity factor *Le/L* are expected. The magnitude of the affect would depend on the relative size, orientation, content and material composition of the particles. This is schematically represented for the case of 2D particles in Figure 5-2.

Donohue and Wensrich (2008) investigated the impact of fibrous materials on the tortuosity factor. Their research was developed using numerical modelling to create assemblages of fibres with aspect ratios (AR) in the range of 1 to 40. The pore space was modelled as a chain of spheres passing through the assemblage of fibres. The length of that chain was used as an indication of the length of the flow path. Their results showed that arrangements of fibres have greater tortuosities than those of spherical elements (e.g *Le/L* 1.5-2.8 vs 1.2). The highest tortuosities were observed in fibre arrangements with 5<AR<20. The minimum AR that caused a significant increase in the tortuosity was 5 (i.e. 25%) whilst fibres with AR of 20 caused the tortuosity to increase by 133%. They also observed that fibres with 5<AR<20 tend to orientate horizontally and create the longest void passages. The orientation of fibres with AR>20 differed from the horizontal axis and created arrangements less efficiently packed with lower tortuosities (≈1.5).

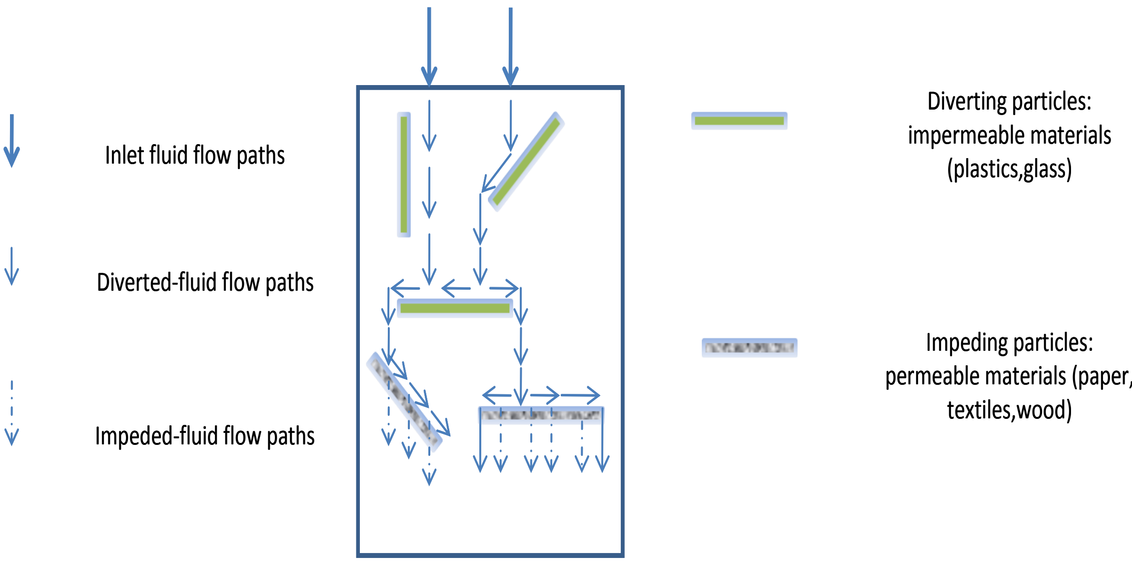

Figure 5-2 Conceptual model to explain flow through landfilled waste (adapted from thin sheet model Xie et al., 2006)

Results for fibrous materials, although best conceptualised as 1D and 3D particles, give an indication of the effect that 2D particles could have on the tortuosity of a porous medium. Findings by Donohue and Wensrich (2008) suggest that in solid wastes, 2D particles could increase the medium tortuosity by a magnitude that would depend on their relative size.

5.1.1.3. Evidence of the structure of solid wastes and preferential flow

Results by Donohue and Wensrich (2008) suggest that impermeable 2D particles in landfilled waste could divert fluid flow, extend flow paths and consequently increase flow tortuosity. Their results also suggest that if the particles are horizontally oriented, i.e. perpendicular to the direction of flow, the longer they are the greater the impact on the tortuosity. Placement methods during landfilling favour the horizontal orientation of materials. This has been observed during field excavations by Rees-White (2004), at laboratory scale by Caicedo et al. (2010) and suggested as the reason for the anisotropy in the hydraulic conductivity by Hudson (2007).

Whilst investigating the ineffectiveness of leachate extraction wells in a landfill site in the UK, Rees-White (2004) led a site excavation which exposed a series of waste profiles. Some of the images of the exposed profiles taken during the study are presented in Annex 5-2. The images evidence the layered structure where each compacted layer of waste is followed by a layer of daily cover material. The excavation revealed that the wells were in good condition and that there was no serious microbial growth that could be causing well clogging. Thus, a different explanation for the ineffectiveness of the leachate extraction wells was necessary and the layered structure, which favours horizontal flow paths, was argued as the most likely reason.

The anisotropy in the hydraulic conductivity of solid wastes was studied by Hudson (2007) by measuring the vertical and horizontal hydraulic conductivity in fresh and old MSW and finding the horizontal hydraulic conductivity between five to ten times greater than the vertical. Hudson (2007) argued that was the result of the layered structure produced by the presence of horizontally oriented elongated components. Hudson et al.(2010) studied the horizontal spreading characteristics of a 40 year old MSW. In that study water was injected on the centre top of the waste sample and collected at the bottom through a segmented basal collector system. Experiments were performed at different flow rates under unsaturated conditions. Their results showed that horizontal dispersion was significant and increased with flow rate (e.g. 42.9% for 5.94 l/h vs 14% for 0.57 l/h).

The evidence provided by Hudson (2007) and Hudson et al.(2010) indicates that horizontal flow paths in solid waste may be more prevalent than those in the vertical direction. When water is injected at one single point, the nearest flow channels become saturated and the excess of water moves laterally until it encounters adjacent unsaturated vertical paths before moving downwards. This favours the presence of preferential flow paths (phenomena further discussed in Section 5.1.2). Experimental work in columns packed with solid waste has indicated the presence of channelling flow in fresh MSW, usually by measuring moisture contents and the distribution of flow at the discharge of waste packed columns (Zeiss and Major, 1992, Korfiatis et al., 1984). In other studies also using fresh MSW, tracer tests have revealed the presence of stagnant zones and flow channelling, indicating the presence of preferential flow phenomena (Johnson et al., 2001, Bendz and Singh, 1999).

Recirculation of liquids required for the remediation of landfill sites, is therefore expected to be influenced by the layered and anisotropic structure of solid wastes and by the presence of preferential flow. However, experimental evidence at both laboratory and field scale is still limited. There is particularly a lack of studies that can be used to describe old deposits where the presence of preferential flow had been related to waste characteristics. Also, there are limited studies comparing the impact of different injection methods on preferential flow phenomenon. Moreover, the impact of pre-treated materials (i.e. MBT waste) on the structure and the presence of channelling and preferential flow in landfills has only seen a limited number of studies (Fernando et al., 2009). Research discussed in this chapter provides some evidence to address these gaps.

5.1.2. The use of invasive methods for the study of preferential flow and the structure in porous media

Given that the number of studies of structure and preferential flow in solid wastes is limited, so is the knowledge of the most appropriate methods to investigate flow for porous media of this type. The purpose of this and following sections is to discuss the different methods, as well as their principles and applications.

The study of the structure of porous media has been traditionally approached using indirect invasive methods such as field observations (Beven and Germann, 1982, Shipitalo et al., 2004); laboratory analysis of cores by thin sectioning, resin impregnation and imaging (Mooney and Morris, 2008, Flury et al., 1994); indirect analysis using tracer injection breakthrough curves from fluid flow experiments (Mooney and Morris, 2008) and observation of flow path patterns revealed by dye staining (Flury et al., 1994, Morris and Mooney, 2004).

Of special interest for the study of fluid flow and transport process in porous systems is the presence of preferential routes or flow pathways. This type of phenomenon is commonly referred as preferential flow and is used to describe flow mechanisms where transport of water, as well as dissolved and suspended matter, are primarily associated with a smaller fraction of the total pore space. Field measurement of mass movement of liquids and gases in soils often shows faster transport than is predicted from mathematical modelling, a phenomenon that has been frequently associated with preferential flow occurring through macro-pores (e.g. earthworm burrows and cracks), or caused by soil layering or hydrophobicity (Beven and Germann, 1982, Allaire et al., 2009).

The study of preferential flow mechanisms in natural and semi-natural systems has gained attention during recent decades due to its incidence in physical processes with high environmental and human health implications. In soils, preferential routes may accelerate or delay the movement of dissolved matter and contaminants. Faster transport of contaminants to groundwater sources reduces the contact time with chemically reactive soil layers (Morris and Mooney, 2004, Flury et al., 1994).

Diverse techniques ranging from the observation of structures likely to lead to preferential flow (Garner, 1953, Munyankusi et al., 1994, Beven and Germann, 1982, Shipitalo et al., 2004, Mooney et al., 2006) to the use of tracers breakthrough curves (Mooney and Morris, 2008) and dyes to visualise flow paths (Lipsius and Mooney, 2006, Van Ommen et al., 1988, Andreini and Steenhuis, 1990, Flury et al., 1994, Weiler and Flühler, 2004, Hangen et al., 2004, Morris and Mooney, 2004) have been applied in preferential flow studies with soils and in other systems such as packed beds (Ravindra et al., 1997).

The observation of disturbing structures, i.e. cavities, fissures, in-homogeneities, can be achieved during field excavations by in situ inspection or in the laboratory. Careful selection of sampling methods is required to ensure negligible changes in the specimens original structure (Clayton et al., 1982). Specific steps during specimen preparation (e.g. thin sectioning and resin impregnation); depend on factors such as specimen nature, degree of detail expected and techniques availability (e.g. visual, microscopic or scanning).

In tracer studies, conservative substances (non-reactive, non-degradable and highly detectable) are used as surrogates to mimic the transport of water and other dissolved and suspended substances. Once applied, the tracer travels through the system and is characterized by monitoring its concentration in the effluent. The response curve so obtained is influenced by the flow behaviour and the medium structure. Different chemicals are used for this purpose. Ions such as Cl^- and Br^- are particularly good at tracing water movement; whereas dyes are generally considered suitable surrogates for contaminants (Flury et al., 1994).

Dyes are coloured substances highly soluble in the carrying solvent, properties that are exploited in preferential flow studies. As the solvent flows, dyes stain such contact areas and make the visual recognition of flow paths possible. Dyes are, due to their high sorption capacity, non-conservative (Ketelsen and Meyer-Windel, 1999, Germán-Heins and Flury, 2000) which has limited their use in breakthrough curves studies , where conventional tracers are used.

Of special interest in preferential flow studies are those dyes with high water solubility , such as Brilliant Blue (BB), which due to its high mobility, visibility and low toxicity has been extensively used to understand flow paths in soils studies (Andreini and Steenhuis, 1990). Visualisation, using image processing techniques, has allowed the qualitative description of dye spatial distribution (Flury et al., 1994). Some degree of quantification has also been achieved with the calibration of photograph colour using the amount of dye adsorbed (Morris and Mooney, 2004, Lipsius and Mooney, 2006). Further exploitation of dye patterns information to infer flow regimes was published by Weiler and Flühler (2004). In their study, texturally diverse soils (i.e. loam to sand) were infiltrated with Brilliant Blue at different irrigation rates and initial moisture conditions. Photographs taken of vertical and horizontal sections together with the analysis of the extent and distribution of the stained areas were used to classify flow types into those occurring only in the soil matrix and those occurring as the result of interactions between the soil matrix and macropores.

The use of dyes for preferential flow studies in solid wastes has not been reported. The current research used a dye for the visualisation of flow paths. This was considered a reasonable approach to learn about the fundaments of how 2D particles affect fluid flow. For example, diverted flow paths could be visually assessed with the stained paths created by the coloured dye.

The use of invasive techniques for the study of structure and preferential flow paths provide fundamental knowledge to understand better the impact of macro-structural features of porous media on flow phenomena. However, when a higher level of detail is necessary or when the specimen structure has to be carefully preserved, non-invasive methods are a better option.

5.1.3. Non-invasive methods for the study of structure

The acquisition of images using non-invasive techniques is faster and causes far less disturbance than progressive thin sectioning. Non-invasive techniques are based on the principle that the properties of the internal structure of a specimen can be inferred from the detection of a signal, passed through the specimen. These techniques were originally developed for diagnostic medicine and have enabled the non-invasive study of the human body. In recent decades increased availability has led to the use of these techniques for research purposes in areas such as archaeology, palaeontology, petro-physics, geology and materials engineering.

Physical properties of the signal used vary between non-invasive technologies and include X-rays in Computed Tomography (CT), Magnetic fields in Magnetic Resonance Imaging and gamma rays in Positron Emission Tomography. Since the response of a particular material is dependent on the signal type, selection of the appropriate technique requires careful consideration of the type of material being investigated. The use of non-invasive methods for the study of the structure of solid waste is still very limited. However, research by Watson et al. (2006) and (2007) suggests that solid waste is suited to examination using CT. During the research discussed in this chapter, a locally available microfocus-CT (μCT) equipment was used.

CT has been successfully used in porous media research since the early 1990s, and has revealed highly detailed information on both the structure and the pore space architecture, improving our understanding of fluid flow (Heijs et al., 1995, Amos et al., 1996) and other porous medium interaction processes (Sato and Suzuki, 2003, Kettridge and Binley, 2008). A review of the principles of CT and applications in porous media follow in the next sections.

5.1.3.1. Principles of X-Ray Computed Tomography

CT is a radiographic method that uses X-rays for digitally cutting a specimen to reveal its interior details. X-rays are high energy electromagnetic waves produced inside X-ray vacuum systems, where a cathode is heated to produce electrons which are accelerated by a high voltage to a rotating anode which typically re-radiates less than 1% of the electron energy in the form of X-rays (Pope. J.A., 1999). This process establishes a flow of X-rays with wavelengths in the range 0.01 to 10 nm.

CT scanners work by emitting a cone of X-rays, which pass through the object of interest to one or more detectors. In μCT, the object is rotated in relation to the X-ray source to create a series of two dimensional images which can then be computationally assembled into a three dimensional object.

A detector measures X-ray intensity before the beam enters the object and after it passes through it, and using the Beer-Lambert law (Equation 5-5) calculates μ, the linear X-ray attenuation coefficient for the material being scanned. I_0 and $I_{(x)}$ are the initial and transmitted beam intensities respectively and x the length of the x-ray path through the material. If the scanned medium is inhomogeneous, the intensity is expressed as shown in Equation 5-6:

$$I_{(x)} = I_O e^{(-\mu x)}$$ Equation 5-5

$$I_{(x,y)} = I_{(0,0)} e^{\left(-\int_{(0,0)}^{(x,y)} \mu(x,y)\,dl\right)}$$ Equation 5-6

In Equation 5-6, μ is the unknown variable constrained by many equations for each point along each X-ray path. Image reconstruction consists of finding values for μ that provide solutions to these equations (Brooks et al., 1981, Denison and Carlson, 1997). The most commonly used reconstruction algorithm, known as filtered back projection, was invented by Allan Cormack who shared the 1979 Nobel Prize for Medicine and Physiology with Godfrey Hounsfield inventor of the CT scanner and relates the measured projection data to the two-dimensional Fourier transform of the object cross section. Once reconstructed, objects can be visualized in 2D and 3D and features qualitatively or quantitatively assessed using various image processing software packages available both free and commercially (Kak and Slaney, 1988).

Attenuation of the X-rays is caused by beam – matter interactions, primarily Compton scattering and photoelectric absorption, both of which are strongly dependent on the density of the absorbing medium, the atomic number and the energy of the incoming X-ray beam (ASTM 1441-00, 2005). Mathematical functions to describe the relationship between physical properties of the matter and the attenuation of X-rays have been extensively discussed (Denison and Carlson, 1997, McCullough, 1975, Brooks, 1977) and approximate equations have been proposed. Equation 5-7 is an example, where ρ is the electron density (related to mass density by the number of atomic units per electron), Z is the effective atomic number and E is the energy of the incoming X-ray beam. The relationship shows that μ is directly proportional to the electron density of the material (ASTM 1441-00, 2005).

Differentiation of features within a specimen is therefore possible because at each point, μ depends directly on the material properties (Brooks et al., 1981, Denison and Carlson, 1997).

$$\mu(x, y) = \rho\left(a + \frac{bZ^{3.8}}{E^{3.2}}\right) \qquad \text{Equation 5-7}$$

Images obtained from CT are monochromatic representations of the spatial distribution of μ where the grey shade represents intensity. Images are conventionally mapped so that brighter regions correspond to those volume elements (voxels) with higher μ values. The format selected for storing the image controls the number of levels in the grey scale range, e.g. in 8 bit, the grey level has values in the range 0-255.

Medical CT scanning applications can successfully image metre sized objects with millimetre scale resolutions. Demand for higher resolution tomography in denser and smaller objects eventually led to the development of μCT which scans millimetre sized objects at 1-10 μm resolution. The physical principles that control CT and μCT are the same. With decreasing size, radiography becomes more difficult as the specimen must absorb a sufficient portion of the incident beam to produce a measurable signal, which in a small specimen demands high attenuation per unit length, a condition that is only satisfied at low X-ray energies which are insufficient to penetrate dense objects. Precisely focused beams are also required to minimize blurring of fine details (Dunsmuir et al., 1991). These difficulties were successfully addressed by D'Amico et al. (1992) with the development of a microfocus X-ray source which forms the basis of μCT. In μCT, X-rays are first highly collimated to achieve beam focus on the anode of only few micrometres diameter.

5.1.3.2. Image processing principles

Once images are reconstructed, imaging processing takes place. This process follows the same principles as for images obtained with digital cameras and other imaging sources. The first step is the recognition and digital correction of noise or artefacts. Noise is defined as the random variation of the grey value not present in the object imaged; whilst artefacts refer to anything in the image that does not correspond to a physical feature in the test object (ASTM 1441-00, 2005). Minimization of noise and artefacts is addressed through the mathematical transformation of images for which a wide range of algorithms are available according to the specific situation (Kak and Slaney, 1988). Digital enhancement of contrast, defined as the extent to which a parameter of interest differs for a set of features, is also used to ease the subsequent steps in the image processing sequence: segmentation and feature extraction.

In segmentation, images are subdivided into a number of uniformly homogeneous regions. The segmented image is therefore defined by a set of connected regions, so that each voxel in a segment acquires a unique region property. The set of properties includes grey levels, contrast, spectral values, or textural properties (Acharya and Ray, 2005a). Segmentation algorithms are based on one of the two basic properties of grey-level-values discontinuity and similarity among the pixels. In the first category, the image is partitioned based on abrupt changes in grey level. Whilst in the second, the partition is based on the similarity among the pixels within a region. The well-established segmentation techniques include: histogram-based thresholding, region growing, region splitting and merging and clustering or classification (Acharya and Ray, 2005a). The next step in the feature extraction aims to recognize the segmented object. A set of objects possessing similar features are said to belong to a certain pattern class. There are many types of features and each feature has a specific technique for measurement (Acharya and Ray, 2005b).

5.1.3.3. Applications of CT and μCT in porous media research

Following successful application in the medical field, CT rapidly gained popularity among those studying the structure of porous media in fields such as hydrogeology and geosciences. A vast number of references are available and comprehensive review papers within these fields are given by Ketcham & Carlson (2001); Allaire et al. (2009) and Werth et al. (2010).

Petroleum engineers pioneered the use of CT within geological sciences to characterise density, porosity, saturation and complex mineralogies in oil-reservoir rocks, imaging fluid flow patterns and studying rock mechanics (Wellington and Vinegar, 1987, Withjack, 1988). Scientists from a diverse range of porous media research areas then found medical CT a feasible method for studying, with a high level of detail, density and water distributions (Withjack, 1988, Amos et al., 1996); solid matrix structure (Kettridge and Binley, 2008) ; pore space structure (Mooney et al., 2006, Peyton et al., 1992, Heijs et al., 1995, Perret et al., 2003) ; soil interaction (Mooney et al., 2006, Kettridge and Binley, 2008) and flow transport processes (Anderson et al., 1992)

The use of μCT was introduced in geosciences by petrologists interested in studying pore interconnectivity and geometry in rocks (Denison and Carlson, 1997, D'Amico et al., 1992, Beall et al., 1996, Denison et al., 1997). This was later extended to the study of the microstructure of bentonites (Sato and Suzuki, 2003), sediments (Gaillard et al., 2007) and organic soils (Kettridge and Binley, 2008). In recent years μCT has been used for the study of flow paths and to produce 3D morphological models for flow simulations using computational fluid dynamics methods (Chen et al., 2009, Grader et al., 2009). Combination of CT and μCT has gained popularity in petrophysics research. The complementary use of these two methods allows imaging at multiple scales that increases the precision of digital 3D representations. For example, low resolution images by CT guide decisions about location and size of higher resolution images to be obtained by μCT (Grader et al., 2009).

CT has seen limited use in the study of waste structure and fluid flow phenomena, with Watson et al. (2006) and Watson et al. (2007) being the only references identified at the time of writing. Watson et al. (2007) used medical CT to investigate the change in structure of the organic fraction of MSW as it degraded anaerobically over a period of two years. They found that CT scanning was able to show structural changes in the waste occurring over the period of degradation and that particle size was reduced over the same time. The use of μCT for the study of the structure in solid wastes was pioneered during this research.

Details for the development of a method to use for the study of the structure of waste analogues are published in Caicedo D et al. (2010) and Caicedo D et al.(2011). In this Chapter, the methodology was further extended for the study of the structure of a sample of MSW.

5.2. Methods and materials

5.2.1. Materials

The waste specimen used in this study corresponds to the MSW described and characterised in Chapter 2 and was used during the study of settlement processes in landfills by Ivanova et al. (2008). In that study, a purpose built consolidating anaerobic reactor (CAR) was used according to the design described by Parker et al. (1999). The reactor is a Perspex cylinder (935-mm height and 480-mm ID) with a loading system that applies a constant surcharge to the waste, which in this case was set at 50kPa. This load would be equivalent to a 5-m waste depth in a landfill if a 10 kN/m^3 bulk unit weight is assumed for the residue.

The sample was placed and degraded following a process that is representative of that occurring in landfill sites and which lead to the formation of highly structured materials (Dixon and Jones, 2005). The specimen served as a control sample as given in full by Ivanova (2007). Progressive layers of material were placed inside the CAR and highly compressed to 500-mm height. After placement, the sample was saturated using a prepared mineral media containing 10% of anaerobically digested sewage sludge to accelerate anaerobic digestion. Leachate was intermittently recirculated, however, as the purpose of the sample was to work as a control, it was initially acidified, and the degradation inhibited during the initial 345 days of the 919 days of total experimentation. A total settlement of 18.6% (350-mm final sample height), was reported as the result of consolidation and bio-degradation processes (Ivanova, 2007).

5.2.2. Methods

After settlement was completed, the opportunity was taken to investigate the structure and flow paths in the waste. Description of the methods developed for both studies follows. They are presented in the chronological order followed during the investigation.

5.2.2.1. Sampling

The sample was removed from the reactor, with every effort made to preserve the original structure. This step was of great importance since it is recognized that damage caused to the structure as a result of sampling may cause potential bias to structures favouring preferential flow. The core was extruded from the cell using a piston and then wrapped with cling film. Following extrusion, the core which was originally contained in the 480-mm Perspex cylinder, was 479-mm diameter over the upper part (300-mm height) and 487-mm over the bottom one (50-mm height), suggesting that the original structure was likely to have been reasonably well preserved.

5.2.2.2. Thin sectioning

The structure was investigated following a thin sectioning method developed to deconstruct the MSW specimen in slices of 80 mm thickness, and followed by analysis in μCT which produced 0.125 mm thickness digital slices. The thin sectioning involved cutting the specimen into vertical slices using a band saw. Initial trials revealed that horizontal slicing was relatively easy, but less so for in the vertical direction. This was because of the preferential horizontal orientation of many 2D materials contained within the waste sample, as was confirmed once the slices were produced. To achieve high quality cutting, the sample was covered with a plaster layer that once dried, created a strong yet easily cut protective layer that prevented any structural damage during the slicing process and facilitated core manipulation. The core was then cut horizontally at a height of 230 mm using an electric knife. This step had two purposes: to make the sample fit into the 300 mm throat of the band saw and preserve the bottom portion for the study of flow paths. The top portion was cut into 8 cm thick vertical slices using the band saw, which produced cleanly cut flat surfaces. A schematic representation of the cutting process is presented in Figure 5-3. Photographs of each exposed surface were taken as shown in Figure 5-7.

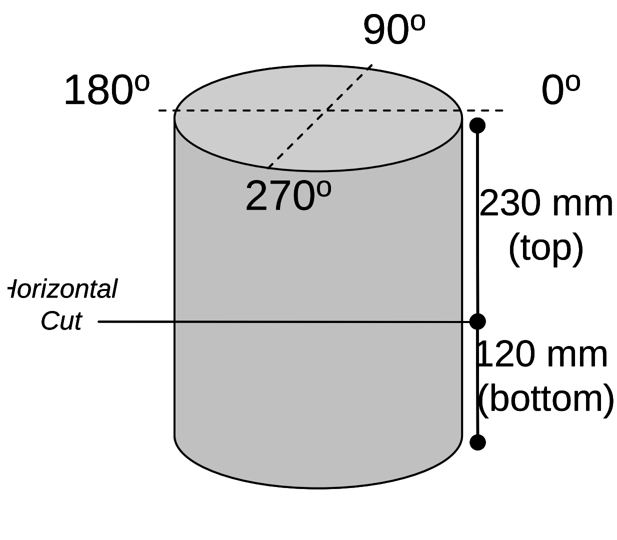

a. Initial core representation with imaginary reference points (dashed lines) and initial horizontal cut

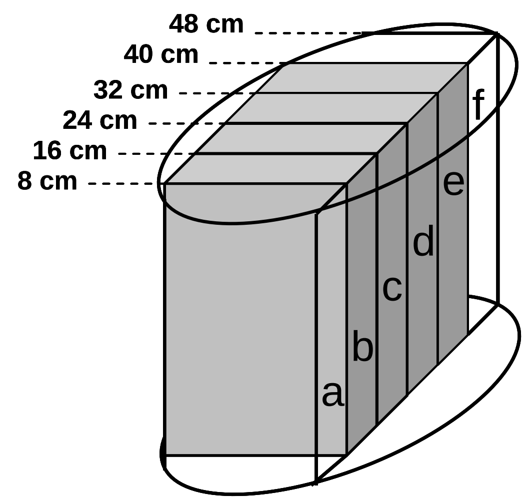

b. Thin sectioning carried out on the top subcore

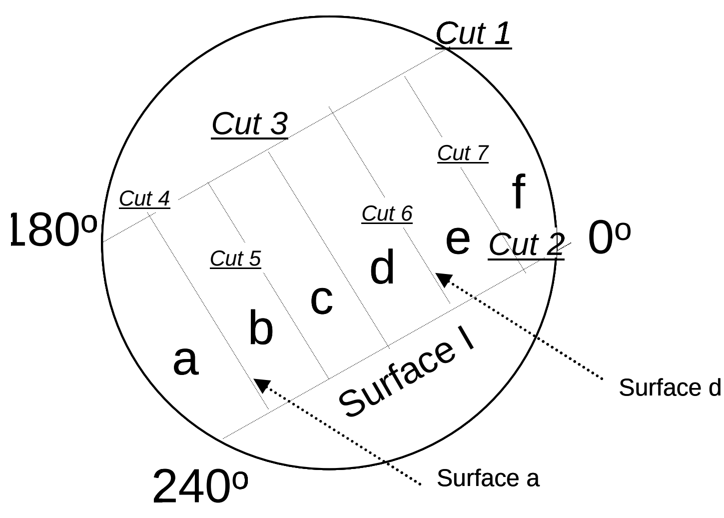

c. Cross sectional view of the thin sectioning process

Figure 5-3 Schematic representation of the cutting process during the study of preferential flow in specimen of MSW

5.2.2.3. Flow paths

Description of specimen

A block sample (310 x 320 x 120 mm) was produced from the remaining bottom portion of the sample as described in Section 5.2.2.2, by cutting it vertically with the band saw. No further horizontal slicing was necessary. Once cut, three of the exposed surfaces were covered with a plaster layer to preserve the structure during the test. The fourth face was left uncovered for visualisation of dye flow paths during the experiment. The bottom surface was carefully attached to a strong mesh (with a large aperture size of approx. 1 cm) to support the specimen whilst not causing major flow disruptions. The sample was mounted to permit the location of five concentric containers at the bottom, aligned with its centre, which allowed the collection and measurement of the outflow distribution. The experimental arrangement is schematised in Figure 5-5. The dimensions of each container and their areas are included, which are equivalent-when represented as percentage- to the percentage of the total flow that should occur for each region for conditions of uniform flow through the specimen.

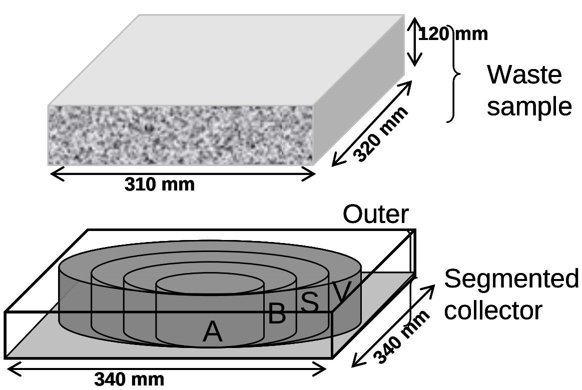

Sector	Diameter (cm)	Area of circle (m^2)	Sector area (m^2) [a]
A	6.3	0.0031	0.0031
B	12.2	0.0117	0.0086
S	22	0.0380	0.0263
V	31.5	0.0779	0.0399
Outer	na	na	0.0213

a. Corresponds to the effective area that collects volume.
Example, for B =0.0117-0.0031= 0.0086

Figure 5-4 Schematic representation of block sample used during the study of flow paths. Outflow was collected in concentric containers with the dimensions presented in the table

Description of tests

Flow paths were studied by two methods using only water first which was then replaced with a dye solution. The application of water was complemented with the quantification of the relative outflow collected in each container, which gave an indication of flow distribution. With the purpose of evaluating the effect of the injection method, water was initially applied through a single point to recreate a pulse injection event, and then evenly irrigated over an area on the specimen to recreate an irrigation event. A schematic representation of the experimental set up is presented in Figure 5-6.

For the pulse injection event, a needle connected to a peristaltic pump was located 5 cm above the centre of the specimen. A Watson Marlow 505S pump was operated at 3 rpm (Q 100 ml/min) and switched every 5 minutes from on to off mode. Outflow was reported once steady state was reached and measurements taken every 10 minutes, i.e. after the on/off cycle. The test was run for 40 minutes.

For the irrigation event, a rainfall simulator device, similar to the one used by Ravindra et al. (1997), was purpose built (by second author of Caicedo et al. (2010)). The device was made of a Perspex cylinder and a needles shower. The flow rate capacity, controlled by the liquid head in the cylinder, was in the range of 39 ml/min to 49 ml/min. A schematic representation of the rainfall simulator is presented in Figure 5-5. The irrigation test was run in two phases. First water alone, was irrigated at a rate of 43 ml/min, over a central circular area, I in Figure 5-6 (16-cm D), on the top of the waste surface, and until a steady state was reached, indicated by the measured flow rates in and out of the sample being the same after 60 minutes . Then, the supply of water was replaced by the dye solution and the test was run for a further 1 hour. Both, the total outflow and the concentric distribution were measured every 30 minutes.

Rain simulator

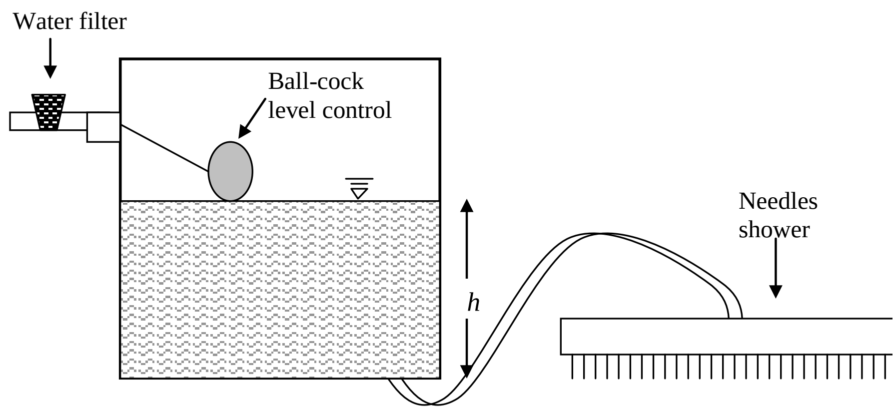

Figure 5-5 Schematic representation of rainfall simulator used during the investigation of flow paths

The dye used was an aqueous solution of Acid Blue 9 (also known as Brilliant Blue R), a commercially available food grade colorant (CAS No 3844-45-9). The dry colorant was supplied by Sigma Aldrich and a 1g/l aqueous solution prepared to irrigate the waste sample. This concentration, although less than those reported in the literature for soils (3 to 5 g/l; Flury and Flühler (1995); Germán-Heins and Flury (2000) and Mooney & Morris (2008)) provided a sufficient visual contrast with the waste matrix and was considered adequate for the test. The use of the rainfall simulator minimised bias during the dye application that could have favoured preferential infiltration of the dye solution. Photography's were taken during this part of the experiment to assist the visualisation of flow paths.

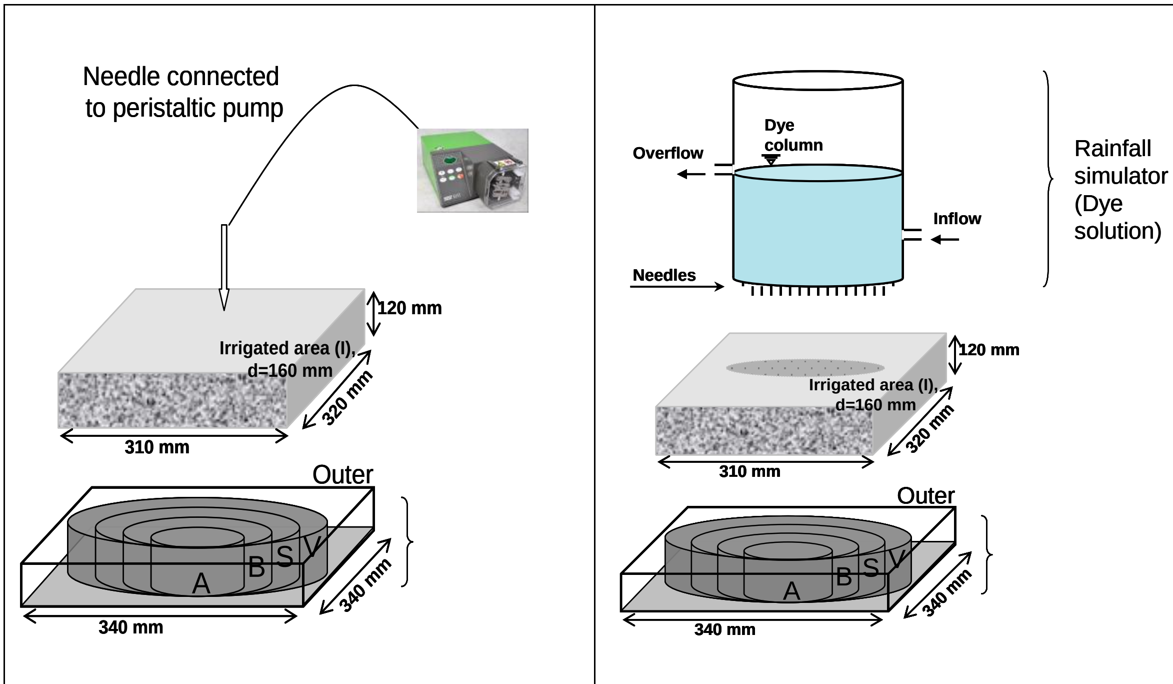

a. Injection point event: Pulse regime

b. Irrigation Event

Figure 5-6 Schematic representation of experimental set up for the study of flow paths. a-Injection point event, a needle connected to a peristaltic pump was used and b-Irrigation event , a rainfall simulator was used to irrigate a square sample obtained from the MSW specimen. Outflow was collected in concentric containers

Flow rates used during both the injection point and irrigation events correspond to unsaturated conditions. An estimation of the flow rate necessary for saturated conditions follows. $K_{saturated}$ was estimated using Powrie and Beaven (1999) values for crude household waste samples. MSW specimen was compressed under 50 kPa and its dry density calculated by Ivanova (2007) as 0.343 t/m^3. Powrie and Beaven (1999) reported $K_{saturated}$ between 1.5 x 10-4 and 1.9 x 10-5m/s for solid wastes under 87-kPa and dry density values ranging 0.32 – 0.39 t/m3. This indicates that $K_{saturated}$ for the MSW specimen should be in the order of 10-5 m/s. Using Darcy's equation (Equation 4-3 with i =1) gives $Q_{saturated}$ of 60 ml/min, and flow rates below that will therefore create unsaturated conditions.

For the case of the irrigation event, where the rainfall simulator was operated at 43 ml/min, $Q_{experimental}$ was approximately 30% less than $Q_{saturated}$. Whilst in the case of the injection point pulse event, the pump was operated at 100 ml/min in an on off mode (5 minutes each) which gives a $Q_{average}$ of 50 ml/min. Running the study under unsaturated conditions was considered a reasonable approach. First of all, given the existing regulations and concerns about groundwater contamination, operation of bioreactor landfills are likely to occur predominantly through the unsaturated zone (Environment Agency, 2009, Benson et al., 2007). Secondly, experiments reported by Hudson et al. (2010) on horizontal spreading were carried out under unsaturated conditions, thus equivalent conditions for the research described in this chapter were considered appropriated for comparison purposes.

5.2.2.4. μCT

The use of μCT during this research had two main purposes:

- To extend the investigation by thin sectioning and get a more detailed understanding of the structure of an specimen of solid waste by looking at aspects such as layering, distribution and orientation of flow diverting elements
- And to characterize in three dimensions the pore space of such specimen.

Layering, distribution and orientation of flow diverting elements were visually assessed and followed the same principles explained in section 5.2.2.2 for thin sectioning. However, μCT retrieved information based on 0.125 mm layers (i.e. voxel size) in contrast with the 80 mm layers by thin sectioning.

Characterisation of the pore space required scanning under conditions that produce images with a resolution to resolve details at the scale of pores, i.e. fraction of millimetres. This involved not only the selection of the right scanning parameters (e.g. distance from sample to panel detector) but also of the specimen size (i.e. the smaller the sample the higher the resolution). The specimen was selected from the slices produced by thin sectioning according to the process described in section 5.2.2.2. The slice d (see Figure 5-3), a cuboid of

210 x 210 x 80 mm, located in the central upper section of the MSW sample, was considered representative and chosen for this study.

The method followed in this study was similar to that detailed in Caicedo et al. (2011) which was developed for the μCT analysis of a specimen of MBT waste. The main aspects of the method are detailed in the next paragraphs.

The process started with the acquisition of images in a high voltage μCT X-Tek XT H 450 (X-Tek Systems Ltd, Tring, Hertfordshire, UK) equipped with a 2000 × 2000 pixel PerkinElmer 1621 X-ray flat panel detector with pixel size 200 μm x 200 μm. This equipment arrangement provided a resolution limit of 100 μm (i.e. 0.1 mm). The scanning conditions were selected after a trial and error process. The nature of the sample investigated (i.e. heterogeneity, specimen size, material composition, etc.) and the quality of the images (i.e. high signal to noise ratio, artefacts, etc.) were considered to adjust the conditions. Optimal conditions were identified as 200 kV beam voltage, 68 μA current and 1mm thick copper filter. The total scanning time was 52 minutes and comprised 3142 radiographic projections each with an exposure time of 1s.

After the acquisition, reconstruction took place using a filter back projection algorithm. This produced a 3D object composed of volume images that were analysed using two commercial software packages: Mimics 14, developed by Materialise (Leuven, Belgium) and VG-Studio Max V2.0 developed by Volume Graphics GmbH (Heidelberg, Germany). In addition to the analysis of the 3D images, a stack of 2D images was produced and analysed in Image J, a free Java-based image processing program developed at the U.S. National Institute of Health. The reconstruction produced 986 and 1940 slices in the x-y and x-z planes respectively each with 0.125 mm thickness (i.e. voxel size).

The next step was the processing of images. This involved mapping the images to 8 bits, i.e. adjustment of the voxels greyscale to the 0 to 255 range. In the resulting images set, denser materials such as glass and metals were displayed as bright objects with grey values at the lower end of the scale. Lighter components like pores were displayed as dark objects with grey values at the upper end of the grey scale. Whilst materials with intermediate densities, which correspond to 2D materials (i.e. plastics, textiles and paper-see Chapter 3), shown in middle grey tones.

Once mapped, the images were qualitatively and quantitatively assessed. Visual inspection of the mapped 2D images was carried out in Image J. This evaluation aided in the location of big pores and the identification of the nature of the structure that created them (e.g. hollow rigid plastics, expanded polystyrene, etc.). Also, some pores were measured using the sizing tool in Image J and the orientation of 2D materials visually assessed.

The qualitative examination in Image J was followed by a quantitative three dimensional study of the pore space using the pore analysis module in Mimics 14. This study was computationally demanding and required the creation of a smaller file (i.e. excluded information of covering materials as cling and foil film). This new file is in imaging processing referred as a region of interest (ROI), i.e. a region that has features of interest. The ROI, a cuboid of 175 x 175 x 62.5mm, was composed of 500 slices in the x-y and 1400 in x-z plans. Figure 5-7 illustrates the specimen, the ROI and the coordinate arrangement used.

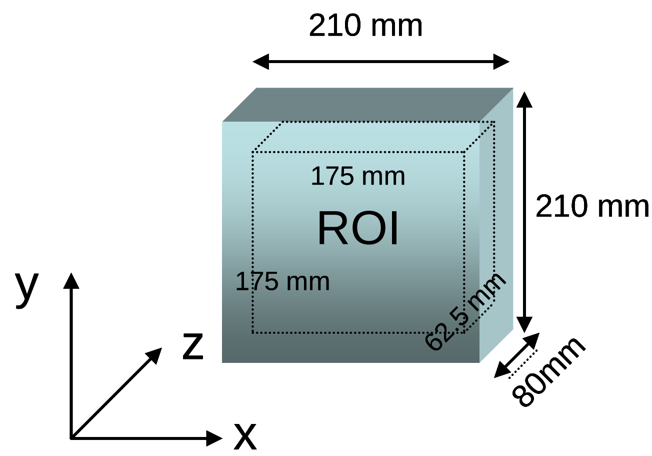

Figure 5-7 Schematic representation of a subsample for scanning taken from the degraded MSW

A 3D volume and its grey value histogram were created for the ROI. Using these two files, a manual segmentation process based on histogram thresholding was performed and the pore space extracted, i.e. pore voxels were identified and separated. Selection of the threshold grey value was an iterative process. An initial threshold was manually selected and adjusted. The threshold separated voxels in two groups and produced a new 3D volume composed by two voxel groups (i.e. above and below the threshold). The resulting 3D volume was visually assessed until a reasonable separation between pores and solids was achieved. Otherwise, the grey value was adjusted to attain a better separation. For comparison purposes, two automatic thresholding algorithms (i.e. Huang and Otsu) traditionally applied for the segmentation of the pore space in soils were used. The resulting grey values did not differ in more than 5% from those obtained with the manual thresholding.

Additionally, the qualitative separation between two voxel groups was quantitatively validated. The number of voxels in the pore space and in the entire 3D object was determined using the volume measurement tool. The pore space volume was calculated as a fraction of the total volume. The result was compared with the total porosity reported for the MSW specimen 31.39% (Ivanova, 2007) . A grey value of 152 produced 32.69% pores volume, a number that differed in less than 5% from the total porosity, was chosen as the final threshold.

With the pore space segmented, a 3D volume was produced and a quantitative analysis performed. The segmented 3D volume was loaded into the pore analysis module in Mimics 14 which follows an algorithm developed by Sweeney and Martin (2003). The Sweeney & Martin (2003) algorithm approximates the pore space to a chain of tangentially connected spheres. First, a voxel inside the pore space is identified at the edge of the 3D object. The biggest sphere is fitted inside the pore and the amount of voxels needed to fill the pore measured. The inserted sphere could have a size of a voxel fraction and be smaller than the voxel size (i.e. 0.125 mm for this study). The sphere diameter is estimated multiplying the number of voxels of the inserted sphere and the voxel size. The sphere volume is calculated. A second sphere is tangentially fitted to the first sphere and grows until it touches the solid matrix edges. The process is repeated and the totality of the pore space is fitted with the spheres. A report of the number of pores (i.e. spheres), diameter and volume is generated. Cumulative distributions are produced to have an overview of the overall pore space geometry.

The Sweeney and Martin (2003) algorithm demands high computational and time resources. To facilitate the analysis, eight smaller representative sub-regions of interest (sub-ROIs) were created and the pore analysis performed in each sub-ROI. Each sub-ROI, created from top to bottom in the x-z plane, was a 6.25 mm layer comprised by 50 slices of 0.125 mm thickness (i.e. the voxel size). The porosity was estimated in each segmented sub-ROIs using the volume analyser tool in Mimics 14 and compared with the total porosity of the specimen studied.

In addition to pore geometry, the connectivity between pores was studied. This analysis used the region growing algorithm, a procedure where a voxel of interest (i.e. seed pore region. The seed voxel and the tolerance were chosen considering the grey value histogram, particularly the pore space range. The seed voxel was a voxel inside a pore with a grey value in the middle of the pore space range (i.e. from 152 to 255). The tolerance was calculated from the difference between the maximum and minimum of the range. Whilst the seed grows, voxels complying with the tolerance criterion are coloured. This facilitates the identification of the region where the seed voxel has growth which can be used to assess whether the pores are connected (e.g. continuous region) and in which direction (i.e. horizontal or vertical).

5.3. Results and analysis

5.3.1. Thin sectioning

The deconstruction of the specimen revealed it to be a highly structured material. Vertical slicing was difficult and required the use of specialised equipment. The specimen, although requiring plaster coating to prevent damage during the experiments, was sufficiently stable to not fall apart before being covered, which agrees with the reinforcing effect of materials such as plastics and textiles discussed by Fernando et al. (2009); Dixon and Jones (2005) and Kölsch (1995).

During the deconstruction a total absence of nuisance smells coming from the sample indicating that the readily degradable components, e.g. food and yard waste (Meraz et al., 2004) have been degraded by this time, was noticed. This agrees with the material characterisation reported in Chapters 3 (see Table 3-6) which showed that the content of food and yard waste only decreased during the degradation from 2.27% and 18.40% to 0.16% and 3.38% dry mass respectively.

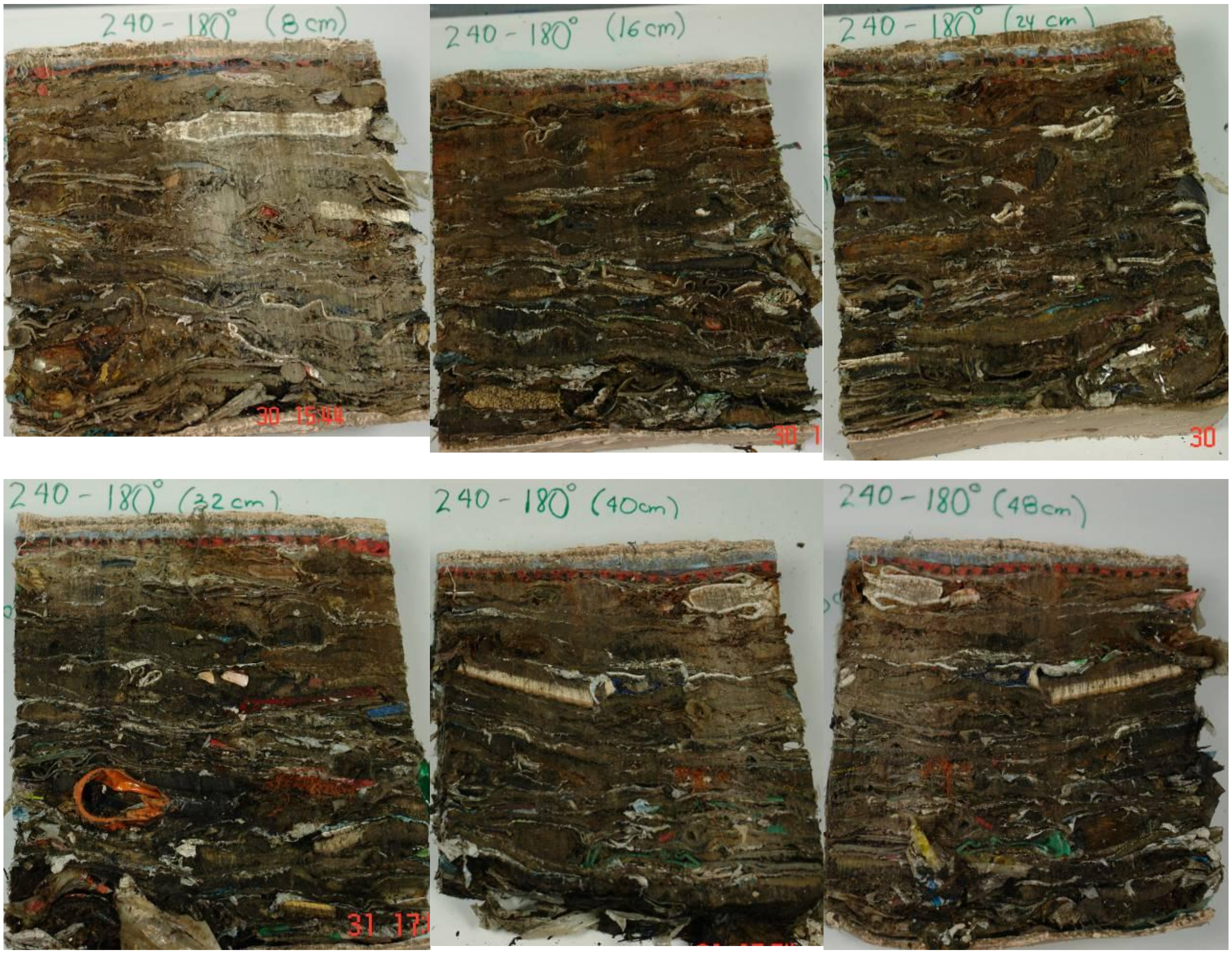

Figure 5-8 Surfaces exposed after slicing every 8 cm of the MSW sample (the planes of view are perpendicular to surface I in Figure 5-3). The notation given in degrees correspond to a preliminary study (not reported here) where a red-dye was injected to the specimen as reported in Caicedo et al. (2010)

Six slices, each of 80 mm thick, were produced following the sectioning procedure show schematically in Figure 5-3. Photographs of each slice are presented in Figure 5-8. Visual inspection evidences a layered structure. This type of structure agrees with the observations reported by Rees-White (2004) at field scale (see Annex 5-2). The layered structure also indicates that the method used by Ivanova (2007) for placing the material in the CAR is comparable to the placement conditions used in landfills.

Visual inspection of the slices showed that, despite more than 1.5 years of anaerobic degradation in the CAR, many pieces of 2D materials (e.g. plastic and textiles) remained easily identifiable. Judging from the appearance of the surfaces exposed during cutting and from the structural stability of the specimen, 2D materials constituted a significant portion of the specimen. This agrees with the results of material characterisation, which showed that the content of plastics and textiles increased with degradation from 20.03% and 3.08% to 28.35% and 6.62% dry mass respectively. The inspection shows also that 2D materials are distributed through the sample and are preferentially horizontally oriented. This supports the argument by Hudson (2007) that the horizontal orientation of elongated materials is the reason for the anisotropy in the hydraulic conductivity observed in solid wastes.

An effort was made to quantify the orientation of 2D particles. The step would involve segmentation of the images such that the particles of interest could be extracted and their angles measured. This proved to be a challenging task. First of all, 2D particles come from diverse material sources and show a wide range of colours. Difference in colour between 2D particles and the surrounding materials, although evident for the human eye, was not always sufficiently high for system recognition. This complicated the application of the simpler segmentation method, i.e. histogram-based thresholding (color frequency distribution). More sophisticated methods could have been explored, e.g. region growing, but that would require either the manual selection of the particles of interest or an elaborated method to define the initial seed and region growth parameters. Time constraint during this research limited the possibility of this further exploration.

Table 5-1 Composition by dry mass of MSW sample. Results obtained before and after degradation at different sieve sizes are presented. Particle density information reported by Mantell and Salzberg (1958) and Fernando *et al.* (2009) is included for discussion of μCT results.

<table>
<tr><th></th><th></th><th></th><th colspan="9">After
Sieve Size (mm)</th><th></th></tr>
<tr><th>Materials</th><th>Dim</th><th>B4</th><th>> 75</th><th>75-63</th><th>63-37.5</th><th>37.5-20</th><th>>75-20</th><th>20-10</th><th><10</th><th><20</th><th>Total</th><th>Particle density (Mg/m^3)</th></tr>
<tr><td>Flexible Plastics</td><td>2D</td><td>10.16%</td><td>0.88%</td><td>0.93%</td><td>6.36%</td><td>4.47%</td><td rowspan="6">52.15%</td><td>0.80%</td><td>0.00%</td><td rowspan="6">10.86%</td><td>13.44%</td><td>0.8336 [b]</td></tr>
<tr><td>Glass</td><td>2D</td><td>2.63%</td><td>0.00%</td><td>0.00%</td><td>0.00%</td><td>1.21%</td><td>5.21%</td><td>0.00%</td><td>6.42%</td><td>2.5098 [b]</td></tr>
<tr><td>Metals</td><td>2D</td><td>6.78%</td><td>0.00%</td><td>0.00%</td><td>0.15%</td><td>0.00%</td><td>0.00%</td><td>0.00%</td><td>0.15%</td><td>2.7000 [a]</td></tr>
<tr><td>Rigid Plastics</td><td>2D</td><td>9.87%</td><td>0.10%</td><td>2.15%</td><td>8.65%</td><td>3.49%</td><td>0.53%</td><td>0.00%</td><td>14.91%</td><td>1.0599 [b]</td></tr>
<tr><td>Paper</td><td>2D</td><td>27.34%</td><td>0.00%</td><td>0.80%</td><td>8.23%</td><td>8.49%</td><td>3.94%</td><td>0.00%</td><td>21.46%</td><td>1.2000 [a]</td></tr>
<tr><td>Textiles</td><td>2D</td><td>3.08%</td><td>0.03%</td><td>0.00%</td><td>2.87%</td><td>3.34%</td><td>0.38%</td><td>0.00%</td><td>6.62%</td><td>1.1400 [a]</td></tr>
<tr><td>Combustible</td><td>3D</td><td>2.96%</td><td>0.00%</td><td>0.00%</td><td>0.15%</td><td>0.65%</td><td rowspan="4">6.70%</td><td>0.03%</td><td>0.00%</td><td rowspan="4">1.47%</td><td>0.83%</td><td>1.7315 [b]</td></tr>
<tr><td>Food</td><td>3D</td><td>2.27%</td><td>0.00%</td><td>0.00%</td><td>0.00%</td><td>0.00%</td><td>0.16%</td><td>0.00%</td><td>0.16%</td><td>1.7315 [b]</td></tr>
<tr><td>Wood</td><td>3D</td><td>3.19%</td><td>0.00%</td><td>0.00%</td><td>1.82%</td><td>1.27%</td><td>0.73%</td><td>0.00%</td><td>3.81%</td><td>1.1042 [b]</td></tr>
<tr><td>Yard waste</td><td>3D</td><td>18.40%</td><td>2.19%</td><td>0.00%</td><td>0.30%</td><td>0.34%</td><td>0.56%</td><td>0.00%</td><td>3.38%</td><td>1.7315 [b]</td></tr>
<tr><td>Unidentified</td><td>0D</td><td>13.32%</td><td>0.00%</td><td>0.00%</td><td>0.00%</td><td>0.00%</td><td>0.00%</td><td>0.00%</td><td>28.82%</td><td>28.82%</td><td>28.82%</td><td>1.7315 [b]</td></tr>
</table>

a Specific gravity reported in materials handbook by Mantell & Salzberg (1958)
b Measured in laboratory using material selected from waste sample by Fernando et al (2009)

5.3.2. Flow paths tests

5.3.2.1. Injection point event

The flow distribution, expressed as a percentage of the total outflow, is presented in Figure 5-9. The needle was located at the centre of the specimen, thus considering water flowing linearly from the injection point to the base, i.e. neglecting flow spreading, all the outflow should come from the central region A. This is represented in the graph as expected outflow-vertical flow. The percentage area covered by each sector of the segmented collector is shown in Table 5-2, and these are equivalent to the percentage of the total flow that should occur for each region for uniform flow through the sample. They are represented as the white columns referred as expected outflow-uniform flow.

Table 5-2. Percentage of area covered by each sector of the segmented collector

Sector	Diameter (cm)	Area of circle (m^2)	Sector area (m^2) [a]	% Area [b]
A	6.3	0.0031	0.0031	3.1%
B	12.2	0.0117	0.0086	8.6%
S	22	0.0380	0.0263	26.5%
V	31.5	0.0779	0.0399	40.2%
Outer	na	na	0.0213	21.4%
Total	na	na	0.0992	

a. Corresponds to the effective area that collects volume.
Example, for B =0.0117-0.0031= 0.0086
b. Calculated as percentage of the total area.
Example, for B = 0.0086/0.0992=8.6%

The results showed that the greatest flow proportion was collected in the outer (88-94%) sector. Almost four times the expected outflow-uniform flow for that sector. No fluid was collected in the sector A. In remaining the sectors B, S and V the collected fluid was less than 12% whilst the expected outflow-uniform flow for the three regions grouped was 75.3%.

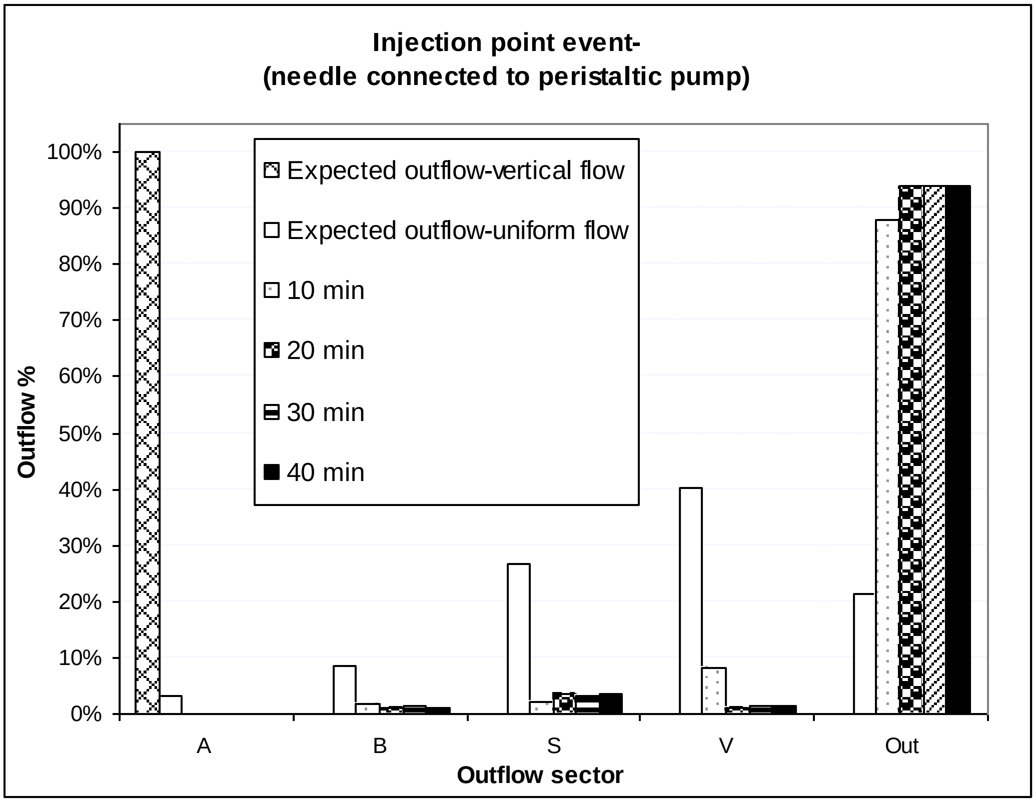

Figure 5-9 Outflow distribution during injection point test. Data for the expected outflow considers linear water flow and negligible spreading.

5.3.2.2. Irrigation Event

The flow distribution, expressed as a percentage of the total outflow, is presented in Figure 5-10. Expected flows in Table 5-3 were calculated as percentages of the total flow, considering an ideal situation in which water flows uniformly and purely vertically. In that case, fluids irrigated over the area I (diameter 16 cm), should be collected only in sectors A, B and S (diameters 6.3, 12.2 and 22 cm respectively). V and outer sectors are geometrically outside the influence of I with diameters greater than 22 cm. The experimental data, however, showed that the greatest flow proportion was collected in the outer (39-46%), and V (19-21%) sectors. No fluid was collected in the sector A, whereas the expected flow was of 16%. In sectors B and S, the collected fluid was less than 50%, of the expected value. Water alone was irrigated during the first 59 minutes of the test. The supply was then changed to Brilliant Blue solution and run for 60 more minutes.

Table 5-3 Percentage of area covered by each sector of the seented collector

Sector	Diameter (cm)	Area of circle (m^2)	Sector area (m^2) [a]	% Expected flow [b]
I	16	0.0201	na	na
A	6.3	0.0031	0.0031	15.5
B	12.2	0.0117	0.0086	42.6
S	22	0.0380	0.0263	41.9
V	31.5	0.0779	0.0399	0
Outer	na	na	0.0213	0

a. Corresponds to the effective area that collects volume.
Example, for B =0.0117-0.0031= 0.0086
b. Calculated as percentage of I. Example, for B = 0.0086/0.0201=42.6

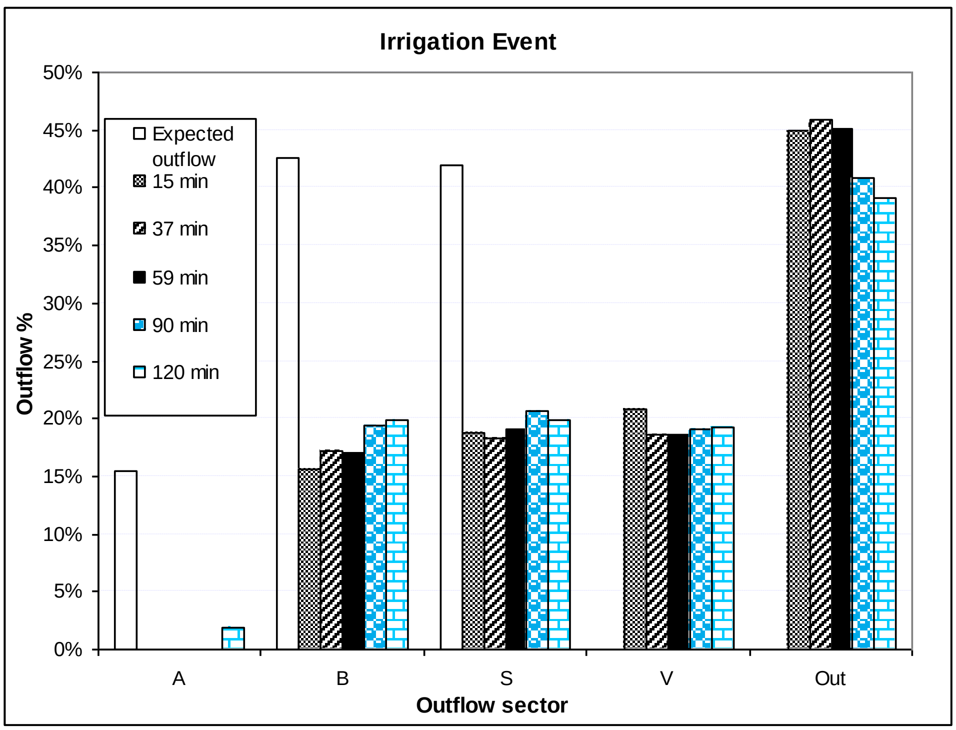

Figure 5-10 Outflow distribution during the irrigation event test. Data for the first 59 minutes (white and black bars) correspond to water irrigation; the supply was then changed to dye solution (blue bars)

Figure 5-10 illustrates that the flow distribution was reasonably steady over the whole 120 minutes and was not considerably affected by the dye injection at 59 minutes. This suggests that dye solution moved through similar flow paths to the water, and thus acted as a representative tracer to visualise water movement. The test was stopped after 2 hours when the obstruction of some of the needles was detected, which could have been caused by un-dissolved solid particles coming either from the solid dye or from solution drying over small localised areas. This could be minimised filtering the mixture or adding a small amount of a retardant solvent.

Photographs were taken during the test to record progress of dye staining with time. Selected images are presented in Figure 5-11.

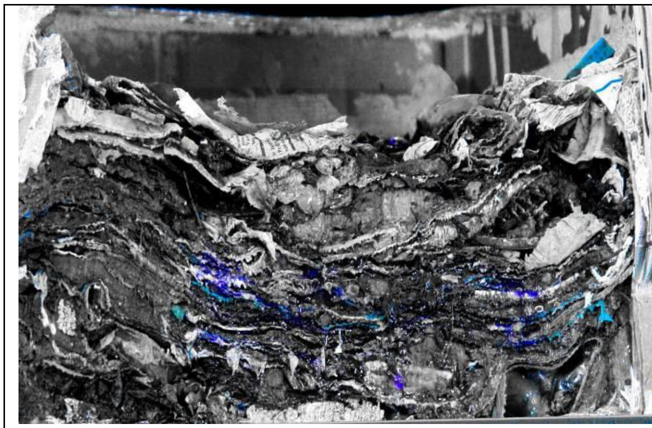

i. start of dye injection (59 min)

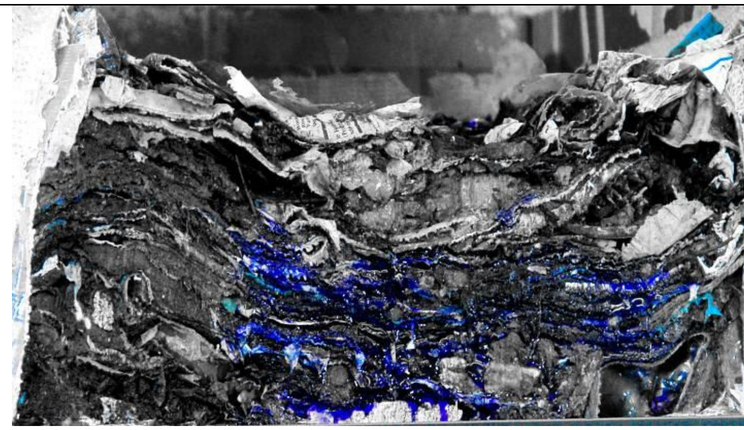

ii. 4 minutes after Brilliant Blue injection

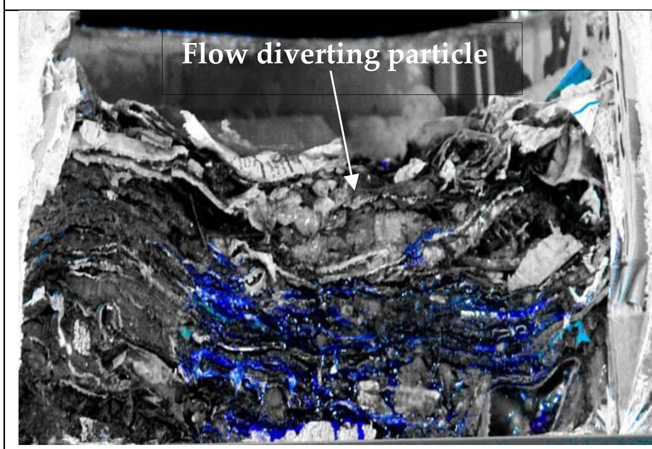

iii. 9 minutes after Brilliant Blue injection

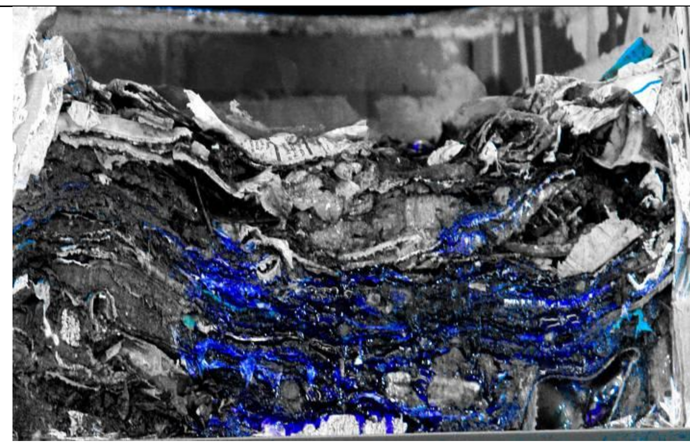

iv. 40 minutes after Brilliant Blue injection

Figure 5-11 Exposed surface of MSW after irrigation with 1g/litre solution of Brilliant Blue. Dark blue regions indicate areas that were dye- stained.

Visual observation during Brilliant Blue irrigation confirmed that a significant proportion of the dye solution was flowing towards the external surface, through channel(s) connecting the irrigated area with the external surface below the top of the specimen. This situation needs more analysis. The external exposed surface was not recovered with plaster, and in a layered material it is inevitable that any vertical boundary will represent a preferential flow path that would not exist in reality. Additionally, although significant steps were taken to minimise structural distortion of the specimen and any inclination, those efforts were not sufficient to entirely preserve the original structure, and some layer bending (concave downwards), was evident that could have affected the waste body and preferential flow. Therefore, sample disturbance and stress could depend on size of preferential flow channels.

Table 5-4 summarises data of the two experiments whilst running with water only. The comparison shows that outflow through the periphery was, in both experiments, significantly high, i.e. 92.49% and 45.28% for injection and irrigation respectively, whilst the area of the region was only 21.40%. During the point injection event, the peripheral outflow was twice that for irrigation. This may be explained by the fact that with point injection it is easier for water to form a pond on the specimen surface. Water will then look for the easiest way to flow which may be a horizontal channel(s) connecting the centre of the top of the specimen with the periphery. Comparatively speaking, irrigation enhanced flow distribution through the sample, reflected by the increase from 7.51 to 54.72% in the outflow collected from the middle area. Nevertheless, approximately half of the flow was still collected from the periphery suggesting the presence of horizontal channels that could have favoured preferential flow. None of the experiments showed outflow coming from the inner area. This gives an indication of the tortuous paths. Fluid particles initiate their journey on the top centre of the specimen and during their trip are diverted by many particles to finish their journey at a radial distance of at least 3.15 cm from the centre (the radius of the inner sector A). These results suggest that as a consequence of the layered structure, the horizontal hydraulic gradient could probably be several times larger than the vertical gradient and could produce horizontal channelling.

Efforts were made to compare the results from this study. However, research on flow paths in solid waste is scarce and studies for direct comparison (i.e. similar experimental set up and conditions) could not be identified. The investigation by Hudson et al. (2010), which explored flow spreading using a very different experimental set up (i.e. hydraulically constrained at circular boundary), was considered only for indirect comparison.

Hudson et al. (2010) studied a 40 years old solid waste excavated from landfill and found that the horizontal spreading increased with flow rates. Their results suggest that the tendency for water flowing through channels decreases with flow rate, which differs from the results reported here. This divergence can be explained in the light of the structural differences between materials. In Annex 5-1 some of the images taken during loading the 40 years old solid waste are shown. The images illustrate a predominantly soil like material with some content of 2D plastics, but that do not form continuous impermeable layers. In contrast, the structure of the MSW specimen showed in Figure 5-8 and Figure 5-12 evidences predominantly layers of 2D materials, which by diverting flow can limit the horizontal spreading.

Table 5-4 Comparison of outflows: between injection point and irrigation tests during the study of flow paths and data reported by Hudson et al.**(2010) of a study of horizontal spreading in solid waste**

				Average outflows [a] (using only water)				Hudson et al (2010)		
	Sector	% Area Sector		Injection Point		Irrigation		% Area	Test-lower flow rate (0.57 l/h)	Test-higher flow rate (5.94 l/h)
Q/A (m/s)				8.40E-06		7.22E-06			8.33E-07	8.68E-06
Inner area	A	3.10%	3.10%	0.00%	0.00%	0.00%	0.00%	10.20%	21.00%	8.10%
Middle area	B	8.60%	75.30%	1.32%	7.51%	16.61%	54.72%	50.70%	65.00%	49.10%
	S	26.50%		3.15%		18.73%				
	V	40.20%		3.03%		19.38%				
Periphery	Outer	21.40%	21.40%	92.49%	92.49%	45.28%	45.28%	39.10%	14.00%	42.90%

a-Averages of outflows were calculated considering only data for tests running with water (no dye solution)

5.3.3. μCT

Some of the images reconstructed in the x-y plane are presented in
Figure 5-12. The relative position of each image is referred to the entire specimen and to the sub-ROIs as explained in section 5.2.2.4. Visual assessment of images shows the denser components as bright objects, pores as dark areas and a strongly layered structure where the 2D components (i.e. materials with intermediate densities) are horizontally orientated.

Some examples of the 2D images in the x-z plane are presented in Figure 5-13 . Images a to d illustrate different types of structures developed in the specimen. For example, image a shows a big pore formed inside a hollow rigid plastic. Images b and c show a structure created from permeable materials with smaller pores, and image d a structure inside a big synthetic piece of expanded polystyrene. The size of the pores was measured which evidenced the presence of pores as large as 53.87 mm (see Figure 5-12 for images a and b; and Figure 5-13 for image a). The examination was expanded with a three dimensional analysis as detailed in sections 5.2.2.4 and 5.3.4.

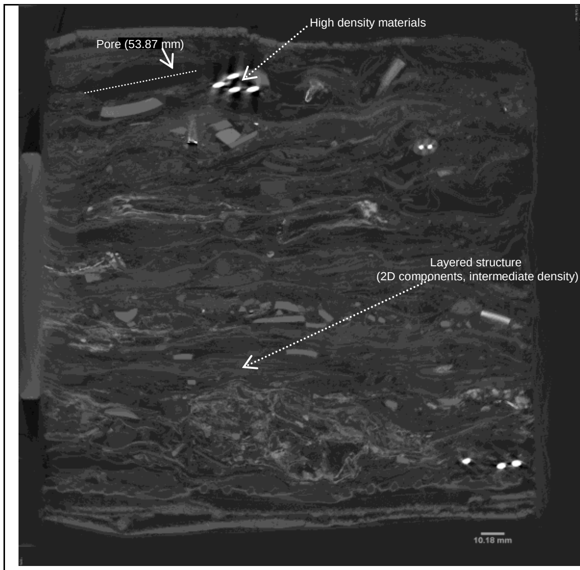	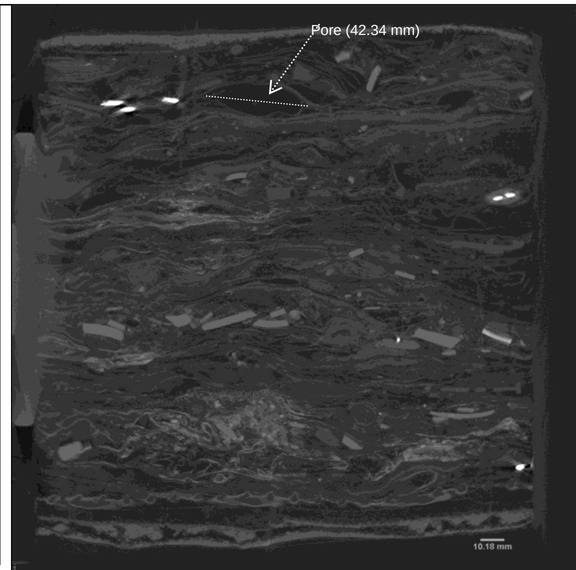
a. x-y plane. Slice # 180 in specimen (0 mm inside the ROI)	b. x-y plane. Slice # 380 in specimen (25 mm inside the ROI)
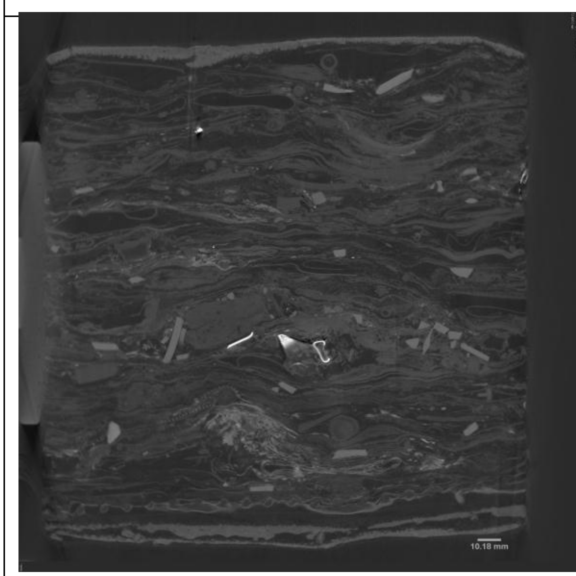	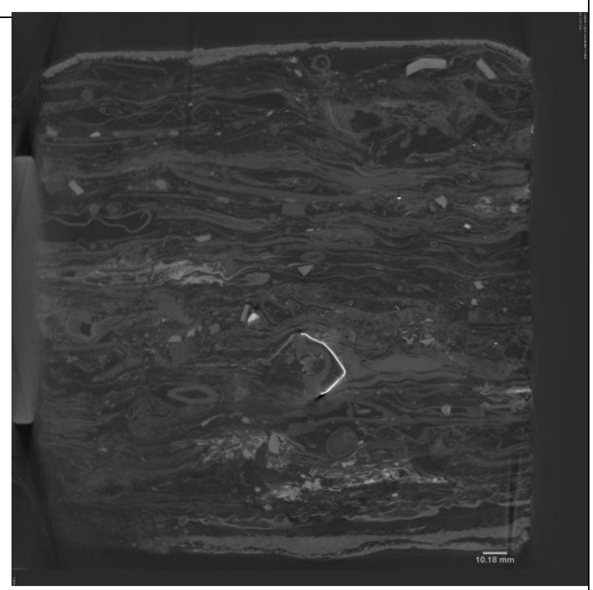
c. x-y plane. Slice # 580 in specimen (50 mm inside the ROI)	c. x-y plane. Slice # 680 in specimen (62.5 mm inside the ROI)

Figure 5-12 Examples of slice views obtained by μCT of MSW specimen in the x-y plane. Darker features are pores whereas brighter areas correspond to denser components such glass and metals. Grey materials correspond to middle density materials such as plastics, textiles and expanded polystyrene.

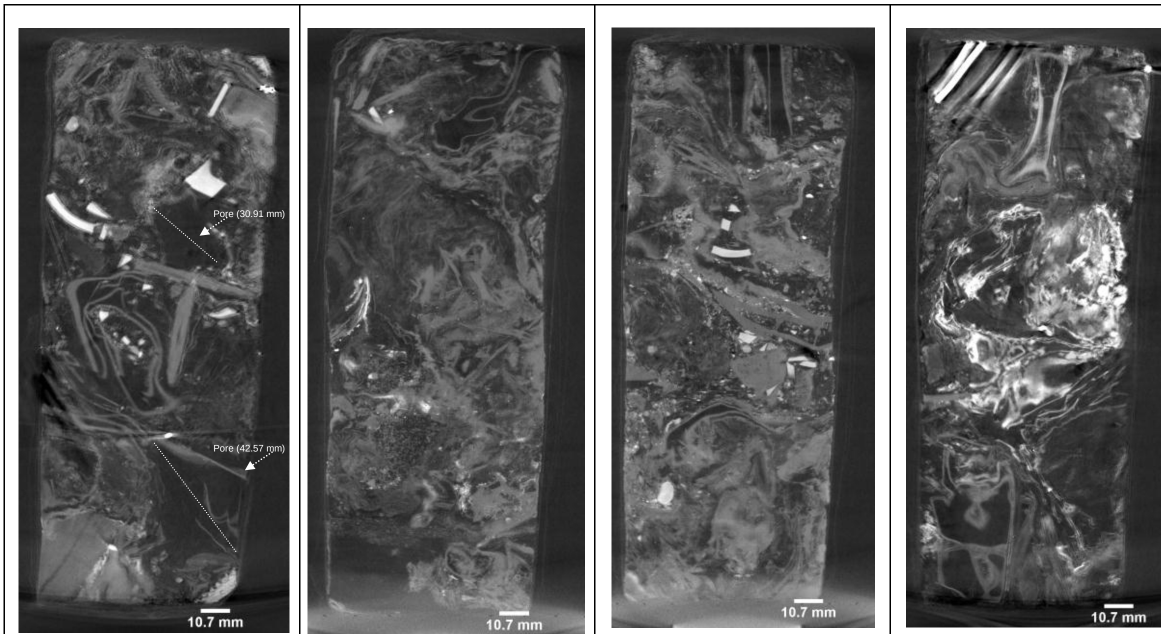

a. x-z plane. Slice # 200 in specimen (0 mm inside the ROI)	b. x-z plane. Slice # 800 in specimen (75 mm inside the ROI)	c. x-z plane. Slice # 1000 in specimen (100 mm inside the ROI)	d. x-z plane. Slice # 1600 in specimen (175 mm inside the ROI)

Figure 5-13 Examples of slice views obtained by μCT of MSW specimen in the x-z plane.

5.3.4. 3D characterization of pore space

A 3D object, where the pore space was segmented from the solid matrix, was achieved following the iterative process described in Section 5.2.2.4. Figure 5-14 shows examples of 3D objects rendered at different grey values.

<table>
<tr><td>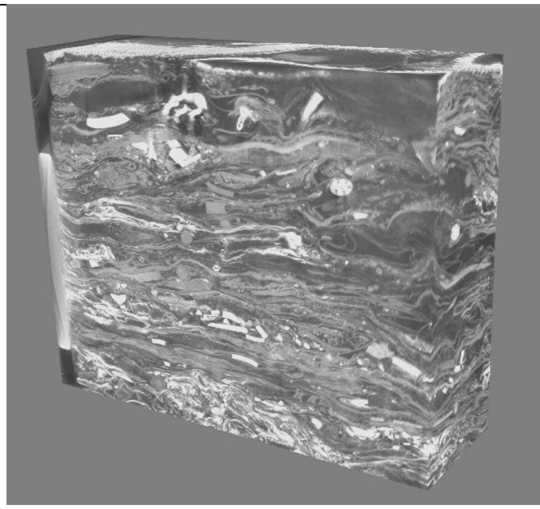</td><td>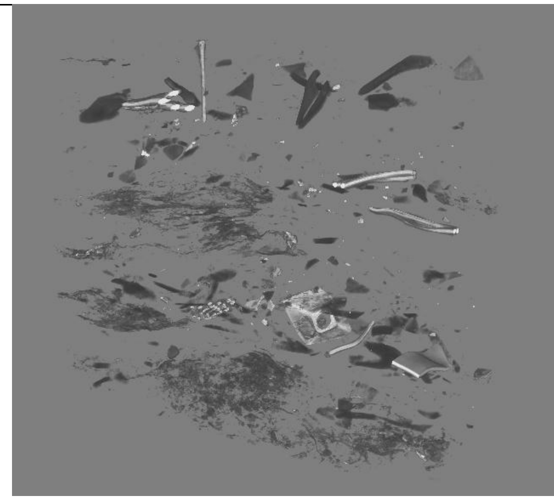</td></tr>
<tr><td>a. Complete MSW specimen</td><td>b. High density materials (glass and metals)</td></tr>
<tr><td rowspan="2">Figure 5-14 Examples of 3D objects obtained by μCT at different grey values thresholds of the MSW specimen. Materials with different densities are rendered. The background was left in these images to ease visualization but was removed and ROI prepared for quantification.</td><td>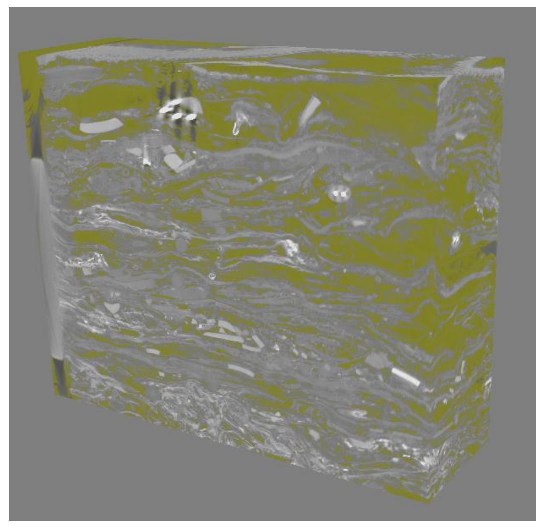</td></tr>
<tr><td>c. Low density materials are rendered in yellow colour (pores and background)</td></tr>
</table>

It was explained in section 5.2.2.4 that eight sub-ROIs were created to reduce the computational demand during the quantitative pore space analysis. Table 5-5 details the location of each sub-ROI in the x-z plane (from top to bottom). The distance from top to bottom is equivalent to the depth within the specimen. The eight sub-ROIs covered a total thickness of 175 mm (i.e. the specimen total depth).

Table 5-5 Slices selected for pore analysis in the x-z plan. The position refers to the depth within the ROI of the MSW specimen

Sub-ROI number	Slices range number	Position within ROI in the x-z plan top to bottom (mm)	Average distance (mm)
1	200-250	0-6.25	3.125
2	400-450	25-31.25	28.125
3	600-650	50-56.25	53.125
4	800-850	75-81.25	78.125
5	1000-1050	100-106.25	103.125
6	1200-1250	125-131.25	128.125
7	1400-1450	150-156.25	153.125
8	1550-1600	168.75-175	171.875

Figure 5-15 shows the porosity for each sub-ROI as a function of depth expressed as the average distance from top to bottom for each layer (Table 5-5). The higher porosities were seen in the upper and lower layers, i.e. 52.12% and 40.57 % for 0-6.25 and 168.75-175 mm respectively. This could be the result of distortions to the structure caused by cuts made during the preparation of the sample. In the internal layers, two regions are identified. From 6.25 to 81.25 mm the average porosity was 35.09%, whilst in the deeper region from 81.25 to 156.25 mm was 25.20%. This difference reflects the increase in compaction, and the consequent reduction of the volume of pores with depth.

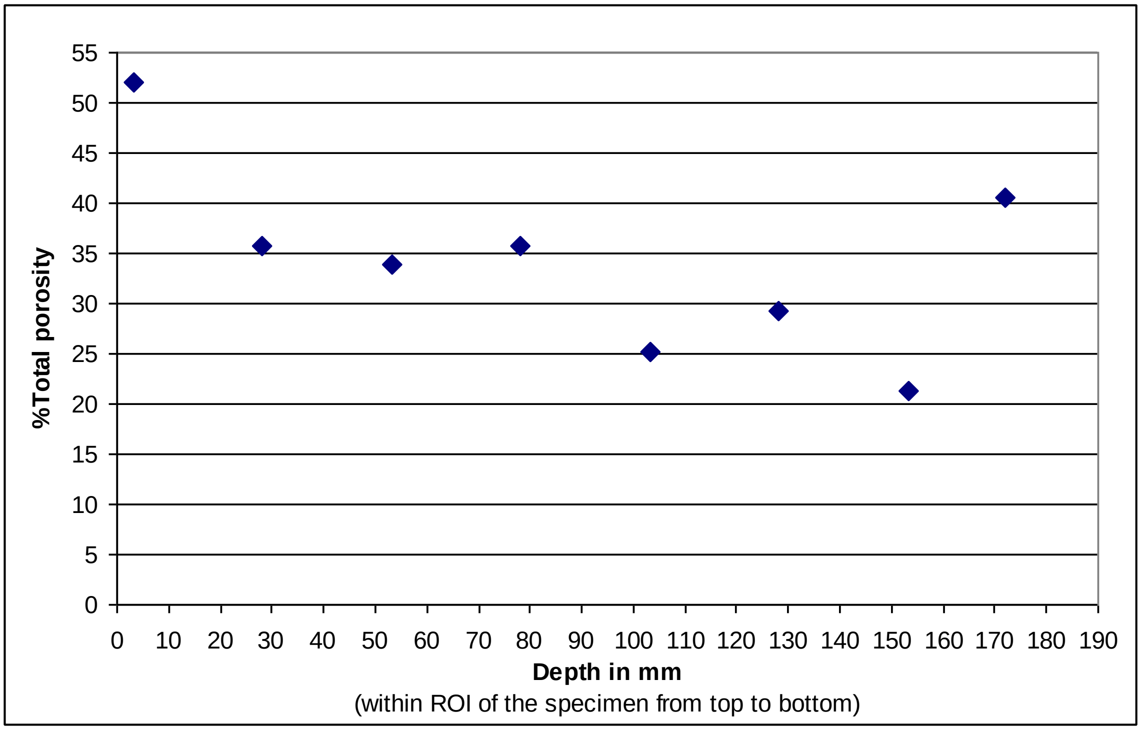

Figure 5-15 Variations with depth in the porosity of a specimen of MSW. The analysis was run in a ROI using the pore analysis module in Mimics 14

Results of the pore size distribution by number and volume are summarized in Figure 5-15 and Figure 5-16 respectively. There are no clear differences in either the number or volume pore size distribution between layers in the specimen. This suggests that although the deeper layer (81.25- 156.25 mm) has a lower porosity, the reduction in the total volume of pores was uniform and did not produce net changes in the pore size distribution.

Comparison between the two lines shows that 95% of the pores by number have a size of less than 1mm but they represent only 25% by volume. Additionally, 50% of the pores by number have a size between 0.26 and 0.41 mm, yet they represent less than 5% by volume. Large pores, i.e. ≥ 2mm size, are less than 5% in number but more than 25% in volume (and up to 75% depending of the layer). Large pores are important in fluid flow processes. As in soils, large pores can favour preferential flow (Beven and Germann, 1982), especially if they are well connected. The high percentage (by volume) of large pores indicates that this may be the case for the MSW specimen. Visual examination of image c in Figure 5-14 (pores rendered in yellow colour) suggests that the pores are connected, especially in the horizontal direction.

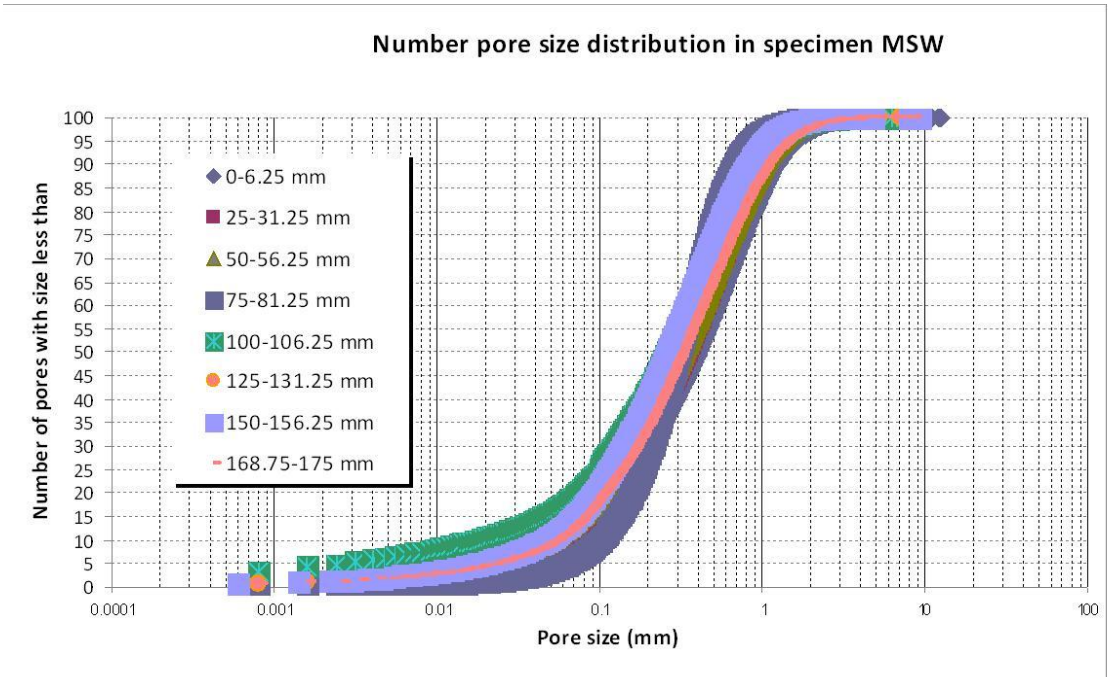

Figure 5-16 Variations in number pore size distribution of a specimen of MSW. The analysis was run in a ROI using the pore analysis module in Mimics 14. Different plots correspond to different layers in the specimen

Figure 5-18 presents the pore size distributions for the whole specimen and the PSD obtained during the characterization of the MSW sample in Chapter 2.

The PSD shows that the MSW specimen is a coarse material with particles as large as 75 mm and with 50% by mass with size above 20 mm. In Table 3-6 can be seen that large materials > 20mm correspond to 2D particles. These large 2D particles are expected to form large pores as it is evidenced by the volume pore size distribution where 50% by volume of the pores have a size above 1.60 mm. This shows that the D_{50} by volume of pores is one order of magnitude less than the D_{50} by mass of particles, whilst the D_{50} by number of pores is two orders of magnitude less than the D_{50} by mass of particles.

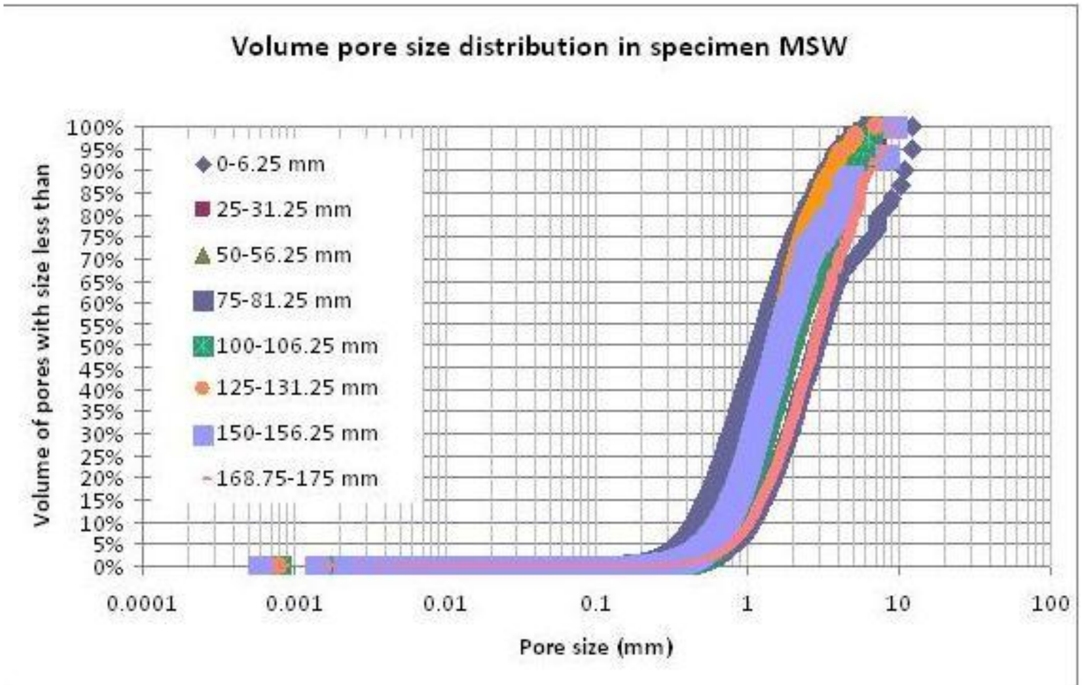

Figure 5-17 Variations in volume pore size distribution of a specimen of MSW. The analysis was run in a ROI using the pore analysis module in Mimics 14. Different plots correspond to different layers in the specimen

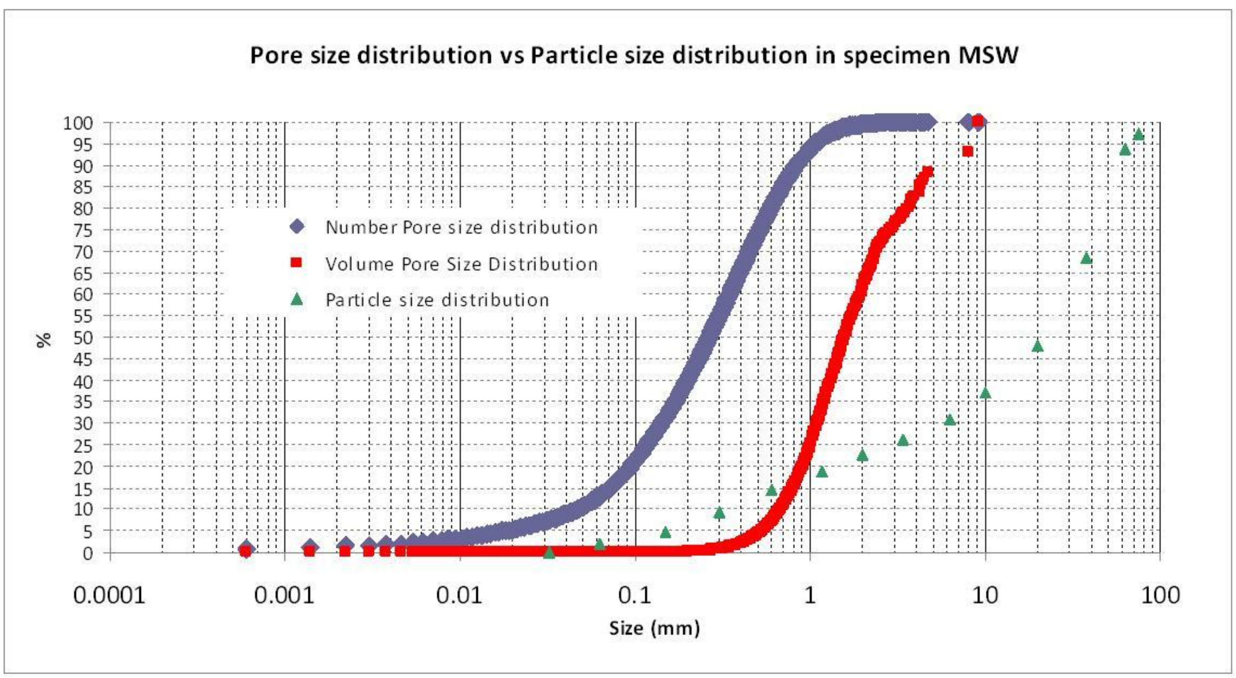

Figure 5-18 Variations in volume pore size distribution of a specimen of MSW.

The pore analysis here described provided detailed information about the pore size distribution in the specimen of MSW studied, however there are some limitations that need consideration. First of all, the Sweeney and Martin (2003) algorithm simplifies the complex geometry of the pores in solid waste by modelling the space as a chain of spheres. However, the high heterogeneity in solid wastes suggests that the pore architecture could differ from a chain of spheres. In consequence, some places inside the pores could not be reached by the spheres (e.g. edges) and therefore not be considered in the analysis.

Also, the analysis does not consider the connectivity between the pores, a factor of importance in flow conduction. For example, a single large pore with a throat would be reported as a sequence of spheres (e.g. one fitting the entrance throat and other the pore body) rather than a single body. Therefore, the analysis presented using the Sweeney & Martin (2003) algorithm should be taken only as an approximation. Further research is necessary to develop algorithms that consider more complex geometries and a more realistic description of the pore architecture in solid waste.

5.4. Summary

During this research three techniques, i.e. visualization of flow paths with dye tracers, thin sectioning and μCT, were developed and successfully applied for the study of preferential flow and structure in solid wastes.

Results showed that preferential flow is a likely phenomenon during fluid flow through layered structured landfill waste. The application of thin sectioning exposed a layered structure in a sample of anaerobically degraded MSW. This type of structure resulted from the presence of large 2D materials (>20 mm), i.e. plastics, textiles and paper, horizontally oriented and that given their low degradability remained unaffected during the degradation. The use of μCT revealed detailed information of the structure and pore architecture unknown up to now. 50% by volume of the pores was found to be of horizontally connected large pores above 1.60 mm size. Large pores can be the cause of the presence of preferential flow channels.

The use of Brilliant Blue as a dye tracer was shown to be a useful tool for the visual identification of water flow paths in waste. Colour contrast between the waste matrix and the dye was sufficient to achieve visual differentiation between stained and unstained areas.

The use of μCT, introduced during this research, for the study of solid waste is under research. Some of the areas that need more investigation include the development of scanning routines to systematically study different types of solid waste and of algorithms for a more realistic description of the pore space architecture. Also, more research is required to understand the role of pores of different architecture in fluids conduction and how to estimate fluid flow properties from pores geometry. Chapter 6 explores how to link data for pores geometry with fluids flow properties.

6. General Discussion

This thesis has demonstrated that landfilled waste is a complex material, potentially comprising many different components with particles that widely vary in size and shape. The physical nature, and particularly the structure of waste, is recognised to have a major control over processes that act on waste, such as fluid flow and degradation. Research by others (Beaven, 1996, Powrie and Beaven, 1999, Stoltz et al., 2010) has demonstrated the importance of waste density linked to effective stress and compaction on hydraulic properties. At a particulate level however, one of the fundamental controls on the hydraulic conductivity are the size and shape of the particles. This thesis concentrated on: understanding the effect of PSD and the content and size of 2D particles on flow and on developing characterisation and assessment methods to aid interpretation.

Chapters 2 and 3 studied the geometric properties that describe a particulate matter at the scale of individual particles. The properties investigated were the particle size and particle shape. The study evidenced that alike other particulate materials, the PSD in solid wastes can be described using mathematical models and that the type of model depends on the nature and treatment history of the residue. It was also shown that to fully represent the mathematical model it is only required to know the model parameters; i.e. one parameter for Normal and Rosin-Rammler (RR) models or two parameters for fractal models, and the range of particles size where the model is applicable. This finding implies that the graphical representation of the PSD can be replaced by an analytical expression. The analytical expression can be used in calculations that involve information about the material particles size such as the estimation of the pore size and the hydraulic conductivity.

The importance of the particle shape was demonstrated by a detailed material classification which evidenced that the proportion of 2D materials in solid waste is significant and by analogue waste experiments which highlighted the need to consider the relative size to matrix and proportion (both volume and mass) of 2D impeding particles.

Results from analogue waste experiments showed that the hydraulic conductivity of a medium modified with 2D particles is controlled by the volume content (*VC*) and the relative size (*RS*) of the modifying particles (see Figures 4-9 and 4-10). Also, the mathematical model developed by Maxwell(1954) for conduction through a heterogeneous media estimates the hydraulic conductivity using a single term p which is a function of the volumetric content of 2D particles.

Similar controls are expected for solid wastes. For example, Figure 4-9 and 4-10 show that when *VC* and *RS* exceed 20% (i.e. 7.3% by mass) and 15 respectively, the reduction on the hydraulic conductivity surpasses 30%. Results from material characterisation in solid wastes (see chapter 3) suggests that *VC* and *RS* could exceed those limits and reductions in the hydraulic conductivity therefore envisaged.

Estimation of *VC, RS* and p are necessary to confirm this hypothesis. This estimation requires information of at least three characteristics: particle size, material characterisation and particle density. With the PSD and the material characterisation, the mass fraction of potentially flow diverting or impeding 2D materials and the *RS* of the 2D particles could be estimated. Information on particle density could be incorporated to estimate the proportion by volume of 2D particles.

The structure of solid waste was studied by thin sectioning and tracer experiments which verified the importance of layering.

The novel use of μCT showed waste structure. μCT was used to investigate pore size distributions within real samples of waste opening new research possibilities. The ability to examine pore geometry with μCT provides an experimental link between PSD analyses and pore network models. For example, pore size distributions obtained from mathematical models based on PSD (e.g. White and Beaven (2008)) could be contrasted with experimental measurements from μCT. Then, the description of the pore space architecture could be used as a tool to study the interaction between the structure and processes such as flow and degradation. One alternative is to use the pore space description to mathematically model flow using pore network models as it has been discussed by Nayagum et al. (2010). This has been a usual approach in soils and particulate media (Heijs et al., 1995, Amos et al., 1996).

As with most non-invasive techniques, constraints in the resolution of the images obtained with μCT, imply limitations in the size of features resolved (i.e. size of the smaller pores). This is a restraint that has been addressed with highly focussed X-ray beams (D'Amico et al., 1992) and multiscale images (Grader et al., 2009). To obtain multiscale images, the object is progressively cut to reduce its size and images are obtained every time. Acquisition of multiscale images in specimens of solid waste could be feasible providing the structure is preserved. Structure preservation could be achieved for example using the techniques for thin sectioning described in Chapter 5.

This Chapter focusses on demonstrating the use of PSD information through the incorporation of the PSD models into a methodology developed by White and Beaven (2008) for the estimation of the characteristics of the pore space (i.e. length and area) and the associated hydraulic conductivity.

Also in this chapter, a graphical approach that links waste characterisation with the impact on the hydraulic conductivity is discussed. The approach integrates the use of the ternary plots, introduced in Chapter 3 where materials in solid waste were classified according to their dimensionality, with their impact on hydraulic conductivity according to the framework proposed by Velkushanova et al. (2009). Results obtained in Chapter 4, that dealt with the impact of 2D particles on the hydraulic conductivity of a matrix are used to develop further the use of material characterisation for the estimation of the hydraulic conductivity in solid wastes.

6.1. The use of PSD for the estimation of fluid flow properties in solid wastes

6.1.1. Background

Efforts have been made by researchers to find expressions to estimate the hydraulic conductivity using particle size data (Hazen, 1911, Krumbein, 1936b, Dullien, 1992, Boadu, 2000). Equation 2-4 for example, is a general expression that estimates the intrinsic permeability k as a function of d, the system characteristic size parameter. The equation indicates that the better the estimation of d, the more accurate the calculated k. In Chapter 2, focus was placed on finding a mathematical model to describe the PSD of solid wastes. The advantages of having a PSD mathematical model were discussed. They include the benefits of getting an analytical expression to express the PSD data and the consequently easier and more precise calculations of material properties (e.g. pore size distribution and permeability) that involve particle size information. This is equivalent to improving the accuracy in the estimation of d and the intrinsic permeability k.

In solid wastes, the use of particle size data and PSDs models to estimate fluid flow properties is still highly unexplored. Nevertheless , the approach presented by White and Beaven (2008), one of the few in this field, provides a method for the estimation of the characteristics of the pore space in solid wastes. White and Beaven (2008) considered the mathematical representation of the PSD with a generic polynomial expression that fits the s shape of a PSD graph. Then, using the data generated with the PSD model, the properties of the pore space are estimated using size dependent functions that relate the size of the particles with the pores size (i.e. length and area). A downside of the White and Beaven (2008) method is that the polynomial expression proposed to represent the PSD, does not have a physical meaning and is not used in the particle industry to represent the PSD for a material type. This condition could be addressed with a more robust PSD representation such as the models explored in Chapter 2 (e.g. normal, RR or fractal).

6.1.1. Method description

The method proposed by White and Beaven (2008) allows mapping of PSD data into micro-scale network models and can be used to derive model parameter values for application in more complex macro-scale landfill models. The basic assumption is that as particulate materials are composed by particles with a range of sizes, the particles create a porous network system consisting of channels with a range of sizes. If the particles are grouped into narrow size ranges; they create a sub-network with a narrow size range, its own porosity and permeability. The PSD of a waste material can then be converted into a pore size distribution once a function that relates the size of the particles to the size of the pores is defined. White and Beaven (2008) defined a size dependent function (Equation 6-1) that considers the contribution of each particle to an element of channel length l_i ,

$$l_i = f_L\left(\bar{d}_i\right)\bar{d}_i \qquad \text{Equation 6-1}$$

where $f_L\left(\bar{d}_i\right)$ is a size dependent function and $\bar{d}_i$ is the particles defined according to Equation 6-2.

$$\bar{d}_i = \frac{d_i + d_{i-1}}{2} \qquad \text{Equation 6-2}$$

The contribution of an individual particle to an element channel is calculated with Equation 6-1. The contribution of all the particles within the size range can be calculated considering the total amount of particles N_i. The mass of particles in the range d_i to d_{i-1} is y_{retained} . If the particles are assumed to be spherical, the ratio between the volume occupied by all the particles and the volume of a single spherical particle with an average diameter $\bar{d}_i$ gives the number of particles in the range of sizes of interest. Then, considering the elemental volume of waste is V_E and that it has a porosity n, the particles in the range d_i to d_{i-1} will occupy a solid volume equal to $y_{retained}(1-n)V_E$ and the number of particles in this range of sizes will be (see Equation 6-3),

$$N_i = \frac{y_{retained}(1-n)V_E}{\frac{4}{3}\pi\left(\frac{\bar{d}_i}{2}\right)^3} \qquad \text{Equation 6-3}$$

N_i is the total number of particles in the elemental volume V_E, if V_E is assumed to be a cubic metre, the number of particles contributing to the channel length L_i will be approximately the cube root of N_i. Thus, L_i can be expressed as (see Equation 6-4):

$$L_i = N_i^{0.33} f_L(\bar{d}_i)\bar{d}_i \qquad \text{Equation 6-4}$$

Similarly, the channel diameter can be estimated with another size function $f_D(\bar{d}_i)$ defined in Equation 6-5 which converts the particle size $\bar{d}_i$ into a channel diameter D_i.

$$D_i = f_D(\bar{d}_i)\bar{d}_i \qquad \text{Equation 6-5}$$

The area of flow in an individual channel a_i can be estimated from the diameter of an individual channel according to Equation 6-6.

$$a_i = \pi\left(\frac{D_i}{2}\right)^2 \qquad \text{Equation 6-6}$$

The total channel flow area can be estimated with the total number of particles contributing to this flow area. This is approximately N_i to the power of 2/3. Then, the total channel flow area A_i can be estimated as:

$$A_i = N_i^{2/3}\pi\left(\frac{D_i}{2}\right)^2 \qquad \text{Equation 6-7}$$

L_i and A_i calculated with Equations 6-4 and 6-7 are the length and area of the pores for the channels formed with particles within a small size interval. The calculations are repeated to cover the complete size range and a pore size distribution obtained with the y_{retained} and the values for L_i and A_i.

Each of the channels within the network can be theorised as an arrangement of pipes, and the flow rate through them q_i estimated with the Poiseuille´s equation. The flow rate estimated with Poiseuille`s equals the amount calculated with Darcy´s law (see Equation 6-8).

$$q_i = A_i\frac{\rho g D_i^2}{64\mu}\frac{\Delta h}{L_i} = \frac{A_i}{\sum A_i}A_E K_i\frac{\Delta h}{L_E} \qquad \text{Equation 6-8}$$

In Equation 6-8, ρ and μ are the fluid density and viscosity, g is the acceleration due to gravity and Δh the hydraulic gradient driving the flow. K_i is the effective permeability for the channel within the network, and A_E and L_E are the area and length of the element of volume V_E respectively. Equation 6-9, obtained from Equation 6-8, is an expression for K_i in terms of the channel geometry and fluid properties.

$$K_i = \frac{\sum A_i}{L_i} \frac{L_E}{A_E} \frac{\rho g D_i^2}{64\mu} \quad \text{Equation 6-9}$$

With the K_i for each group of channels within the network, the permeability of the network K can be estimated as the sum of the products between K_i and the fraction area for the associated group of channels (see Equation 6-10)

$$K = \sum K_i \frac{A_i}{\sum A_i} \qquad \text{Equation 6-1}$$

The different steps involved in White and Beaven (2008) method demonstrate how to use PSD data to estimate the geometrical properties of the pore space and the associated permeability. Discussion on some aspects of the method is the focus of the next paragraphs.

White and Beaven (2008) used empirically selected values for $f_L(\bar{d}_i)$ and $f_D(\bar{d}_i)$. Although they did not present clear reasons for the selection of the numbers used, they recognised the need for the determination of those geometric functions for solid wastes. Some discussion on the possible numbers follows. The channel diameter for example, should be a fraction of the particle size, perhaps of less than 10% of the particle size. This is a suggestion based on the geometrical construction of a pore space (Donohue and Wensrich, 2008) and on the empirical equations where the permeability and the particle size are related with a factor of less than one (Hazen, 1911, Krumbein, 1938b). Then, it is reasonable to think that $f_D(\bar{d}_i)$ should adopt values of less than 1, maybe of less than 0.1. On the other hand, the channel length is the result of solid particles located vertically and creating a pore space, therefore it should not have the same restriction. Instead, the channel length could be several times larger than the particle size which implies that $f_L(\bar{d}_i)$ could adopt values of more than 1.

One of the implications of the White and Beaven (2008) approach is that changes in the PSD due to compression, deformation, biodegradation and crushing can be reflected in the pore length and pore area distributions. In particular, the application of the method has the potential to indicate the magnitude of the variation in the pore size distribution and permeability resulting merely from the biodegradation process. This is an aspect explored during the present chapter. Results from chapter 2 indicate that changes in PSD can be expected as the result of biodegradation. White and Beaven (2008) method was applied to PSDs obtained in chapter 2 and results are presented and discussed along the present chapter. The values of the functions $f_L(\bar{d}_i)$ and $f_D(\bar{d}_i)$ were selected considering the reasons discussed. Furthermore, the fitness of the values selected was evaluated comparing the permeability obtained with the White and Beaven (2008) method and the permeability experimentally found for the specimens of MSW by Ivanova (2007) and for UK MBT and German MBT by Siddiqui (2011) and ensuring that both values had the same order of magnitude. For comparison purposes, the values selected were kept unaltered for each sample before and after degradation.

6.1.2. Results

Results obtained from the application of White and Beaven (2008) method are summarised in Table 6-2 and Annexes 6-1 to 6-5. PSD data were generated using the parameters of the PSD model summarised in Table 2-15. The parameters are those of the model that showed the highest fit to experimental data and that was judged to give the best PSD representation, i.e. Fractal Model for UK MBT and MSW and RR for German MBT. The parameters $f_L(\bar{d}_i)$ and $f_D(\bar{d}_i)$ were selected as described in Section 6.1.1. The porosities agree with the experimental drainable porosities reported by Siddiqui (2011) and by Ivanova (2007) for the specimens of solid waste. Data taken for UK MBT and German MBT was for the initial conditions during the experimentation in the CARs, i.e. absence of compression. The hydraulic conductivity reported for Siddiqui (2011) and Ivanova (2007) under no compression was used for comparison with the results from the model and then to adjust $f_L(\bar{d}_i)$ and $f_D(\bar{d}_i)$. Table 6-1 is a summary of the parameters used.

Table 6-1 Summary of parameters used for the application of White and Beaven (2008) method to samples of solid waste

	Stress (Kpa)	Average Drainable Porosity (%)	Average $K_{experimental}$ (m\s)	n	Source	f_D	f_L	PSD model
UK MBT B4	0	40	7.47E-05	0.4	Siddiqui 2011	0.04	2.3	Fractal
German MBT B4	0	37	6.37E-05	0.37	Siddiqui 2011	0.02	2.3	Rosin Rammler
MSW B4	0	34	8.45E-05	0.34	Ivanova 2007	0.02	2.3	Fractal

An example of data generated from application of the White and Beaven (2008) model to the PSD data presented in Chapter 2 is given in Table 6.2, with analyses of all PSDs given in Annexes 6-1 to 6-5.

Table 6-2 Application of White and Beaven (2008) method to UK MBT B4 sample

Sieve size mm	y retained	Average d mm	Channel diameter Di m	Channel lenght Li m	Channel area Ai m^2	Channel effective permeability Ki m/s	Sigma KiAi/A m/s
0,032	0,0500						
0,063	0,0186	0,048	1,90E-06	0,63	9,49E-05	2,79E-09	8,53E-11
0,15	0,0342	0,107	4,26E-06	0,77	1,43E-04	1,14E-08	5,25E-10
0,3	0,0391	0,225	9,00E-06	0,81	1,56E-04	4,87E-08	2,46E-09
0,6	0,0540	0,450	1,80E-05	0,90	1,94E-04	1,75E-07	1,09E-08
1,18	0,0724	0,890	3,56E-05	1,00	2,36E-04	6,20E-07	4,72E-08
2	0,0746	1,590	6,36E-05	1,01	2,41E-04	1,96E-06	1,52E-07
3,35	0,0929	2,675	1,07E-04	1,08	2,79E-04	5,15E-06	4,64E-07
6,3	0,1487	4,825	1,93E-04	1,27	3,83E-04	1,43E-05	1,77E-06
7	0,0293	6,650	2,66E-04	0,74	1,30E-04	4,67E-05	1,96E-06
8	0,0393	7,500	3,00E-04	0,82	1,58E-04	5,38E-05	2,74E-06
9	0,0367	8,500	3,40E-04	0,80	1,51E-04	7,07E-05	3,44E-06
10	0,0346	9,500	3,80E-04	0,78	1,45E-04	9,01E-05	4,22E-06
11	0,0328	10,500	4,20E-04	0,77	1,40E-04	1,12E-04	5,06E-06
12	0,0312	11,500	4,60E-04	0,76	1,36E-04	1,37E-04	5,97E-06
15	0,0862	13,500	5,40E-04	1,06	2,67E-04	1,34E-04	1,15E-05
20	0,1251	17,500	7,00E-04	1,20	3,42E-04	1,99E-04	2,20E-05
				A (m^2)	3,10E-03	**K (m/s)**	5,94E-05
						$K_{experimental}$ (m/s)	7,47E-05

Model Parameters		
Fractal dimension	2,5354	
n	0,40	
f_D	0,04	
f_L	2,3	
g	9,81	m/sec^2
mu liquid	1,00E-03	kg/m/sec
ro liquid	1000	kg/m^3

6.1.3. Discussion

Results from the application of White and Beaven (2008) method are summarised in Table 6-3. Changes in the hydraulic conductivity (K) with degradation were estimated in the specimens as a percentage of the K of the specimen before degradation.

Table 6-3 Comparison of K estimated with White and Beaven (2008) method in specimens of solid waste before and after degradation

	$K_{w\&b}$ (m\s)	%change in $K_{w\&b}$ with degradation	$K_{measured}$ (m\s)
UK MBT B4	5,94E-05	6,23%	7,47E-05
UK MBT AF	6,31E-05		NA
German MBT B4	1,95E-05	1,03%	6,37E-05
German MBT AF	1,97E-05		NA
MSW B4	4,09E-05	3,42%	8,45E-05
MSW AF	4,23E-05		NA
w&b	White and Beaven (2008)		

The results show that the K estimated with the White and Beaven (2008) method increased with the degradation of the specimens and was caused by a general increase in particle size with degradation discussed in Chapter 2. Although there are no independent experimental measurements of K following degradation to support these results, it is believed that the presence of coarser particles creates a coarser pore space which could create a higher hydraulic conductivity and consequently higher flows.

The results also show the potential magnitude of the changes in K. They indicate that K is not expected to increase by more than 10% as a result of the biodegradation occurring in the specimens studied. Some differences between the specimens are evidenced. For example, the specimen with the smaller increase in K of 1.03 % was the German MBT. This sample had the smaller and statistically un-significant variation in the PSD from the specimens of solid waste investigated. Whilst the specimens of UK MBT and MSW showed higher increases in K, i.e. 6.23 and 3.42% respectively, and both specimens had been demonstrated to experience significant variations in their PSDs with degradation.

The results suggest that the changes in structure caused by the biodegradation of a solid waste material may have a secondary impact on the variation observed in properties such as the hydraulic conductivity. Some other processes such as crushing and compression may have a stronger impact on the structure and consequently on the hydraulic conductivity. This is an area of some limited research over the last years (Dixon et al., 2008, McDougall et al., 2004), but worthy of further attention.

The procedure illustrated in this chapter to use PSD data for the estimation of the hydraulic conductivity could be extended to incorporate changes in PSD that arise from crushing or compression processes. This would require investigating the type of PSD model that best represents the experimental data both before and after the process. The type of model required will possibly change according to the process experienced by the residue. For example, Rosin-Rammler could give a reasonable representation of the PSD of the material before crushing, when the content of coarser particles is still significant. Whereas the fractal model could be a better model for the material after crushing, when the content of finer particles has increased.

The application of the White and Beaven (2008) method to specimens of solid waste from different origins here discussed, demonstrates the potential to incorporate PSD data into the estimation of macro properties of solid wastes such as the hydraulic conductivity. The study demonstrated some of the advantages attained when the PSD is represented with an analytical expression. For example, the simplicity in producing the entire PSD curve using, depending on the type of model, only one or two parameters (i.e. one parameter for fractal and two for RR). Additionally, there is the possibility of creating a new PSD for the degraded material by adjusting the PSD model parameters to reflect the extension of the degradation.

The results suggest also that in all the specimens $K_{\text{estimated}}$ and K_{measured} have the same order of magnitude (e.g. 5.94x10^{-5} vs 7.47 x10^{-5} m/s for UK MBT B4 estimated and experimental respectively). This could be an indication that the values selected for the functions $f_L(\bar{d}_i)$ and $f_D(\bar{d}_i)$ were of the correct order. However, as the values for those functions were empirically selected and not determined from values found in the literature , further analysis of the characteristics of $f_L(\bar{d}_i)$ and $f_D(\bar{d}_i)$ is required. To increase the confidence of the values estimated with the White and Beaven (2008) method, the functions $f_L(\bar{d}_i)$ and $f_D(\bar{d}_i)$ require to be determine in solid wastes of different natures. This was acknowledged by the authors White and Beaven (2008) and is emphasised here following the application of their method to solid wastes from different origins.

Although the method developed by White and Beaven (2008) is still under development and further research is necessary for a better estimation of the size functions, the application to solid waste specimens from different sources was demonstrated. One of the possibilities is the potential to incorporate changes in the structure of the solid waste into the estimation of the hydraulic conductivity. This offers an alternative to incorporate information about the structure of solid wastes into more complex macro-scale models. This may be possible by selecting an appropriate mathematical model (e.g. Fractal, RR or normal) to describe the PSD. It is also possible to include the associated changes in structure resulting from processes such as crushing, compression and biodegradation by adjusting or changing the PSD model according to the nature of changes under investigation. The inclusion of information about the structure of solid wastes is an area that has been recognised as important by most modellers but that has been in the practice neglected in most macro-scale landfill models. The use of mathematical models to represent PSD data and the use of such data to estimate the hydraulic conductivity with for example the use of White and Beaven (2008) method could be a reasonable alternative to address such difficulty. The procedure to attain such information has been illustrated in Chapters 2 and 6 of this thesis.

6.2. The influence of material composition on the hydraulic conductivity of solid wastes

Material composition of raw and processed specimens of solid waste was discussed in Chapter 3. Results illustrated the differences found between specimens and also the changes arising from degradation. In addition to conventional material characterisation, the framework introduced by Velkushanova et al.(2009) was extended to classify materials according to their shape expressed as their dimensionality. Dimensionality and material composition were combined to develop a criterion to classify materials according to their potential to affect flow. Material composition was transformed into the content of 0D, 1D, 2D and 3D components. The fraction composed for 2D materials, was theorised as to have the potential to be flow impeding or diverting. This hypothesis was confirmed in the experiments presented in Chapter 4. It was shown that when 2D materials are sufficiently large in comparison to the particles in the surrounding matrix, and constitute over a certain percentage of the residue, they could influence the flow properties. The experiments showed that to be considered as potentially flow diverting or impeding, 2D particles need to have at least 15 times the size of the particles of the surrounding matrix and account for at least 7.3% by mass in the residue. The potential to affect flow of the 2D particles was measured as the magnitude of the reduction in the hydraulic conductivity *K* of the matrix material without 2D particles. Only reductions in *K* over 30% were considered as significant. Once only those 2D particles 15 times larger than the matrix particles are defined as flow diverting or impeding , the mass content of 2D particles can be used to evaluate the composition of a waste material and assess whether that content is high enough (i.e. > 7.3% by mass) to cause an important impact on the flow properties of the residue. The criterion can then be incorporated into the ternary plots introduced in Chapter 3 and be used to discriminate between composition regions where an impact on flow properties is expected from those where such impact is not expected. In Figure 6-1, a graphical representation between two regions according to the mass content of 2D particles is presented. Region 1 represents those residues with low 2D particles mass content (i.e. < 10%), and therefore with a non-significant impact on flow properties. Whilst region 2 represents those residues with an important content of 2D particles and consequently a significant impact on flow properties.

With the regions defined, a discussion for the specimens of solid waste studied during this research follows. In the first instance, the definition applied in chapter 3 for flow diverting and impeding particles needs an adjustment in the light of the results discussed in chapter 4. In Velkushanova et al. 2009, it was considered that 2D particles 5 times the size of the particles in the matrix could be considered either as flow diverting or impeding. However, the experimental results suggest that those particles are not sufficiently large to cause a significant reduction in K (i.e. > 30%) and that they need to be at least 15 larger than the size of the particles in the matrix. With this adjustment, Figure 3-6 was modified for the specimens that have a completed characterisation (i.e. material classification for each size fraction) and the resulting ternary plot presented in Figure 6-2. The adjusted mass content of diverting and impeding materials were calculated using Tables 3-8 to 3-13. For the UK MBT and German MBT specimens, a representative matrix particle size of 1mm was defined which means that 2D particles need to be approximately 15 mm long to be considered as flow diverting or impeding. Only 2D particles in the fraction from 12-20 mm and over were summed up to obtain the amount of diverting and impeding particles. A comparison between Figure 3-6 and Figure 6-2 evidences that with the adjusted definition, the amount of flow diverting and impeding particles decreased from over 30% by mass to less than 17%. Nevertheless, contrasting Figures 6-1 and 6-2 evidences that the composition of the specimens is still located within the region 2 where the content of 2D particles is high enough to cause an effect on the residue flow properties.

This type of ternary representation could be used in practice to move from a general material characterisation to infer whether the hydraulic conductivity could see a reduction of more than 30% resulting from the important content of 2D materials that can have an impact on the flow properties of the solid waste material.

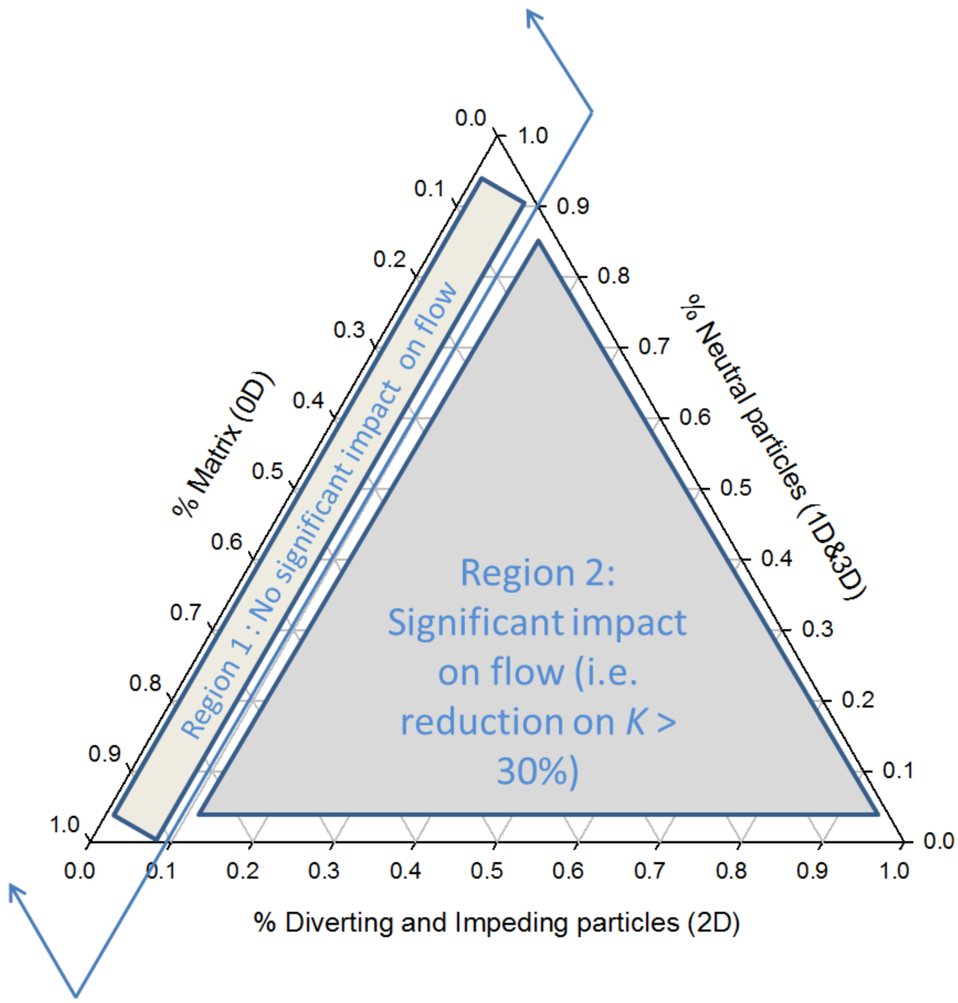

Figure 6-1 Ternary Plot illustrating different regions according to the impact on flow caused by the presence of 2D particles

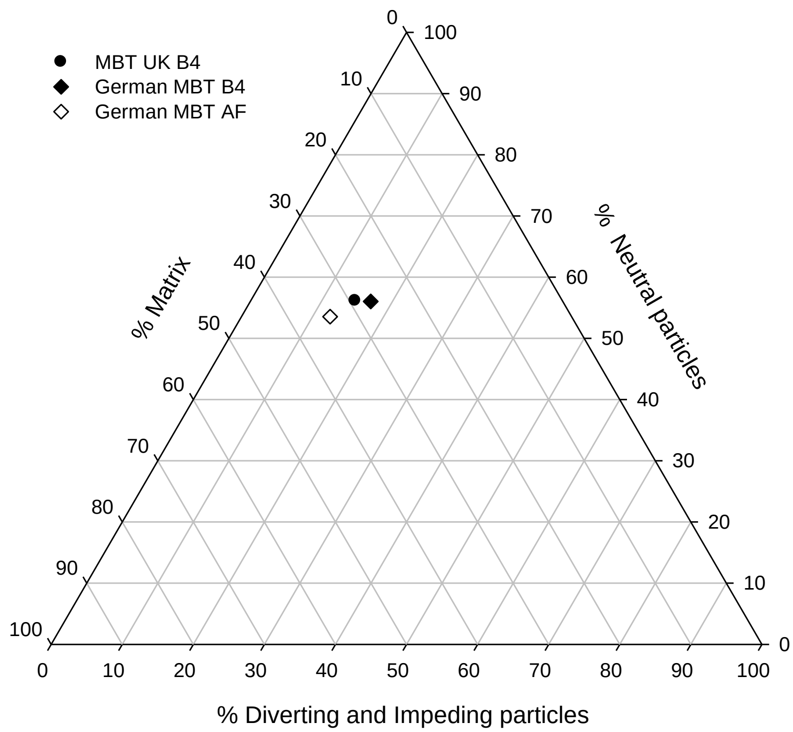

	Diverting & Impeding	Neutral	Matrix
MBT UK B4	14.73%	56.12%	29.15%
German MBT B4	16.96%	56.02%	27.02%
German MBT AF	12.48%	53.55%	33.97%

Figure 6-2 Adjusted comparative Ternary Plot of specimens of solid waste classified according to the content of particles that affect flow. The diverting or impeding particles are at least 15 the average matrix particle size

7. Summary and Conclusions

This chapter presents the summary and key conclusions drawn from the research discussed in this thesis and outlines areas of future work.

Results from analyses on particle size and particle shape in specimens of MSW and MBT suggest that these two properties differ between specimens and change with degradation. Particle size and shape play an important role in the type of the structure that develops in landfilled solid wastes which in turn influences fluid flow processes. Results from this research suggest that landfilled solid wastes could experience structural changes with degradation undergoing an increase in the average particle size and in the content of 2D materials. The magnitude of such changes appears to depend on the material's initial state of degradation. For example, the specimen of waste with more pre-treatment (i.e. German MBT with aerobic-anaerobic treatment) showed minor changes than those seen in specimens of MSW and partially pre-treated MBT residues (i.e. UK MBT).

Experiments with waste analogues and waste specimens suggest that 2D particles influence fluid flow processes reducing the saturated hydraulic conductivity, increasing flow paths tortuosity and favouring preferential flow paths. Reduction in the hydraulic conductivity was found to be within one order of magnitude and to be a function of the 2D particles relative content and size.

Based on the results of this study, the framework described by Velkushanova et al. (2009) needs adjustment. In Velkushanova et al.(2009), 2D particles are classified as potentially flow diverting or impeding if they are at least 5 times larger than the size of the particles in the matrix. However, the study detailed along this thesis showed that 2D materials might reduce the hydraulic conductivity by more than 30% when they are 15 times larger than the surrounding matrix and constitute at least 7.3% (by dry mass) of the solid waste. This suggest that 2D particles may need to be 15 times larger than the size of the particles in the matrix and represent more than 7% by dry mass to be consider as potentially flow diverting or impeding.

Results from the experiments in a specimen of MSW suggest that the presence of inert coarse 2D materials could influence the development of a strong and layered structure, where large pores are horizontally connected and favoured preferential flow. More research is necessary to understand the impact of 2D materials in residues of different nature (e.g. MBTs)

Three techniques, i.e. visualization of flow paths with dye tracers, thin sectioning and μCT, were pioneered and successfully applied during this research to study the structure in solid waste and the presence of preferential flow. The use of μCT to characterise the structure of MSW was demonstrated.

The findings from the previous chapters are summarized below:

7.1. The nature of particle size and shape in solid wastes

The following was drawn from the study of particle size and shape:

1. Particle size was successfully described using physically based PSD mathematical models, an approach un-explored in solid wastes. This opens the possibility of incorporating analytical expressions into existing waste-behavioural mathematical models to characterise the particle size; and consider changes with degradation by tuning the parameters values in the analytical expressions.

2. The nature and waste processing history of the residue investigated has an influence on the type of model that best describes its PSD.

3. Changes in particle size distribution with degradation were statistically significant in the specimen of a partially pre-treated MBT (i.e. UK MBT) and in the specimen of MSW, but insignificant in a sample of the highly pre-treated MBT (i.e. German MBT). In the specimens investigated, the controlled degradation in the CAR produced an increase in the average particle size. This could indicate that the specimens underwent a degradation mechanism where readily degradable smaller particles were degraded earlier than those of inert coarser materials.

4. 2D materials were found to be predominantly coarse inert and slowly degradable materials, i.e. flexible and rigid plastics, glass, paper and textiles. In the specimens investigated, 2D particles comprised over 30% by dry mass which suggests that they may constitute a significant proportion in residues from different sources. The content of 2D particles experienced a further increase of 4 to 6% with degradation indicating that 2D materials may experience little or non-degradation.

7.2. The role of 2D particles on permeability

Results from the experiments using waste analogues provide an indication of the magnitude of the changes expected in the hydraulic conductivity in solid wastes. The study also indicates that the reduction in the hydraulic conductivity could be a function of the 2D materials content and relative size.

The following is a proposed approach that could be used to incorporate the findings of this research into calculating changes in hydraulic conductivity as a result of 2D particles. The idea is to include variations in *K* that result from changes in the structure and geometry which may result from degradation or other processes (e.g. crushing). An initial characterisation that includes PSD and material composition would be necessary:

1. First, the initial hydraulic conductivity (K_o) could be estimated using Powrie and Beaven (1999) equation using the depth or effective stress conditions. Alternatively, the initial PSD can be used to estimate K_o considering a soil or granular media with a similar grading to the residue studied. In this case only the magnitude of the changes in *K* are meaningful.

2. The initial material characterisation could be used to estimate the proportion of 2D particles. For example, 2D plastic and glass pieces could be considered as potentially flow diverting. While the waste analogue experiments were performed with plastic 2D particles, it may be reasonable to consider a comparable effect from 2D glass pieces. Paper and textiles are semi-permeable materials and could be conceptualised as flow impeding particles. Data for impeding materials is unavailable. An alternative might be to consider only a fraction (e.g. 50-70%) as potentially diverting. The initial mass content of 2D particles could be calculated with these considerations.
3. The size of the 2D particles is considered. The maximum in the PSD curve indicates the size of the largest 2D particles (assuming that the bulky 3D particles had been removed). Considering the results in chapter 3, the matrix materials content could be approximated to 30%. The D_{50} in the matrix, equivalent to the D_{15} of the entire PSD, gives a reasonable estimation of the median size of the matrix particles. The ratio between 2D particles and matrix median could then be calculated. The result gives an indication of the *RS*.

4. If the mass content of 2D particles is less than 7.3% (relative volumetric content VC < 20) and relative size (*RS)* is less than 15, there is no need to include a correction factor for the initial waste as K/Ko would not be greater than 0.7. However, as degradation evolves, the final content of 2D particles can increase by an extra 4 to 6%. Further analysis could be necessary according to step 8 below.

5. If the mass content of 2D particles is between 7.3% and 13.7% (20 ≤VC <40) and 15 ≤ *RS* < 25, a correction factor can be applied considering the relation $K/Ko = -0.005VC + 0.81$ (see Figure 4-9). *K*/*Ko* will take values between 0.71 and 0.61.

6. If the mass content of 2D particles is between 7.3% and 13.7% (i.e. 20 ≤VC <40) and *RS*=25, a correction factor can be applied considering the relation $K/Ko = -0.0094VC + 0.72$ (see Figure 4-9). *K*/*Ko* will take values between 0.53 and 0.34.

7. For mass contents exceeding 13.7% and *RS* above 25, a reduction in the hydraulic conductivity of one order of magnitude can be applied, and the correction factor equals 0.1.

8. The impact of a waste aging on its hydraulic conductivity could be estimated if the content of 2D particles caused by degradation increases significantlyby using the new composition factors within steps 4 to 7 above.

9. Changes in PSD with degradation could be incorporated considering the nature of the residue investigated. More research is necessary to extend the findings explained in chapter 2 to other specimens of solid waste, yet the curves presented in chapter 2 could be used as an indication.

   i. For dual aerobic and anaerobic pre-treated wastes, changes in PSD with degradation could be considered as negligible
   ii. For raw municipal solid wastes and aerobic pre-treated wastes, the general trend observed in the specimens of MBT UK and MSW could be used as an indication of how PSDs may change, and hence have an impact on permeability.
   iii. With the new PSD, K_o is updated and calculations start again

7.3. Preferential flow and waste structure

The following was drawn from the study of preferential flow and waste structure in a specimen of degraded MSW:

1. Preferential flow was found to be predominant in a strong layered structured degraded MSW which was tested under unsaturated flow rate conditions ($Q \approx 0.7$ $Qsat$) using two different methods, i.e. injection and irrigation, with 92.49% and 45.28% peripheral flow respectively.

2. The layered type of the structure seemed to be influenced by the high content of coarse 2D materials, i.e. over 50% (by dry mass) and 20 mm size, horizontally oriented and that remained unaffected during the degradation.

3. The use of μCT revealed detailed information of the structure and pore architecture in the specimen of MSW investigated. 50% by volume of the pores were found to be of horizontally connected large pores above 1.60 mm size. Large pores could be the cause of the presence of preferential flow channels.

7.4. Future Work

The study detailed along this thesis produced a level of new understanding in the following areas (see Table 1-1):

At the particle level: particles size and shape were described using PSDs mathematical models and dimensional descriptors. Results from the study indicate that particle size and shape diverge between residues from different origins. The treatment story and changes with degradation could change the PSD, the material composition and influence the type of PSD model. Emphasis was placed to the quantification of 2D materials which were shown to constitute an important mass fraction of the specimens investigated.

At the level of packed bed: techniques to study the structure in solid residues (i.e. μCT , thin sectioning and dye staining) were developed and applied to a degraded specimen of MSW. Using those techniques, structural features such as layering and pore space architecture were investigated with a pioneer detailed level.

At the level of fluid flow behaviour: the influence of 2D materials on hydraulic conductivity was studied using analogues. The study demonstrated that 2D materials can reduce the hydraulic conductivity of a matrix. The larger and more abundant the 2D particles, the greater the reduction. 2D materials were also shown to influence the presence of preferential flow channels.

The following suggestions for future work are made:

1. At the level of fluid flow behaviour:

    a. Further experiments are required to investigate the impact on the hydraulic conductivity of other type of 2D materials, i.e. glass, paper and textiles, which may reduce the hydraulic conductivity at different conditions than those observed in plastics 2D materials (i.e. *RS* 15 and *VC* 20).

    b. The experiments in the permeameter were carried out to represent the proportion of 2D plastics in the specimens of MBT studied. It is necessary to extend the investigation to cover higher contents of plastic 2D materials (i.e. mass contents over 13.7%) to represent the higher contents observed in MSWs.

    c. To have a more comprehensive understanding of the effect of 2D materials on the hydraulic conductivity of solid wastes, it is recommended to validate the results in solid wastes using a waste derived matrix material modified with controlled amounts of 2D particles.

d. More work on mathematical models other than Maxwell is recommended to help understand the impact of 2D particles on K on a theoretical level.

2. At the level of packed bed, at least two areas for further research are proposed:

a. The presence of preferential flow paths could generate operational difficulties during the application of remediation strategies resulting from the poor access of fluids to some of the areas in the landfill and consequent spatial variation in contaminants flushing. Further research for a better understanding of the influence of factors such as waste composition, pre-treatment, placement method and waste age on the nature of the structure developed and flow through preferential flow paths is necessary.

b. CT and μCT could be applied to characterise the structure of landfilled waste adopting a multiple scale imaging approach. This could provide significant insights to aid understanding of, for example, how the structure of waste changes over time as it degrades through variations in pore size and interconnectivity; or the difference in the structure that develops in residues with different characteristics.

8. Annexes

Annex 2-1 PSD and hydraulic conductivity in samples of raw (DM3) and pulverised (PV1) pre-landfilled directive household wastes, from Beaven (2000)

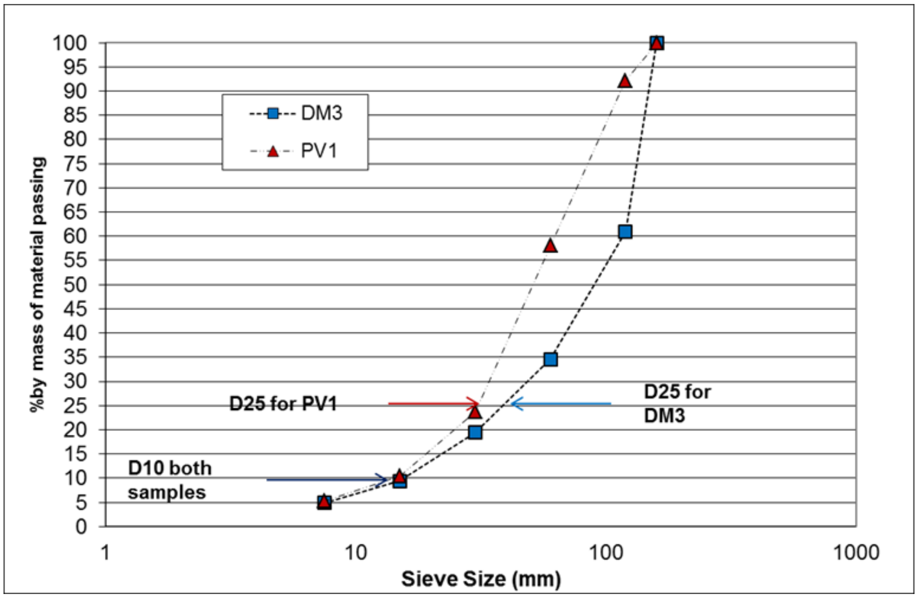

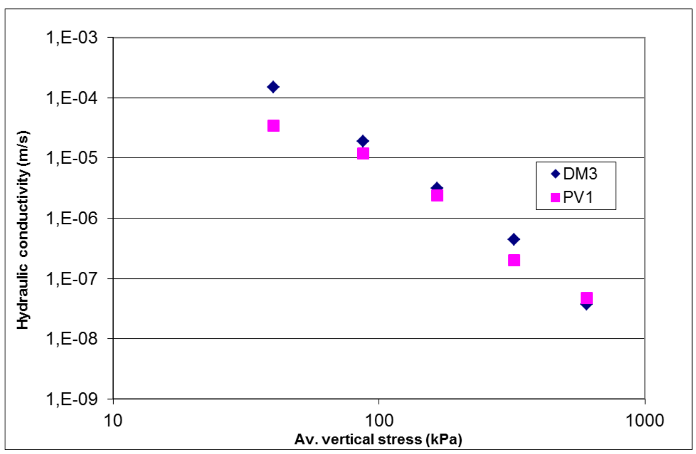

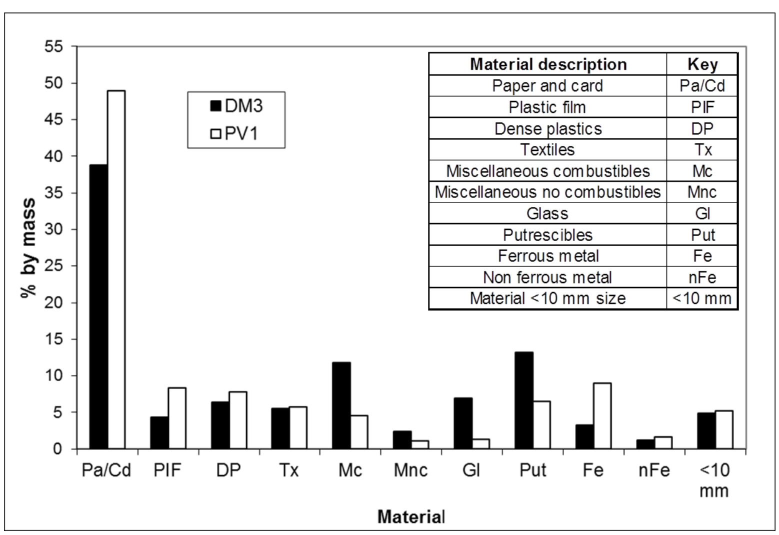

Annex 2-2 Graphical representation of simulated PSDs for solid waste following diverse mathematical models for particle size distribution

Properties and differences between the mathematical models to describe particle size, i.e. Normal, Rosin Rammler distributions and Fractal. Simulated particle size distributions were created for a solid waste following each of the models. Parameters for each model were selected from those obtained for German MBT.

Normal distribution			Rosin Rammler distribution			Fractal scaling	
Distribution parameters		Observations	Distribution parameters		Observations	Parameters	
Z_{mean}	1,9890	The distribution is normal in the Ln (sieve size), and can be referred as log-normal. Parameters were selected from those obtained with the normal model for German MBT	d'	10,2964	Parameters selected from those obtained with the RR model for German MBT	D	2,4581
Sg	1,1757		v	1,0395		Observations	Parameters selected from those obtained with Fractal model for German MBT
X_{mean}	7,3085						
S	0,1618					Calculations using Equation 2-24	
		Calculation using function NORMDIST-Excel which correspond to Equation 2-15	Calculations using Equation 2-22				$(R/R_L)^{\wedge 3-D}$
Sieve size (mm)	Ln sieve size	Normal (log-normal)	$(x/d')^v$		Rosin Rammler	R/R_L	Fractal
75	4,3175	0,9762	7,8792	0,0004	0,9996	1,0000	1,0000
63	4,1431	0,9665	6,5730	0,0014	0,9986	0,8400	0,9098
37,5	3,6243	0,9179	3,8331	0,0216	0,9784	0,5000	0,6869
20	2,9957	0,8041	1,9941	0,1361	0,8639	0,2667	0,4886
10	2,3026	0,6051	0,9701	0,3790	0,6210	0,1333	0,3356
6,3	1,8405	0,4497	0,6001	0,5488	0,4512	0,0840	0,2613
3,35	1,2090	0,2535	0,3112	0,7325	0,2675	0,0447	0,1855
2	0,6931	0,1352	0,1821	0,8336	0,1664	0,0267	0,1403
1,18	0,1655	0,0604	0,1052	0,9001	0,0999	0,0157	0,1054
0,6	-0,5108	0,0167	0,0521	0,9493	0,0507	0,0080	0,0731
0,3	-1,2040	0,0033	0,0253	0,9750	0,0250	0,0040	0,0502
0,15	-1,8971	0,0005	0,0123	0,9878	0,0122	0,0020	0,0345
0,063	-2,7646	0,0000	0,0050	0,9950	0,0050	0,0008	0,0215
0,032	-3,4420	0,0000	0,0025	0,9975	0,0025	0,0004	0,0149

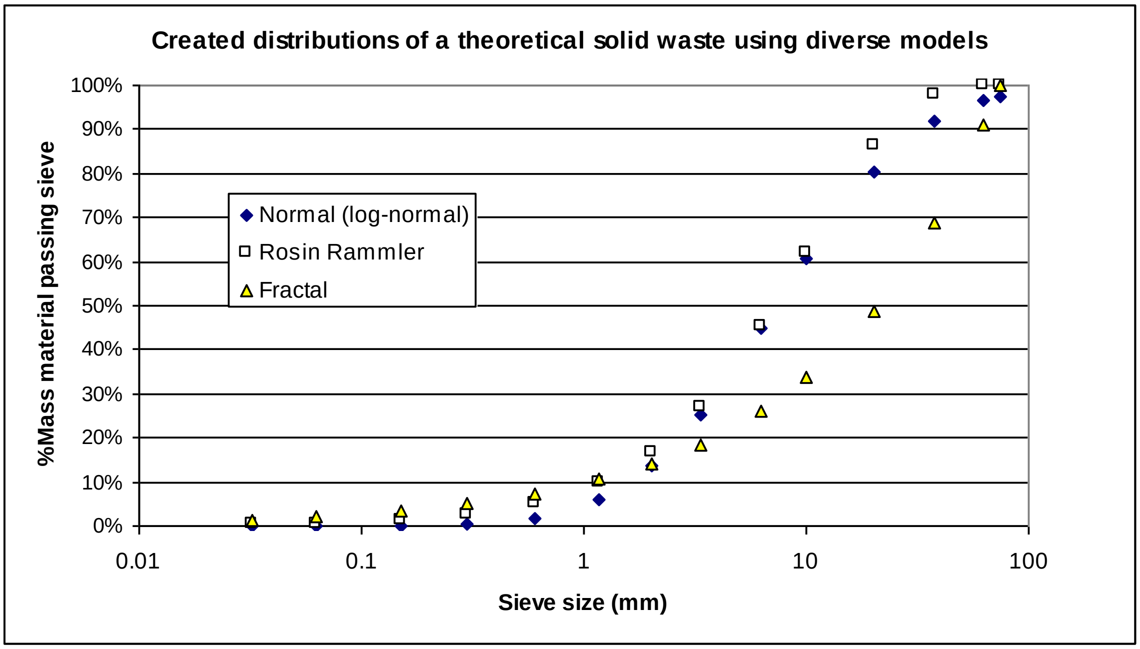
Created distributions of a theoretical solid waste using diverse models
100%
90%
80%
70%
60%
50%
40%
30%
20%
10%
0%
%Mass material passing sieve
Normal (log-normal)
Rosin Rammler
Fractal
0.01
0.1
1
10
100
Sieve size (mm)

Annex 2-3 MBT UK schematic description of the treatment process (after http://www.newearthsolutions.co.uk/residual-waste-treatment/process-description/, last accessed January 25 2010)

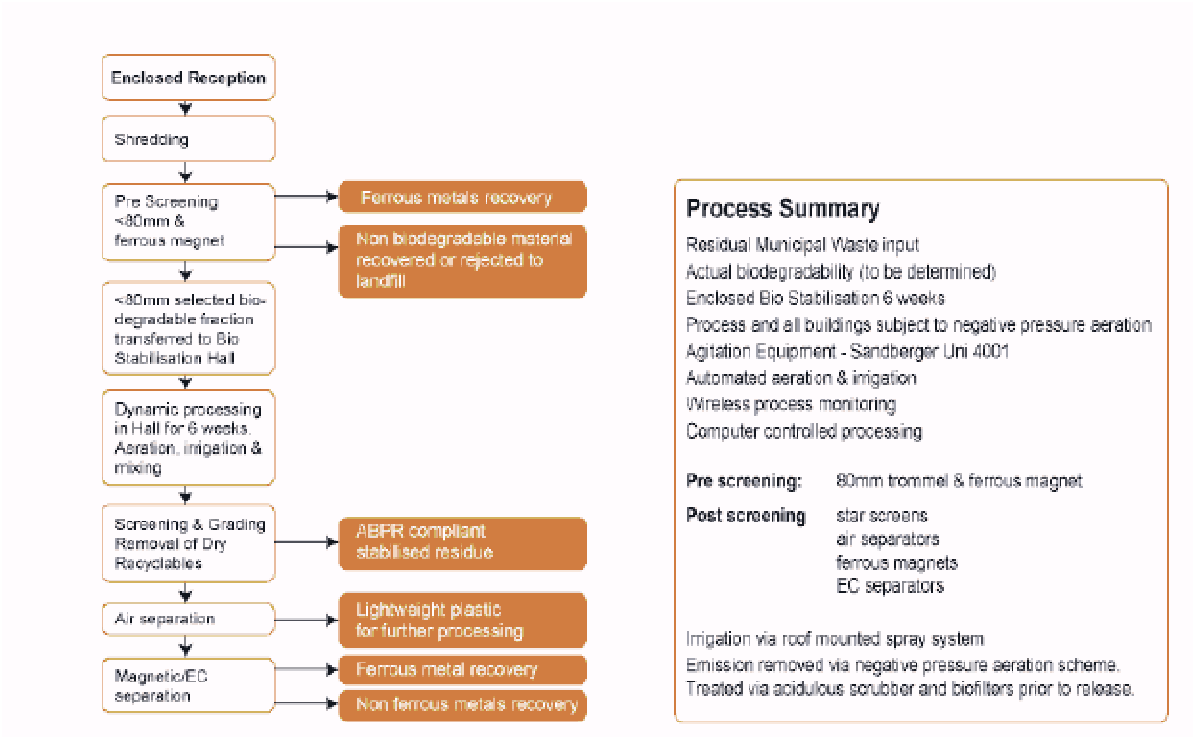

Annex 2-4 Comparison of PSDs with dry and wet sieving methods . a. UK MBT B4, b. German MBT B4, c. MSW AF.

In the two samples of MBT waste dry sieving showed a tendency to underestimate the content of materials retained in mesh sizes< 10 mm. The differences were more pronounced for MBT UK (a) than for German MBT (b). This underestimation can be recognised as a right shifted curve for MBT UK-wet sieving with approximately 5% more content of fines in the range 0.3-3.35 mm size. For German MBT the underestimation is evidenced as a right shifted curve with approximately 2% more content of fines in the range 0.6 to 6.3 mm. For MSW the effect of underestimation of fines is not evident but there is an overestimation of approximately 3% in the content of coarse materials > 10mm size.

a. Comparison of PSDs obtained with dry and wet sieving in sample of MBT UK before degradation

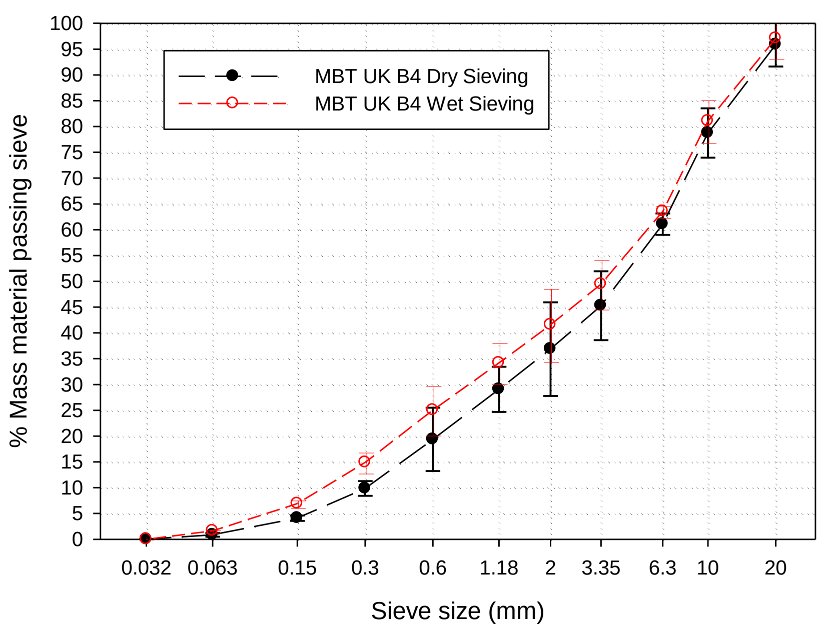

b. Comparison of PSDs obtained with dry and wet sieving in sample of German MBT before degradation

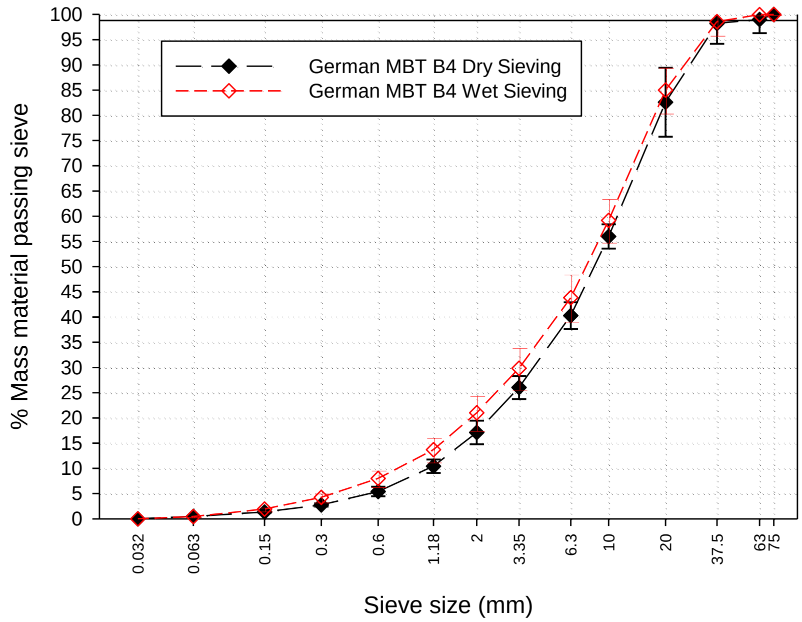

c. Comparison of PSDs obtained with dry and wet sieving in sample of MSW after degradation

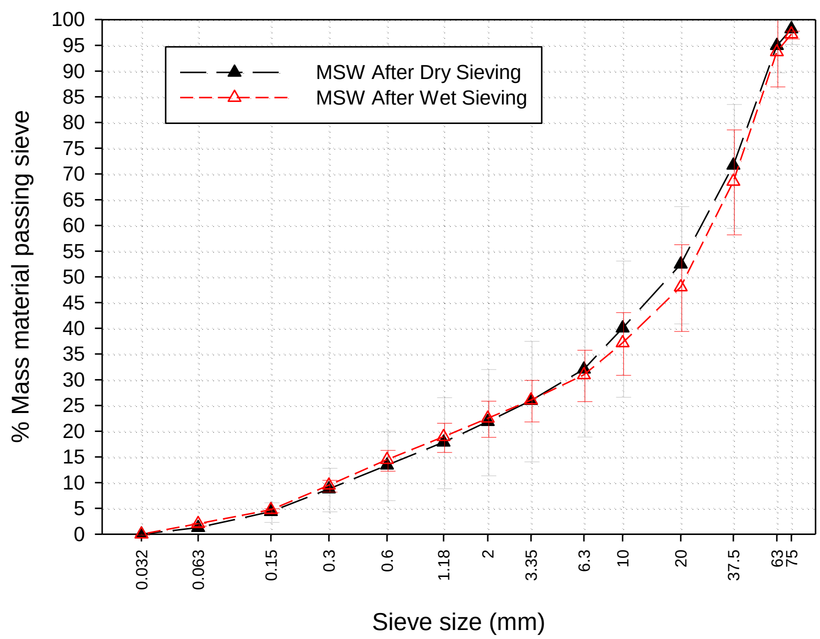

Annex 2-5 PSDs in UK MBT obtained before and after degradation. a. cumulative distributions. b. histogram.

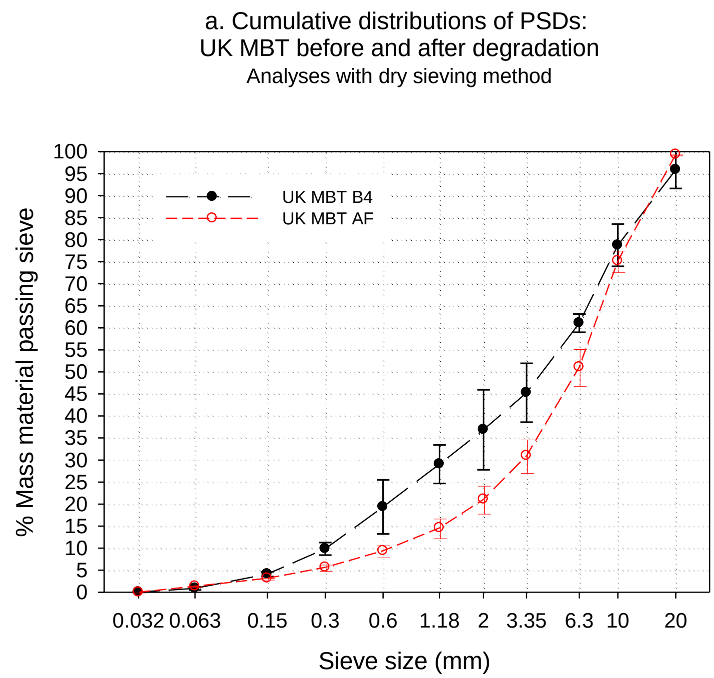

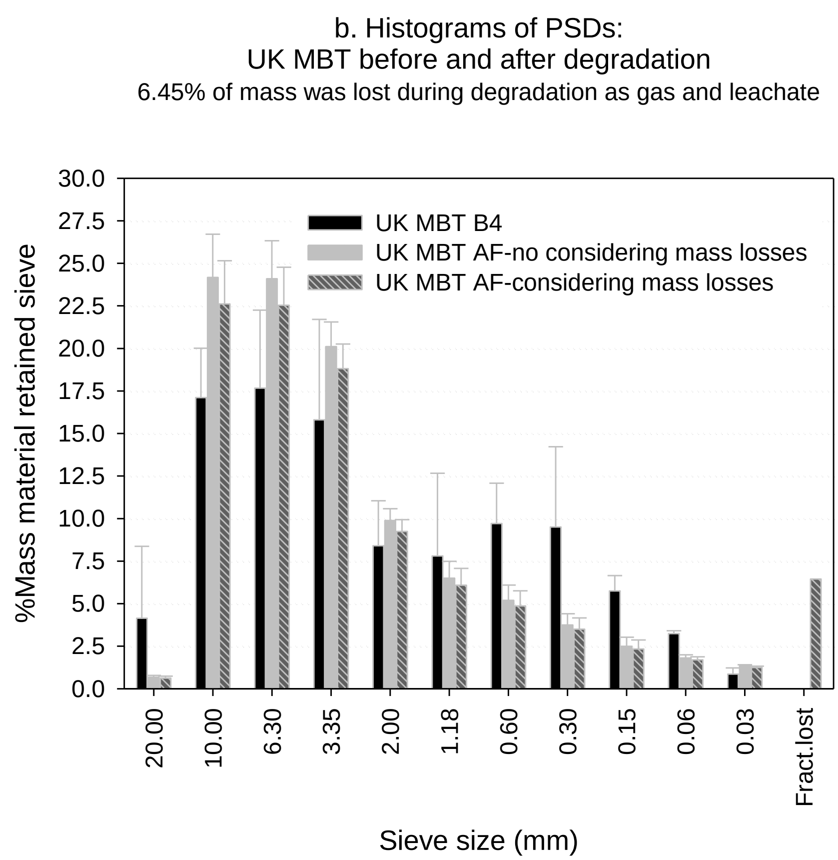

Annex 2-6 PSDs in German MBT obtained before and after degradation. a. cumulative distributions. b. histogram.

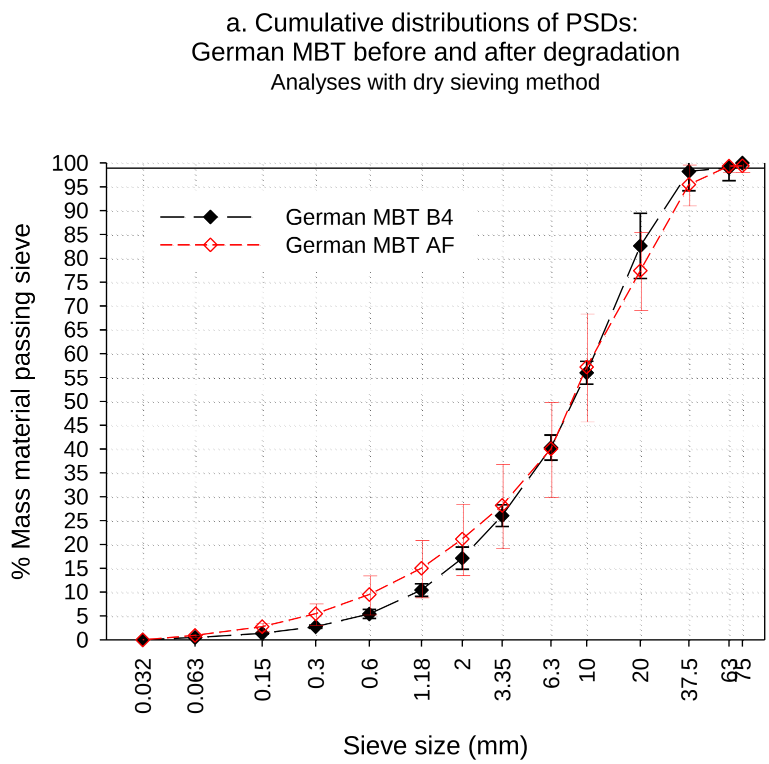

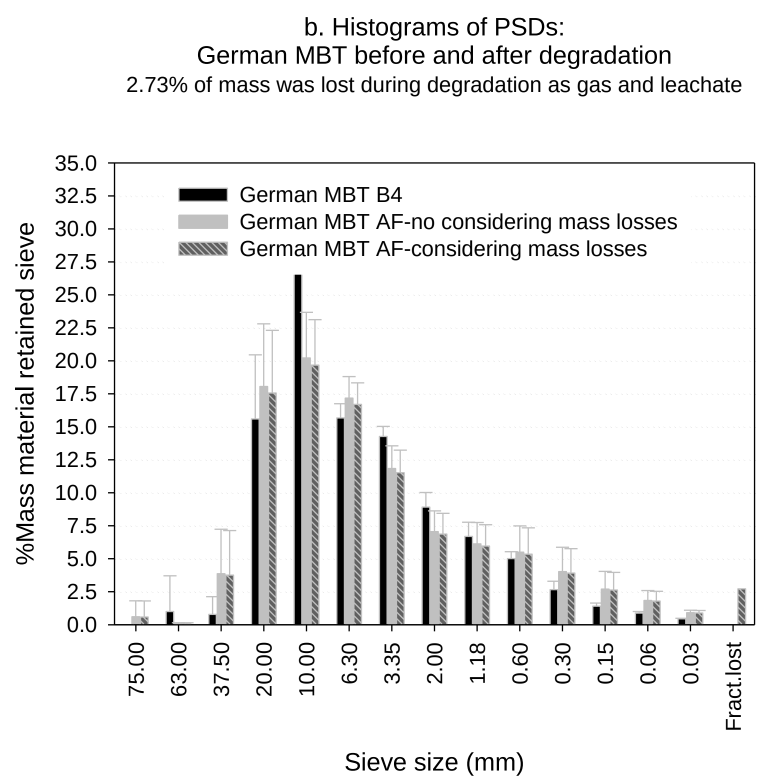

Annex 2-7 PSDs in MSW obtained before and after degradation. a. cumulative distributions. b. histogram.

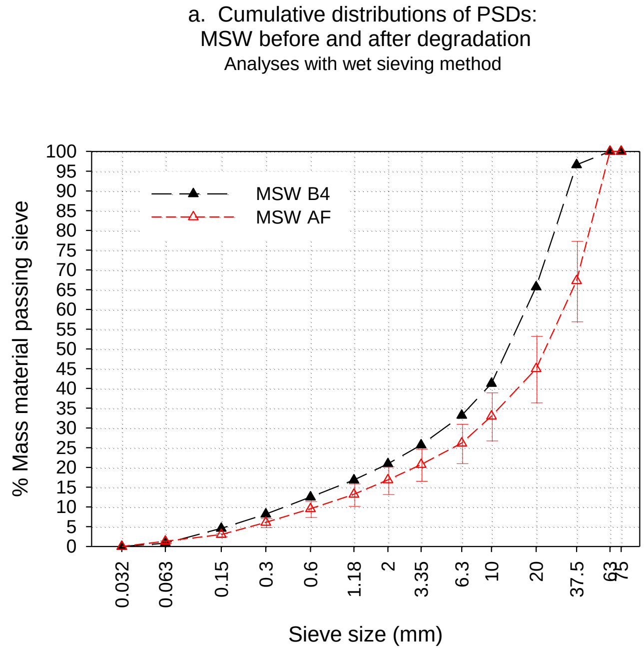

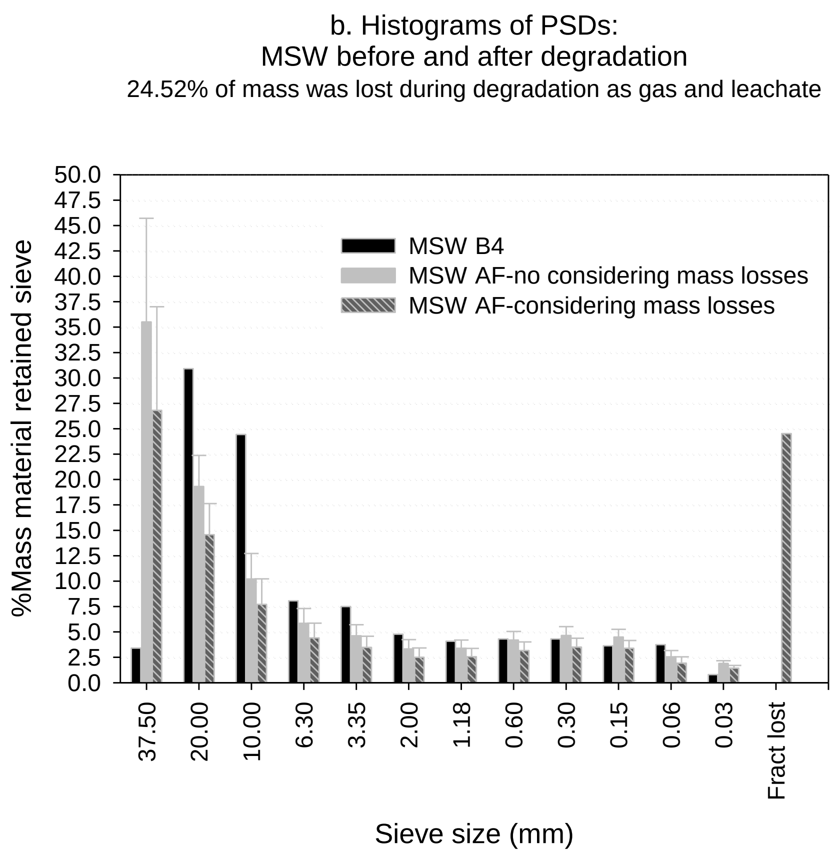

Annex 2-8 Graphical analysis of the cumulative PSD in UK MBT for assessment of normal law using, a. linear-linear, b. logarithmic-linear, c. logarithmic-probabilistic and d. linear-probabilistic scales

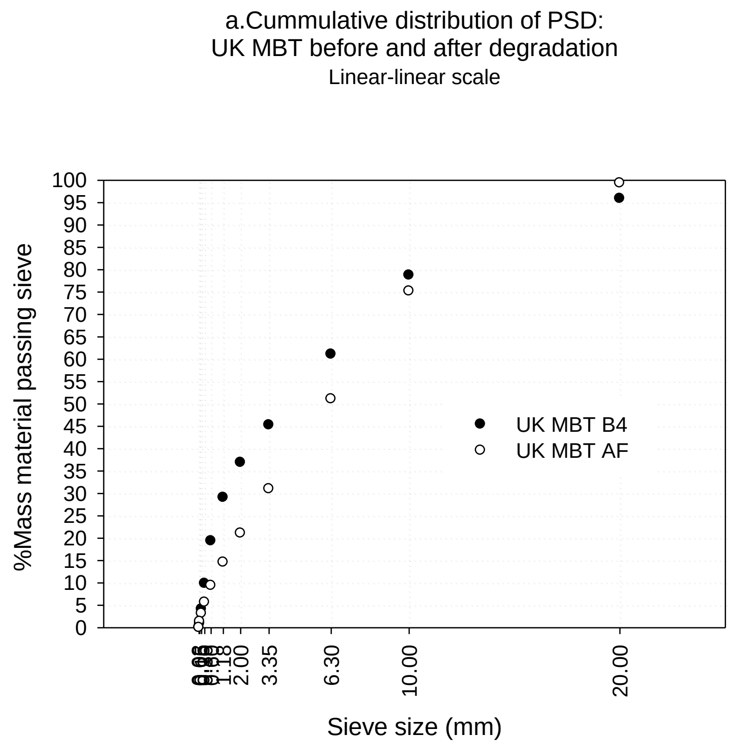

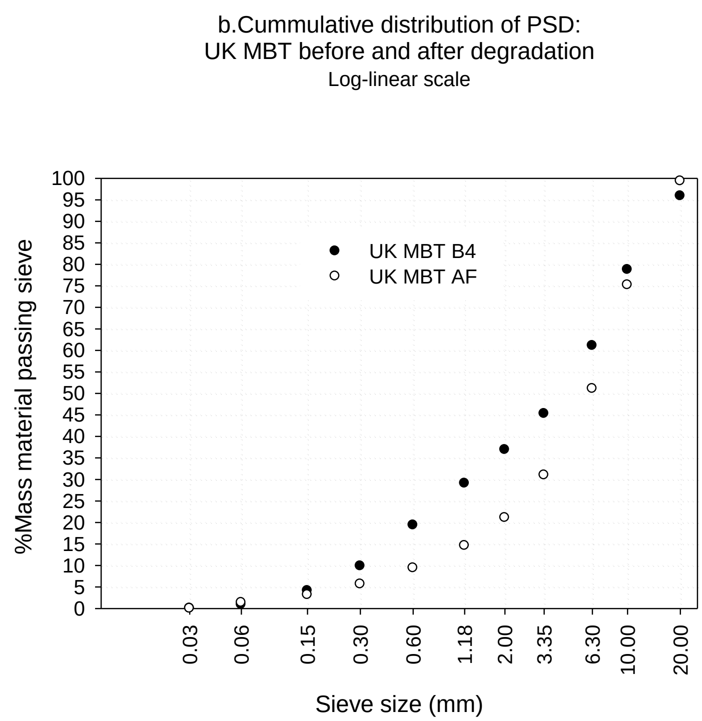

c.Cummulative distribution of PSD:
UK MBT before and after degradation
Log-probabilistic scale

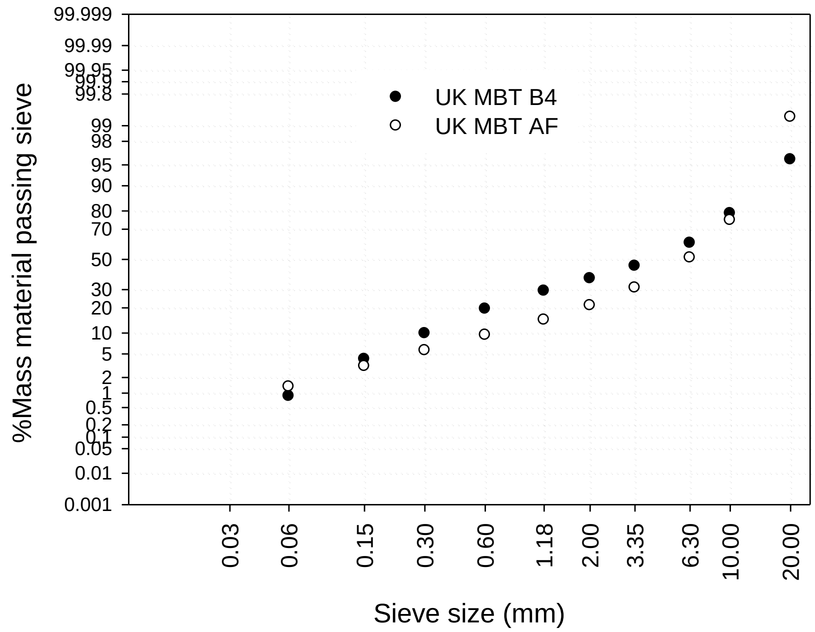

d.Cummulative distribution of PSD:
UK MBT before and after degradation
Linear-probabilistic

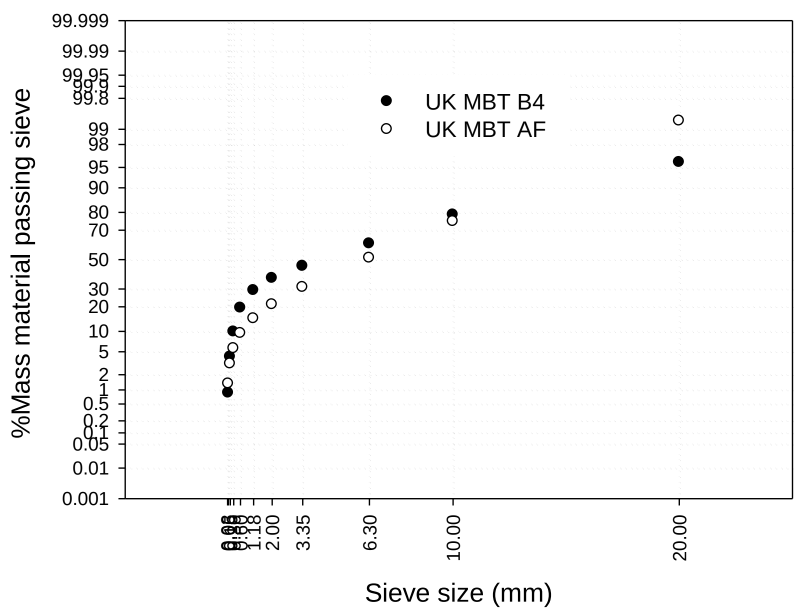

Annex 2-9 Cumulative PSD represented in Log-probabilistic scale for a. German MBT and b. MSW specimens

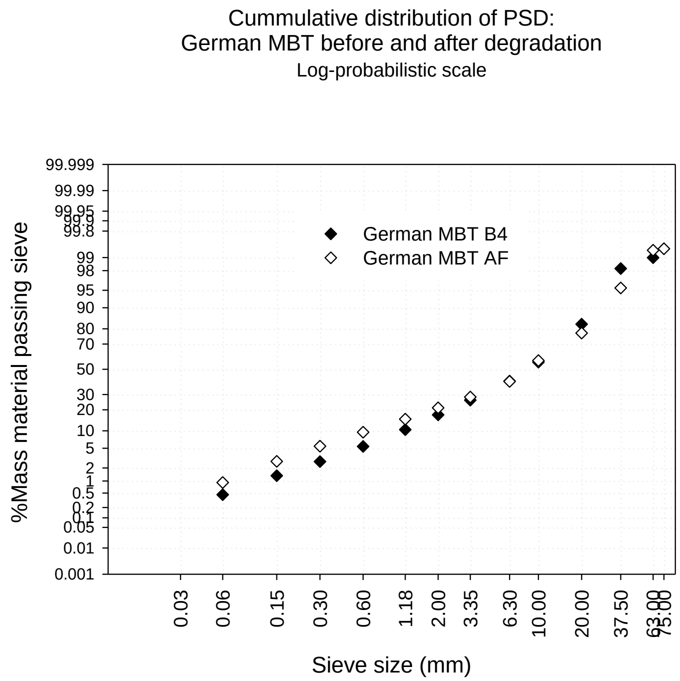

a. Cumulative PSD of German MBT represented in Log-probabilistic

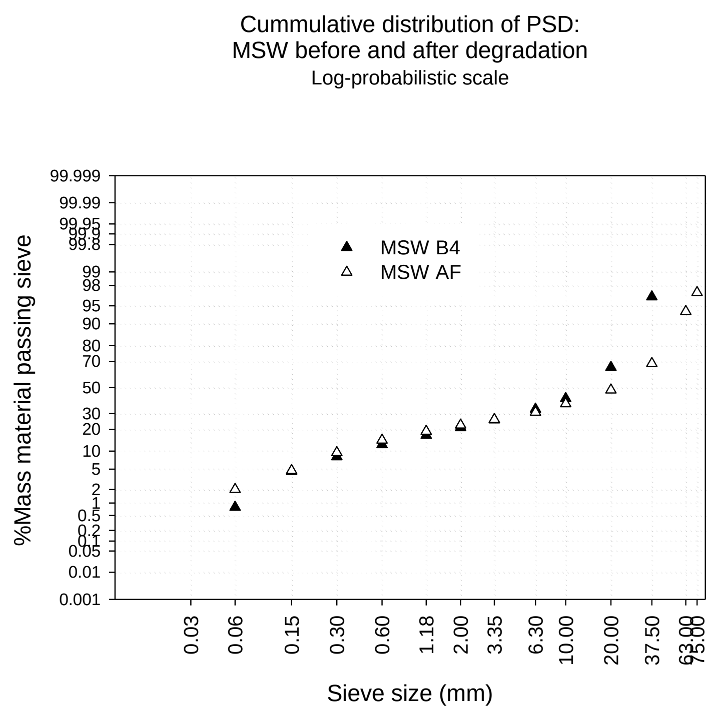

scale

b. Cumulative PSD of MSW represented in Log-probabilistic scale

Annex 2-10 Normal law model fitting to PSDs of UK MBT before and after degradation for different sieve size ranges. a. cumulative 20-0.032 mm , b. cumulative 6.3-0.063 mm, c. linear scale 20-0.032 mm and d. linear scale 6.3-0.063 mm

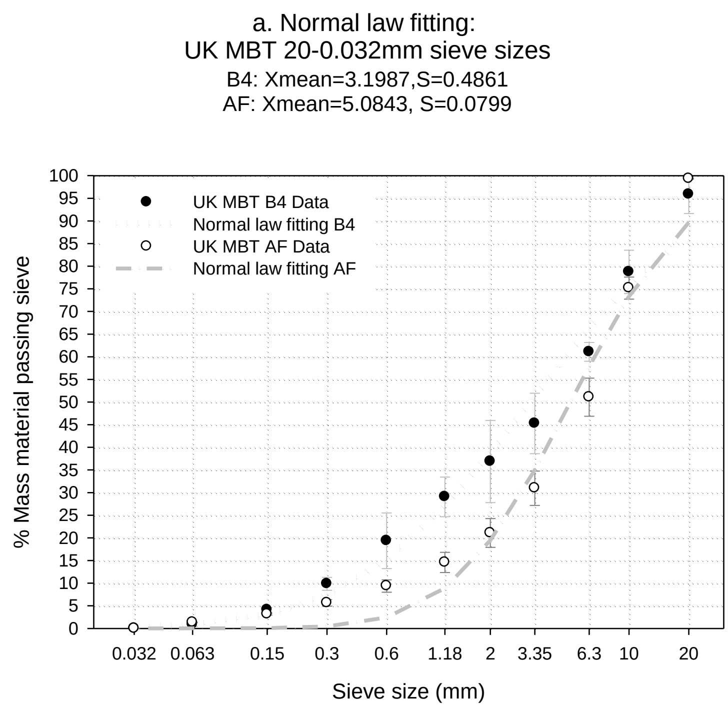

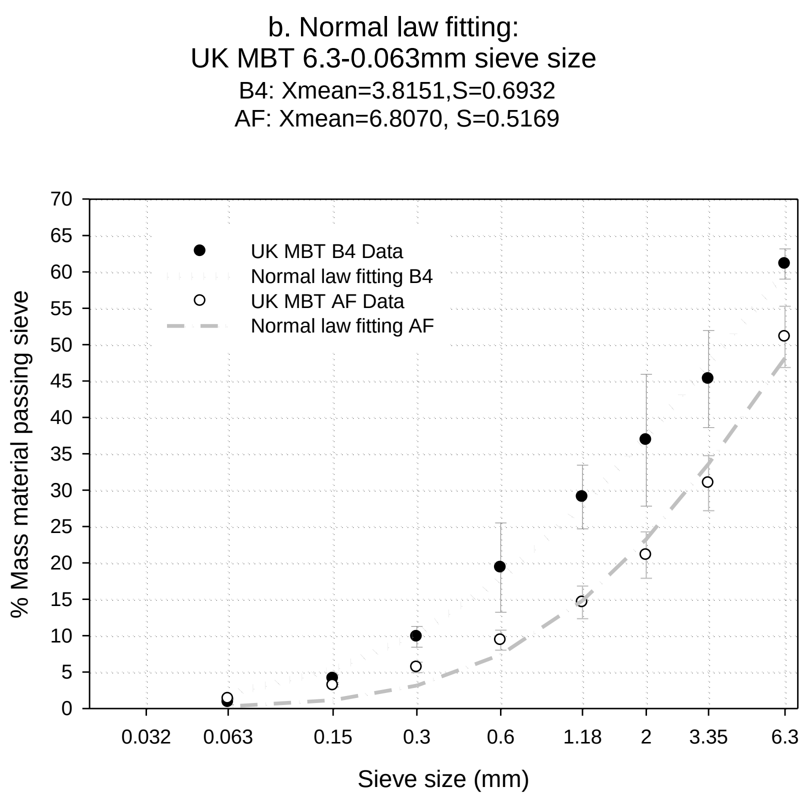

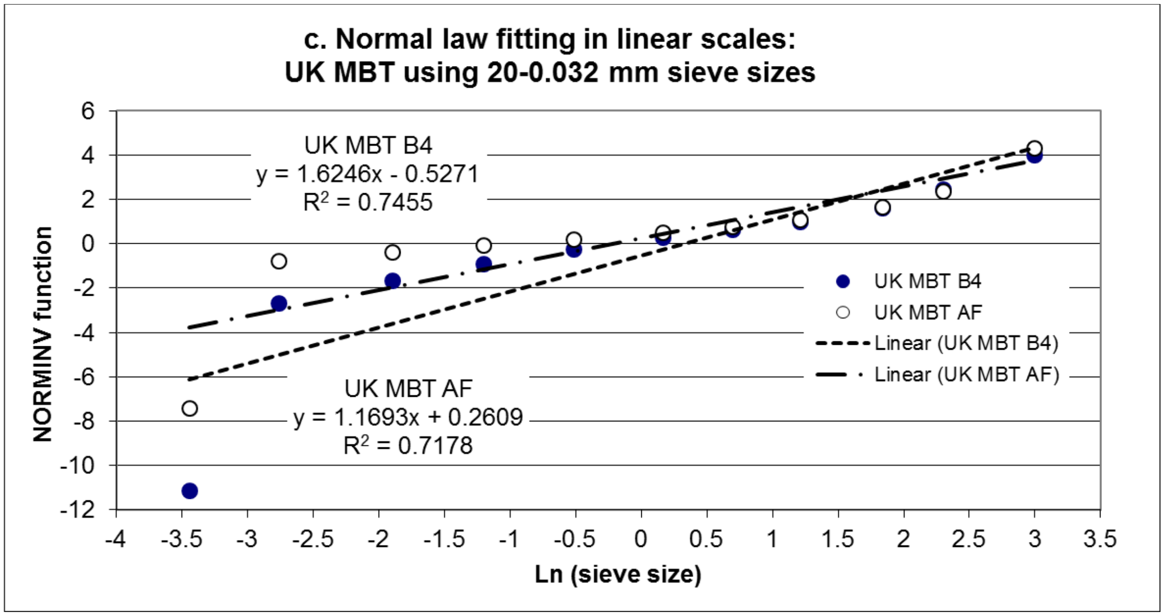
c. Normal law fitting in linear scales:
UK MBT using 20-0.032 mm sieve sizes
UK MBT B4
y = 1.6246x - 0.5271
R2 = 0.7455
UK MBT AF
y = 1.1693x + 0.2609
R2 = 0.7178
UK MBT B4
UK MBT AF
Linear (UK MBT B4)
Linear (UK MBT AF)
NORMINV function
Ln (sieve size)
6
4
2
0
-2
-4
-6
-8
-10
-12
-4
-3.5
-3
-2.5
-2
-1.5
-1
-0.5
0
0.5
1
1.5
2
2.5
3
3.5

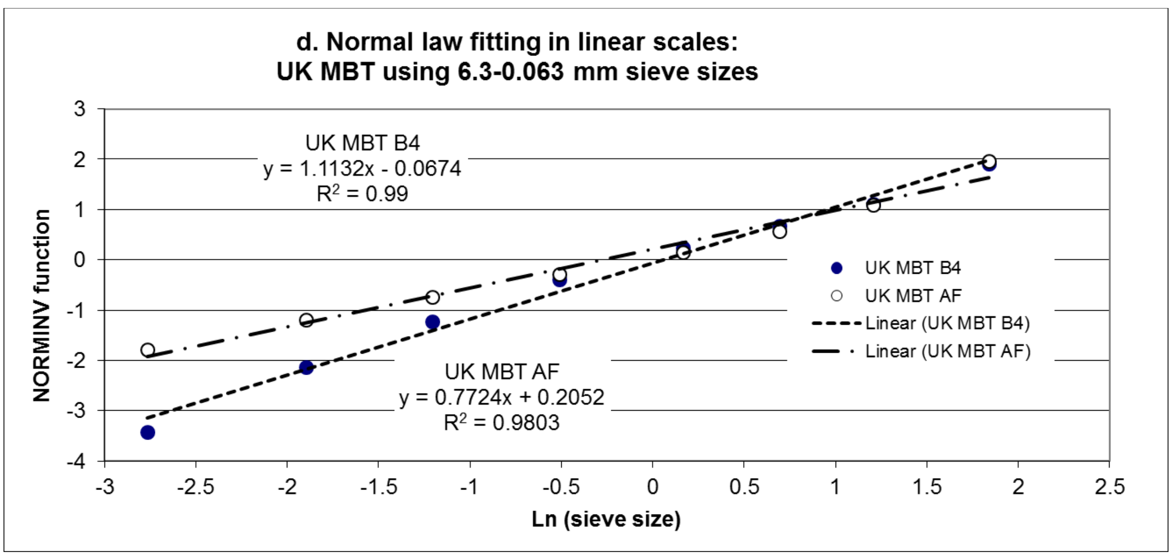
d. Normal law fitting in linear scales:
UK MBT using 6.3-0.063 mm sieve sizes
UK MBT B4
y = 1.1132x - 0.0674
R2 = 0.99
UK MBT AF
y = 0.7724x + 0.2052
R2 = 0.9803
UK MBT B4
UK MBT AF
Linear (UK MBT B4)
Linear (UK MBT AF)
NORMINV function
Ln (sieve size)
3
2
1
0
-1
-2
-3
-4
-3
-2.5
-2
-1.5
-1
-0.5
0
0.5
1
1.5
2
2.5

Annex 2-11 Normal law model fitting to PSDs of German MBT before and after degradation for different sieve size ranges. a. cumulative 75-0.032 mm , b. cumulative 6.3-0.063 mm, c. linear scale 75-0.032 mm and d. linear scale 6.3-0.063 mm

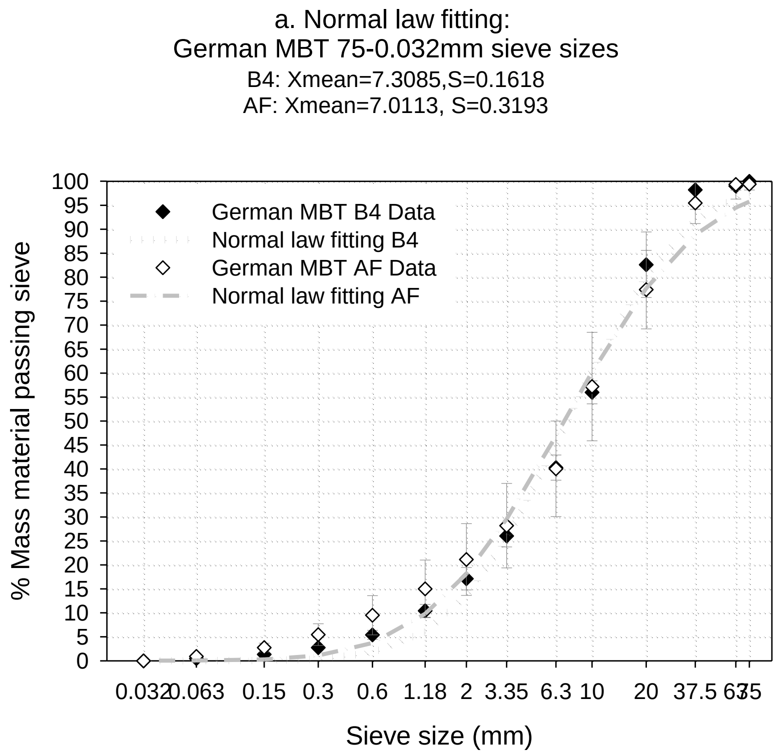

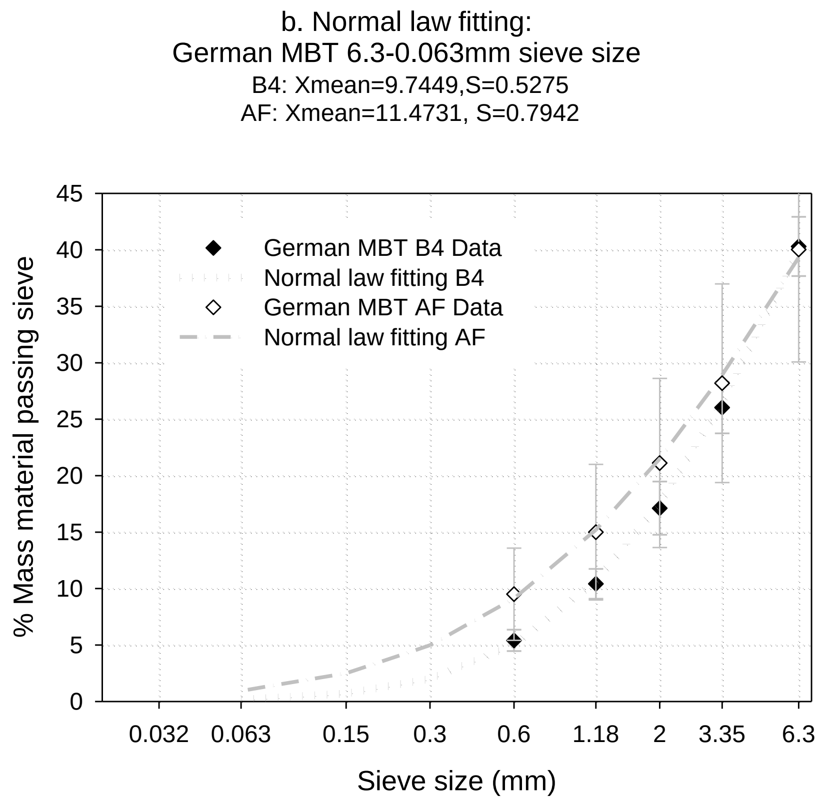
b. Normal law fitting:
German MBT 6.3-0.063mm sieve size
B4: Xmean=9.7449,S=0.5275
AF: Xmean=11.4731, S=0.7942
German MBT B4 Data
Normal law fitting B4
German MBT AF Data
Normal law fitting AF
% Mass material passing sieve
Sieve size (mm)
0
5
10
15
20
25
30
35
40
45
0.032
0.063
0.15
0.3
0.6
1.18
2
3.35
6.3

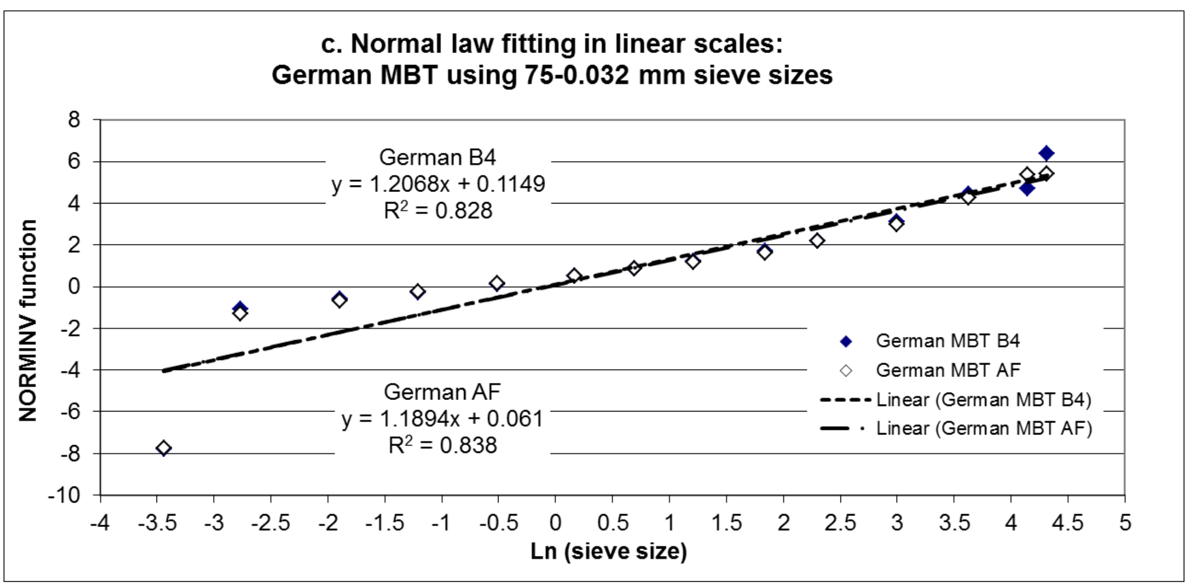
c. Normal law fitting in linear scales:
German MBT using 75-0.032 mm sieve sizes
German B4
y = 1.2068x + 0.1149
R² = 0.828
German AF
y = 1.1894x + 0.061
R² = 0.838
German MBT B4
German MBT AF
Linear (German MBT B4)
Linear (German MBT AF)
NORMINV function
Ln (sieve size)

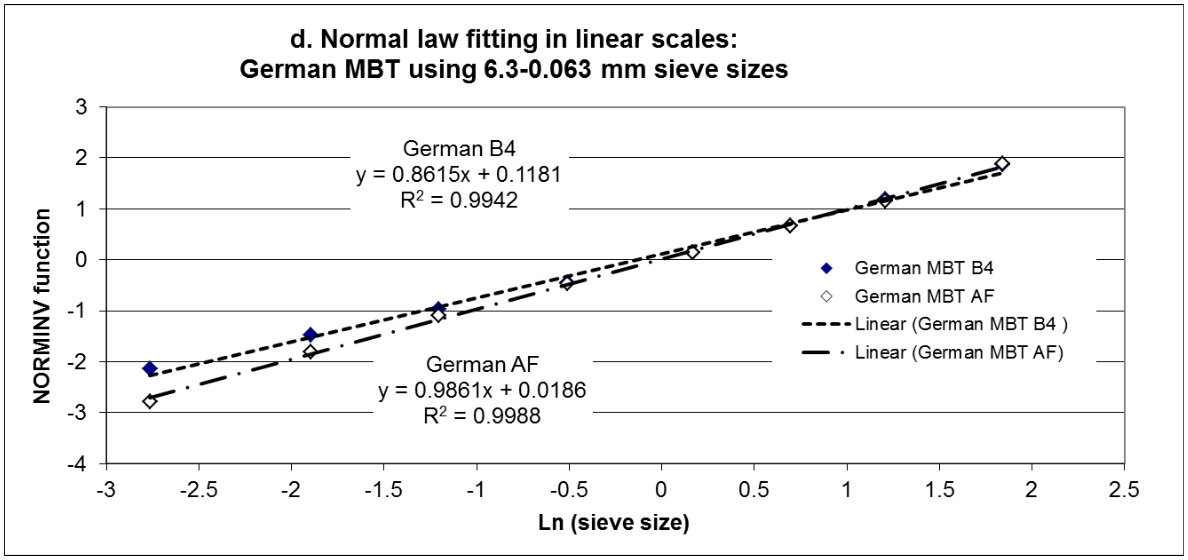

d. Normal law fitting in linear scales:
German MBT using 6.3-0.063 mm sieve sizes
German B4
y = 0.8615x + 0.1181
R2 = 0.9942
German AF
y = 0.9861x + 0.0186
R2 = 0.9988
German MBT B4
German MBT AF
Linear (German MBT B4)
Linear (German MBT AF)
NORMINV function
Ln (sieve size)
3
2
1
0
-1
-2
-3
-4
-3
-2.5
-2
-1.5
-1
-0.5
0
0.5
1
1.5
2
2.5

Annex 2-12 Normal law model fitting to PSDs of MSW before and after degradation for different sieve size ranges a. cumulative 75-0.032 mm , b. cumulative 6.3-0.063 mm, c. cumulative 20-0.032 mm, d. linear scale 75-0.032 mm, e. linear scale 6.3- 0.063 mm and. f. linear scale 20-0.063 mm

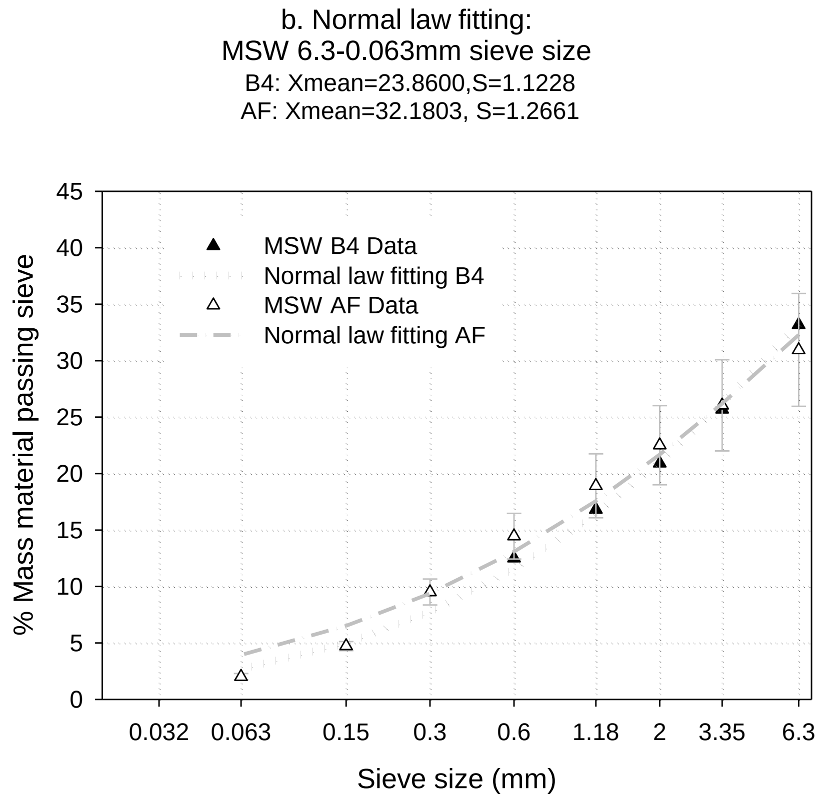

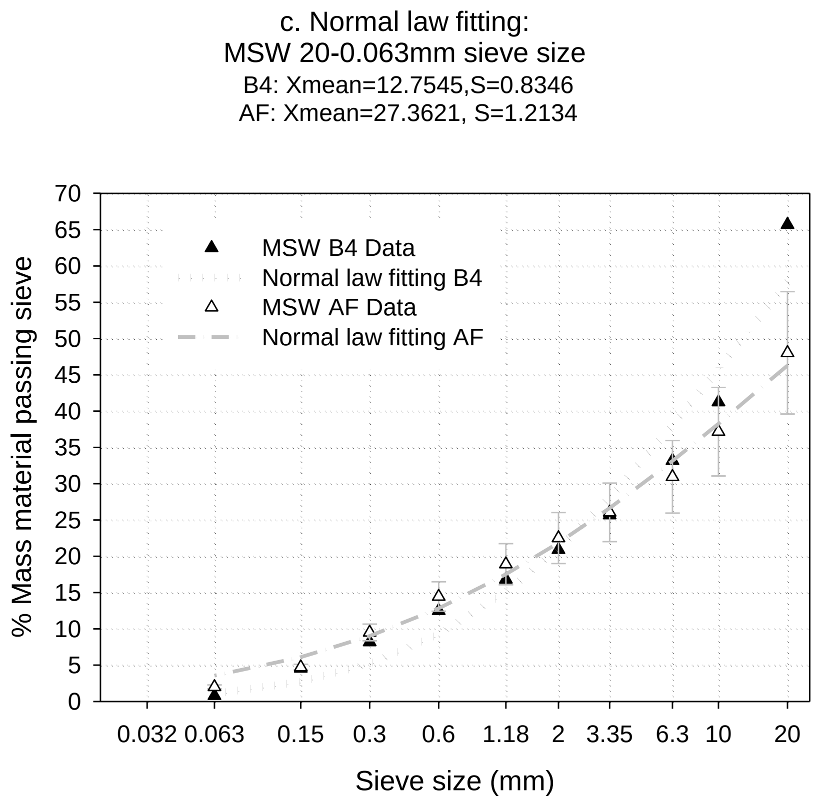
c. Normal law fitting:
MSW 20-0.063mm sieve size
B4: Xmean=12.7545,S=0.8346
AF: Xmean=27.3621, S=1.2134
MSW B4 Data
Normal law fitting B4
MSW AF Data
Normal law fitting AF
% Mass material passing sieve
Sieve size (mm)
0.032 0.063 0.15 0.3 0.6 1.18 2 3.35 6.3 10 20

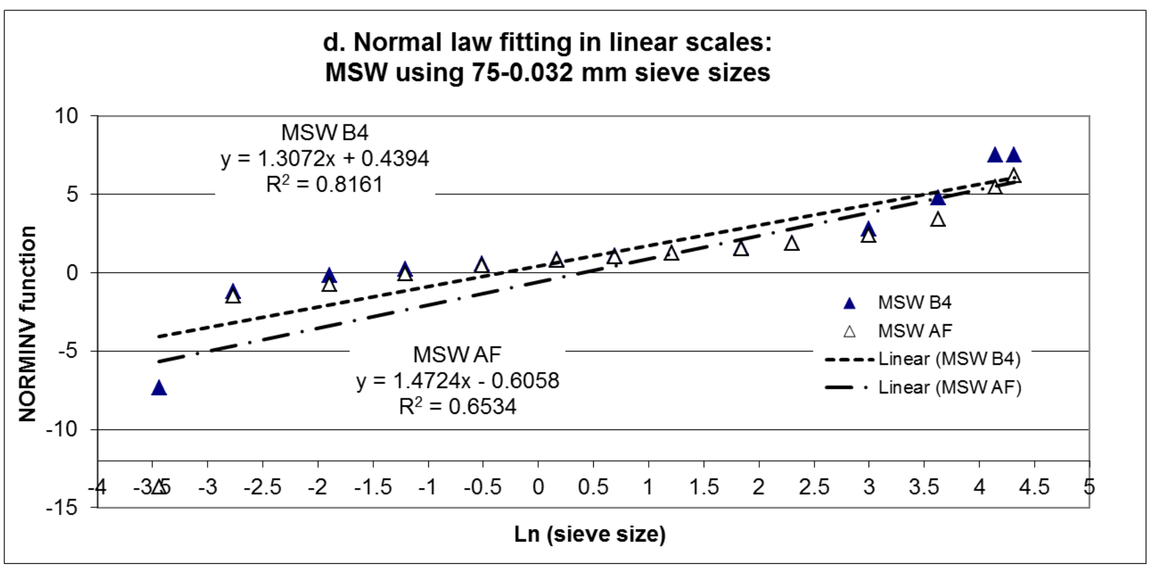
d. Normal law fitting in linear scales:
MSW using 75-0.032 mm sieve sizes
MSW B4
y = 1.3072x + 0.4394
R^2 = 0.8161
MSW AF
y = 1.4724x - 0.6058
R^2 = 0.6534
MSW B4
MSW AF
Linear (MSW B4)
Linear (MSW AF)
NORMINV function
Ln (sieve size)

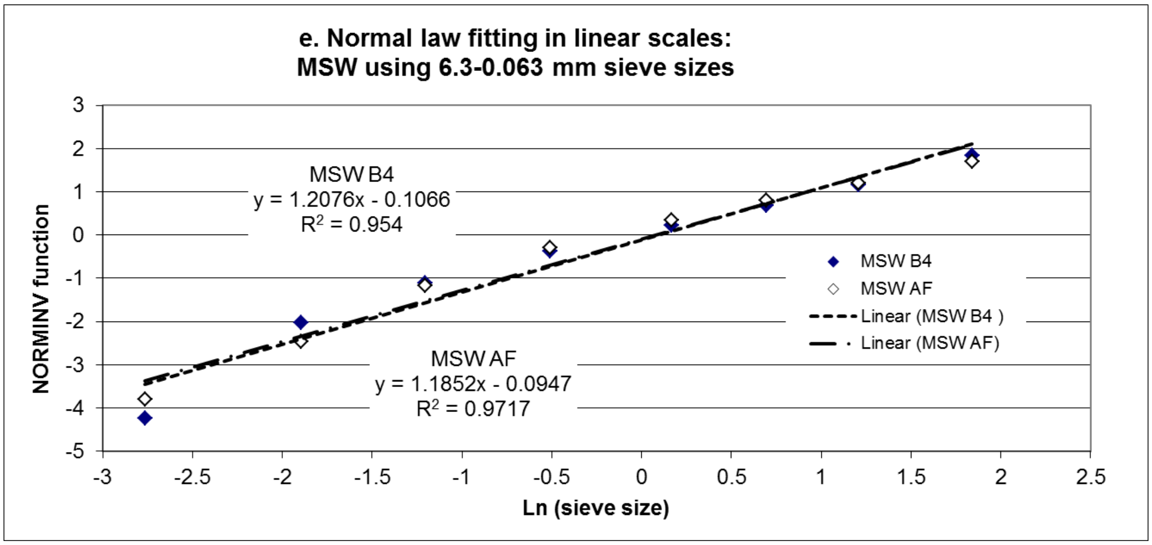

e. Normal law fitting in linear scales:
MSW using 6.3-0.063 mm sieve sizes
NORMINV function
Ln (sieve size)
MSW B4
y = 1.2076x - 0.1066
R² = 0.954
MSW AF
y = 1.1852x - 0.0947
R² = 0.9717
MSW B4
MSW AF
Linear (MSW B4)
Linear (MSW AF)

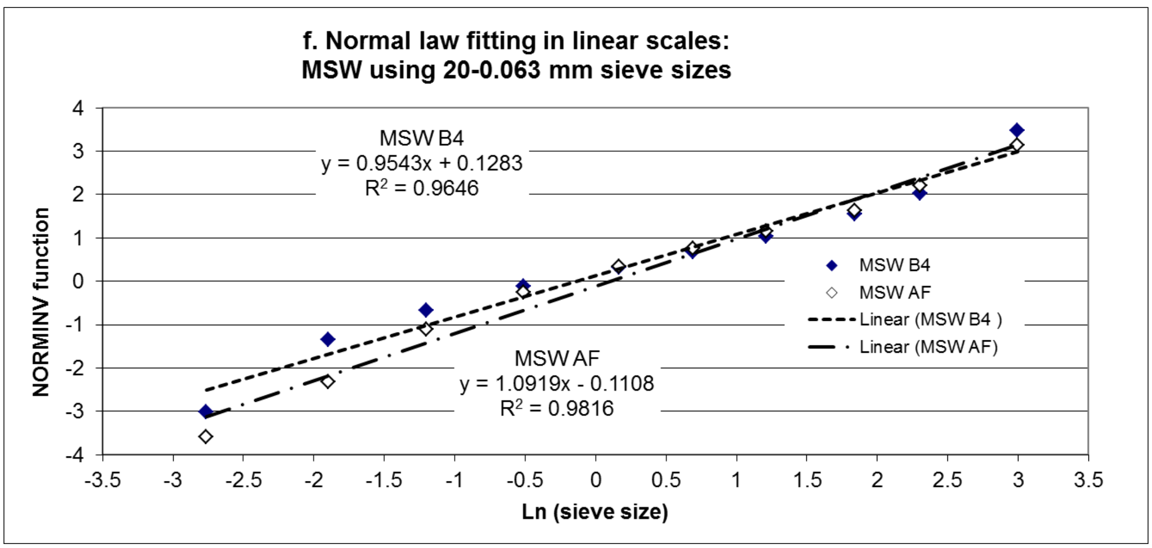

f. Normal law fitting in linear scales:
MSW using 20-0.063 mm sieve sizes
NORMINV function
Ln (sieve size)
MSW B4
y = 0.9543x + 0.1283
R² = 0.9646
MSW AF
y = 1.0919x - 0.1108
R² = 0.9816
MSW B4
MSW AF
Linear (MSW B4)
Linear (MSW AF)

Annex 4-1 Dimensionality analysis of *K* (adapted from Hubbert (1940))

A dimensional analysis by Hubbert (1940) confirmed that the factors and powers included in Equation 4-4 were the correct ones and that no other essential quantities were omitted. Combining Equation 4-3 and Equation 4-4 gives Equation 4-5 where each variable has the dimensions included in the following table.

Dimensions for each of the variables involved in the analysis of *K*

Variables	Dimensions
[Q]	$[L^3T^{-1}]$
[A]	$[L^2]$
[i]	$[L^0]$
[C]	$[L^0]$
$[d^2]$	$[L^2]$
$[\rho]$	$[ML^{-3}]$
$[1/\mu]$	$[M^{-1}LT]$
[g]	$[LT^{-2}]$
Results	
Introducing the information in Equation 4-5 gives: $[L^3T^{-1}L^{-2}L^0]=[L^0L^2ML^{-3}M^{-1}LTLT^{-2}]$ which summarises as: $[LT^{-1}]=[LT^{-1}]$	

which shows dimensional balance and that C is a dimensionless coefficient. Equation 4-5 shows that Q varies with the size and shape characteristics of the solid media.

Annex 4-2 Details of experimental set up for permeability tests

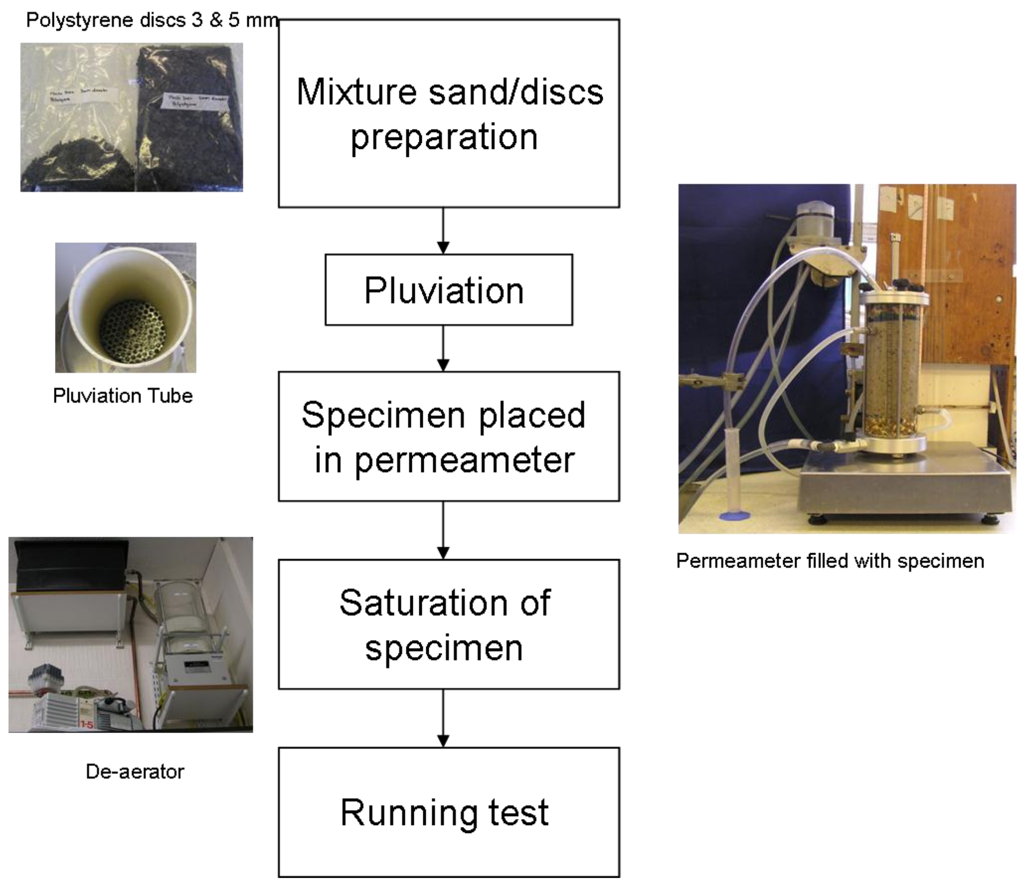

Annex 4-3 Initial trials evaluating the impact on the hydraulic conductivity when using de-aired water

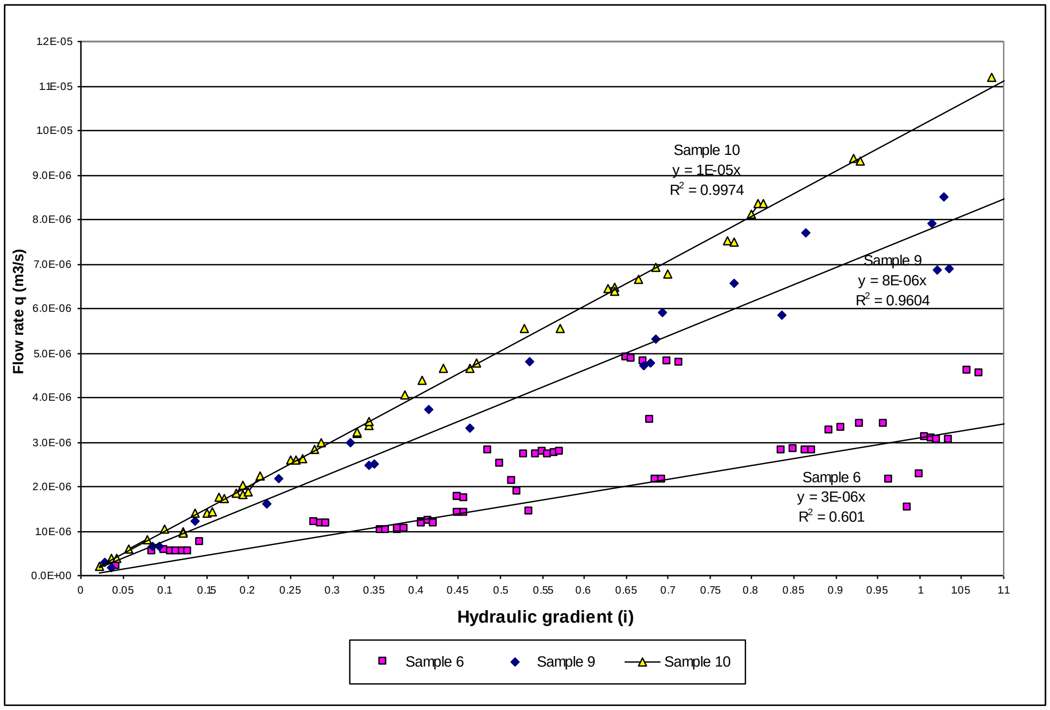

Sample	Description	R^2	S	K (m/s)
6	100 % Sand Direct Tap water	0.601	0.000003	6.79E-04
9	100% Sand Tap water stored and vacuumed	0.9604	0.000008	1.81E-03
10	100% Sand De-aired water	0.9974	0.00001	2.26E-03

Three samples of Leighton Buzzard Sand Fraction B were tested. Sample 6 was tested using tap water continuously entering to the main tank. Samples 8 and 9 were tested using tap water first loaded to the main tank, left in rest and then connected to a vacuum pump. Results from those two samples were very similar, however only Sample 9 is presented. Sample 10 was tested with de-aired water. The hydraulic conductivity of the sample tested with tap water was almost one third the hydraulic conductivity of the sand tested with de-aired water. The correlation coefficient R^2 showed a significant increase with the use of de-aired water.

Annex 4-4 Specifications of Leighton Buzzard sand : material used as matrix

Standard Reference Materials
BS 1881-131:1998

Fractions A to E 2.36mm to 90um
Standard Course Aggregate 5mm – 10mm
To be used for making Concrete Cubes for Testing Cement

Standard Sand

Description: Natural, uncrushed Silica Sand in five fractions, washed, dried and graded. Free from silt, clay or organic matter. Geological classification: Lower Greensand, Leighton Buzzard, Beds, UK.

Particle Shape: Rounded to sub-rounded.

Colour: Light brown / pale silver to brown.

Particle Size: Fractions A – E 2.36mm to 90um

	A	B	C	D	E
Size	2.36mm -1.18mm	1.18mm – 600um	600um - 300um	300um - 150um	150um - 90um
Min. within the stated range	80% minimum	80% minimum	80% minimum	75% minimum	70% minimum
Max. larger than	2.36mm is 10%	1.2mm is 10%	600um is 10%	300um is 10%	150um is 15%
Max. finer than	1.18mm is 10%	600um is 10%	300um is 10%	150um is 15%	90um is 15%

Moisture Content: Less than 0.1% by dry mass when treated by the standard over method described in BS 812: part 2

Air Entrainment: Not exceeding 1.5% when tested to Clause 7.2 to 7.6 of BS 1881-131:1998

Standard Coarse Aggregate:
The coarse aggregate consists of clean, dry, crushed granite, substantially free from dust. Fraction 5mm to 10mm. (maximum > than 10mm is 10%, maximum < 5mm is 10%)

Marking: Sands and aggregates are supplied in suitable bags marked with:

a) Our name and logo
b) the designation of the sand fraction e.g. Fraction A
c) the British Standard reference i.e. BS 1881-131
d) Batch number and weight

Annex 4-5 Derivation of phase relationships for mixtures of Sand and plastic discs

Schematic representation of mixtures Sand and Plastic discs

1

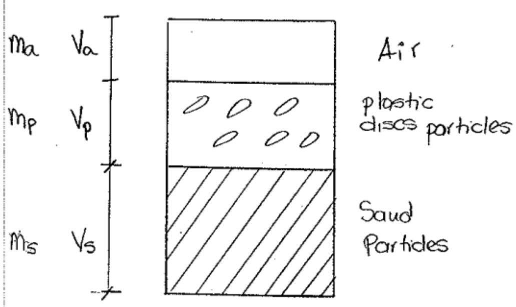

From definitions

$\boxed{\text{Void Ratio}}$, e = $\dfrac{\text{Volume of voids}}{\text{Volume of solids}}$,

Voids ▸ in the dry state, Voids are only filled with air, no water.

Solids ▸ refers to sand and plastic discs

$$e = \frac{V_a}{V_s + V_p} \quad , \quad V_a = e\,(V_s + V_p)$$

$\boxed{\text{Porosity}}$, n = $\dfrac{\text{Volume of voids}}{\text{Total volume}}$

$$n = \frac{V_a}{V_s + V_p + V_a}$$, then dividing by Va follows:

$$n = \frac{\frac{V_a}{V_a}}{\frac{V_s}{V_a} + \frac{V_p}{V_a} + \frac{V_a}{V_a}} = \frac{1}{\frac{V_s + V_p}{V_a} + 1} \quad , \text{ but } \frac{V_s + V_p}{V_a} = \frac{1}{e}$$

so $n = \dfrac{1}{\frac{1}{e}+1} = \dfrac{1}{\frac{1+e}{e}} = \dfrac{e}{1+e}$.

Unit Weight

$$\gamma = \frac{\text{Total weight}}{\text{Total volume}} = \frac{g \times \text{Total mass}}{\text{Total volume}}$$

$$\gamma = \frac{g \times (m_s + m_p + \cancelto{0}{m_a})}{(V_s + V_p + V_a)} \quad , \quad \text{but } m_a \cong 0$$

$V_a = e\,(V_s + V_p)$

$\dfrac{m_s}{V_s} = \rho_s \quad , \quad \rho_s = G_s \rho_w$

$\dfrac{m_p}{V_p} = \rho_p \quad , \quad \rho_p = G_p \rho_w$

replacing gives:

$$\gamma = \frac{g \times (m_s + m_p)}{(V_s + V_p + e\,(V_s + V_p))} = \frac{g \times (m_s + m_p)}{(1+e)\,(V_s + V_p)} =$$

$$= \frac{g \times (m_s + m_p)}{(1+e)\left(\frac{m_s}{\rho_s} + \frac{m_p}{\rho_p}\right)} = \frac{g \times (m_s + m_p)}{(1+e)\left(\frac{m_s}{G_s \rho_w} + \frac{m_p}{G_p \rho_w}\right)} =$$

$$= \frac{g \rho_w}{(1+e)} * \frac{(m_s + m_p)}{\left(\frac{m_s}{G_s} + \frac{m_p}{G_p}\right)} \qquad \text{but } g \rho_w = \gamma_w$$

$$\gamma = \frac{\gamma_w}{(1+e)} \times \frac{(m_s + m_p)}{\left(\frac{m_s}{G_s} + \frac{m_p}{G_p}\right)}$$ (2)

that for e would be:

$$(1+e) = \frac{\gamma_w}{\gamma} \times \frac{(m_s + m_p)}{\left(\frac{m_s}{G_s} + \frac{m_p}{G_p}\right)}.$$; and $\frac{\gamma}{\gamma_w} = \rho_{bulk}$.

if we define $$\overline{G_s} = \frac{(m_s + m_p)}{\left(\frac{m_s}{G_s} + \frac{m_p}{G_p}\right)}$$

so: $$e = \frac{1}{\rho_{bulk}} \cdot \overline{G_s} - 1$$

$$\boxed{e = \frac{\overline{G_s}}{\rho_{bulk}} - 1}$$

Annex 4-6 Pluviation: apparatus, mechanisms and results from testing sands

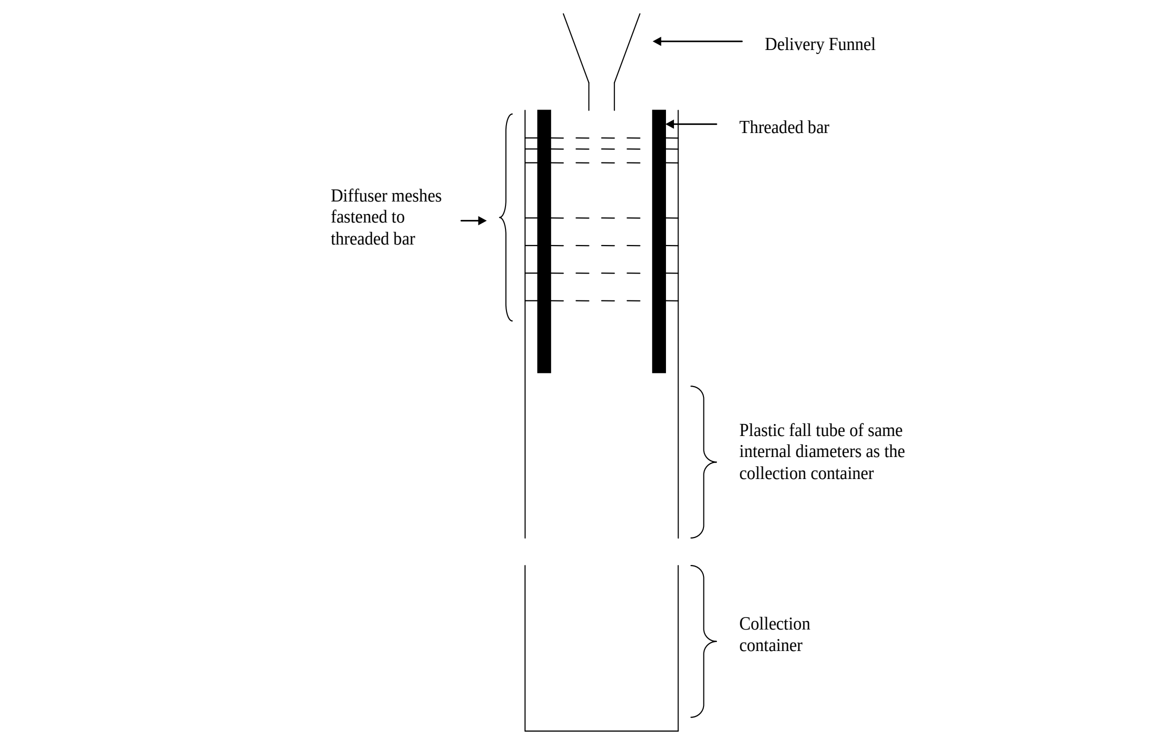

a. Schematic representation of the pluviation apparatus

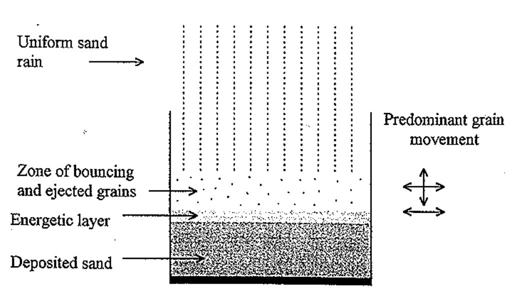

b. Deposition during optimum pluviation (after Fig 5 in (Cresswell et al., 1999))

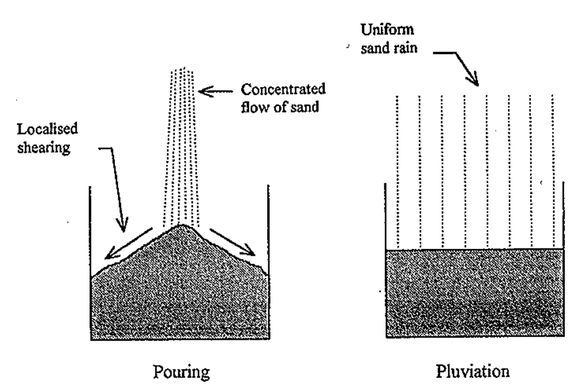

c. The difference in the mechanism of compaction between pouring and pluviation at the same rate (after Fig 8 in (Cresswell et al., 1999))

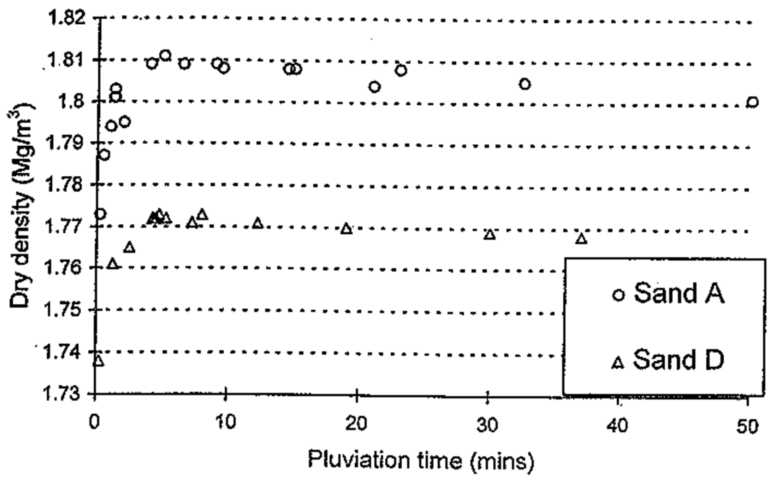

d. Pluviation time versus dry densities reported by Cresswell et.al in different sands (after Fig 3 in Cresswell *et al* (1999)). Sand A is a medium coarse Leighton buzzard sand D_{50} equal to 0.75 mm

Annex 4-7 Graphical method for temperature corrections in the range 10 to 30 Celsius according to Equation 4-10

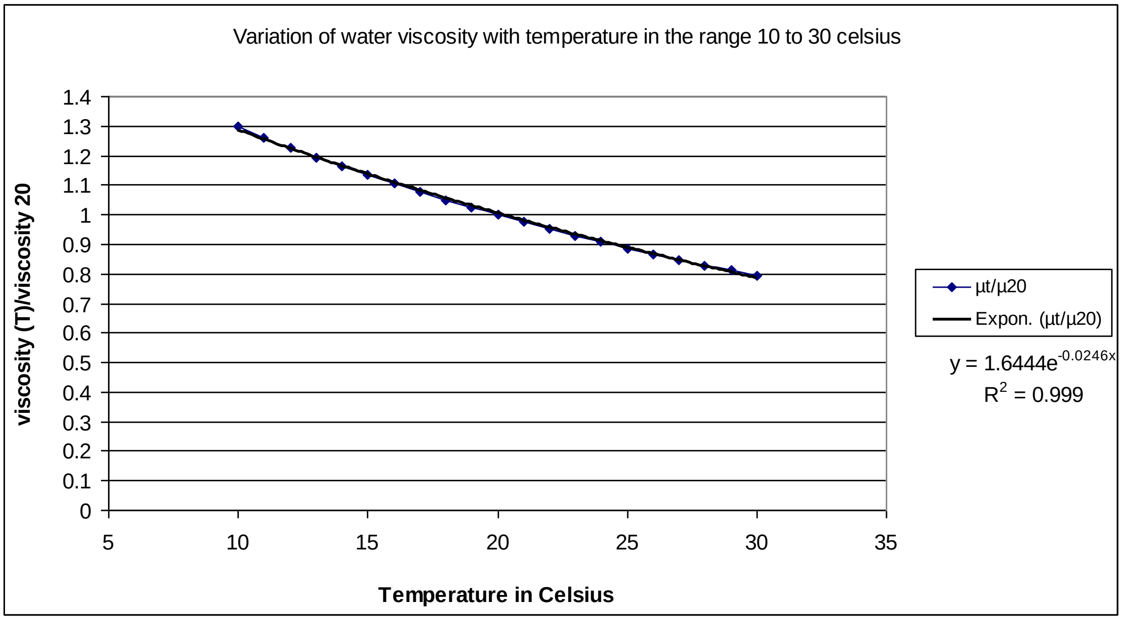

Annex 5-1 Images taking during loading solid waste for a study of horizontal spreading by Hudson et al. (2010)

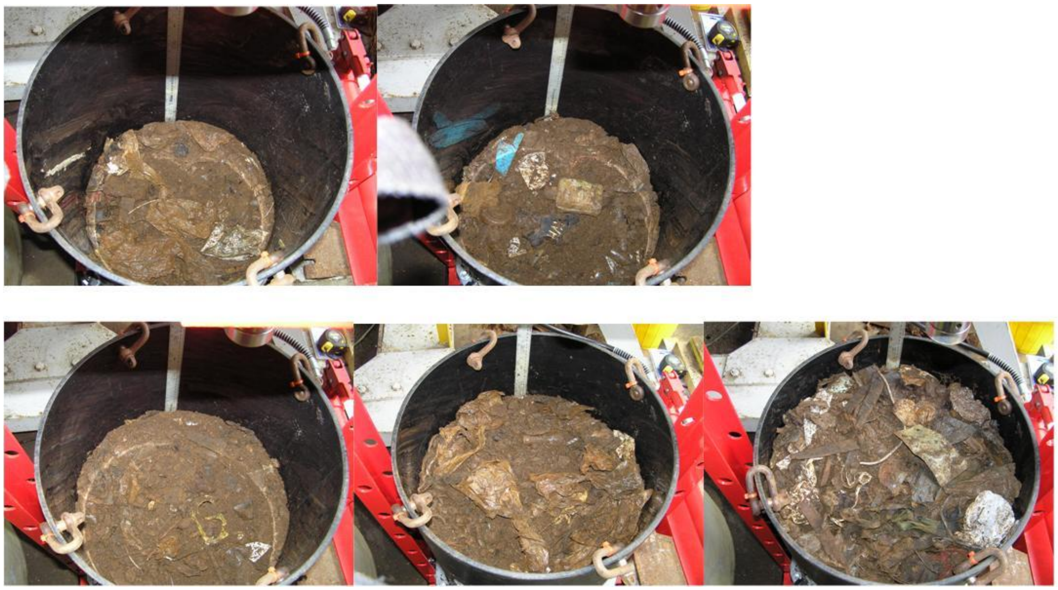

Annex 5-2 The structure of waste, layering and daily cover (adapted from Rees-White (2004))

Annex 6-1 Application of White and Beaven (2008) method to UK MBT AF sample

Sieve size mm	y retained	Average d mm	Channel diameter Di m	Channel lenght Li m	Channel area Ai m^2	Channel effective permeability Ki m/s	Sigma KiAi/A m/s
0,032	0,0180						
0,063	0,0095	0,048	1,90E-06	0,51	6,08E-05	3,51E-09	6,75E-11
0,15	0,0198	0,107	4,26E-06	0,65	9,92E-05	1,38E-08	4,33E-10
0,3	0,0256	0,225	9,00E-06	0,70	1,18E-04	5,65E-08	2,11E-09
0,6	0,0395	0,450	1,80E-05	0,81	1,57E-04	1,95E-07	9,75E-09
1,18	0,0590	0,890	3,56E-05	0,93	2,06E-04	6,68E-07	4,36E-08
2	0,0667	1,590	6,36E-05	0,97	2,24E-04	2,05E-06	1,45E-07
3,35	0,0903	2,675	1,07E-04	1,07	2,74E-04	5,23E-06	4,55E-07
6,3	0,1584	4,825	1,93E-04	1,30	3,99E-04	1,41E-05	1,78E-06
7	0,0330	6,650	2,66E-04	0,77	1,41E-04	4,52E-05	2,01E-06
8	0,0451	7,500	3,00E-04	0,85	1,73E-04	5,18E-05	2,84E-06
9	0,0430	8,500	3,40E-04	0,84	1,68E-04	6,76E-05	3,59E-06
10	0,0412	9,500	3,80E-04	0,83	1,63E-04	8,56E-05	4,42E-06
11	0,0397	10,500	4,20E-04	0,82	1,59E-04	1,06E-04	5,33E-06
12	0,0384	11,500	4,60E-04	0,81	1,55E-04	1,28E-04	6,33E-06
15	0,1085	13,500	5,40E-04	1,14	3,11E-04	1,25E-04	1,23E-05
20	0,1641	17,500	7,00E-04	1,31	4,10E-04	1,83E-04	2,38E-05
				A (m^2)	3,16E-03	**K (m/s)**	6,31E-05

Model Parameters		
Fractal dimension	2,3771	
n	0,40	
f_D	0,04	
f_L	2,3	
g	9,81	m/sec^2
mu liquid	1,00E-03	kg/m/sec
ro liquid	1000	kg/m^3

Annex 6-2 Application of White and Beaven (2008) method to German MBT B4 sample

Sieve size mm	y retained	Average d mm	Channel diameter Di m	Channel lenght Li m	Channel area Ai m^2	Channel effective permeability Ki m/s	Sigma KiAi/A m/s
0,032	0,0020						
0,063	0,0025	0,048	9,50E-07	0,33	6,48E-06	3,67E-10	2,70E-12
0,15	0,0073	0,107	2,13E-06	0,47	1,31E-05	1,30E-09	1,93E-11
0,3	0,0128	0,225	4,50E-06	0,57	1,91E-05	4,79E-09	1,04E-10
0,6	0,0257	0,450	9,00E-06	0,72	3,06E-05	1,52E-08	5,27E-10
1,18	0,0491	0,890	1,78E-05	0,89	4,71E-05	4,78E-08	2,56E-09
2	0,0666	1,590	3,18E-05	0,99	5,77E-05	1,38E-07	9,04E-09
3,35	0,1010	2,675	5,35E-05	1,13	7,63E-05	3,39E-07	2,94E-08
6,3	0,1838	4,825	9,65E-05	1,38	1,14E-04	9,03E-07	1,17E-07
7	0,0368	6,650	1,33E-04	0,81	3,90E-05	2,93E-06	1,30E-07
8	0,0486	7,500	1,50E-04	0,89	4,69E-05	3,40E-06	1,81E-07
9	0,0442	8,500	1,70E-04	0,86	4,41E-05	4,50E-06	2,26E-07
10	0,0401	9,500	1,90E-04	0,83	4,14E-05	5,81E-06	2,73E-07
11	0,0364	10,500	2,10E-04	0,81	3,88E-05	7,33E-06	3,23E-07
12	0,0330	11,500	2,30E-04	0,78	3,63E-05	9,08E-06	3,75E-07
15	0,0816	13,500	2,70E-04	1,06	6,64E-05	9,25E-06	6,99E-07
20	0,0918	17,500	3,50E-04	1,10	7,18E-05	1,50E-05	1,22E-06
30	0,0883	25,000	5,00E-04	1,09	7,00E-05	3,09E-05	2,46E-06
40	0,0313	35,000	7,00E-04	0,77	3,51E-05	8,55E-05	3,42E-06
63	0,0152	51,500	1,03E-03	0,60	2,17E-05	2,35E-04	5,82E-06
75	0,0010	69,000	1,38E-03	0,25	3,60E-06	1,04E-03	4,25E-06
				A (m^2)	8,79E-04	**K (m/s)**	1,95E-05
						$K_{experimental}$ (m/s)	6,37E-05

Model Parameters		
d`parameter (RR model)	10,2964	
v parameter (RR model)	1,0395	
n	0,37	
f_D	0,02	
f_L	2,3	
g	9,81	m/sec^2
mu liquid	1,00E-03	kg/m/sec
ro liquid	1000	kg/m^3

Annex 6-3Application of White and Beaven (2008) method to German MBT AF sample

Sieve size mm	y retained	Average d mm	Channel diameter Di m	Channel lenght Li m	Channel area Ai m^2	Channel effective permeability Ki m/s	Sigma KiAi/A m/s
0.032	0.0070						
0.063	0.0053	0.048	8.93E-07	0.42	9.38E-06	2.28E-10	2.70E-12
0.15	0.0131	0.107	2.00E-06	0.57	1.72E-05	8.45E-10	1.84E-11
0.3	0.0199	0.225	4.23E-06	0.66	2.27E-05	3.28E-09	9.43E-11
0.6	0.0350	0.450	8.46E-06	0.79	3.31E-05	1.09E-08	4.56E-10
1.18	0.0581	0.890	1.67E-05	0.94	4.66E-05	3.59E-08	2.11E-09
2	0.0700	1.590	2.99E-05	1.00	5.27E-05	1.08E-07	7.18E-09
3.35	0.0960	2.675	5.03E-05	1.11	6.52E-05	2.74E-07	2.26E-08
6.3	0.1591	4.825	9.07E-05	1.32	9.13E-05	7.53E-07	8.69E-08
7	0.0306	6.650	1.25E-04	0.76	3.05E-05	2.48E-06	9.54E-08
8	0.0400	7.500	1.41E-04	0.83	3.64E-05	2.88E-06	1.33E-07
9	0.0362	8.500	1.60E-04	0.81	3.41E-05	3.82E-06	1.65E-07
10	0.0329	9.500	1.79E-04	0.78	3.20E-05	4.93E-06	2.00E-07
11	0.0299	10.500	1.97E-04	0.76	3.01E-05	6.21E-06	2.36E-07
12	0.0273	11.500	2.16E-04	0.73	2.83E-05	7.68E-06	2.75E-07
15	0.0689	13.500	2.54E-04	1.00	5.24E-05	7.78E-06	5.16E-07
20	0.0826	17.500	3.29E-04	1.06	5.92E-05	1.23E-05	9.21E-07
30	0.0940	25.000	4.70E-04	1.11	6.45E-05	2.40E-05	1.96E-06
40	0.0455	35.000	6.58E-04	0.87	3.98E-05	6.00E-05	3.02E-06
63	0.0371	51.500	9.68E-04	0.81	3.48E-05	1.39E-04	6.12E-06
75	0.0060	69.000	1.30E-03	0.44	1.03E-05	4.59E-04	5.97E-06
				A (m^2)	7.91E-04	**K (m/s)**	1.97E-05

Model Parameters		
d`parameter (RR model)	10.9739	
v parameter (RR model)	0.8546	
n	0.37	
f_D	0.02	
f_L	2.3	
g	9.81	m/sec^2
mu liquid	1.00E-03	kg/m/sec
ro liquid	1000	kg/m^3

Annex 6-4 Application of White and Beaven (2008) method to MSW B4 sample

Sieve size mm	y retained	Average d mm	Channel diameter Di m	Channel lenght Li m	Channel area Ai m^2	Channel effective permeability Ki m/s	Sigma KiAi/A m/s
0,032	0,0424						
0,063	0,0135	0,048	9,50E-07	0,59	2,04E-05	2,13E-10	4,80E-12
0,15	0,0237	0,107	2,13E-06	0,71	2,98E-05	8,87E-10	2,91E-11
0,3	0,0260	0,225	4,50E-06	0,73	3,17E-05	3,84E-09	1,34E-10
0,6	0,0344	0,450	9,00E-06	0,80	3,83E-05	1,40E-08	5,89E-10
1,18	0,0444	0,890	1,78E-05	0,87	4,54E-05	5,01E-08	2,51E-09
2	0,0442	1,590	3,18E-05	0,87	4,53E-05	1,60E-07	8,01E-09
3,35	0,0534	2,675	5,35E-05	0,93	5,15E-05	4,25E-07	2,42E-08
6,3	0,0827	4,825	9,65E-05	1,08	6,90E-05	1,20E-06	9,10E-08
7	0,0160	6,650	1,33E-04	0,62	2,31E-05	3,93E-06	1,00E-07
8	0,0213	7,500	1,50E-04	0,69	2,79E-05	4,54E-06	1,40E-07
9	0,0198	8,500	1,70E-04	0,67	2,66E-05	5,98E-06	1,75E-07
10	0,0185	9,500	1,90E-04	0,65	2,55E-05	7,63E-06	2,14E-07
11	0,0174	10,500	2,10E-04	0,64	2,45E-05	9,51E-06	2,57E-07
12	0,0165	11,500	2,30E-04	0,63	2,36E-05	1,16E-05	3,02E-07
15	0,0451	13,500	2,70E-04	0,88	4,61E-05	1,14E-05	5,83E-07
20	0,0645	17,500	3,50E-04	0,99	5,86E-05	1,71E-05	1,10E-06
30	0,1048	25,000	5,00E-04	1,17	8,10E-05	2,96E-05	2,65E-06
40	0,0856	35,000	7,00E-04	1,09	7,08E-05	6,21E-05	4,85E-06
63	0,1573	51,500	1,03E-03	1,34	1,06E-04	1,10E-04	1,29E-05
75	0,0686	69,000	1,38E-03	1,01	6,12E-05	2,60E-04	1,75E-05
				A (m^2)	9,07E-04	**K (m/s)**	4,09E-05
					Minimun	**$K_{experimental}$ (m/s)**	1,90E-05
					Maximun	**$K_{experimental}$ (m/s)**	1,50E-04

Model Parameters		
Fractal dimension	2,5927	
n	0,34	
f_D	0,02	
f_L	2,3	
g	9,81	m/sec^2
mu liquid	1,00E-03	kg/m/sec
ro liquid	1000	kg/m^3

Annex 6-5 Application of White and Beaven (2008) method to MSW AF sample

Sieve size mm	y retained	Average d mm	Channel diameter Di m	Channel lenght Li m	Channel area Ai m^2	Channel effective permeability Ki m/s	Sigma KiAi/A m/s
0,032	0,0273						
0,063	0,0101	0,048	9,50E-07	0,53	1,68E-05	2,34E-10	4,36E-12
0,15	0,0185	0,107	2,13E-06	0,65	2,53E-05	9,62E-10	2,68E-11
0,3	0,0212	0,225	4,50E-06	0,68	2,77E-05	4,10E-09	1,25E-10
0,6	0,0293	0,450	9,00E-06	0,76	3,44E-05	1,47E-08	5,59E-10
1,18	0,0392	0,890	1,78E-05	0,84	4,18E-05	5,22E-08	2,41E-09
2	0,0404	1,590	3,18E-05	0,85	4,27E-05	1,65E-07	7,77E-09
3,35	0,0503	2,675	5,35E-05	0,91	4,95E-05	4,34E-07	2,37E-08
6,3	0,0805	4,825	9,65E-05	1,07	6,77E-05	1,21E-06	9,01E-08
7	0,0159	6,650	1,33E-04	0,62	2,30E-05	3,93E-06	9,98E-08
8	0,0213	7,500	1,50E-04	0,69	2,79E-05	4,54E-06	1,40E-07
9	0,0199	8,500	1,70E-04	0,67	2,67E-05	5,96E-06	1,76E-07
10	0,0187	9,500	1,90E-04	0,66	2,57E-05	7,59E-06	2,15E-07
11	0,0178	10,500	2,10E-04	0,65	2,48E-05	9,44E-06	2,58E-07
12	0,0169	11,500	2,30E-04	0,64	2,40E-05	1,15E-05	3,05E-07
15	0,0466	13,500	2,70E-04	0,89	4,72E-05	1,13E-05	5,89E-07
20	0,0677	17,500	3,50E-04	1,01	6,05E-05	1,68E-05	1,12E-06
30	0,1121	25,000	5,00E-04	1,19	8,47E-05	2,90E-05	2,71E-06
40	0,0933	35,000	7,00E-04	1,12	7,50E-05	6,03E-05	4,99E-06
63	0,1752	51,500	1,03E-03	1,39	1,14E-04	1,06E-04	1,33E-05
75	0,0777	69,000	1,38E-03	1,06	6,65E-05	2,49E-04	1,83E-05
				A (m^2)	9,06E-04	**K (m/s)**	4,23E-05

Model Parameters		
Fractal dimension	2,5361	
n	0,34	
f_D	0,02	
f_L	2,3	
g	9,81	m/sec^2
mu liquid	1,00E-03	kg/m/sec
ro liquid	1000	kg/m^3

9. Publications

EXPLORING THE USE OF MICRO-FOCUS COMPUTED TOMOGRAPHY FOR A BETTER CONCEPTUAL UNDERSTANDING OF STRUCTURE IN LANDFILLED WASTE IN THE CONTEXT OF POST-CLOSURE MANAGEMENT FOR LANDFILLS

Diana Milena Caicedo Concha,* Geoff Watson, David Richards and William Powrie

School of Civil Engineering and the Environment
University of Southampton
Southampton SO171BJ, UK

Key Words: Waste structure, waste characterisation, computed tomography, non-invasive methods, pore characterisation

ABSTRACT

Alternative landfill operation strategies are required to reduce the time for which a landfill poses a pollution risk. The application of those alternative strategies, e.g., aeration and flushing, requires recirculation of fluids, consequently their implementation requires better understanding of fluid flow and transport processes in landfills. Research in porous media has revealed that flow and transport processes are strongly controlled by the physical structure, in particular the pore size, geometry and interconnectivity and particle size and shape. It is generally accepted that landfilled municipal solid waste (MSW) develops a heterogeneous and anisotropic structure during placement, degradation and settlement; however our detailed understanding of the structure that develops once MSW is placed into landfills, and how it influences fluid flow is very limited. This paper discusses the use of Micro-Computed Tomography (μCT) for the non invasive study of waste structure. Results are presented for waste analogues which were successfully analysed using threshold segmentation techniques to detect millimetre sized structural features and to quantify the volumetric content of high density materials. Improvements required (e.g., image quality, higher resolution, segmentation techniques) to extend μCT to analyse the structure of landfilled waste samples and characterise pore architecture are also discussed.

INTRODUCTION

Landfilling is generally considered the least desirable option for final disposal of solid waste. Nevertheless, in many countries, landfilling remains the final disposal route for solid wastes. Recalcitrant contaminants contained in landfill sites are likely to persist for centuries rather than decades and liner and leachate collection systems are likely to fail before this time [1]. Thus the risk of pollution posed by active and closed landfill sites extends well beyond the operational period for the site [2].

The search for alternative landfill operation and management strategies has triggered the development of operation of the landfill as a bioreactor, aiming to enhance biodegradation, which has many advantages. These include improved site utilization (through accelerated settlement), leachate management, physico-chemical stabilization and removal of contaminants. The application of these alternatives requires the recirculation of liquids and so their implementation requires better understanding of fluid flow and transport processes in landfills.

Research in porous media, including soils, packed beds and foams, has revealed that flow and transport processes are strongly controlled by the physical structure, in particular the pore size, geometry and interconnectivity and the particle size and shape [3-5]. Landfilled municipal solid waste (MSW) is a porous medium comprising a mixture of highly diverse materials (e.g., plastics, textiles, glass and organic waste). It is recognized that like geological materials and as a result of the deposition in progressive layers, compaction and the heterogeneity, MSW develops a strong structure [6]. Plastics and Textiles, due to their shape, tensile strength and orientation, can enhance the strength (e.g., Kölsch [7] and Dixon et al. [8]), and influence flow behaviour by diverting fluid flow [9,

*Corresponding author
Email: dmc1x07@soton.ac.uk; dicaiced@yahoo.com

10]. However our detailed understanding of the structure that develops once MSW is placed into landfills, and how that structure influences fluid flow is very limited.

Research into the structure of porous media has been traditionally approached using methods such as field observations [4,11]; laboratory analysis of cores by thin sectioning, resin impregnation and imaging [12,13]; indirect analysis using tracer injection breakthrough curves from fluid flow experiments [12]; and observation of flow path patterns revealed by dye staining [13,14].

Non-invasive techniques, particularly X-ray Computed Tomography (CT) have been successfully used in porous media research since the early 1990s, and have revealed highly detailed information on both the structure and the pore space architecture, improving our understanding of fluid flow [15,16] and other porous medium interaction processes [17, 18].

This paper discusses the potential of X-ray CT for studying landfilled waste, and illustrates this with some results obtained from waste analogue specimens. This paper presents a theoretical background of CT. Example applications are discussed to show that non-invasive methods can be applied to the study of landfilled waste. The imaging procedure is explained and the potential for improvement is discussed. Preliminary results of some of the structural features revealed in the analysis of waste analogues are presented, compared with bulk properties and discussed in the context of their potential impact on the long term management of landfill sites.

Non-invasive Techniques Background

Non-invasive techniques are based on the principle that properties of the internal structure of a specimen can be inferred from the detection of a signal, passed through the specimen. They were originally developed for diagnostic medicine and have enabled the non-invasive study of the human body. In recent decades increased availability has led to the use of these techniques for research purposes in areas such as archaeology, palaeontology, petrophysics, geology and materials engineering.

The acquisition of images using non-invasive techniques is faster and causes far less disturbance than progressive thin sectioning. Physical properties of the signal used vary between non-invasive technologies including X-rays in CT, Magnetic fields in Magnetic Resonance Imaging and gamma rays in Positron Emission Tomography. Since the response of a particular material is dependent on the signal type, selection of the appropriate technique requires careful consideration of the type of material being investigated. Watson et al. [19] concluded that landfill waste was suited to examination using CT. During the research discussed in this paper, locally available microfocus-CT (µCT) equipment was used.

Principles of X-ray CT

X-ray CT is a radiographic method that uses X-rays for digitally cutting a specimen to reveal its interior details. X-rays are high energy electromagnetic waves produced inside X-ray vacuum systems, where a cathode is heated to produce electrons which are accelerated by a high voltage to a rotating anode which typically reradiates less than 1% of the electron energy in the form of X-rays [20]. This process establishes a flow of X-rays known as a beam, with wavelengths in the range 0.01 to 10 nm.

CT scanners work by emitting a cone of X-rays, which pass through the object of interest to one or more detectors. In µCT, the object is rotated in relation to the X-ray source to create a series of two dimensional images which can then be computationally assembled into a three dimensional object.

A detector measures X-ray intensity before the beam enters the object and after it passes through it, and using the Beer-Lambert law (Eq. 1) calculates µ, the linear X-ray attenuation coefficient for the material being scanned. I_o and $I_{(x)}$ are the initial and transmitted beam intensities respectively and x the length of the X-ray path through the material. If the scanned medium is inhomogeneous, the intensity is expressed as shown in Eq. 2.

$$I_{(x)} = I_O e^{(-\mu x)} \tag{1}$$

$$I_{(x,y)} = I_{(0,0)} e^{\left(-\int_{(0,0)}^{(x,y)} \mu(x,y)\,dl\right)} \tag{2}$$

In Eq. 2, µ is the unknown variable constrained by many equations for each point along each X-ray path. Image reconstruction involves finding values for µ that provide solutions to these equations [21, 22]. The most commonly used reconstruction algorithm, known as "filtered back projection", was invented by Allan Cormack who shared the 1979 Nobel Prize for Medicine and Physiology with Godfrey Hounsfield inventor of the CT scanner and relates the measured projection data to the two-dimensional Fourier transform of the object cross section. Once reconstructed, objects can be visualized in 2D and 3D and features qualitatively or quantitatively assessed using various image processing software packages available both free and commercially [23].

Attenuation of X-rays is caused by beam matter interactions, primarily Compton scattering and photoelectric absorption, both of which are strongly dependent on the density of the absorbing medium, the atomic number and the energy of the incoming X-ray beam [24]. Mathematical functions to describe the relationship between physical properties of the matter and the attenuation of X-rays have been extensively discussed (e.g., McCullough [25]; Brooks [26] and Denison and Carlson [27]) and approximate equations have been proposed. Equation 3 is an example, where ρ is the electron density (related to mass density by the number of atomic units per electron), Z is the effective atomic number and E is the energy of the incoming X-ray beam. The relationship shows that μ is directly proportional to the electron density of the material [24]. Differentiation of features within a specimen is therefore possible because at each point, μ depends directly on the material properties [21,22].

$$\mu(x,y) = \rho\left(a + \frac{bZ^{3.8}}{E^{3.2}}\right) \qquad (3)$$

Images obtained from CT are monochromatic representations of the spatial distribution of μ where the grey shade represents intensity. Images are conventionally mapped so that brighter regions correspond to those volume elements (voxels) with higher μ values. The format selected for storing the image controls the number of levels in the grey scale range, e.g., in 8 bit, the grey level has values in the range 0-255.

μ may change between equipment and so Hounsfield units and CT numbers, which use the linear attenuation of reference materials such as air and water for calibration, are preferred when diagnostic and quantitative studies are required [15,21].

Medical CT can successfully image metre sized objects with millimetre scale resolutions. Demand for higher resolution tomography in denser and smaller objects eventually led to the development of μCT which scans millimetre sized objects at 1-10 μm resolution. The physical principles that control CT and μCT are the same. With decreasing size, radiography becomes more difficult as the specimen must absorb a sufficient portion of the incident beam to produce a measurable signal, which in a small specimen demands high attenuation per unit length, a condition that is only satisfied at low X-ray energies which are insufficient to penetrate dense objects. Precisely focused beams are also required to minimize blurring of fine details [28]. These difficulties were successfully addressed by D'Amico et al. [29] with the development of a microfocus X-ray source which forms the basis of μCT. In μCT, X-rays are first highly collimated to achieve beam focus on the anode of onlyfew micrometres diameter.

Applications of CT in Porous Media Research

Following successful application in the medical field, CT rapidly gained popularity among those studying the structure of porous media in fields such as hydrogeology and geosciences. A vast number of references are available and comprehensive review papers within these fields are given by e.g., Ketcham and Carlson [30]; Kaestner et al. [31]; Allaire et al. [32] and Werth et al. [33].

Petroleum engineers pioneered the use of CT within geological sciences to characterise density, porosity, saturation and complex mineralogies in oil-reservoir rocks, imaging fluid flow patterns and studying rock mechanics [34,35]. Scientists from diverse porous media research areas then found medical CT a feasible method for studying, with a high level of detail, density and water distributions [15, 16]; structure [18] and soil interaction processes [18, 36].

CT has seen limited use in the study of waste structure and fluid flow phenomena, with Watson et al. [19] and Watson et al. [37] being the only references identified at the time of writing. Watson et al. [37] used medical CT to investigate the change in structure of the organic fraction of MSW as it degraded anaerobically over a period of 2 yr in 35 L reactors. They found that CT scanning was able to show structural changes in the waste occurring over the period of degradation and that particle size was reduced over the same time. The resolution used for the scanning was too small to enable the pore network to be clearly visible. No attempts to use higher resolution computed tomography in waste have been reported.

MATERIALS AND METHODS

1. Materials

As part of an investigation into the effects of two dimensional components on hydraulic conductivity and shear strength, two synthetic specimens were prepared and scanned. Each specimen consisted of two dimensional plastic materials in a relatively homogeneous matrix. This approach was preferred over scanning samples of real landfilled waste. It was considered that the properties being investigated would be well represented but the material would be less complex than real wastes, minimizing uncertainties caused by uncontrolled variables, e.g., continuing degradation; other components acting as reinforcement or flow diverters; as well as reducing complexities in the imaging process.

The first specimen created in a modified 75 mm diameter, 238 mm tall permeameter, was prepared to investigate the effect that two dimensional components have on hydraulic conductivity. The permeameter was modified by replacing the aluminium connecting rods with plastic ones to reduce artefacts due to X-ray scattering from the metal. In this case the matrix material selected was Leighton Buzzard Sand fraction b (grain size 600 μm to 1.18 mm) and polystyrene discs (5 mm diameter x 0.6 mm thick) which represented the two dimensional components. Sand and polystyrenes discs in a dry mass ratio of 6.35:1 (86.4% sand and 13.6% discs) were mixed by hand and deposited in a permeameter cell, using a pluviation method as described by Cresswell et al. [38]. Pluviation uses a cylindrical tube (75 mm diameter) filled with offset sequential interwoven wire diffuser meshes to create an even sand rain effect which produces a high density, evenly distributed specimen. Once placed, the sample level was measured in order to calculate total volume (353.44 cm^3), bulk density (1.76 Mg m^{-3}) and volumetric percentages (54.4% sand, 21.6% discs and 24% pores). The scan aimed to identify the distribution and orientation of the flow diverting elements (polystyrene discs) and evaluate the potential to characterize in two and three dimensions the pore network structure of the specimen.

The second specimen was a modified mechanically biologically treated waste residue (MBT). Details of the MBT residue used can be found in Velkushanova et al. [10] and Fernando et al. [39]. The sample was prepared for shear strength testing in a 60 mm direct shear apparatus by sieving the MBT at the as-received moisture content (26% by dry mass), retaining the fractions from 0 to 2.8 mm (to create a matrix) and then adding 2% by dry mass of 20 x 10 mm High Density Polyethylene (HDPE:25 pieces or 2.4% by volume). The material was placed in the shear box apparatus and compressed under a normal stress of 100 kPa for 24 h but not subjected to shear stresses. The final specimen was a cuboid (6 x 6 x 3 cm; 108 cm^3), with a mass of 85.46 g and a bulk density of 0.79 Mg m^{-3}. The scan was intended to study the distribution and orientation of the HDPE pieces following compression.

2. Methods

The permeameter specimen was scanned using an X-Tek XT H 450 (X-Tek Systems Ltd, Tring, Hertfordshire, UK). This machine was equipped with a 2000 x 2000 pixel PerkinElmer 1621 X-ray flat panel detector with pixel size 200 μm x 200 μm, which provided a resolution limit of 100 μm (limited by the power source size). The scan was run with a beam voltage of 200 kV, a current of 175 μA and a 1 mm thick copper filter. The total scanning time was 3.53 h, and the scan consisted of 3143 radiographic projections with an individual exposure time of about 4 s.

The MBT specimen was scanned using a X-Tek XT H 225 equipped with a 2000 x 2000 pixels PerkinElmer 1620 X-ray flat panel detector with a resolution limit of 3 μm (when used with a 6 mm sample). For the 60 mm MBT sample, the resolution was 30 μm. The scanner settings were 110 kV and 149 μA for beam voltage and current respectively. The total scanning time was 3.75 h and the scan consisted of 3004 radiographic projections with individual exposure time of about 5 s.

In both cases preliminary trial runs were required to find optimal settings to obtain high signal to noise ratio images and minimise artefacts (defined by ASTM [24]) as anything in the image that does not accurately reflect true structure in the sample being inspected). In order to minimise ring artefacts, which had been problematic in earlier scans, the scan was acquired in "ring compensation" mode.

Reconstruction was carried out using a filter back projection algorithm and volume images analysed using VG-Studio Max V2.0 software developed by Volume Graphics GmbH, Heidelberg, Germany. The stack of two dimensional images was processed using Image J — a free, Java-based image processing program developed at the U.S. National Institute of Health.

RESULTS AND DISCUSSION

1. Permeameter Sample

The reconstruction of the complete sample produced 1376 horizontal slices separated by 0.059 mm. A subsection (70 mm depth, 75 mm diameter) located between the lower two piezometer ports in the permeameter was selected as the region of interest (ROI). This region was selected as some of its fluid flow properties had been determined (e.g., saturated hydraulic conductivity). This ROI, consisting of 1083 horizontal slices with a voxel size of 2.15 x 10^{-4} mm^3, was used for further analyses. It was first divided from bottom to top into four sub-regions: ROI-1, ROI-2, ROI-3 (each with 250 slices) and ROI-4 (with 331 slices) to reduce the computational demand and accelerate processing. All images were stored as 8 bit grey scale images.

Inspection of the horizontal and vertical views (Fig. 1) allowed visual identification of the plastic pieces. They were preferentially oriented in the x-y plane, and distributed along the sample with a concentration increasing from bottom to top.

Figure 2 shows the grey value distribution for each of the ROIs, as well as the result of summing the four ROIs. All the histograms show two peaks clearly divided at a grey value of around 143. As images were mapped for brighter materials to be displayed with the higher grey levels, those voxels with grey values above 143 correspond to sand. This was verified during visualisation in 3D by disabling the interval 0-143. The rendered volume showed only sand grains confirming that materials in the range

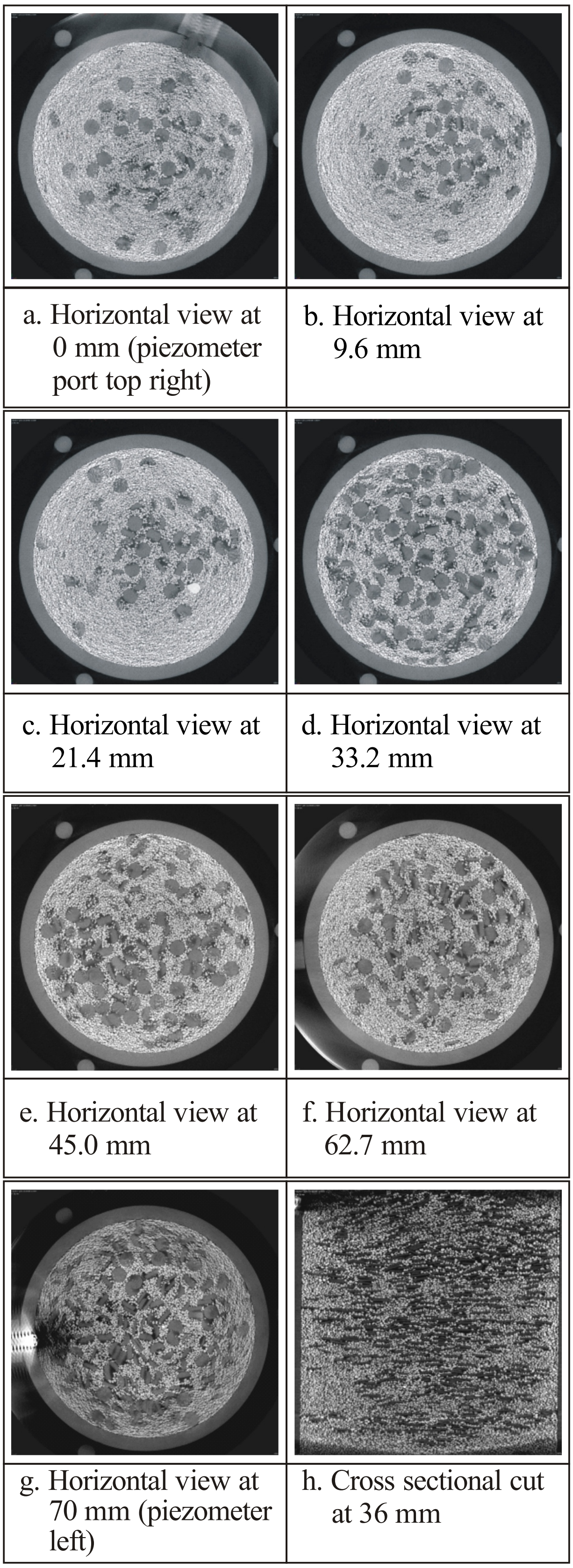

Fig. 1. Selected slice views in the permeameter specimen. Dark grey features are the 5 mm plastic discs incorporated to the sample. Distances given are from the bottom of the specimen.

0-143 correspond to plastic discs and pores.

The cumulative distribution of grey values is illustrated in Fig. 3. The y-axis is the percentage of voxels with a grey value < x. Therefore, the graph represents the volumetric content of the components in the specimen. Volumetric concentrations of pores and discs were calculated for each ROI using a threshold of 143 and the corresponding quantity on the y-axis. They were compared against the percentages determined during the specimen preparation (54.4% sand, 21.6% discs and 24% pores). Results from the sum of all ROIs showed close agreement with the actual composition (see the sum of all ROIs in Fig. 3). Differences in the volumetric contents between the four ROIs suggest a gradual increase in the content of plastic discs, from bottom to top, and this is also shown in the horizontal views.

Differentiation between discs and pores based on grey level was more difficult. Grey value histograms under 143 do not show clear peaks to distinguish between these two materials. Although the distribution for ROI-4 (Fig. 2) suggests that the curve is the result of two different distributions - the first with a maximum at around 60 presumably for pores and the second with a maximum at around 118 presumably for plastics - they share a significant region of grey values making any unambiguous differentiation un reliable.

At the time of writing no further attempts have been made to achieve segmentation between plastics and pores. This could have been possible using alternative segmentation algorithms like those based on differences in shape (i.e., Hough transform, template matching) or on the statistical treatment of histogram to obtain two separated normal distributions [40]. This will be the subject of further research.

2. MBT Specimen

The reconstruction of the complete sample produced 731 horizontal slices separated by 0.052 mm. A subsection was created to approximate the real shape of the sample and disregard the wrapping which held the sample together, as well as the background information. A ROI of approximately 6 x 6 x 3 cm size was created. It was composed of 594 horizontal slices and had a voxel size of 1.41×10^{-4} mm^3. All images were stored as 8 bit grey scale and mapped so that denser/brighter components were displayed at the higher grey values.

Visual inspection of the 2D slices showed six, sub-horizontally aligned reinforcing particles (the dark grey rectangular features in Fig. 4a-4d), located at 2.55, 4.52, 10.04, 11.60, 15.70 and 16.54 mm (measured from the base of the sample). Four further reinforcing particles lay on the external top layer of the specimen. This corresponds to 40% of the total

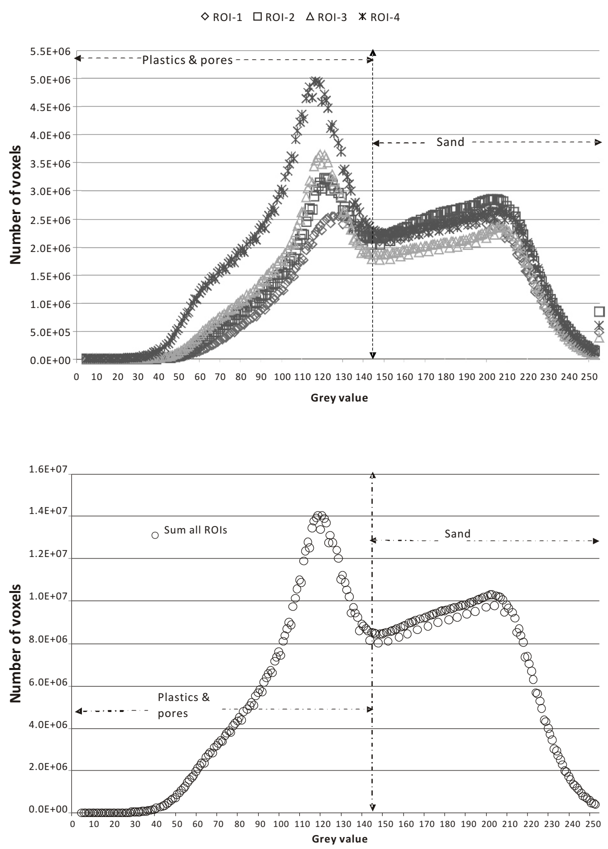

Fig. 2. Grey value distribution for the permeameter sample. Y axis represents the number of voxels with a grey value equal to X. The grey scale is in the range 0-255 as a result of images being stored in 8 bit format.

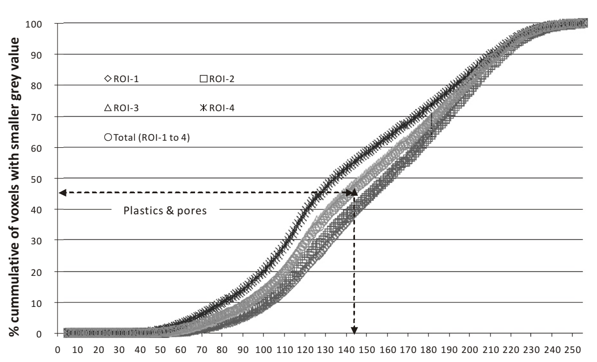

		From voxel information Threshold grey value=143				
Materials	%Vol[a]	ROI-1	ROI-2	ROI-3	ROI-4	Sum all ROIs
Plastic pieces & pores	45.6	37.4	39.3	47.3	54.5	45.5
sand	54.4	62.6	60.7	52.7	45.5	54.5

a: data from preparation

Fig. 3. Cumulative grey value distribution in the permeameter specimen. Y axis represents the percentage of voxels as the total sample volume with a grey value less than X. The threshold grey value of 143 corresponds to the point dividing the peaks for sand and plastics and pores in Fig. 5.

number of pieces added to the specimen (25 in total). The remaining 15 pieces were placed vertically or with some angle of inclination as can be seen in the vertical cuts shown in Figs. 4e and 4f. White features in the images correspond to high density materials, due to the convention chosen during mapping the images, and are likely to be small glass and metal pieces contained in the matrix.

Figure 5a shows the grey value histogram for the ROI. The variety of components in waste and their wide range of densities lead to a distribution that, unlike the one obtained for the permeameter sample, does not show clearly distinguished peaks. This situation caused difficulties during the segmentation of components and showed the need to enhance contrast between materials if quantification, rather than simply detection, was the aim of imaging MSW and MBT samples. At the time of writing strategies for increasing the contrast are being explored. These include filling macro-pores with an aqueous solution of a contrast enhancing compound (e.g., potassium iodide) and increasing the overall contrast by imaging smaller regions with lower energy beams.

Despite this difficulty, the potential use of the information obtained from μCT was further explored by performing an approximated segmentation which used some information extracted from the grey value distribution (Fig. 5a) and the 3D rendering tool. The histogram in Fig. 5a, displays at least three weak peaks at grey values of around 50, 106 and 120. Those peaks are likely to represent maximum grey values for three types of materials: low, medium and high density.

Figure 5 (b and c) shows three dimensional representations of the complete specimen (b) and only the high density materials (c). The object represented in c was created by iteratively adjusting the threshold, starting at 120 as suggested by the histogram, and until a satisfactory representation was achieved: only glass and metal pieces were rendered. A threshold of 170 produced an object that was visually judged to be composed entirely of glass and metals.

The volumetric content of high density materials with grey value > 170 was calculated as 5.43%. Information of this nature is useful for the characterisation of solid waste. The specimen studied was created using the finest fraction (0-2.8 mm) of an MBT waste sample. This fraction is usually termed "soil like" as the components are too small to be characterised using manual or mechanical sorting [10] and plays a significant role in fluid flow processes. Fine particles

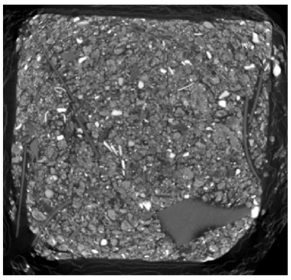

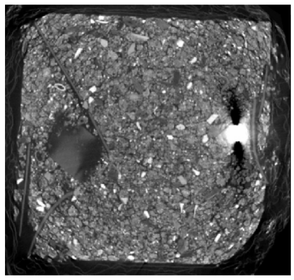

a. Horizontal reinforcing element at 10.04 mm

b. Horizontal reinforcing element at 11.60 mm

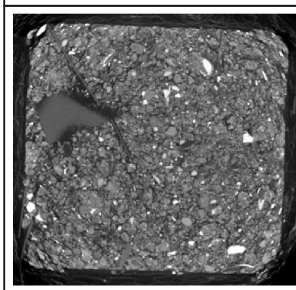

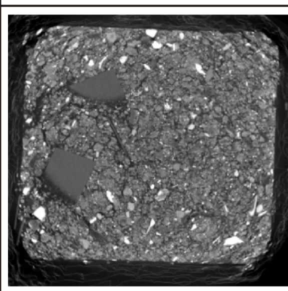

c. Horizontal reinforcing element at 15.70 mm

d. Horizontal reinforcing elements at 16.54 mm

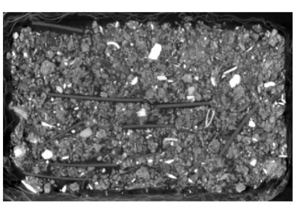

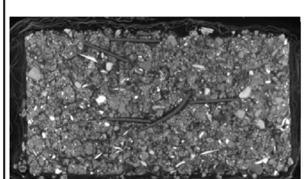

e. Vertical view at 9.67 mm with 8 reinforcing elements

f. Vertical view at 22.15 mm with 5 reinforcing elements

Fig. 4. Selected views in the MBT specimen where reinforcing plastic pieces were identified. (a) Long linear features indicate presence of particles with some angle of inclination; (b, c, d, e and f) rectangular features (dark grey) are the reinforcing pieces. White features are high density materials likely to be glass and metals. Distances given are from the bottom of the specimen.

can fill the pores formed by coarser materials and control the hydraulic conductivity [41-43]. Hence a detailed characterisation will improve the estimation of fluid flow characteristics in landfilled waste. Particles of glass and metals would be expected to behave differently from similar size particles of organic materials. Organic materials are readily biodegradable and consequently likely to exhibit changes in size during degradation. It is clear that a particle size characterisation will not provide the complete picture of these changes as it will not distinguish between materials. Analogous information could be obtained in undisturbed solid waste samples (e.g., *in situ* landfill cores) offering the possibility of non-invasive material characterisation. Segmentation of other features, such as plastic pieces, soil-like materials and pores was less clear using the grey value threshold and 3D rendering tool. Iterative changes in the threshold < 120 did not produce objects that, once visually assessed, were composed of only one type of material. As previously discussed, improvements in image contrast and more complex algorithms for segmentation are to be explored at later stages of research.

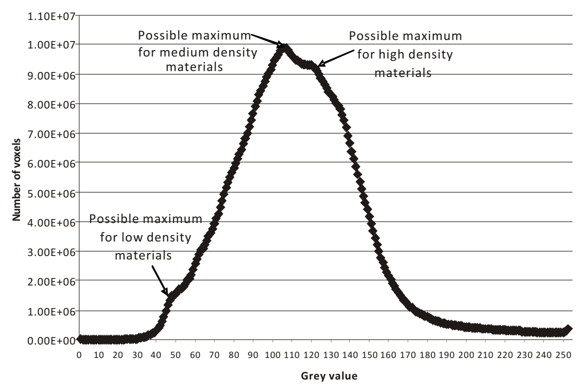

a. Grey value distribution for the MBT sample. Lines were placed as indicative of peaks to assist during the segmentation.

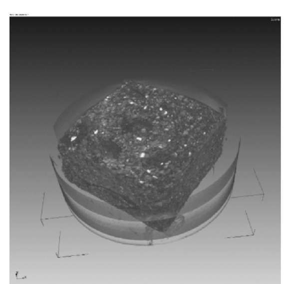

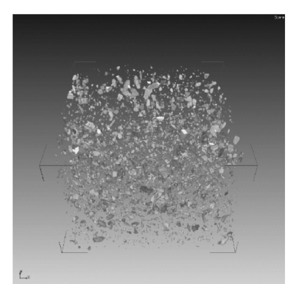

b. Complete specimen. Dark features at the top correspond to plastic pieces.

c. High density materials (grey value over 170), probably glass and metals.

Fig. 5a is the grey value distribution in the MBT specimen scanned with slow acquisition routine. The Y axis represents the percentage of voxels as the total sample volume with a grey value less than X. B and c are three dimensional reconstructions of the MBT specimen in VGStudio Max2 using the Volume Render (Scatter HQ) algorithm.

3. Discussion

The visual inspection of horizontal and vertical μCT slices allowed the detection of elements which modify the structure and the viewing of both specimens with a high level of detail.

Furthermore, the histograms produced useful information on the structure of the permeameter specimen and detected axial structural variations, e.g., differences in concentration of plastic discs. As a consequence of modifications to the structure using flow diverting elements, the saturated hydraulic conductivity in the permeameter specimen was reduced by 26% when compared with an equivalent specimen without structural alterations. The purpose of this ongoing investigation is to increase our fundamental understanding of the role of materials contained in MSW such as plastics, textiles and paper, which, due to their shape, size and composition are thought to impact the fluid flow properties [9,10,44, 45] and the mechanical properties [7,10,39] of the landfilled waste. μCT provides the possibility of obtaining detailed information on the structure (disc distribution) that otherwise could only be obtained by the destruction of the sample.

The possibility of obtaining information on the pore architecture is of particular interest for the estimation of fluid flow properties. Dullien [5] examined how mathematical models that consider the pore space as a bundle of capillaries work well in predicting the hydraulic conductivity and hence are a well founded modelling approach. However given the lack of accurate and detailed information on the pore structure, their use in porous media studies is still limited. In solid waste, this information is even scarcer than for other materials such packed beds and soils where more recent progress has been made [15,36,46,47]. The heterogeneity of waste may also lead to further complexity in the pore geometry [48]. The lack of information on waste pore structure param eters e.g., pore size distribution and tortuosity, has constrained modellers to use soil data for waste modelling. Recent numerical modelling of waste behaviour has inferred the pore size distribution from particle size information to estimate gas and liquid hydraulic conductivities as well as the capillary pressure [49,50]. It is therefore clear that better estimation of pore space parameters will improve modelling accuracy and have a positive impact in the design and operation of strategies for landfill remediation.

The major challenge in applying imaging to a real landfill is the preparation or recovery of a sample representative of the field in terms of both size and structure. Large scanners can accommodate specimens up to about 600 mm in diameter, which should be sufficient to be representative of a processed waste such as MBT with a maximum particle size of up to, say, 60 mm. Regions of interest could then be highlighted, physically extracted and scanned at micron resolution, as has been done in petrophysics research [51]. Potential methods of sample recovery from the field and preservation, including freezing [52] and impregnation [19], have been proposed but further work is needed.

CONCLUSIONS

The use of μCT to identify structural features (reinforcing and flow diverting elements) in waste analogue materials has been demonstrated. The method was also effective in quantifying the content of high density materials, e.g., sand and glass.

The results suggest that μCT could be applied to characterise the structure of landfilled waste such as MBT, for which the particle size and hence representative elemental volume are not too large. A multiple scale imaging approach could be adopted to reveal a level of detail which would increase our understanding of fluid flow and mechanical processes in landfills.

The use of CT and μCT to study solid waste could provide significant insights to aid understanding of, for example, how the structure of waste changes over time as it degrades through variations in pore size and interconnectivity; or the difference in the structure that develop in residues with different characteristics. The current paper has demonstrated this potential.

REFERENCES

1. Hall, D.H., D. Drury, J.R. Gronow, S.J.T. Pollard and R. Smith, Estimating pollutant removal requirements for landfills in the UK: III. Policy analysis and operational implications. Environ. Technol., 28(1), 25-32 (2007).
2. Hudgins, M. and S. Harper, Operational characteristics of two aerobic landfill systems. Seventh International Waste Management and Landfill Symposium. Cagliari, Italy, Oct. 4-8 (1999).
3. Collins, R.E., Flow of Fluids through Porous Materials. Reinhold Publishing , New York (1961).
4. Beven, K. and P. Germann, Macropores and water-flow in soils. Water Resour. Res., 18(5), 1311-1325 (1982).
5. Dullien, F.A.L., Porous Media: Fluid Transport and Pore Structure. 2nd Ed., Academic Press, San Diego, CA (1992).
6. Dixon, N. and D.R.V. Jones, Engineering properties of municipal solid waste. Geotext. Geomembranes, 23(3), 205-233 (2005).
7. Kölsch, F., Material values for some mechanical properties of domestic waste. Fifth International Waste Management and Landfill Symposium. Cagliari, Italy, Oct. 2-6 (1995).

8. Dixon, N., U. Langer and P. Gotteland, Classification and mechanical behavior relationships for municipal solid waste: Study using synthetic wastes. J. Geotech. Geoenviron., 134(1), 79-90 (2008).
9. Xie, M.L., D. Aldenkortt, J.F. Wagner and G. Rettenberger, Effect of plastic fragments on hydraulic characteristics of pretreated municipal solid waste. Can. Geotech. J., 43(12), 1333-1343 (2006).
10. Velkushanova, K., D. Caicedo, D.J. Richards and W. Powrie, A detailed characterisation of an MBT waste. Twelfth International Waste Management and Landfill Symposium. Cagliari, Italy, Oct. 5-9 (2009).
11. Shipitalo, M.J., V. Nuutinen and K.R. Butt, Interaction of earthworm burrows and cracks in a clayey, subsurface-drained, soil. Appl. Soil Ecol., 26(3), 209-217 (2004).
12. Mooney, S.J. and C. Morris, A morphological approach to understanding preferential flow using image analysis with dye tracers and X-ray computed tomography. Catena, 73(2), 204-211 (2008).
13. Flury, M., H. Flühler, W.A. Jury and J. Leuenberger, Susceptibility of soils to preferential flow of water: A field study. Water Resour. Res., 30 (7), 1945-1954 (1994).
14. Morris, C. and S.J. Mooney, A high-resolution system for the quantification of preferential flow in undisturbed soil using observations of tracers. Geoderma, 118(1-2), 133-143 (2004).
15. Heijs, A.W.J., J. de Lange, J.F.T Schoute and J. Bouma, Computed tomography as a tool for non-destructive analysis of flow patterns in macroporous clay soils. Geoderma, 64(3-4), 183-196 (1995).
16. Amos, C.L., T.F. Sutherland, B. Radzijewski and M. Doucette, A rapid technique to determine bulk density of fine-grained sediments by X-ray computed tomography. J. Sediment Res., 66(5), 1023-1025 (1996).
17. Sato, H. and S. Suzuki, Fundamental study on the effect of an orientation of clay particles on diffusion pathway in compacted bentonite. Appl. Clay Sci., 23(1-4), 51-60 (2003).
18. Kettridge, N. and A. Binley, X-ray computed tomography of pent soils: Measuring gas content and peat structure. Hydrol. Process., 22(25), 4827-4837 (2008).
19. Watson, G.V.R., W. Powrie and A.P. Blades, Particle scale classification and identification of the structure of processed municipal solid waste by CT scanning. International Symposium on Geomechanics and Geotechnics of Particulate Media. Yamaguchi, Japan, Sep. 12-14 (2006).
20. Pope. J.A., Medical Physics: Imaging. Heinemann Educational Publishers, Oxford, UK (1999).
21. Brooks, R.A., L.G. Mitchell, C.M. Oconnor and G. Dichiro, On the relationship between computed-tomography numbers and specific gravity. Phys. Med. Biol., 26(1), 141-147 (1981).
22. Denison, C., W.D. Carlson and R.A. Ketcham, Three-dimensional quantitative textural analysis of metamorphic rocks using high-resolution computed X-ray tomography .1. Methods and techniques. J. Metamorph. Geol., 15(1), 29-44 (1997).
23. Kak, A.K. and M. Slaney, Principles of Computerized Tomographic Imaging. IEEE Press, New York (1988).
24. American Society for Testing and Materials (ASTM), Standard Guide for Computed Tomography (CT) Imaging. ASTM E 1441-00, West Conshohocken, PA (2005).
25. McCullough, E.C., Photon attenuation in computed tomography. Med. Phys., 2(6), 307-320 (1975).
26. Brooks, R.A., The physics of computer assisted tomography. 1977 Electro Conference Record. New York, Electro, p.23/1/1-23/1/6 (1977).
27. Denison, C. and W.D. Carlson, Three-dimensional quantitative textural analysis of metamorphic rocks using high-resolution computed X-ray tomography .2. Application to natural samples. J. Metamorph. Geol., 15(1), 45-57 (1997).
28. Dunsmuir, J.H., S.R. Ferguson, K.L. D'Amico and J.P. Stokes, X-Ray microtomography: A new tool for the characterization of porous media. SPE Annual Technical Conference and Exhibition. Dallas, TX, Oct. 6-9 (1991).
29. D'Amico, K.L., J.H. Dunsmuir, S.R. Ferguson, B.P. Flannery and H.W. Deckman, The Exxon microtomography beam line at the National Synchrotron Light-Source. Rev. Sci. Instrum., 63(1), 574-577 (1992).
30. Ketcham, R.A. and W.D. Carlson, Acquisition, optimization and interpretation of X-ray computed tomographic imagery: Applications to the geosciences. Comput. Geosci., 27(4), 381-400 (2001).
31. Kaestner, A., E. Lehmann and M. Stampanoni, Imaging and image processing in porous media research. Adv. Water Resour., 31(9), 1174-1187 (2008).
32. Allaire, S.E., S. Roulier and A.J. Cessna, Quantifying preferential flow in soils: A review of different techniques. J. Hydrol., 378(1-2), 179-204 (2009).
33. Werth, C.J., C.Y. Zhang, M.L. Brusseau, M. Oostrom and T. Baumann, A review of non-invasive imaging methods and applications in

contaminant hydrogeology research. J. Contam. Hydrol., 113(1-4), 1-24 (2010).
34. Wellington, S.L. and H.J. Vinegar, X-Ray computerized-tomography. J. Petrol. Technol., 39 (8), 885-898 (1987).
35. Withjack, E.M., Computed tomography for rock-property determination and fluid-flow visualization. SPE Formation Eval., 3(4), 696-704 (1988).
36. Mooney, S.J., C. Morris and P.M. Berry, Visualization and quantification of the effects of cereal root lodging on three-dimensional soil macrostructure using X-ray computed tomography. Soil Sci., 171(9), 706-718 (2006).
37. Watson, G.V.R., W. Powrie and A.P. Blades, An investigation into the effects of degradation on waste structure. Eleventh International Waste Management and Landfill Symposium. Cagliari, Italy, Oct. 1-5 (2007).
38. Cresswell, A., M.E. Barton and R. Brown, Determining the maximum density of sands by pluviation. Geotech. Test. J., 22(4), 324-328 (1999).
39. Fernando, S., W. Powrie, G. Watson and D.J. Richards, The impact of the reinforcing content on the shear strength of mechanically biologically treated waste. Third International Workshop "Hydro-Physico-Mechanics of Landfills". Braunschweig, Germany, Mar. 10-13 (2009).
40. Nixon, M. and A. Aguado, Feature Extraction and Image Processing. 2nd Ed., Academic Press, Oxford, UK (2008).
41. Hazen, A., Discussion of aams on sand foundations. T. Am. Soc. Civ. Eng., 73, 199-203 (1911).
42. Krumbein, W.C. and G.D. Monk, Permeability as a function of the size parameters of unconsolidated sand. T. Am. Soc. Civ. Eng., 151, 153-163 (1942).
43. Powrie, W., Soil Mechanics: Concepts and Applications. 2nd Ed., Spon Press, Oxon, UK (2004).
44. Donohue, T.J. and C.M. Wensrich, A numerical investigation of the void structure of fibrous materials. Powder Technol., 186(1), 72-79 (2008).
45. Caicedo, D., J.J. Sandoval, G.V.R. Watson, D.J. Richards and W. Powrie, Exploring the use of a modified dye-adsorption method for the study of landfilled waste structure and some implications for post-closure management in landfills. Global Waste Management Symposium. San Antonio, TX, Oct. 3-6 (2010).
46. Peyton, R.L., B.A. Haeffner, S.H. Anderson and C.J. Gantzer, Applying X-ray CT to measure macropore diameters in undisturbed soil cores. Geoderma, 53(3-4), 329-340 (1992).
47. Perret, J.S., S.O. Prasher and A.R. Kacimov, Mass fractal dimension of soil macropores using computed tomography: From the box-counting to the cube-counting algorithm. Eur. J. Soil Sci., 54(3), 569-579 (2003).
48. Felske, C., E. Kraft, C. Zeiss and W. Bidlingmaier, Geometric characterisation of residential waste with special consideration to the fluidflow behaviour in landfills. Eighth International Waste Management and Landfill Symposium. Cagliari, Italy, Oct. 1-5 (2001).
49. White, J.K. and R.P. Beaven, The role of pore space geometry, waste descriptors, and microscale network modelling in the design of macroscale landfill models. Global Waste Management Symposium. Copper Mountain, CO, Sep. 7-10 (2008).
50. Nayagum, D., J. White, K. Zardava and R. Beaven, The use of a numerical model to extrapolate laboratory scale results on waste to full scale landfill remediation applications. Global Waste Management Symposium. San Antonio, TX, Oct. 3-6 (2010).
51. Grader, A.S., A.B.S. Clark, T. Al-Dayyani and A. Nur, Computations of porosity and permeability of sparic carbonate using multiscale CT images. 23rd International Symposium of the Society of Core Analysts. Noordwijk aan Zee, Netherlands, Sep. 27-30 (2009).
52. Watson, G.V.R., R.P. Beaven, C.R.I. Clayton and A.P. Hudson, Development of techniques for freeze sampling of wastes using liquid nitrogen. Ninth International Waste Management and Landfill Symposium. Cagliari, Italy, Oct. 6-10 (2003).

Discussions of this paper may appear in the discussion section of a future issue. All discussions should be submitted to the Editor-in-Chief within six months of publication.

Manuscript Received: June 28, 2010
Revision Received: January 18, 2011
and Accepted: January 24, 2011

Exploring the use of a modified dye-adsorption method for a better understanding of landfilled waste structure in the context of post-closure management strategies in landfills

Caicedo C. Diana M[1] , Sandoval C. John J[2], Watson, Geoff V.R[3], Siddiqui, Asif A, Richard, David J and Powrie, William [4]

ABSTRACT

It is generally accepted that landfilled municipal solid waste develops a heterogeneous and anisotropic structure during placement, degradation and settlement. Thus structure is significant as it affects the flow properties for liquids and gas. This paper describes the results of a test carried out on a specimen of degraded MSW to investigate the effectiveness of emulsion paint and brilliant blue dye in identifying preferential liquid flow paths. Some promising initial results are presented and suggestions for improvements to the techniques and future work are made.

INTRODUCTION

Final disposal of solid waste into landfills is considered as the least desirable option within integral solid waste management systems. Nevertheless, in many countries, landfilling remains as the main solid waste final disposal solution. Evidence suggests that recalcitrant contaminants contained in landfills are likely to persist for centuries as well as the risk of pollution posed by both active and closed sites.

The search for adequate landfill operation and management strategies has triggered the development of various engineering alternatives aiming to enhance biodegradations processes, sites utilization rates (i.e. settlement), improved leachate management, physicochemical stabilization and removal of contaminants, among others. Alternatives explored include the recirculation of liquids and in situ aeration. Implementation of any of these alternatives requires understanding of flow and transport processes in landfills.

In porous media flow and transport processes are strongly controlled by the medium physical structure, which can be analyzed in terms of pores geometry and interconnectivity (Collins, 1961; Beven and Germann, 1982; Dullien, 1992). No much is known about the physical structure that develops once solid waste is placed into landfills and how that structure influences flow phenomena. It is recognized though that, similarly to other geological materials , municipal solid

[1]PhD student , School of Civil Engineering and the Environmental, University of Southampton, United Kingdom, University Road, Southampton, SO17 1BJ, dmc1x07@soton.ac.uk.

[2]PhD student , School of Civil Engineering and the Environmental, University of Southampton, United Kingdom, University Road, Southampton, SO17 1BJ, jjs1x07@soton.ac.uk .

[3]Research Fellow, School of Civil Engineering and the Environmental, University of Southampton, United Kingdom, University Road, Southampton, SO17 1BJ, gvrw@soton.ac.uk.

[4]Professor, School of Civil Engineering and the Environmental, University of Southampton, United Kingdom, University Road, Southampton, SO17 1BJ, wp@soton.ac.uk.

waste (MSW) can constitute highly structured materials due to the deposition in progressive layers, high compaction and composition, material's size and material's shape heterogeneity (Dixon and Jones, 2005). Plastics and textiles, due to their shape and orientation, can reinforce the structure strength (Ashby and Jones, 1986, Kölsch, 1995 , Dixon et al., 2008) and influence flow behaviour by blocking or impeding fluids movement (Xie et al., 2006 and Velkushanova et al., 2009)

Of special interest for the study of fluid flow and transport process in porous systems is the presence of preferential routes or flow pathways. This type of phenomenon is commonly referred as preferential flow and is used to describe flow mechanisms where transport of water, as well as dissolved and suspended matter, are primarily associated with a smaller fraction of the total pore space. Field measurement of mass movement of liquids and gases in soils often shows faster transport than it is predicted from mathematical modelling, a phenomenon that has been frequently associated with preferential flow occurring through macropores (e.g. earthworm burrows and cracks), or caused by soil layering or hydrophobicity (Beven and Germann, 1982, Allaire et al., 2009)

The study of preferential flow mechanisms in natural and semi-natural systems has gained attention during the recent decades due to its incidence in physical processes with high environmental and human health implications. In soils, preferential routes may accelerate or delay the movement of dissolved matter and contaminants. Faster transport of contaminants to groundwater sources reduces the contact time with chemically reactive soil layers (Morris and Mooney, 2004 and Flury et al., 1994).

Diverse techniques ranging from the observation of structures likely to lead to preferential flow (Garner, 1953, Beven and Germann, 1982, Munyankusi et al., 1994, Shipitalo et al., 2004,, Mooney et al., 2006) to the use of tracers breakthrough curves (Mooney and Morris, 2008) and dyes to visualise flow paths (Van Ommen et al., 1988, Andreini and Steenhuis, 1990, Flury et al., 1994, Weiler and Flühler, 2004, Hangen et al., 2004, ,Morris and Mooney, 2004, Lipsius and Mooney, 2006) have been applied in preferential flow studies with soils and in other systems such packed beds (Ravindra et al., 1997).

The observation of disturbing structures, i.e. cavities, fissures, in-homogeneities, can be achieved during field excavations by in situ inspection or in the laboratory. Careful selection of sampling methods is required to ensure negligible changes in the specimen' original structure (Clayton et al., 1982). Specific steps during specimen preparation (e.g. thin sectioning and resin impregnation); depend on factors such as specimen nature, degree of detail expected and techniques availability (e.g. visual, microscopic or scanning).

In tracer studies, conservative substances (non-reactive, non-degradable and highly detectable) are used as surrogates to mimic the transport of water and other dissolved and suspended substances. Once applied, the tracer travel through the system is characterized by monitoring its concentration in the effluent. The response curve so obtained is influenced by the flow behaviour and the medium structure. Different chemicals are used for this purpose. Ions such as Cl^- and Br^- are particularly good at tracing water movement; whereas dyes are generally considered suitable surrogates for contaminants.

Dyes are coloured substances highly soluble in the carrying solvent, properties that are exploited in preferential flow studies. As the solvent flows, dyes stain such contact areas and make the visual recognition of flow paths possible. Dyes are due to their high sorption capacity, non-conservative (Ketelsen and Meyer-Windel, 1999 and Germán-Heins and Flury, 2000) which has limited their use in breakthrough curves studies , where conventional tracers are used.

Of special interest in preferential flow studies are those dyes with high water solubility , such as Brilliant Blue (BB), which due to its high mobility, visibility and low toxicity has extensively been used to understand flow paths in soils studies (Andreini and Steenhuis, 1990). Visualisation, using image processing techniques, has allowed the qualitative description of dye spatial distribution (Flury et al., 1994). Some degree of quantification has also achieved with the calibration of photograph colour using the amount of dye adsorbed (Morris and Mooney, 2004, Lipsius and Mooney, 2006). Further exploitation of dye patterns information to infer flow regimes was published by Weiler and Flühler, 2004. In their study, textural diverse soils (i.e. loam to sand) were infiltrated with Brilliant Blue at different irrigation rates and initial moisture conditions. The use of photographs taken of vertical and horizontal sections together with the analysis of the extent and distribution of the stained areas was used to classify flow types into those occurring only in the soil matrix and those occurring as the result of interactions between the soil matrix and macropores.

As observed in some soil systems, preferential flow routes seem to develop within landfill units. Some experimental work has indicated the presence of channelling flow in municipal solid waste , usually by measuring moisture contents and the distribution of flow at the discharge of waste packed columns (Zeiss and Major, 1992, Korfiatis et al., 1984). In other studies in MSW, tracer tests have revealed the presence of stagnant zones and flow channeling, indicating the presence of preferential flow phenomena (Johnson et al., 2001, Bendz and Singh, 1999). During remediation of landfill sites, flushing and aeration effectiveness are expected to be strongly influenced by the presence of preferential flow mechanisms; however, experimental evidence in this sense at both laboratory and field scale is still limited. No studies reporting the use of dye tracers for flow visualisation in waste have being published

This paper presents a case of study in which dye tracing methods were explored to visualize flow routes in a nearly undisturbed municipal solid waste (MSW) sample in response to liquid infiltration events. The study was carried out under two different liquid injection methods and using different dye types. In the first method, a water diluted emulsion paint was poured on the top of the sample whereas in the second an aqueous solution of Brilliant Blue was irrigated using a device that simulates an even irrigation event. The structure of the specimen was also analysed, with special attention to the examination of the orientation of those materials that have the potential to modify flow patterns. The paper explains the results obtained during these experiments, examines the potential of dye tracing methods in the study of flow and transport processes in landfilled waste and discusses the implication of those results in the context of post-closure management strategies for landfills.

MATERIALS

The waste specimen used in this study corresponds to fresh household waste (MSW) acquired from a local landfill facility in the UK and was used during the study of settlement processes in landfills published by Ivanova et al., 2008. Large particles (>40-mm) were shredded. The resulting sample was characterized according to its particle size and components, as can be seen in Figure 1. In that study, a built purpose consolidating anaerobic reactor (CAR) was used according to the design described by Parker et al., 1999. The reactor is a Perspex cylinder (935-mm height and 480-mm ID) with a loading system that applies a constant surcharge to the waste, which in this case was set at 50kPa. This load would be equivalent to a 5-m waste depth in a landfill if a 10 kN/m^3 bulk unit weight is assumed for the residue.

The sample was placed and degraded following a process that represents well those occurring in landfill sites that lead to the formation of highly structured materials (Dixon and Jones, 2005). The specimen served as a "control sample" as given in full by Ivanova, 2007. Progressive layers of material were placed inside the CAR and highly compressed to 500-mm height. After placement, the sample was saturated using a prepared mineral media containing 10% of anaerobically digested sewage sludge to accelerate anaerobic digestion. Leachate was intermittently recirculated , however, as the purpose of the sample was to work as a "control", it was initially acidified, and the degradation inhibited during the initial 345 days of the 919 days of total experimentation. A total settlement of 18.6% (350-mm final sample height), was reported as the result of consolidation and bio-degradation processes (Ivanova, 2007).

METHODS

After settlement was completed, the opportunity was taken to trial some techniques developed during this study to investigate preferential flow on much smaller waste samples. The methods were based on the application of two types of dye to reveal flow paths in waste in two different flow regimes. The first dye was diluted emulsion paint added to the surface of the resaturated waste. The second was an aqueous solution of Brilliant Blue that was irrigated using a device simulating rainfall.

Dye-tracing using diluted paint

At the start of this study, the MSW sample was slowly re-saturated by pumping water through the base of the CAR at a rate of 1.25 ml/s. The water level in the reactor was raised up to 1 mm above the waste surface. Then two litres of diluted (1:1 by mass) red emulsion paint were then allowed to pond at the top of the saturated waste and allowed to drain. Once the drainage finished the CAR was wrapped in an electric heating blanket and insulation to dry both the waste and the infiltrated paint.

After two weeks, the sample was removed from the reactor, whilst every effort was made to preserve the original structure. This step was of great importance since it is recognized that damage caused to the structure as a result of sampling may cause potential biases to structures favouring preferential flow. The core was extruded from the cell using a piston and then wrapped with cling film. Following extrusion, the core which was originally contained in the 480-mm Perspex cylinder, was 479-mm diameter over the upper part (300-mm height) and 487-mm over the bottom one (50-mm height), suggesting that the original structure was likely to have been reasonably well preserved.

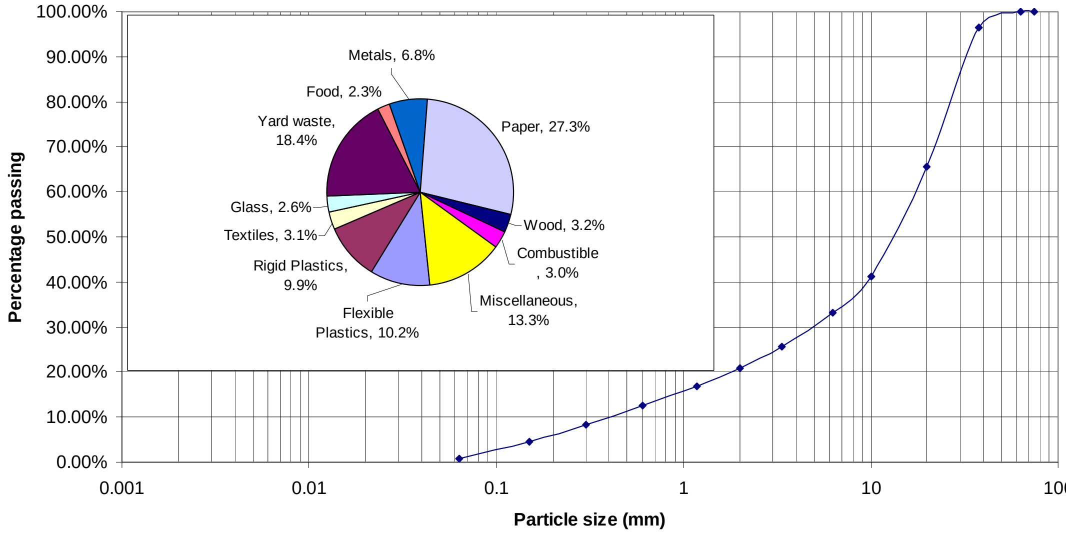

Figure 1 Particle size distribution and material composition of the MSW at the beginning of settlement studies (after Table 5.2 and 5.3 in Ivanova, 2007)

To visualise the areas through which the paint penetrated, the external surface of the sample was inspected and photographs taken at different angles after reference pins were placed every 60^{o} around the sample (e.g. red pins in Figure 4 are the reference points at 180^{o}). A thin sectioning method to allow visualisation on the internal structure was developed, involving cutting the specimen into vertical slices using a band saw. Initial trials revealed that horizontal slicing was relatively easy, but not vertical. This was, because of the preferential horizontal orientation of many sheet-like materials , e.g. plastics, textiles, etc., contained within the waste sample, as was confirmed once the slices were produced. To achieve high quality cutting, the sample was covered with a plaster layer that once dried, created a strong yet easily to cut coat that prevented any structural damage during the slicing process and facilitated core manipulation. The core was then cut horizontally at height of 230-mm using an electric knife. This step had two purposes: to make the sample fit into the 300-mm throat of the band saw and preserve the bottom portion for the Brilliant Blue tests. The top portion where, the paint had penetrated the most, was cut into 8 cm thick vertical slices using the band saw, which produced cleanly cut flat surfaces. A schematic representation of the cutting process is presented in Figure 2. Photographs of each exposed surface were taken as shown in Figure 5 and Figure 6 and used for analysis.

Dye-tracing using Brilliant Blue

In the second test Acid Blue 9 (also known as Brilliant Blue R), a commercially available food grade colorant (CAS No 3844-45-9), was used as dye. The dry colorant was supplied by Sigma Aldrich and a 1g/litre aqueous solution prepared to irrigate the waste sample. This concentration, although less than those reported in the literature for soils (3 to 5 g/l; Flury and Flühler, 1995; Germán-Heins and Flury, 2000 and Mooney and Morris, 2008) provided a sufficient visual contrast with the waste matrix and was considered adequate for the test.

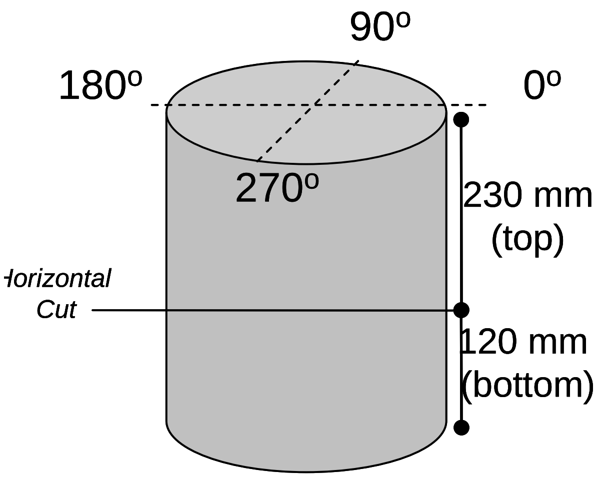

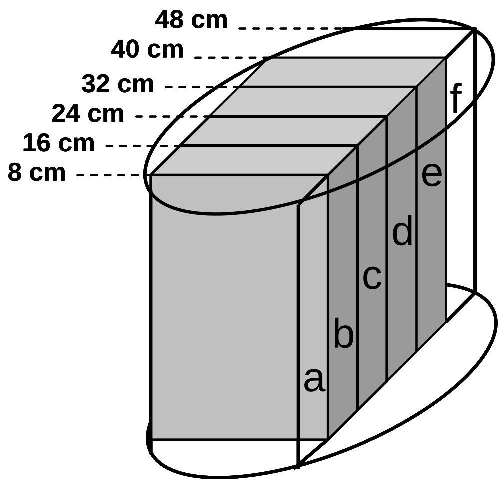

a. Initial core representation with imaginary reference points (dashed lines) and initial horizontal cut

b. Thin sectioning carried out on the top subcore

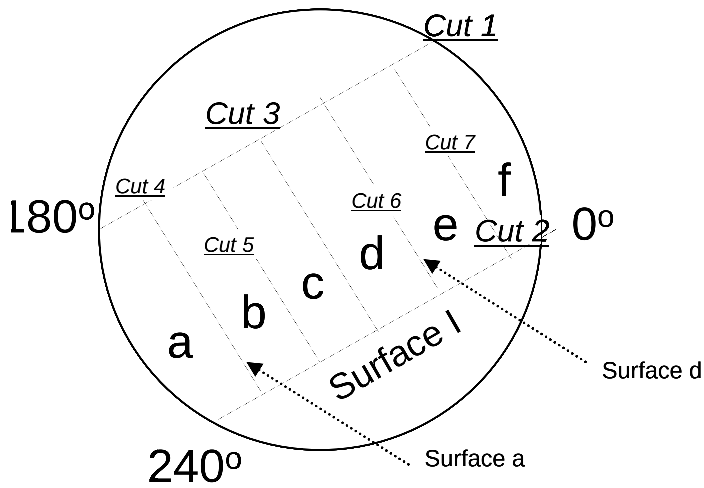

c. Cross sectional view of the thin sectioning process

Figure 2 Schematic representation of the cutting process during the study of preferential flow in specimen of MSW

The dye tracer was applied using a rainfall simulator device that produced an even irrigation of the sample at very low flow rates. A schematic representation of the experimental set up is presented in Figure 3. The device is made of a Perspex cylinder and a needles shower. The flow rate, controlled by the liquid head in the cylinder, is in the range of 39 ml/min to 49 ml/min. The use of the rainfall simulator was essential for this study as made possible the minimisation of any bias during the dye application that could have favoured preferential infiltration of the dye solution.

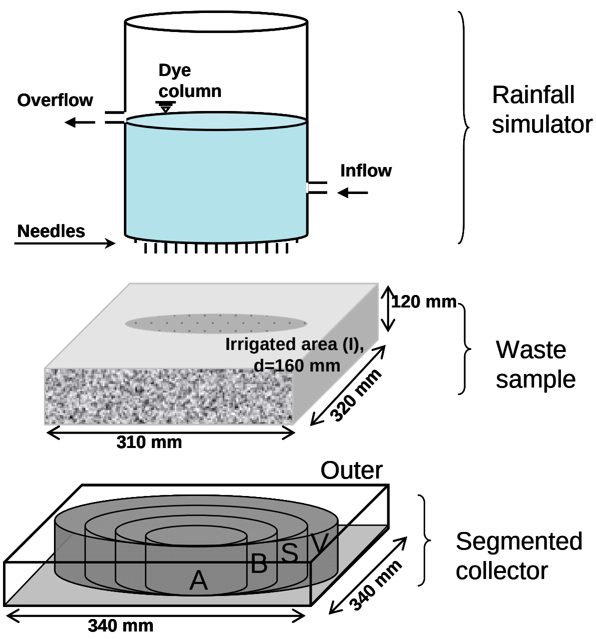

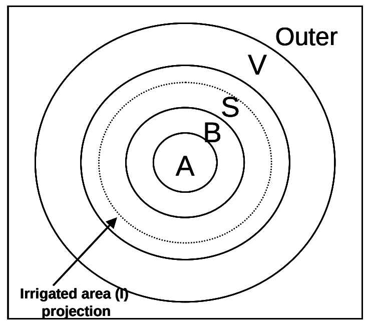

Segmented collector cross section

Sector	Diameter (cm)	Area of circle (m2)	Sector area (m2) [a]	% Expected flow [b]
I	16	0.0201	na	na
A	6.3	0.0031	0.0031	15.5
B	12.2	0.0117	0.0086	42.6
S	22	0.0380	0.0263	41.9
V	31.5	0.0779	0.0399	0
Outer	na	na	0.0213	0

a. Corresponds to the effective area that collects volume. Example, for B =0.0117-0.0031= 0.0086
b. Calculated as percentage of I. Example, for B = 0.0086/0.0201=42.6

Figure 3 Schematic representation of the experimental set up used during Brilliant Blue tests. A rainfall simulator was used to irrigate a square sample obtained from the MSW specimen. Outflow was collected in concentric containers with the dimensions presented in the table

Powrie and Beaven, 1999 reported saturated hydraulic conductivity values between 1.5 x 10^{-4} to 1.9 x 10^{-5}m/s for crude household waste samples under 87-kPa compression conditions, corresponding to measured dry density values ranging 0.32 – 0.39 t/m^3. A dry density value of 0.343 t/m^3 was calculated by Ivanova for the waste sample used in this study based in the results reported by Powrie and Beaven (1999). This suggest that the saturated hydraulic conductivity for the sample should be at least in the order of 10^{-5} m/s. Based on this data, the head column in the rainfall simulator was set in order to produce the flow rates required for the experiments.

A square (310 x 320 x 120 mm) specimen was produced from the remaining bottom portion of the sample, by cutting it vertically with the band saw. No further horizontal slicing was necessary. Once cut, three of the exposed surfaces were covered with a plaster layer to preserve the structure during the test, as previously described. The fourth face was left uncovered for visualisation of dye flow paths during the experiment. The bottom surface was carefully attached to a strong mesh (with a large aperture size of approx. 1-cm) to support the specimen whilst not causing major flow disruptions. The sample was mounted so as to permit the location of five concentric containers at the bottom, aligned with its centre, which allowed the collection and measurement of the outflow distribution.

The test was run in two phases. First water alone, was irrigated at a rate of 43 ml/min, over a central circular area, I in Figure 3 (16-cm D), on the top of the waste surface, and until a steady state was reached, indicated by the measured flow rates in and out of the sample being the same after 60 minutes . Then, the supply of water was replaced by the dye solution and the test was run for a further 1 hour. Both, the total outflow and the concentric distribution were measured every 30 minutes.

RESULTS

Dye-tracing using diluted paint

Photographs were taken and processed using Adobe Photoshop Lightroom, using the saturation tool that allows colour filtration (red in this case) and facilitates visual analysis (Figure 4). Over most of the surface, the dye penetrated approximately 6 cm. However, in some areas, infiltration was substantially higher. In the 180-240^{o} section, penetration of the dye was up to 15 cm (Figure 4 a); region that was selected for a more detailed analysis using thin sectioning (Figure 2). The maximum dye penetration was 27 cm, detected in the 300-0^{o} section in a hollow plastic bottle, which could presumably have acted as a macropore (Figure 4 b).

Six slices each 8 cm thick, were produced to visualise the dye spatial distribution as indicated in Figure 2. Photographs were recorded and presented in Figure 5 and Figure 6. This inspection showed negligible average infiltration of the paint, <1 cm, and evidenced the preference of the paint to flow along the external surface. Examination of the structure was achieved through inspection of the slices as shown in Figure 6, which confirmed that materials such as plastics and textiles were mostly horizontally orientated.

Brilliant Blue Tests

The flow distribution, expressed as a percentage of the total outflow, is presented in Figure 7. The area of each sector (Figure 3), was used to estimate an “expected outflow” considering water flowing linearly from the irrigated area to the base, i.e. neglecting flow spreading. Water alone was irrigated during the first 59 minutes of the test. The supply was then changed to Brilliant Blue solution and run for 60 more minutes.

Photographs were taken during the test to record progress of dye staining with time. Selected images are presented in Figure 8, for which a blue filter was used. The dark blue areas represent those regions coloured with Brilliant Blue while those in light blue are original blue pieces of material, not dye-stained.

DISCUSSION

The two dye tests carried out during this study indicated the presence of preferential flow, especially at the external surface of the sample. The factors causing this behaviour can be related primarily to the structural properties of the solid medium.

Examination of the structure revealed that, despite more than 1.5 years of active anaerobic degradation and 3 more sitting in the CAR, many pieces of plastic and textiles remained easily

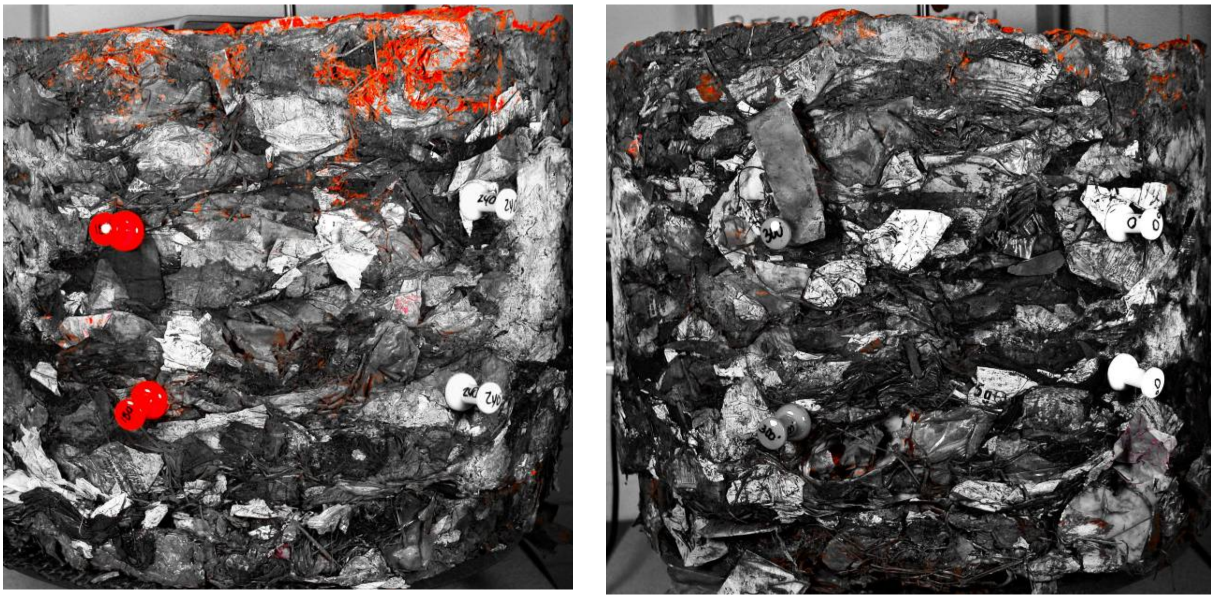

a. 180-240 ^{o} region, showing dye penetration up to 15 cm. The red pins identified as 180^{o}, are the reference points placed at that angle (originally red).

b. 300-0 ^{o} region, showing a localised dye penetration up to 27 cm

Figure 4 Selected photographs of the external surface of the MSW sample after infiltration of a paint . Red regions indicate paint stained areas.

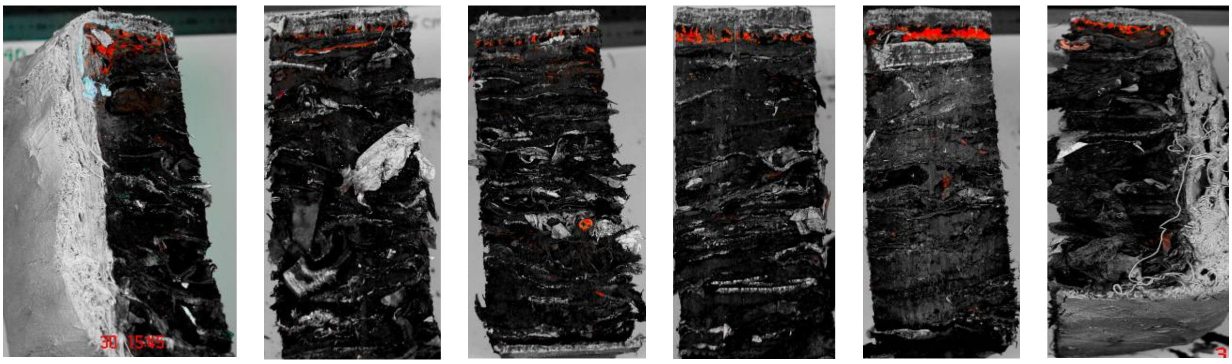

a. 8 cm | b.16 cm | c. 24 cm | d. 32 cm | e. 40 cm | f. 48 cm

Figure 5 Slices produced by sequential sectioning of the 180-240 ^{o} region (the view is of Surface I indicated in Figure 2 c)

identified. They were well distributed through the sample and preferentially horizontally orientated. These materials, due to their shape, impede or block the flow of fluids. They can, therefore lead to preferential flow. The original mass content of plastics and textiles was 20% and 3% by dry mass respectively. Material characterisation has not yet been carried out for the degraded sample; however, judging from the visual inspection, plastic content is likely to be much higher. The total absence of nuisance smells coming from the sample also indicates that the readily degradable components, e.g. organic matter and paper, have been degraded by this time. Further material analysis will be carried on within the next few months to better understand the changes in waste structure resulting from biodegradation.

Deconstruction of the sample revealed it to be a highly structured material. Vertical slicing was difficult and required the use of specialised equipment. The specimen, although requiring plaster coating to prevent damage during the experiments, was sufficiently stable to not fall apart before being covered, which reflects the high reinforcing potential of materials such as plastics and textiles.

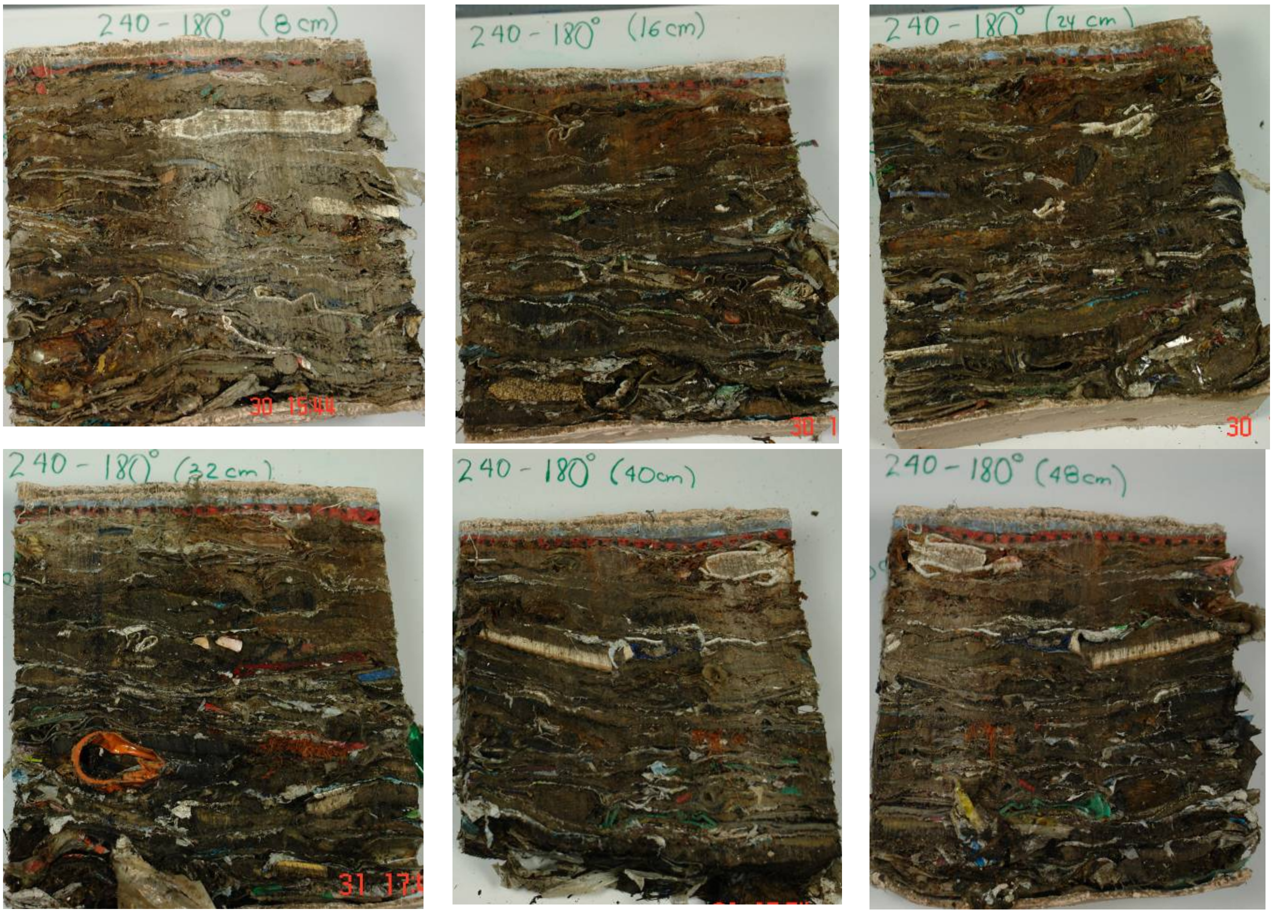

Figure 6 Surfaces exposed after slicing every 8 cm of the MSW sample (the planes of view are perpendicular to surface I in Figure 2c)

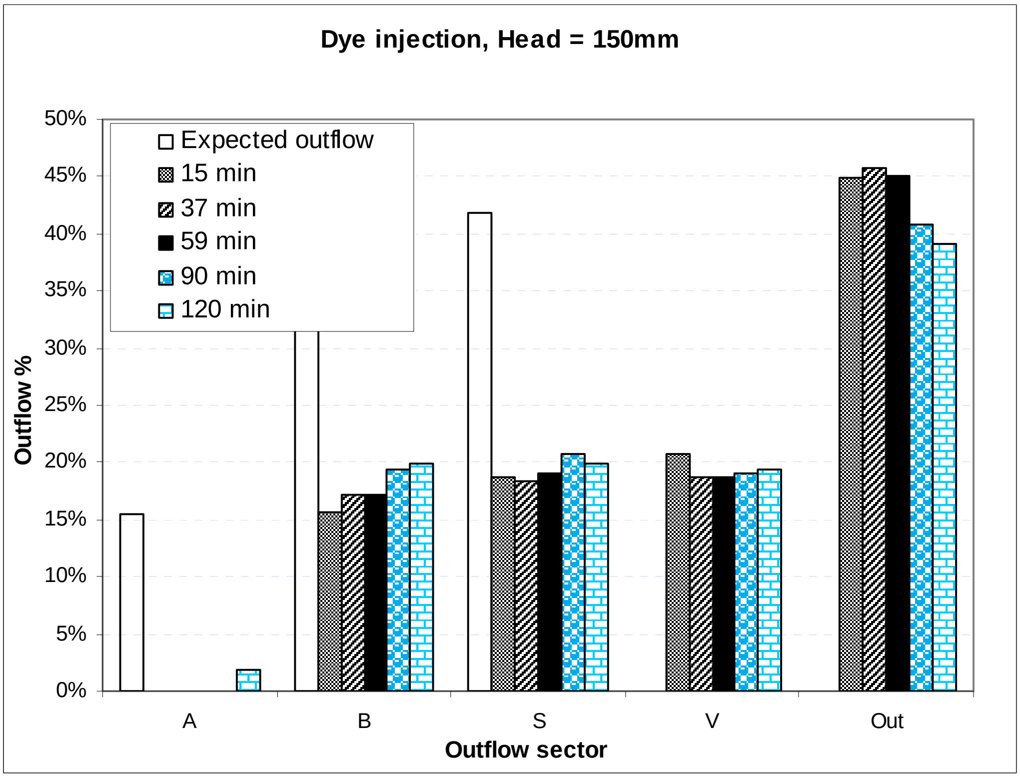

Figure 7 Outflow distribution during Brilliant Blue infiltration test. Data for the first 59 minutes (white and black bars) correspond to water irrigation; the supply was then changed to dye solution (blue bars)

During the experiment using Brilliant Blue the flow distribution differed substantially from that expected in the absence of preferential flow. Expected outflows (Figure 7) were calculated as percentages of the total flow, considering an ideal situation in which water flows uniformly and purely vertically. In that case, fluids irrigated over the area I should be collected only in sectors A, B and S as shown in Figure 3. V and outer sectors are geometrically outside the influence of I with diameters greater than 22 cm. The experimental data, however, showed that the greatest flow proportion was collected in the outer (39-46%), and V (19-21%) sectors. No fluid was collected in the sector A, whereas the expected flow was of 16%. In sectors B and S, the collected fluid was less than 50%, of the expected value.

Development of leachate recirculation and flushing techniques for landfills has become a priority in order to assess the long term environmental impact of the source term associated with waste disposal and management. One of the challenging aspects of describing the dynamics of contaminants in landfills is understanding and simulating their movement in the unsaturated zone. The flow rates employed in the dye-tracing tests with Brilliant Blue were conceived to be low enough to establish unsaturated flow conditions through the waste sample under irrigation. BB addition followed establishment of unsaturated flow conditions in the system, as indicated by the consistency in the outflow percentages measured for every sector of the segmented collector, as shown in Figure 7. In this form the routes followed by the solution, indicated by the stained sections in the sample, can be associated with flow pathways leaved by the liquid under an unsaturated flow regime.

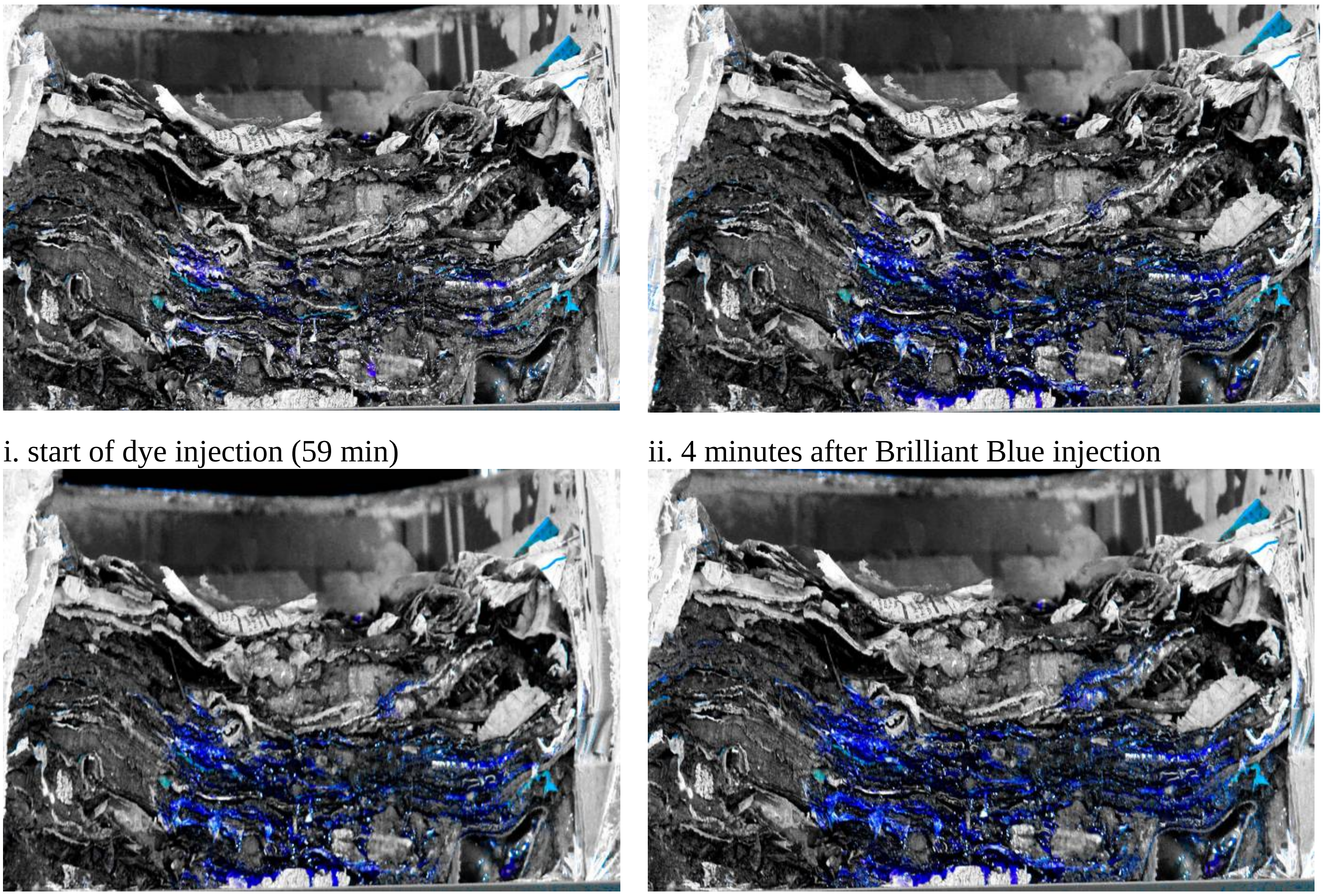

i. start of dye injection (59 min) ii. 4 minutes after Brilliant Blue injection

iii. 9 minutes after Brilliant Blue injection iv. 40 minutes after Brilliant Blue injection

Figure 8 Exposed surface of MSW after irrigation with 1g/litre solution of Brilliant Blue. Dark blue regions indicate areas that were dye- stained.

Visual observation during Brilliant Blue irrigation confirmed that a significant proportion of the dye solution was flowing towards the external surface (Figure 8), through channel(s) connecting the irrigated area with the external surface below the top of the specimen. This situation needs more analysis. The external –exposed surface was not recovered with plaster, and in a layered material it is inevitable that any vertical boundary will represent a preferential flow path that would not exist in reality. Additionally, although significant steps were taken to minimise structural distortion of the specimen and any inclination, those efforts were not sufficient to entirely preserve the original structure, and some layer bending (concave downwards), was evident that could have affect the waste body and preferential flow.

Figure 7 illustrates that the flow distribution was reasonably steady over the whole 120 minutes and not affected by dye injection at 59 minutes. This suggests that the BB solution moved through similar flow paths to the water, and thus acted as a representative tracer to visualise water movement. The test was stopped after 2 hours when the obstruction of some of the needles was detected, which could have been caused by undissolved solid particles coming either from the solid dye or from solution drying over small localised areas. This could in the future, be prevented by filtering the mixture and adding a small amount of a retardant solvent.

Results after paint drainage also indicated preferential flow. Inspection of the external surface suggested preferential flow with a pattern that, according to the classification inferred by Weiler and Flühler, 2004 , corresponds to flow occurring in a heterogeneous matrix with fingering present. This result is, however, not conclusive as other biasing factors, e.g. slight inclination towards the 180-240^{o} region, not strictly controlled during the test, could have caused preferential flow.

The paint used showed poorer infiltration capacity than the Brilliant Blue. This might have been caused by some of its properties. The suspension has higher solids content than water and dye soluble systems and likely to have higher viscosity, which will result in an increase of the fluid flow resistance. The mixture also has a faster drying rate compared to other, more conventional water based systems. Estimation of the amount of dye necessary to guarantee significant infiltration should account for losses in the permeation capacity resulting from faster drying. Nevertheless, the paint system offers advantages over BB for example when dry; it becomes insoluble making it then possible to examine different flow conditions in the same sample, using other dyes.

CONCLUSIONS

Coloured based tracers (dye and paint) have been shown to be a useful tool for the visual identification of flow paths in waste. Contrast between colours of the waste matrix and the paint and dye was sufficient to achieve visual differentiation between stained and unstained areas. Brilliant Blue was found to be a reasonably good method of visualising water flow paths. Latex emulsion and Brilliant Blue dye methods can be further improved to overcome some of the operational difficulties, i.e. insufficient infiltration and injection needle obstruction, experienced during this study.

The use of thin sectioning, image processing and sectored fluid collection were of substantial benefit during this research, offering important information for better understanding flow spatial distribution and waste structure.

Results obtained during this study suggest that preferential flow is likely during fluid flow through a landfill waste. This could generate operational difficulties during the application of remediation strategies resulting from the poor access of fluids to some of the areas in the landfill and consequent spatial variation in contaminants flushing. These results, suggest the need for further research to better understand the influence of factors such as waste composition, pre-treatment, placement method and waste age on the nature of the structure developed. Better understanding of the structure of landfilled waste would help to improve the effectiveness of the design and application of different post-closure remediation technologies in landfills aimed at more sustainable landfill management.

ACKNOWLEDGEMENTS

The work described in this paper was carried out as part of EPSRC research grant EP/E041965: Science and strategies for the long-term management and remediation of landfills.

REFERENCES

Allaire, S. E., Roulier, S. & Cessna, A. J. (2009) Quantifying preferential flow in soils: A review of different techniques. *Journal of Hydrology,* **378,** 179-204.

Andreini, M. S. & Steenhuis, T. S. (1990) Preferential paths of flow under conventional and conservation tillage. *Geoderma,* **46,** 88-102.

Ashby, M. F. & Jones, D. R. H. (1986) *Engineering materials 2: An introduction to microstructures, processing and design,* Oxford, England, Pergamon Press.

Bendz, D. & Singh, V. P. (1999) Solute transport under steady and transient conditions in biodegraded municipal solid waste. *Water Resources Research,* **35,** 2333-2345.

Beven, K. & Germann, P. (1982) Macropores and water flow in soils. *Water Resources Research,* **18,** 1311-1325.

Clayton, C. R. I., Simons, N. E. & Matthews, M. C. (1982) *Site investigation,* London, Granada Publishing.

Collins, R. E. (1961) *Flow of fluids through porous materials,* New York, Reinhold Publishing Corporation.

Dixon, N. & Jones, D. R. V. (2005) Engineering properties of municipal solid waste. *Geotextiles and Geomembranes,* **23,** 205-233.

Dixon, N., Langer, U. & Gotteland, P. (2008) Classification and mechanical behavior relationships for municipal solid waste: Study using synthetic wastes. *Journal of Geotechnical and Geoenvironmental Engineering,* **134,** 79-90.

Dullien, F. A. L. (1992) *Porous media: Fluid transport and pore structure,* San Diego, California.

Flury, M. & Flühler, H. (1995) Tracer characteristics of brilliant blue fcf. *Soil Science Society of America Journal,* **59,** 22-27.

Flury, M., Flühler, H., Jury, W. A. & Leuenberger, J. (1994) Susceptibility of soils to preferential flow of water: A field study. *Water Resources Research,* **30,** 1945-1954.

Garner, M. R. (1953) The preparation of latex casts of soil cavities for the study of tunneling activities of animals.

Germán-Heins, J. & Flury, M. (2000) Sorption of brilliant blue fcf in soils as affected by ph and ionic strength. *Geoderma,* **97,** 87-101.

Hangen, E., Gerke, H. H., Schaaf, W. & Hüttl, R. F. (2004) Flow path visualization in a lignitic mine soil using iodine-starch staining. *Geoderma,* **120,** 121-135.

Ivanova, L. K. (2007) Quantification of factors affecting rate and magnitude of secondary settlement of landfills. *University of Southampton (UK.* Thesis for the degree of Doctor of Philosophy.

Ivanova, L. K., Richards, D. J. & Smallman, D. J. (2008) The long-term settlement of landfill waste. *Proceedings of Institution of Civil Engineers: Waste and Resource Management,* **161,** 121-133.

Johnson, C. A., Schaap, M. G. & Abbaspour, K. C. (2001) Model comparison of flow through a municipal solid waste incinerator ash landfill. *Journal of Hydrology,* **243,** 55-72.

Ketelsen, H. & Meyer-Windel, S. (1999) Adsorption of brilliant blue fcf by soils. *Geoderma,* **90,** 131-145.

Kölsch, F. (1995) Material values for some mechanical properties of domestic waste. IN Christensen, T. H., Cossu, R. & Stegmann, R. (Eds.) *Proceedings Sardinia 1995, Fifth International Waste Management and Landfill Symposium.* S. Margherita di Pula, Cagliari, Italy, CISA, Environmental Sanitary Engineering Centre, Ital.

Korfiatis, G. P., Demetracopoulos, A. C., Bourodimos, E. L. & Nawy, E. G. (1984) Moisture transport in a solid waste column. *Journal of Environmental Engineering,* **110,** 780-796.

Lipsius, K. & Mooney, S. J. (2006) Using image analysis of tracer staining to examine the infiltration patterns in a water repellent contaminated sandy soil. *Geoderma,* **136,** 865-875.

Mooney, S. J. & Morris, C. (2008) A morphological approach to understanding preferential flow using image analysis with dye tracers and x-ray computed tomography. *CATENA,* **73,** 204-211.

Mooney, S. J., Morris, C. & Berry, P., M. (2006) Visualization and quantification of the effects of cereal root lodging on the three-dimensional soil macrostructure using x-ray computed tomography. *Soil Science,* **171,** 706-718.

Morris, C. & Mooney, S. J. (2004) A high-resolution system for the quantification of preferential flow in undisturbed soil using observations of tracers. *Geoderma,* **118,** 133-143.

Munyankusi, E., Gupta, S. C., Moncrief, J. F. & Berry, E. C. (1994) Earthworm macropores and preferential transport in a long-term manure applied typic hapludalf. *Journal of Environmental Quality,* **23,** 773-784.

Parker, L. J., White, J. K. & Powrie, W. (1999) The measurement of the geotechnical and hydro-geological properties of degrading solid waste *Sardinia 2009, Seventh International Waste Management and Landfill Symposium.* S. Margherita di Pula, Cagliari, Italy; 4-8 October 1999.

Powrie, W. & Beaven, R. P. (1999) Hydraulic properties of household waste and implications for landfills. *Proc Instn Civil Engineers Geotechnical Engineering.*

Ravindra, P. V., Rao, D. P. & Rao, M. S. (1997) Liquid flow texture in trickle-bed reactors: An experimental study. *Industrial & Engineering Chemistry Research,* **36,** 5133-5145.

Shipitalo, M. J., Nuutinen, V. & Butt, K. R. (2004) Interaction of earthworm burrows and cracks in a clayey, subsurface-drained, soil. *Applied Soil Ecology,* **26,** 209-217.

Van Ommen, H. C., Dekker, L. W., Dijksma, R., Hulshof, J. & Van der Molen, W. H. (1988) A new technique for evaluating the presence of preferential flow paths in nonstructured soils. *Soil Science Society of America Journal,* **52,** 1192-1993.

Velkushanova, K., Caicedo, D., Richards, D. J. & Powrie, W. (2009) A detailed characterisation of an mbt waste. *Proceedings Sardinia 2009, Twelve International Waste Management and Landfill Symposium.* S. Margherita di Pula, Cagliari, Italy.

Weiler, M. & Flühler, H. (2004) Inferring flow types from dye patterns in macroporous soils. *Geoderma,* **120,** 137-153.

Xie, M., Aldenkortt, D., Wagner, J.-F. & Rettenberger, G. (2006) Effect of plastic fragments on hydraulic characteristics of pretreated municipal solid waste. *Can. Geotech. J.,* **43,** 1333–1343

Zeiss, C. & Major, W. (1992) Moisture flow through municipal solid waste: Patterns and characteristics. *Journal of Environmental Systems,* **22**.

From Sanitary to Sustainable Landfilling
- why, how, and when?
1st International Conference on Final Sinks
23rd – 25th September 2010, Vienna

Exploring the use of Micro-focus Computed Tomography for a better conceptual understanding of flow and structure in landfilled waste in the context of post-closure management for landfills

Caicedo Concha. D.M. (1), Watson, G.V.R. (2), Richards, D.J. (3) and Powrie, W. (4)

(1) University of Southampton, UK (dmc1x07@soton.ac.uk), (2) University of Southampton, UK (g.watson@soton.ac.uk), (3) University of Southampton, UK (djr@soton.ac.uk), (4) University of Southampton, UK (wp@soton.ac.uk)

Abstract

Alternative landfill operation strategies are required to reduce the time for which a landfill poses a pollution risk. The application of those alternatives, e.g. aeration and flushing, requires recirculation of fluids, consequently their implementation requires better understanding of fluid flow and transport processes in landfills. Research in porous media has revealed that flow and transport processes are strongly controlled by the physical structure, in particular the pore size, geometry and interconnectivity and particle size and shape. It is generally accepted that landfilled municipal solid waste (MSW) develops a heterogeneous and anisotropic structure during placement, degradation and settlement, however our detailed understanding of the structure that develops once MSW is placed into landfills, and how it influences fluid flow is very limited. This paper discusses the use of Micro-Computed Tomography (μCT) for the non invasive study of waste structure. Results are presented for waste analogues which were successfully analysed using threshold segmentation techniques to detect millimetre sized structural features and quantify the volumetric content of high density materials. Improvements required (e.g. image quality, higher resolution, segmentation techniques) to extend μCT to analyse the structure of landfilled waste samples and characterise pore architecture are also discussed.

Keywords: please given 4 – 6 keywords
Waste structure, waste characterisation, computed tomography, non invasive methods, pore characterisation

1 Introduction

Landfill is generally considered the least desirable option for final disposal of solid waste. Nevertheless, in many countries, landfilling remains the final disposal route for solid wastes. Recalcitrant contaminants contained in landfill sites are likely to persist for centuries rather than decades and liner and leachate collection systems are likely to fail before this time (Hall et al., 2007). Thus the risk of pollution posed by active and closed landfill sites extends well beyond the operational period for the site (Hudgins & Harper, 1999).

The search for alternative landfill operation and management strategies has triggered the development of operation of the landfill as a bioreactor, aiming to enhance biodegradation, which has many advantages. These include improved site utilization (through accelerated settlement), leachate management, physicochemical stabilization and removal of contaminants. The application of these alternatives requires the recirculation of liquids and so their implementation requires better understanding of fluid flow and transport processes in landfills.

Research in porous media; including soils, packed beds and foams, has revealed that flow and transport processes are strongly controlled by the physical structure, in particular the pore size, geometry and interconnectivity and the particle size and shape (Collins, 1961; Beven & Germann, 1982; Dullien, 1992). Landfilled municipal solid waste (MSW) is a porous medium comprising a mixture of highly diverse materials (e.g. plastics, textiles, glass and organic waste, etc). It is recognized that like geological materials and as a result of the deposition in progressive layers, compaction and the heterogeneity, MSW develops a strong structure (Dixon & Jones, 2005). Plastics and textiles, due to their shape, tensile strength and orientation, can enhance the strength (e.g. Kölsch, 1995 and Dixon et al., 2008), and influence flow behaviour by diverting fluid flow (Xie et al., 2006 and Velkushanova et al., 2009). However our detailed understanding of the structure that develops once MSW is placed into landfills, and how that structure influences fluid flow is very limited.

Research into the structure of porous media has been traditionally approached using methods such as field observations (Beven & Germann, 1982, and Shipitalo et al., 2004); laboratory analysis of cores by thin sectioning, resin impregnation and imaging (Mooney & Morris, 2008, Flury et al., 1994); indirect analysis using tracer injection breakthrough curves from fluid flow experiments (Mooney & Morris, 2008) and observation of flow path patterns revealed by dye staining (Flury et al., 1994, Morris & Mooney, 2004).

Non-invasive techniques, particularly X-ray Computed Tomography (CT) have been successfully used in porous media research since the early 1990s, and have revealed highly detailed information on both the structure and the pore space architecture, improving our understanding of fluid flow (e.g., Heijs et al., 1995 and Amos et al., 1996) and other porous medium interaction processes (e.g. Sato & Suzuki, 2003, Kettridge & Binley, 2008).

This paper discusses the potential of X-ray Computed Tomography (CT) for studying landfilled waste, and illustrates this with some results obtained from waste analogue specimens. This paper presents a theoretical background to CT. Example applications are discussed to show that non-invasive methods can be applied for the study of landfilled waste. The imaging procedure is explained and the potential for improvement is discussed. Preliminary results of some of the structural features revealed in the analysis of waste analogues are presented, compared with bulk properties and discussed in the context of their potential impact on the long term management of landfill sites.

2 Non-invasive techniques background

Non-invasive techniques are based on the principle that properties of the internal structure of a specimen can be inferred from the detection of a signal, passed through the specimen. They were originally developed for diagnostic medicine and have enabled the non-invasive study of the human body. In recent decades increased availability has led to the use of these techniques for research purposes in areas such as archaeology, palaeontology, petro-physics, geology and materials engineering.

The acquisition of images using non-invasive techniques is faster and causes far less disturbance than progressive thin sectioning. Physical properties of the signal used vary between non-invasive technologies and include X-rays in Computed Tomography (CT), Magnetic fields in Magnetic Resonance Imaging (MRI) and gamma rays in Positron Emission Tomography (PET). Since the response of a particular material is dependent on the signal type, selection of the appropriate technique requires careful consideration of the type of material being investigated. As discussed by Watson *et al.*, 2006, landfill waste is ideally suited to examination using CT. During the research discussed in this paper, locally available microfocus-CT (μCT) equipment was used.

2.1 Principles of X-ray Computed Tomography (CT)

X-ray Computed Tomography (CT) is a radiographic method for digitally cutting a specimen to reveal its interior details. The principles that control CT are similar to those of conventional radiography where differences in X-ray absorption are shown by grey scale differences in medical radiographs. X-rays are high energy electromagnetic waves produced inside X-ray vacuum systems where the cathode of a high voltage power source emits electrons that are collected in the anode. This process establishes a flow of electrical current known as *beam*, which has a wavelength of 0.01-10 nm.

CT scanners work by emitting a cone of X-rays, which pass through the object of interest to one or more detectors. In μCT, the object is rotated in relation to the X-ray source to create a series of two dimensional images which can then be computationally assembled into a three dimensional object.

A detector measures X-ray intensity before the beam enters the object and after it passes through it, and converts them to grey values using the Beer-Lambert law (Equation 1). I_o and $I(x)$ are the initial and transmitted beam intensities respectively, μ the linear x-ray attenuation coefficient for the material being scanned, and x the length of the X-ray path through the material. If the scanned medium is inhomogeneous, the intensity is expressed in terms of Cartesian coordinates as shown in Equation 2.

$$I_{(x)} = I_O e^{(-\mu x)} \qquad \textit{Equation 1}$$

$$I_{(x,y)} = I_{(0,0)} e^{\left(-\int_{(0,0)}^{(x,y)} \mu(x,y)\,dl\right)} \qquad \textit{Equation 2}$$

In Equation 2, μ is the unknown variable constrained by many equations for each point along each X-ray path. Image reconstruction consists of finding values for μ that provide solutions to these equations (Brooks et al., 1981, Denison et al., 1997). The most commonly used algorithm is known as "filtered back projection" was invented by Allan Cormack who shared the 1979 Nobel Prize for medicine and physiology with Godfrey Hounsfield inventor of the CT scanner and relates the measured projection data to the two-dimensional Fourier transform of the object cross section. Once reconstructed, objects can be visualized in 2D and 3D and features qualitatively or quantitatively assessed using various image processing software available both free and commercially (Kak & Slaney, 1988).

Differentiation of features within a specimen is possible because at each point, μ depends directly on the material's electron or bulk density, effective atomic number and on the energy of the incoming x-ray beam

(Brooks et al., 1981 and Denison et al., 1997). Linear attenuation coefficients may change between equipment. Hounsfield units and CT numbers, which use the linear attenuation of reference materials such air and water for calibration, are preferred when diagnostic and quantitative studies are required (Brooks et al., 1981 and Heijs et al., 1995).

Medical CT can successfully image metre sized objects with millimetre scale resolutions. Demand for higher resolution tomography in denser and smaller objects eventually led to the development of μCT which scans millimetre sized objects at 1-10 μm resolution. The physical principles that control these CT and μCT are the same. With decreasing size, radiography becomes more difficult as the specimen must absorb a sufficient portion of the incident beam to produce a measurable signal, which in a small specimen demands high attenuation per unit length, a condition that is only satisfied at low X-ray energies which are insufficient to penetrate dense objects. Precisely focused beams are also required to minimize blurring fine details (Dunsmuir et al., 1991). These difficulties were successfully addressed by D'Amico *et al.*, (1992) with the development of a microfocus X-ray source which forms the basis of μCT. In μCT, X-rays are first highly collimated to achieve beam focus on the anode of only few micrometers diameter.

2.2 Applications of CT in porous media research

Following successful application in the medical field, CT rapidly gained popularity among those studying the structure of porous media in fields such as hydrogeology and geosciences. A vast number of references are available and comprehensive review papers within these fields are given by e.g. Ketcham & Carlson, (2001), Kaestner *et al.*, (2008), Allaire *et al.*, (2009) and Werth *et al.*, (2010).

Petroleum engineers pioneered the use of CT within geological sciences to characterise density, porosity, saturation and complex mineralogies in oil-reservoir rocks, imaging fluid flow patterns and studying rock mechanics (Wellington & Vinegar, 1987 and Withjack, 1988).

Scientists from diverse porous media research areas then found medical CT a feasible method for studying, with a high level of detail, density and water distributions (e.g. Heijs et al., 1995 and Amos et al., 1996), characterize structures (Kettridge & Binley, 2008) and soil interaction processes (e.g. Mooney et al., 2006, Kettridge & Binley, 2008).

CT has seen limited use in the study of waste structure and fluid flow phenomena, with Watson *et al.*, 2006 and Watson et al., 2007 being the only references identified at the time of writing. Watson *et al.*, (2006 & 2007) used medical CT to investigate the change in structure of the organic fraction of MSW as it degraded anaerobically over a period of two years in 35 l reactors. No attempts to use higher resolution computed tomography in waste have been reported.

3 Material and Methods

3.1 Materials

As part of an investigation into the effects of two dimensional components on shear strength and hydraulic conductivity, two synthetic specimens were prepared and scanned. Each specimen consisted of two dimensional plastic materials in a relatively homogeneous matrix. This approach was preferred over scanning samples of real landfilled waste. It was considered that the properties being investigated would be well represented but the material would be less complex than real wastes, minimizing uncertainties caused by uncontrolled variables, e.g. continuing degradation; other components acting as reinforcement or flow diverters; and reduce complexities in the imaging process.

The first specimen was a modified mechanically biologically treated waste residue (MBT). Details of the MBT residue used can be found in Velkushanova *et al.*, (2009) and Fernando *et al.*, (2009). The sample was prepared for shear strength testing in a 60mm direct shear apparatus by sieving the MBT at the as-received moisture content (26 % by dry mass), retaining the fractions from 0 to 2.8 mm (to create a matrix) and then adding 2 % by dry mass of 20 × 10 mm HDPE (25 pieces or 2.4 % by volume). The material was placed in the shear apparatus and consolidated under a normal stress of 100 kPa for 24 hours but not subjected to shear stresses. The final specimen was a dense cuboid (6 × 6 × 3 cm; 108 cm^3), with a mass of 85.46 g and a bulk density of 0.7913 Mgm^{-3}. The sample was wrapped with aluminium foil before the scan which was intended to study the distribution and orientation of the HDPE pieces following consolidation.

The second specimen, created in a modified 75mm permeameter, was prepared to investigate the effect that two dimensional components have on hydraulic conductivity. In this case the matrix material selected was Leighton Buzzard Sand fraction b (grain size 600 μm to 1.18 mm) and polystyrene discs (5 mm diameter x 0.6 mm thick) which represented the two dimensional components. Sand and polystyrene discs were mixed in a dry mass ratio of 6.35/1 (86.4% sand and 13.6% discs by dry mass), mixed by hand and deposited in a permeameter cell, using a pluviation method as described by Cresswell et al., 1999. Pluviation uses a cylindrical tube (75mm diameter) filled with offset sequential interwoven wire diffuser meshes to create an even sand rain effect which produces a high density, randomly distributed specimen. Once placed the sample level was measured to calculate its total volume 353.44 cm^3, bulk density 1.7618 Mgm^{-3} and volumetric percentages 54.4% sand, 21.6% discs and 24% pores. The permeameter cell was 75 mm in diameter, 238 mm tall and designed for testing hydraulic conductivity in granular soils. The permeameter was modified to remove the metal components as these cause scattering of X-rays which lead to artefacts in the scan data, reducing the image quality. In this case, the scan aimed to identify the distribution and orientation of the flow diverting elements and evaluate the potential to characterize in two and three dimensions, the pore network structure of the specimen

3.2 Methods

The equipment used was an X-Tek Benchtop 160Xi scanner (X-Tek Systems Ltd, Tring, Hertfordshire, UK) equipped with a 1248 × 1248 pixels Hamamatsu C7943 X-ray flat panel sensor (Hamamatsu Photonics, Welwyn Garden City, Hertfordshire, UK), with an ultimate resolution limit of 10 μm. Given the size of the MBT and permeameter specimens (60 mm and 75mm), the resolutions expected in each case are 0.05 mm and 0.06 mm respectively. Preliminary trial runs were required to find the optimal combination of settings to obtain high signal to noise ratio images and to minimise artefacts.

The MBT specimen was scanned at a beam voltage and current of 97 kV and 104 μA respectively using a tungsten target; 1 mm copper filter; a magnification factor of 1.35 and digital gain of 1. Scanning time was about 2 hours using the fast scan routine, based on 1910 radiographic projections and an individual exposure time of ~2 s. The permeameter sample was scanned at a beam voltage and current of 112 kV and 85 μA respectively with no filter, the rest of parameters remained as in the MBT scan.

Reconstruction was carried out using a filter back projection algorithm and volume images analysed using VG-Studio Max V2.0 software developed by Volume Graphics GmbH, Heidelberg, Germany. The stack of two dimensional images was processed using Image J - a free, Java-based image processing program developed at the National Institute of Health.

4 Results and Discussion

4.1 MBT specimen

The reconstruction of the MBT specimen produced 483 thin, horizontal cuts with a separation of approximately 0.06mm and volume element (voxel) size 0.0001042 mm^3. Visual inspection of the 2D views showed six reinforcing particles – the dark grey rectangular features in Figure 1, horizontally aligned located at 1.47, 3.69, 8.61, 10.65, 14.79 and 15.27 mm (measured from bottom to top) and 4 more pieces horizontally placed on the specimen external top layer. This corresponds to 40% of the total number of pieces added to the specimen (25 in total). The remaining 15 pieces would have been placed vertically or with some angle of inclination, making their identification more difficult as only the horizontal slices were analysed. White features in the images correspond to high density material, which are likely to be small glass and metal pieces contained in the matrix.

Figure 2 shows three dimensional representations of the complete specimen (a) and the segmented high and medium density materials (b and c). Creation of these 3D representations for the segmented materials was achieved using the grey value distribution generated after the reconstruction which converts linear attenuation into grey values (range 0-255). A manual segmentation process was performed where an initial grey value was selected as a threshold. Only those materials with grey values over the threshold, or within a specified range, are rendered. The appearance of the resulting 3D representation is visually judged and the threshold iteratively adjusted until a satisfactory representation achieved. In Figure 2 high density materials are rendered as voxels with grey values over 194 whilst medium density by voxels between 156 and 194.

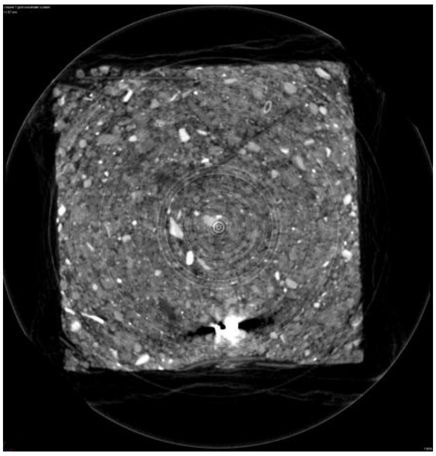	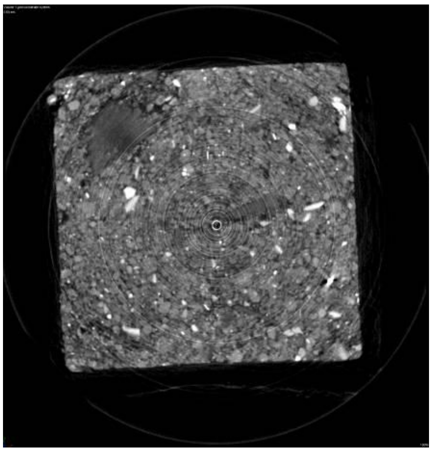	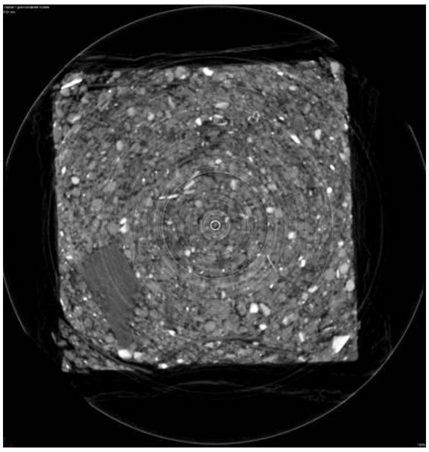
a. Slice at 12.05 mm with no evidence of horizontal reinforcing particles	b. Horizontal reinforcing element at 3.69 mm	c. Horizontal reinforcing element at 8.61 mm

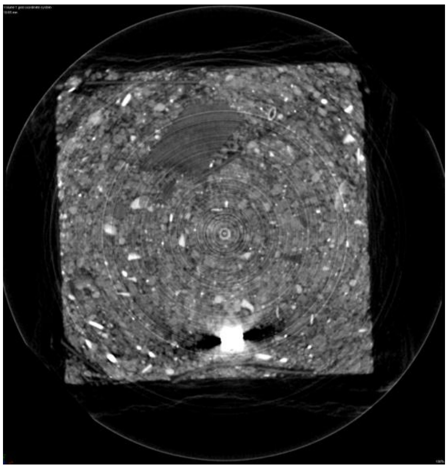	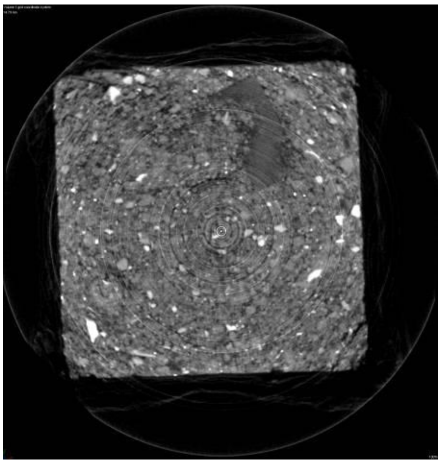	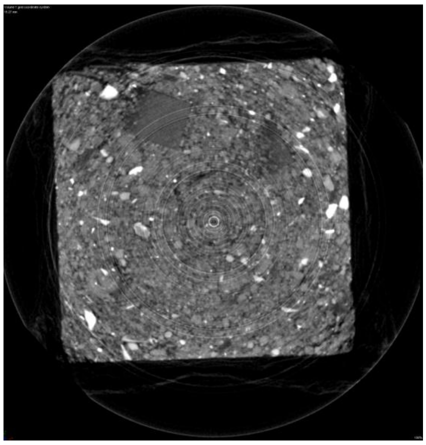
d. Horizontal reinforcing element at 10.65 mm	e. Horizontal reinforcing element at 14.79 mm	f. Horizontal reinforcing element at 15.27 mm

Figure 1 Selected views in the MBT specimen where reinforcing plastic pieces were identified. (a) Long linear features indicate presence of particles with some angle of inclination; (b,c,d,e,f) rectangular features (dark grey) are the reinforcing pieces. White features are high density materials (might be glass and metals).

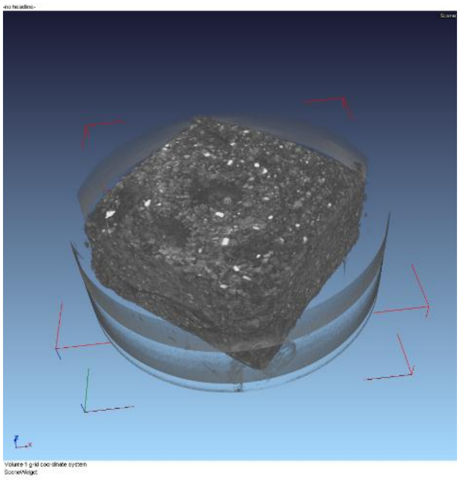	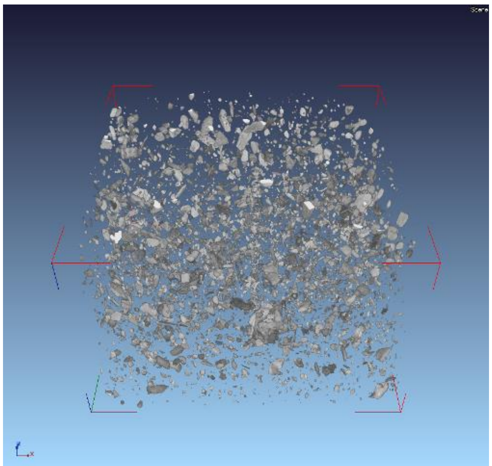	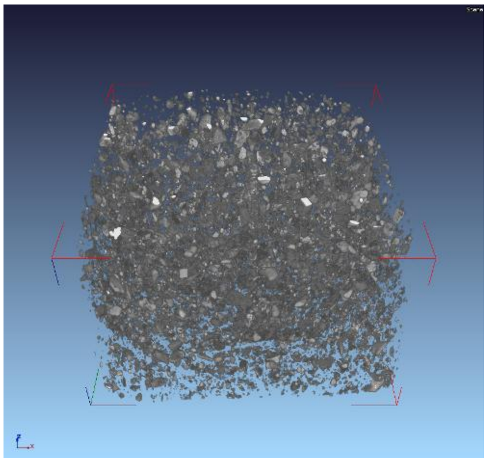
a. Complete specimen. Dark features at the top correspond to plastic pieces	b. High density materials (grey value over 194), could be glass and metals	c. Medium density materials (grey value 156-194), could be materials such as bones, wood, etc

Figure 2 Three dimensional reconstructions of the MBT specimen in VGStudio Max2 using Volume Render (Scatter HQ) algorithm, and fast scan routine

Quantitative analysis of the equivalent volume for these materials was carried out using the volume analyser tool, which displays the grey value distribution with the corresponding number of voxels. The voxel size (0.0001042 mm^3) is used as a conversion factor to calculate the volume of the specimen for each grey value.
Figure 3 shows grey value distribution resulting from a fast scanning against a second run, for comparison purposes, carried out using similar *X*-ray settings and reducing the sample rotation speed resulting in a total scanning time of 10 hours. Differences between the two scans might be the result of not having performed a

Hounsfield calibration, changes in the X-ray spectrum and flux not registered during the operation, and divergences in the region of interest selected for the reconstruction. Using Figure 3 the volumetric content of high density materials was calculated as 1.98 and 1.64 % in the slow and fast scan respectively. Segmentation of other features, such as plastic pieces, soil-like materials and pores was not possible using grey value threshold (as their grey values do not differ significantly). More complex algorithms for segmentation will be explored at later stages to achieve this.

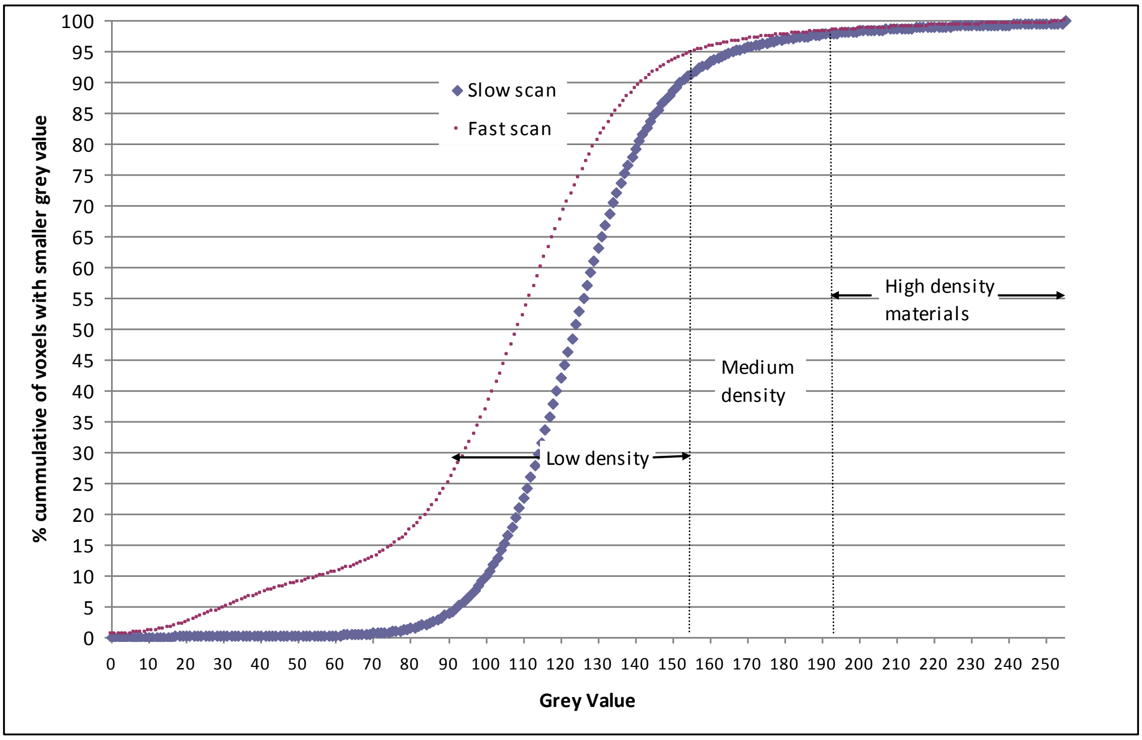

Figure 3 Grey value distribution in the MBT specimen scanned with slow and fast acquisition routines. Y axis represents the percentage of voxels as the total sample volume with a grey value less than X.

4.2 Permeameter sample

A subsection of 20 mm depth, corresponding to ¼ of the total volume, located between 80 and 100 mm elevation in the permeameter (bottom to top, 238mm total height) was selected for reconstruction. This subsection was selected since it is located between two points where the hydraulic conductivity will be measured, which will provide fluid flow data to complement structural information provided by the µCT analysis. Selection of a subsection is a standard practice in image reconstruction as it reduces the computational memory requirements and produces more reliable object representations. The reconstruction generated 343 slices separated by 0.058 mm with a voxel size of 0.00010086 mm^3. Inspection of the views, Figure 4, allowed visual identification of the horizontally orientated plastic pieces. Figure 5 shows the grey value distribution for the reconstructed subsection. Segmentation of sand grains was achieved using 144 as grey value threshold. Materials rendered in the range between 97 and 143 correspond to plastic discs and pores, those under 97 to background (permeameter walls). Quantitative analysis was carried out using the volume analyser tool and results compared against the actual sample composition. A slight decreasing in the threshold, from 143 to 137, did not affect significantly the rendering quality and produced percentages in close agreement with the actual composition. Differentiation between plastics and pores was not successful using grey value threshold. Improvements in image quality (e.g. minimisation of rings artefacts) and use of alternative algorithms will be explored to achieve this.

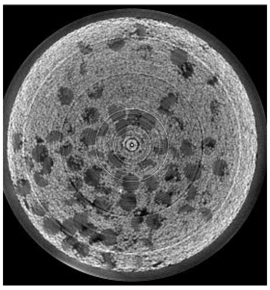	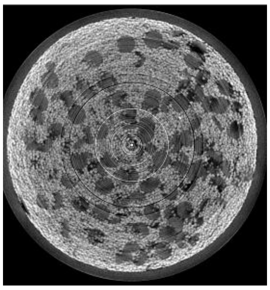		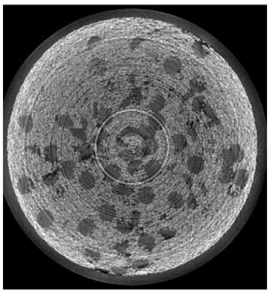
a. Horizontal view at 0 mm	b. Horizontal view at 2.9 mm	c. Horizontal view at 5.8 mm	d. Horizontal view at 8.7 mm
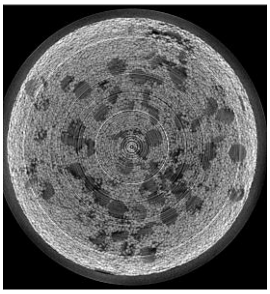	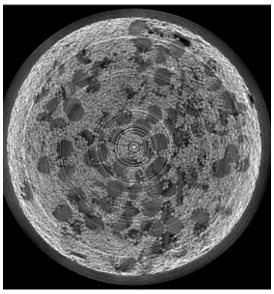		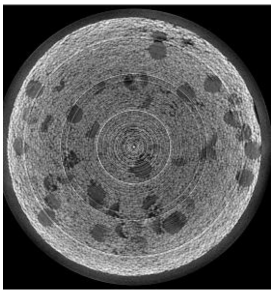
e. Horizontal view at 11.7 mm	f. Horizontal view at 14.6 mm	g. Horizontal view at 17.5 mm	h. Horizontal view at 20 mm

Figure 4 Selected slices views in the Permeameter specimen. Dark grey features are the 5mm plastic discs incorporated to the sample

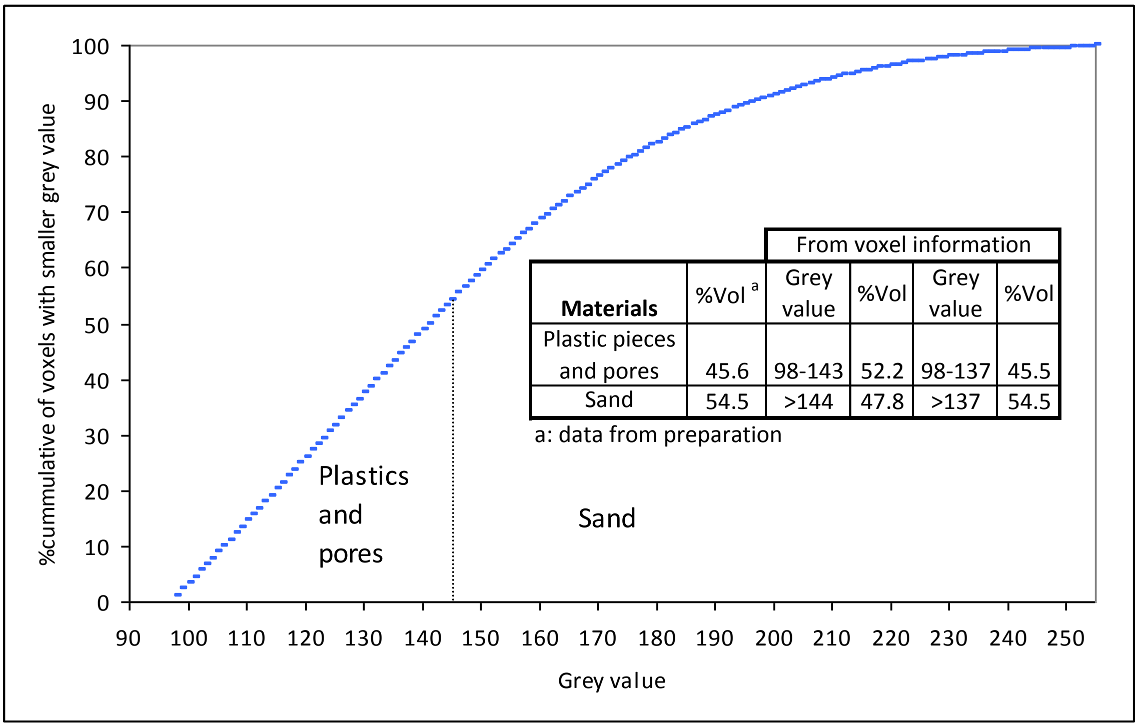

Materials	%Vol [a]	Grey value	%Vol	Grey value	%Vol
Plastic pieces and pores	45.6	98-143	52.2	98-137	45.5
Sand	54.5	>144	47.8	>137	54.5

Figure 5 Grey value distribution for the permeameter sample. Y axis represents the percentage of voxels as the total sample volume with a grey value less than X

5 Conclusions

The potential to use Micro-Computed Tomography was illustrated with examples where it was successfully used in the inspection of structural features (reinforcing and flow diverting elements) in waste analogue specimens. The method was also effective in quantifying the content of high density materials, e.g. glass and sand. The characterisation of pore structure in landfilled waste is viable as several algorithms are available to measure parameters such as pore size and interconnectivity, however this requires better image quality, higher resolution (decreasing sample size) and more complex segmentation procedures that those explored in the examples discussed in this paper. These preliminary results suggest that μCT can be successfully applied to characterise the structure of landfilled waste, where a multi-scale imaging approach could be adopted to reveal high level of details which would increase our understanding of fluid flow and mechanical processes in landfill.

6 References

Allaire, S. E., Roulier, S. & Cessna, A. J. (2009). Quantifying preferential flow in soils: A review of different techniques. *Journal of Hydrology* **378**(1-2): p.179-204.

Amos, C. L., Sutherland, T. F., Radzijewski, B. & Doucette, M. (1996). A rapid technique to determine bulk density of fine-grained sediments by X-ray computed tomography. *Journal of Sedimentary Research* **66**(5): p.1023-1024.

Beven, K. & Germann, P. (1982). Macropores and Water Flow in Soils. *Water Resources Research* **18**(5): p.1311-1325.

Brooks, R. A., Mitchell, L. G., O'Connor, C. M. & DiChiro, G. (1981). On the relationship between computed tomography numbers and specific gravity. *Physics in Medicine and Biology* **26**(1): p.141.

Collins, R. E. (1961). *Flow of Fluids through porous materials*. New York, Reinhold Publishing Corporation.

Cresswell, A., Barton, M. E. & Brown, R. (1999). Determining the maximum density of sands by pluviation. *Geotechnical Testing Journal* **22**(4): p.324-328.

D'Amico, K. L., Dunsmuir, J. H., Ferguson, S. R., Flannery, B. P. & Deckman, H. W. (1992). The Exxon microtomography beam line at the National Synchrotron Light Source (invited). *Review of Scientific Instruments* **63**(1): p.574-577.

Denison, C., Carlson, W. D. & Ketcham, R. A. (1997). Three-dimensional quantitative textural analysis of metamorphic rocks using high-resolution computed X-ray tomography: Part I. Methods and techniques *Journal of Metamorphic Geology* **15**(1): p.29-44.

Dixon, N. & Jones, D. R. V. (2005). Engineering properties of municipal solid waste. *Geotextiles and Geomembranes* **23**(3): p.205-233.

Dixon, N., Langer, U. & Gotteland, P. (2008). Classification and mechanical behavior relationships for municipal solid waste: Study using synthetic wastes. *Journal of Geotechnical and Geoenvironmental Engineering* **134**(1): p.79-90.

Dullien, F. A. L. (1992). *Porous Media: Fluid Transport and Pore Structure*. San Diego, California.

Dunsmuir, J. H., Ferguson, S. R., D'Amico, K. L. & Stokes, J. P. (1991). X-Ray Microtomography : A New Tool for the Characterization of Porous Media *SPE Annual Technical Conference and Exhibition*, Dallas, Texas, Society of Petroleum Engineers, Inc, p.423.

Fernando, S., Powrie, W., Watson, G. & Richards, D. J. (2009). The Impact of the reinforcing content on the shear strength of mechanically biologically treated waste. *Third International Workshop " Hydro-Physico-Mechanics of Landfills"*, Braunschweig, Germany.

Flury, M., Flühler, H., Jury, W. A. & Leuenberger, J. (1994). Susceptibility of soils to preferential flow of water: A field study. *Water Resources Research* **30**(7): p.1945-1954.

Hall, D. H., Drury, D., Gronow, J. R., Pollard, S. J. T. & Smith, R. (2007). Estimating Pollutant Removal Requirements for Landfills in the UK: III. Policy Analysis and Operational Implications. *Environmental Technology* **28**: p.25-32.

Heijs, A. W. J., de Lange, J., Schoute, J. F. T. & Bouma, J. (1995). Computed tomography as a tool for non-destructive analysis of flow patterns in macroporous clay soils. *Geoderma* **64**(3-4): p.183-196.

Hudgins, M. & Harper, S. (1999). Operational characteristics of two aerobic landfill systems. *Proceedings Sardinia 99. Seventh International Waste Management and Landfill Symposium*, S.Margherita di Pula, Cagliari, Italy, p.327-333.

Kaestner, A., Lehmann, E. & Stampanoni, M. (2008). Imaging and image processing in porous media research. *Advances in Water Resources* **31**(9): p.1174-1187.

Kak, A. K. & Slaney, M. (1988). *Principles of Computerized Tomographic Imaging*. New York, IEEE Press.

Ketcham, R. A. & Carlson, W. D. (2001). Acquisition, optimization and interpretation of X-ray computed tomographic imagery: applications to the geosciences. *Computers & Geosciences* **27**(4): p.381-400.

Kettridge, N. & Binley, A. (2008). X-ray computed tomography of peat soils: Measuring gas content and peat structure. *Hydrological Processes* **22**(25): p.4827-4837.

Kölsch, F. (1995). Material values for some mechanical properties of domestic waste. In: T. H. Christensen, R. Cossu & R. Stegmann (Eds.) *Proceedings Sardinia 1995, Fifth International Waste Management and Landfill Symposium*, S. Margherita di Pula, Cagliari, Italy, CISA, Environmental Sanitary Engineering Centre, Ital, p.711-729.

Mooney, S. J. & Morris, C. (2008). A morphological approach to understanding preferential flow using image analysis with dye tracers and X-ray Computed Tomography. *CATENA* **73**(2): p.204-211.

Mooney, S. J., Morris, C. & Berry, P., M. (2006). Visualization and quantification of the effects of cereal root lodging on the three-dimensional soil macrostructure using x-ray computed tomography. *Soil Science* **171**(9): p.706-718.

Morris, C. & Mooney, S. J. (2004). A high-resolution system for the quantification of preferential flow in undisturbed soil using observations of tracers. *Geoderma* **118**(1-2): p.133-143.

Sato, H. & Suzuki, S. (2003). Fundamental study on the effect of an orientation of clay particles on diffusion pathway in compacted bentonite. *Applied Clay Science* **23**(1-4): p.51-60.

Shipitalo, M. J., Nuutinen, V. & Butt, K. R. (2004). Interaction of earthworm burrows and cracks in a clayey, subsurface-drained, soil. *Applied Soil Ecology* **26**(3): p.209-217.

Velkushanova, K., Caicedo, D., Richards, D. J. & Powrie, W. (2009). A detailed characterisation of an MBT waste. *Proceedings Sardinia 2009, Twelfth International Waste Management and Landfill Symposium*, S. Margherita di Pula, Cagliari, Italy.

Watson, G. V. R., Powrie, W. & Blades , A. P. (2006). Particle scale classification and identification of the structure of processed municipal solid waste by CT scanning. In: M. a. N. Hyodo (Ed. *International Symposium on Geomechanics and Geotechnics of Particulate Media* Yamaguchi, Japan.

Watson, G. V. R., Powrie, W. & Blades , A. P. (2007). An investigation into the effects of degradation on waste structure. *Proceedings Sardinia 2007, Eleventh International Waste Management and Landfill Symposium*, S. Margherita di Pula, Cagliari, Italy.

Wellington, S. L. & Vinegar, H. J. (1987). X-Ray Computerized Tomography *Journal of Petroleum Technology* **39**(8): p.885-898.

Werth, C. J., Zhang, C., Brusseau, M. L., Oostrom, M. & Baumann, T. (2010). A review of non-invasive imaging methods and applications in contaminant hydrogeology research. *Journal of Contaminant Hydrology* **113**(1-4): p.1-24.

Withjack, E. M. (1988). Computed Tomography for Rock-Property Determination and Fluid-Flow Visualization. *SPE Formation Evaluation* **3**(4): p.696-704.

Xie, M., Aldenkortt, D., Wagner, J.-F. & Rettenberger, G. (2006). Effect of plastic fragments on hydraulic characteristics of pretreated municipal solid waste. *Can. Geotech. J.* **43**(12): p.1333–1343

A DETAILED CHARACTERISATION OF AN MBT WASTE

K. VELKUSHANOVA, D. CAICEDO, D. RICHARDS AND W. POWRIE

School of Civil Engineering and the Environment, University of Southampton, UK

SUMMARY: Mechanical biological treatment (MBT) of wastes is being used increasingly in Europe to comply with the Landfill Directive. This process will have significant implications for the mechanical (strength) and flow behaviour of such wastes when they are landfilled. This paper describes the detailed characterisation of a particular MBT waste from the UK, with respect to particle size, shape and material. It is argued that the treatment process will eliminate certain types of particle (e.g. large or crushable) present in raw municipal solid waste, but that particles likely to act as reinforcing elements or block fluid flow within a general matrix of indeterminate material will remain. This observation is used to propose a simplified characterisation system in which the shape or “dimension” of the particle is used as an indicator of its potential impact on bulk strength and flow properties. Particle compressibility is not accounted for: the impact of this on the bulk behaviour of the waste remains a subject of continuing investigation.

1. INTRODUCTION

The EU Landfill Directive (EC, 1999) requires amongst other things that biodegradable waste is treated to reduce its biodegradability prior to disposal to landfill. A range of processes known generically as Mechanical-Biological Treatment or MBT have become popular throughout Europe to enable compliance with this requirement. MBT normally involves sorting (in which recyclable and combustible materials are removed), particle size reduction (e.g. by shredding) and partial biodegradation, which may achieved using either aerobic or anaerobic processes.

While an MBT process may fulfil the letter of the Landfill Directive, the real benefits are less clear. In many cases, the quality of the outputs is too low for any utilisation or disposal route other than landfill (Juniper, 2005). After landfilling, the MBT residue or output will probably continue to give off methane, but not at a fast enough rate to make it economically worthwhile to capture and use for electricity generation. Thus the widespread adoption of MBT could exacerbate the problem of fugitive emissions of greenhouse gases from landfills, which the EU Landfill Directive was enacted to address. A further point is that the removal of large reinforcing elements from the waste during the mechanical processing stage will alter its mechanical properties, perhaps reducing landfill stability. The effect of processing on the permeability of the waste is also uncertain.

An indication of the changes in the biodegradability, mechanical and flow properties of waste resulting from mechanical biological treatment might be obtained from a detailed consideration of the constituents of the MBT residue, including the particle size and material type.

Proceedings Sardinia 2009, Twelfth International Waste Management and Landfill Symposium
S. Margherita di Pula, Cagliari, Italy; 5 - 9 October 2009
© 2009 by CISA Publisher, Italy

This paper describes in some detail the characterisation process for an MBT waste from the UK, presents the results, proposes a simplified classification for the material and discusses the implications of the characterisation for the mechanical and flow behaviour.

2. CHOICE OF CHARACTERISATION/CLASSIFICATION SYSTEM

Classification systems for waste have been proposed by a number of authors, often focussing on different attributes. Siegel *et al* (1990) proposed a classification system based on material type. Landva and Clark (1990) distinguished between organic (putrescible and non-putrescible) and inorganic (degradable and non-degradable) components. Grisolia *et al* (1995) recognised the importance of particle deformability, while Kölsch (1995) added the concept of the "dimension" of the particle, which could range from zero (small particles) through one and two dimensions (stick- and sheet-like) to three dimensions (rotund and bulky).

These systems are reviewed by Dixon and Langer (2006), who develop a new framework for waste classification focussing particularly on the factors influencing the mechanical properties of the waste (principally strength and stiffness). Although the attributes of particle size, particle shape and material are all considered, the primary distinction made is between reinforcing, compressible and incompressible particles.

Characterisation of an MBT residue should be more straightforward than characterisation of a raw MSW in two main respects. First, mechanical treatment should reduce substantially the range of particle sizes in the waste. Secondly, the elimination of breakable or crushable items ("particles") such as bottles and cans made from incompressible materials such as ceramics and metals should give a better correlation between particle material type, shape and contribution of a particle to the overall mechanical behaviour of the waste.

3. MATERIALS AND METHODS

A sample of approximately 500 kg of MBT residue was recovered from a mechanical-biological treatment facility in southern England. The MBT process is shown schematically in Figure. A representative 25 kg sub-sample was sieved by gentle mechanical shaking for 30 minutes through a stack of sieves into five different size fractions: >20 mm, 20-12 mm, 12-7 mm, 7-5 mm and <5 mm. The moisture content of each fraction was determined by oven-drying at a temperature of 70ºC until a constant mass was achieved. Each fraction was then sorted manually into different components/materials, viz.: flexible plastics, rigid plastics, textiles, glass, ceramics, stones, metals, paper, wood, bones, rubber and miscellaneous.

These categories are similar to those suggested by some authors, e.g. Dixon and Langer (2006) but differ from the groups described by other authors, e.g. Grisolia et al (1995); Kölsch (1995); Landva and Clark (1990). They were selected partly because of the need for categories to be amenable to identification by visual inspection, although the smaller particle size of MBT waste makes this more difficult than for raw MSW. This is evidenced by the 58.1% of particles (by mass) placed into the "miscellaneous" category. Glass (22.8%) was the second most prevalent material. Rigid and flexible plastics together accounted for 10.8% of the sample: those two groups were distinguished because of the expected impact of the material on particle shape and mechanical properties, as discussed below. The 25 kg sample was sieved at the as-received water content. It is accepted that this could lead to some error as a result of the agglomeration of fine particles, but this is of little consequence as it is likely to affect only the relatively sticky particles later classified as "matrix" material. A proportion of the finest material (< 5 mm) which was dry-sieved following oven drying as described above.

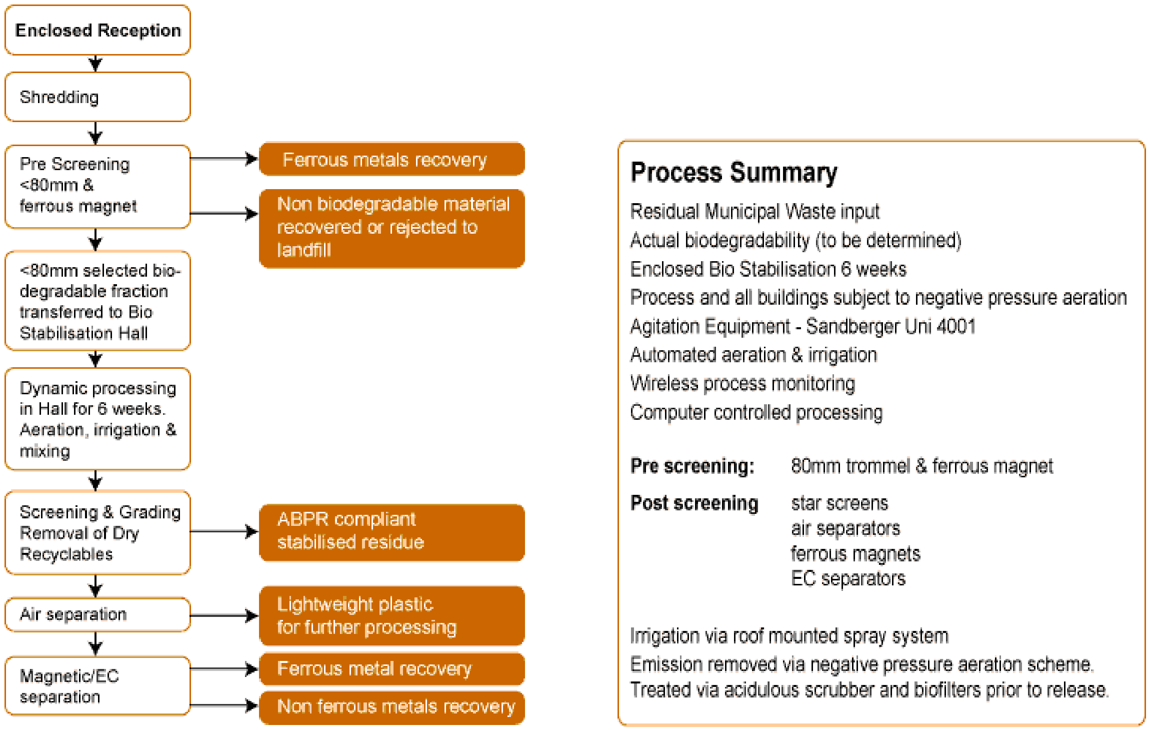

Figure 1. Schematic description of typical MBT process (after New Earth Solutions: http://www.newearthsolutions.co.uk/residual-waste-treatment/process-description/)

4. RESULTS

4.1. Particle size

Figure 2 shows the PSD curve obtained during sorting the MBT waste sample. For comparison, a PSD curve for MSW from the same source as the MBT waste, which had been shredded to a maximum particle size of 80 mm and tested in the Pitsea Compression cell over a period of forty eight months, is also shown, in Figure 3, together with PSD curves for some German MBT wastes reported by Kuhele-Weidemeir (2005), Bauer (2007) and Münnich (2005).

When the Pitsea cell waste PSD curve is adjusted by removing the fraction over 20 mm, it lies just below the PSD for the MBT waste shown in Figure 2.

The maximum particle size for the German MBT waste samples is about 75 mm, compared with 20 mm for the UK MBT waste.

4.2. Moisture Content

The moisture contents of the original (unsieved) sample and the various size fractions obtained by sieving are indicated in Figure 4.

The moisture resides disproportionately in the smallest (<5 mm) fraction. Although the water content of the largest (>20 mm) fraction is also high, this represents just 0.8% of the sample by dry mass and so is insignificant.

Retention of water in the finest fraction is probably explained by the high specific surface area and the absorptive nature of the particle materials (e.g. paper, card and textiles).

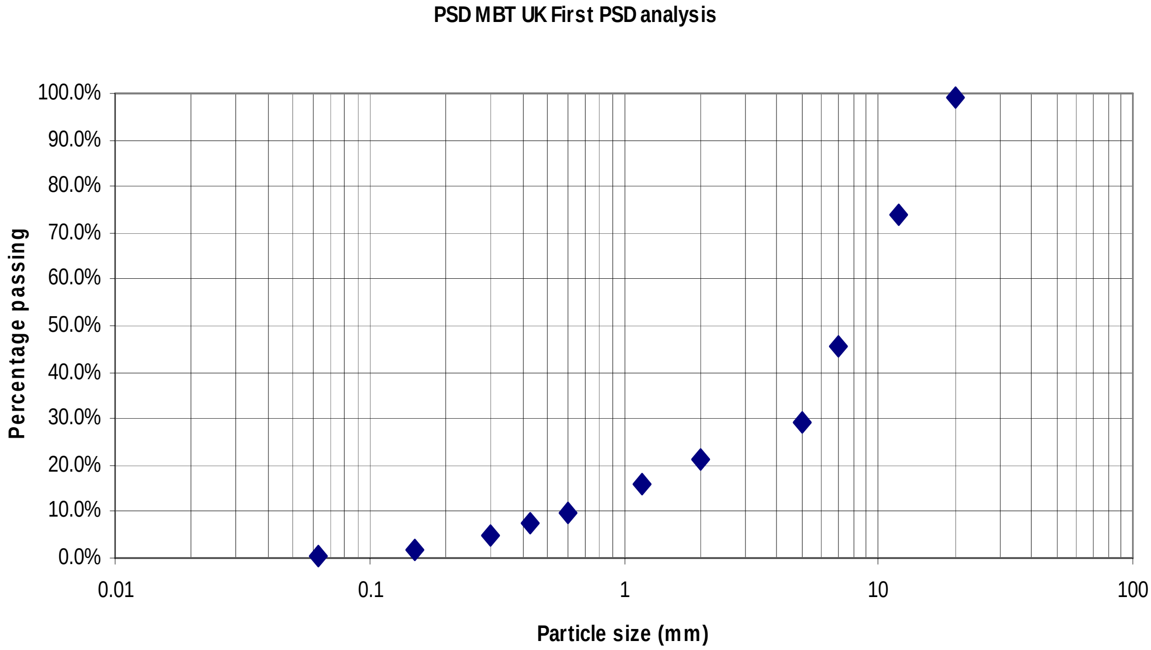

Figure 2. PSD curve obtained by sieving at the as-received water content

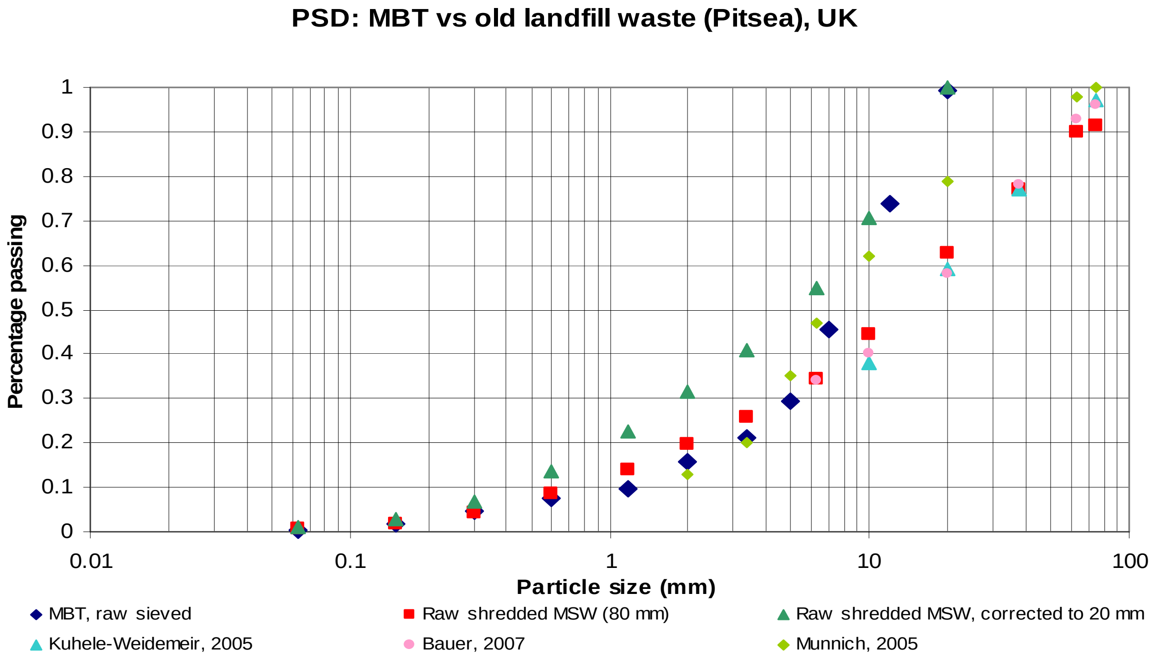

Figure 3. Comparison between PSD curves obtained for MBT, raw MSW shredded to 80 mm, and German MBT waste

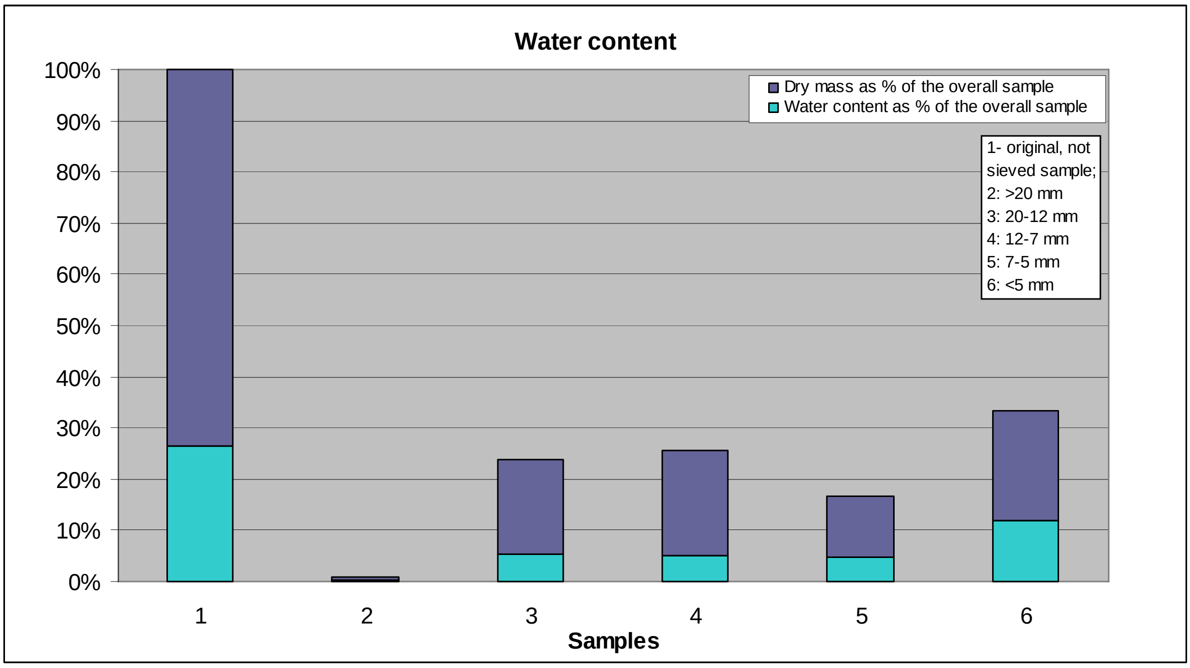

Figure 4. Moisture content of unsieved MBT waste and the different size fractions

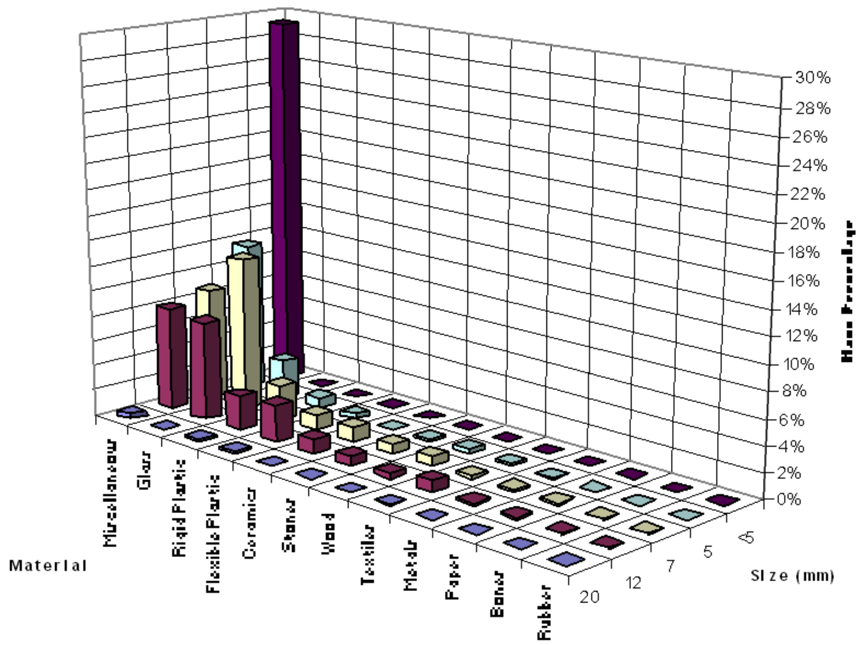

Figure 5. Mass distribution (%) by material type and particle size for the MBT sample (format of graph, suggested by Dixon and Langer, 2006)

4.3. Material type

The composition of the waste by material type and particle size is shown in Figure 5, and summarised quantitatively in Table 1. Percentages by volume were calculated using measured particle densities for the different materials. Owing to their low density, flexible plastics form a relatively small percentage of the whole by mass, but a rather larger proportion by volume.

Photographs of the unsorted waste, and some of the individual particle types and sizes, are given in Figure 6.

Figure 6. MBT waste (a) before sorting; and after manual sorting: (b) “Glass” with size 12-20 mm; (c) “Rigid plastics” with size 12-20 mm; (d) “Flexible plastics” with size bigger than 20 mm; (e) “Textiles” with size 12-20 mm

Table 1. Composition of MBT waste sample by material type and particle size

		Size (mm)					
Material		**<5**	**5-7**	**7-12**	**12-20**	**>20**	**Total**
Bones	% mass	0.00%	0.00%	0.12%	0.12%	0.00%	0.25%
	%volume	0.00%	0.01%	0.19%	0.19%	0.00%	0.39%
Ceramics	% mass	0.00%	0.00%	1.23%	1.07%	0.00%	2.29%
	%volume	0.00%	0.00%	0.88%	0.77%	0.00%	1.65%
Flexible Plastic	% mass	0.00%	0.38%	1.18%	2.87%	0.14%	**4.57%**
	%volume	0.00%	0.78%	2.41%	5.87%	0.29%	9.34%
Glass	% mass	0.00%	3.02%	12.03%	7.70%	0.01%	22.77%
	%volume	0.00%	2.05%	8.17%	5.23%	0.01%	15.45%
Metals	% mass	0.00%	0.07%	0.23%	0.19%	0.00%	0.49%
	%volume	0.00%	0.04%	0.14%	0.12%	0.00%	0.31%
Miscellaneous	% mass	29.15%	11.74%	8.80%	8.01%	0.39%	58.10%
	%volume	28.67%	11.55%	8.66%	7.88%	0.39%	57.15%
Paper	% mass	0.00%	0.04%	0.22%	0.16%	0.01%	0.43%
	%volume	0.00%	0.04%	0.22%	0.16%	0.01%	0.43%
Rigid Plastic	% mass	0.00%	0.75%	2.67%	2.69%	0.16%	**6.27%**
	%volume	0.00%	1.21%	4.28%	4.32%	0.26%	10.07%
Rubber	% mass	0.00%	0.01%	0.08%	0.10%	0.00%	0.18%
	%volume	0.00%	0.01%	0.09%	0.11%	0.00%	0.21%
Stones	% mass	0.00%	0.15%	0.78%	0.81%	0.00%	1.73%
	%volume	0.00%	0.11%	0.57%	0.59%	0.00%	1.28%
Textiles	% mass	0.00%	0.15%	0.22%	0.89%	0.07%	1.33%
	%volume	0.00%	0.14%	0.22%	0.87%	0.07%	1.31%
Wood	% mass	0.00%	0.34%	0.74%	0.49%	0.00%	1.57%
	%volume	0.00%	0.53%	1.13%	0.75%	0.00%	2.42%
Total	**% mass**	**29.15%**	**16.66%**	**28.30%**	**25.10%**	**0.80%**	**100.00%**

4.4. Particle shape

In addition to the particle size and material type, the particle shape will influence the bulk mechanical and flow behaviour of the material. Following Kölsch (1995) and Dixon and Langer (2006), four categories of particle shape may be identified, categorised according to their relative dimensions or aspect ratio. These are:

- Grains (characterised by Kölsch, 1995 as having zero dimensions, D0). Each dimension is less than a certain minimum significant length. In an MBT, these particles form a "matrix" into which the other particles may be considered to be embedded potentially modify its behaviour. Kölsch (1995) identified the minimum significant dimension (such that particles smaller than this are considered as 0D) as 8 mm for a raw MSW: for an MBT waste, the minimum significant dimension will be somewhat smaller.
- Fibres, sticks or strings (one-dimensional, D1). One dimension is long relative to the typical dimension and the other two are smaller. These particles may act as reinforcing elements, potentially enhancing the shear strength of the matrix material.

- Sheets or foils (two-dimensional, D2). These particles are flat, with two long dimensions and one short. They may act as reinforcing elements in terms of their effect on strength, or as elements that block or impede (semi-block) fluid flow, depending on the material of which they are made. Impermeable materials such as plastics and metals will tend to block flow across their area completely, whereas more permeable materials such as textiles and perhaps paper and card may impede rather than fully block flow and are referred to as semi-blocking.
- Bulky (three-dimensional, 3D). These particles are rotund, with all three dimensions greater than the minimum significant value. They may act to block or impede fluid flow, again depending on the material from which they are made and their size relative to the matrix.

The minimum length needed for a 1D or 2D particle to be considered as a reinforcing element is worthy of some consideration.

Dixon and Langer (2006) suggest that to act as a reinforcing element, a 1D or 2D particle must exceed the nominal diameter of the particles around it (i.e., of the particles in the matrix). For fibre-reinforced soils, Michalowski and Zhao (1996) suggest that the length of reinforcing components must be at least an order of magnitude larger than the diameter (D50) of the surrounding grains, but this seems excessive.

In the context of a fibre reinforced composite, Ashby and Jones (1986) show that a certain minimum length of fibre, related to its tensile strength, is needed to develop a significant tension. A reinforcing element has been taken in this paper as one longer than three times the typical particle size in the surrounding matrix.

Figure 7 illustrates various 1-dimensional (1D), 2-dimensional (2D) and 3-dimensional (3D) materials within the sample of MBT waste. The main components in each dimensional and material category are described in Table 2.

Table 3 and Table 4 summarize the mass distribution of particles according to their dimensionality within the two plastic categories (rigid and flexible). Percentages are calculated as a proportion of the total sample dry mass. The majority of particles within both plastic categories are 2D. The dominant dimensions of particles made of other materials are given in Table 5; blank fields indicate that no particles of that material type and size range were present.

5. DISCUSSION

5.1. Mechanical Behaviour

Dixon and Langer (2006) suggest a classification framework for waste components based on shape-related properties as follows:

- Reinforcing components: 1-dimensional and 2-dimensional (e.g. plastic and paper sheets),
- Three-dimensional components: i) Compressible (e.g. putrescible materials, beverage cans) and ii) Incompressible (e.g. pieces of metal). They further divide the compressible category into high- and low-compressibility materials.

As has already been mentioned, the MBT material described in this paper is rather simpler than a raw MSW and might be viewed as a matrix with reinforcing (1D and 2D) and flow-impeding (2D and 3D) elements embedded.

The matrix is represented by the fine fraction (<5 mm): its PSD curve is given in Figure 8 which indicates $D_{50} \sim 1$ mm.

To allow for the gripping of the ends and the development of significant tensile stress, components with one or two long dimensions $\geq 3.D_{50}$ (i.e. ≥ 3 mm) have been considered to be potentially reinforcing.


2 D
> 20
PLASTIC / HEAVY
1 D
3 D


FLEXIBLE PLASTICS
> 20 mm
2D


2 D
12-20mm
Plastics / hard
3 D

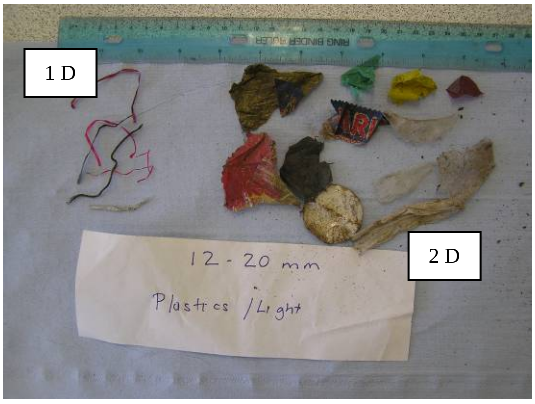
1 D
12 - 20 mm
Plastics / Light
2 D


1 D
2 D
7-12m
PLASTICS / HARD
3 D
RING BINDER RULER


2 D
PLASTICS / LIGHT
7-12m


PLASTICS (HARD)
1 D
2 D
3 D


PLASTICS (LIGHT)
5 - 7 mm
1 D
2 D

Figure 7. Typical 1D and 2D particles found in MBT

Table 2. Description by dimensionality and material of components found in MBT

Fraction (material)	***Size fraction***	***1D***	***2D***	***3D***
Rigid plastics	**>20 mm:** 3D – 55%; 2D – 25%; 1D – 20%	Wires with a plastic cover; lollipop sticks: up to 170×2mm	Sheet-like solid plastic pieces: up to 125×10 mm; 70×30 mm	Parts or whole pens or markers; other bulky items; up to 135×8 mm; 50×8 mm
	12-20 mm: 2D – 55% 3D – 30% 1D – 15%	Pipe-like plastic materials, mostly from lollipops (70×2 mm), wires (115×1.5 mm)	Sheet-like hard plastic pieces (50×12 mm)	Different bulky items (parts of pens, necklaces pines etc.); up to 130x8 mm
	7-12 mm: 2D – 65% 1D – 20% 3D – 15%	Wires (55×1.5 mm); parts of clothes tags (50×0.7 mm)	Sheet like pieces of solid plastic boxes etc. (35 ×8 mm; 40×7 mm)	Bulky items e.g. balls (d ~ 4 mm), parts of toys etc., 40×4 mm
	5-7 mm: 2D – 85% 3D – 10% 1D – 5%	Parts of clothes tags (50 0.7 mm)	Sheet-like hard plastic pieces up to 60×8 mm	Small plastic balls, internal parts of pens up to 12×5 mm
Flexible plastics	**>20 mm:** 2D -100%	-	Mostly pieces of plastic bags and packaging	.
	12-20 mm 2D – 95% 1D – 5%	Parts of plastic packaging (100 ×1 mm; 80×1 mm)	Mostly pieces of plastic bags and packaging (60×40 mm; 50×30 mm)	-
	7-12 mm: 2D – 99 % 1D – 1%	Parts of plastic packaging up to 80×1 mm	Mostly pieces of plastic bags and packaging up to 60×30 mm	-
	5-7 mm: 2D – 98% 1D – 2%	Parts of plastic packaging (80×3 mm; 40×2mm)	Mostly pieces of plastic bags and packaging (50×8 mm; 40×15 mm)	-
Textiles	**>20 mm:** 1D -50% 2D- 50%	Parts of nappies, clothes and hygiene materials (max 165 mm ; min 50 mm)	Parts of clothes	-
	12-20 mm: 1D – 50% 2D – 50%	Parts of nappies, clothes and hygiene materials (max 120 mm ; min 30 mm)	Parts of clothes (50×20 mm; 24×25 mm)	-
	7-12 mm: 1D – 50 % 2D – 50%	Parts of nappies, clothes and hygiene materials (max 60 mm ; min 25 mm)	Parts of clothes (8×12 mm; 25×25 mm)	-
	5-7 mm: 2D – 50% 1D – 50%	Parts of nappies, clothes and hygiene materials (max 80 mm ; min 28 mm)	Parts of clothes (12×12 mm)	-
Glass	**>20 mm:** 3D -80% 2D – 10%	-	Parts of broken bottles	Parts of broken bottles

Fraction (material)	*Size fraction*	*1D*	*2D*	*3D*
	12-20 mm: 3D -80% 2D – 10%	-	Parts of broken bottles (40 mm × 20 mm; 15 mm × 10 mm)	Parts of broken bottles (40 mm × 25 mm × 5 mm;15 mm × 15 mm × 5 mm)
	7-12 mm: 3D - 80% 2D – 10%	-	Parts of broken bottles (35 mm × 10 mm; 15 mm × 15 mm)	Parts of broken bottles (30 mm × 15 mm × 5 mm;15 mm × 15 mm ×5 mm)
	5-7 mm: 3D -100%	-	-	Parts of broken bottles

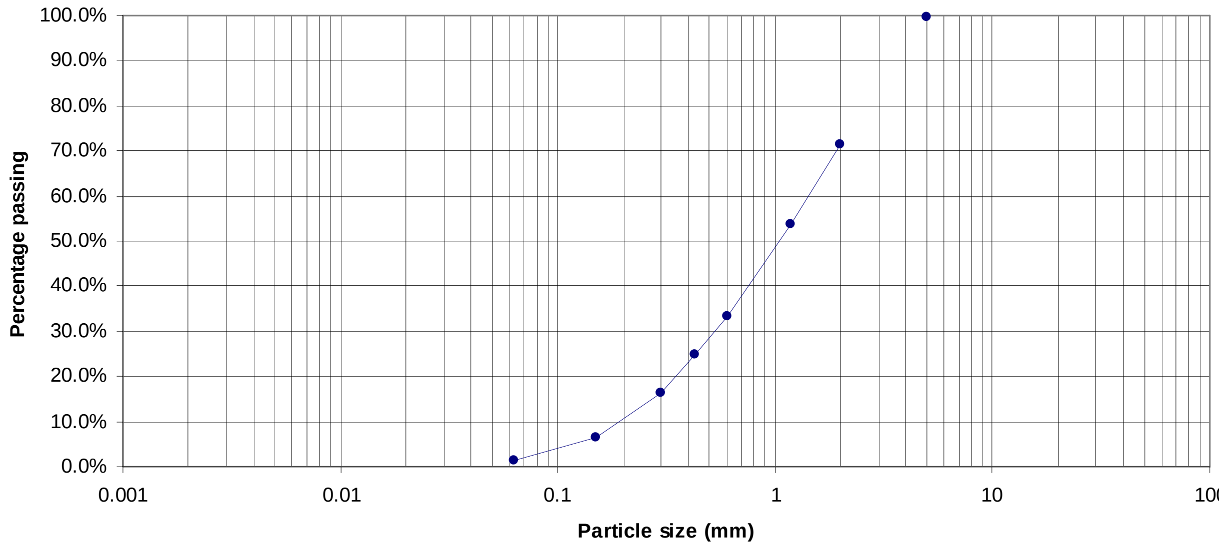

Figure 8. PSD for the Matrix Fraction in MBT (Miscellaneous < 5mm)

Table 3. Rigid Plastics - mass distribution (% dry mass) of particles by dimensional type

			%mass		
Size (mm)	**0D**	**1D**	**2D**	**3D**	**Total**
20	0.00%	0.03%	0.04%	0.09%	0.16%
12	0.00%	0.40%	1.48%	0.81%	2.69%
7	0.00%	0.53%	1.73%	0.40%	2.67%
5	0.00%	0.04%	0.64%	0.08%	0.75%
<5	0.00%	0.00%	0.00%	0.00%	0.00%
Total	**0.00%**	**1.01%**	**3.89%**	**1.37%**	**6.27%**

Table 4. Flexible Plastic - mass distribution (% dry mass) of particles by dimensional type

	%mass				
Size (mm)	**0D**	**1D**	**2D**	**3D**	**Total**
20	0.00%	0.00%	0.14%	0.00%	0.14%
12	0.00%	0.14%	2.73%	0.00%	2.87%
7	0.00%	0.01%	1.17%	0.00%	1.18%
5	0.00%	0.01%	0.37%	0.00%	0.38%
<5	0.00%	0.00%	0.00%	0.00%	0.00%
Total	**0.00%**	**0.16%**	**4.41%**	**0.00%**	**4.57%**

Table 5. Description by dimensions of the materials found in MBT sample

	Size (mm)				
Components	**>20**	**20-12**	**12-7**	**7-5**	**<5**
Flexible Plastic	2D	2D	2D	2D	
Rigid Plastic	3D	2D	2D	2D	
Textiles	1D	1D	1D	1D	
Glass	3D	3D	3D	3D	
Ceramics		3D	3D		
Stones		3D	3D	3D	
Metals	2D	2D	2D	2D	
Paper	2D	2D	2D	2D	
Wood		1D	1D	1D	
Bones		1D	1D	1D	
Rubber		3D	3D	3D	
Miscellaneous	3D	3D	3D	3D	OD

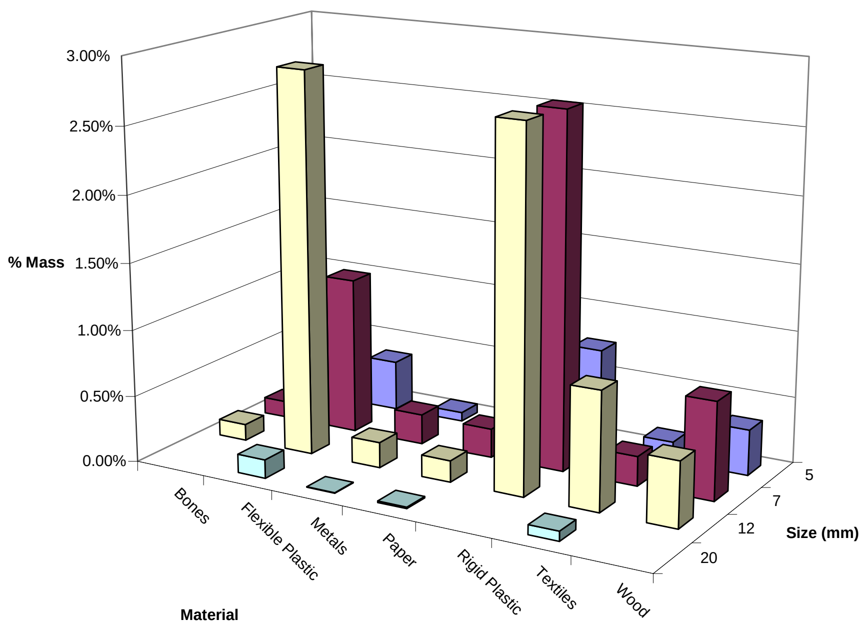

Figure 9. Mass distribution for potentially reinforcing components in MBT sample (following Dixon and Langer, 2006)

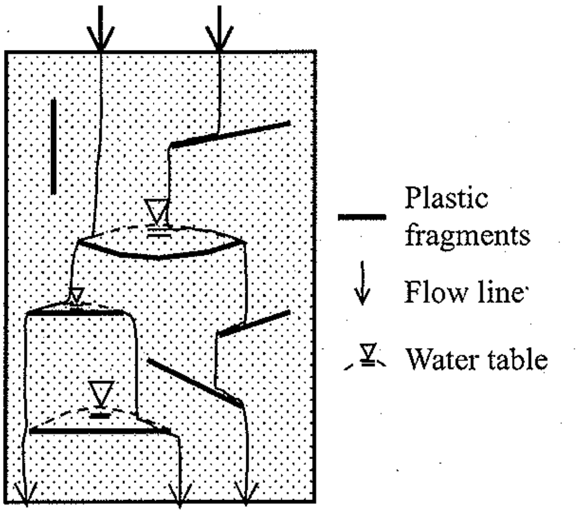

Figure10. Thin-sheet conceptual model for flow through solid wastes (from Xie, 2006)

Table 6. Particle distribution (in % total dry mass) by category and size according to the potential impact on fluid flow in MBT waste

				Size (mm)					
Materials Classification	**Components**		**Dim**	**20**	**12**	**7**	**5**	**<5**	**Total**
Blocking	Rigid Plastic		3D	0.09%	0.81%	0.40%	0.08%	0.00%	1.38%
	Glass		3D	0.01%	7.70%	12.03%	3.02%	0.00%	22.77%
	Ceramics		3D	0.00%	1.07%	1.23%	0.00%	0.00%	2.29%
	Stones		3D	0.00%	0.81%	0.78%	0.15%	0.00%	1.73%
	Rubber		3D	0.00%	0.10%	0.08%	0.01%	0.00%	0.18%
Blocking+ reinforcing	Flexible Plastic	Extensible	2D	0.14%	2.73%	1.17%	0.37%	0.00%	4.41%
	Rigid Plastic	Rigid	2D	0.04%	1.48%	1.73%	0.64%	0.00%	3.89%
	Metals	Rigid	2D	0.00%	0.09%	0.11%	0.04%	0.00%	0.24%
Neutral+ Reinforcing	Textiles	Extensible	1D	0.07%	0.89%	0.22%	0.15%	0.00%	1.33%
	Rigid Plastic	Rigid	1D	0.03%	0.40%	0.53%	0.04%	0.00%	1.00%
	Flexible Plastic	Extensible	1D	0.00%	0.14%	0.01%	0.01%	0.00%	0.16%
	Wood		1D	0.00%	0.49%	0.74%	0.34%	0.00%	1.57%
	Bones		1D	0.00%	0.12%	0.12%	0.00%	0.00%	0.25%
Semiblocking+ reinforcing	Paper		2D	0.01%	0.16%	0.22%	0.04%	0.00%	0.43%
	Textiles		2D	0.00%	0.10%	0.12%	0.03%	0.00%	0.25%
Matrix	Miscellaneous		0D	0.39%	8.01%	8.80%	11.74%	29.15%	58.10%
Total				**0.80%**	**24.28%**	**27.89%**	**17.63%**	**29.15%**	**100.00%**

Only materials of 1D and 2D are considered potentially reinforcing; thus 3D particles of materials such as glass, ceramics and stones are excluded from this category.

Crushable particles are absent, having been eliminated by the processing of the waste. Some of the matrix particles may be compressible and others not, but given that the matrix is composed of fine particles whose material cannot be distinguished it has not been considered fruitful at this stage in the research to attempt to subdivide the matrix material into compressible and incompressible components. (Dixon and Langer, 2006 had to assume that 50% of the fine particles were compressible and 50% were not).

However, the reinforcing particles have been categorised as either “rigid” (metals and hard plastics) or “extensible” (flexible plastics, textiles, paper and card), Table 6.

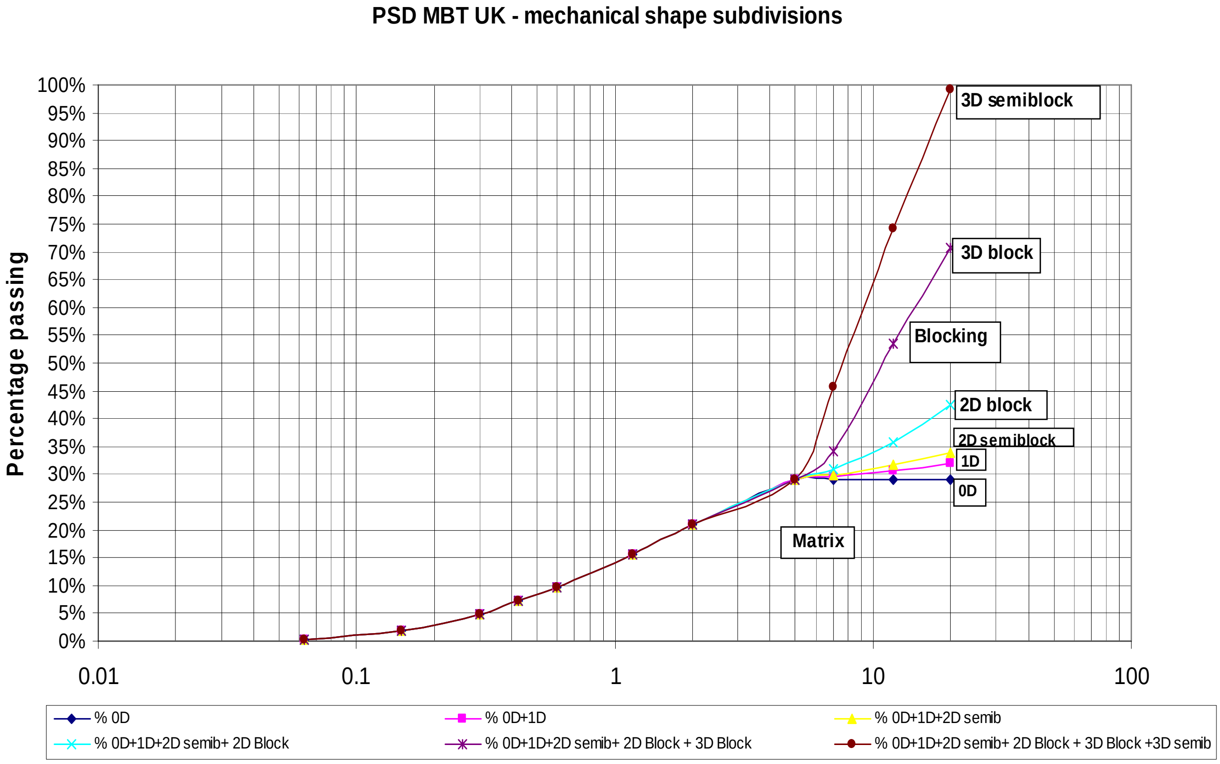

Figure 11. PSD of MBT components as Matrix, Reinforcing, and Flow blocking/impeding

5.2. Flow behaviour: permeability and blocking

In addition to their reinforcing effect, 2D particles embedded within the waste can increase the flow path due to the formation of structure. The larger the sheets and the greater their number, the lower the bulk hydraulic conductivity (permeability).

This is illustrated in the conceptual model developed by Xie (2006): Figure. Large, bulky particles (3D in the Kölsch, 1995 terminology) will also impede flow, as they can be considered as large impermeable or reduced-permeability lumps within the general matrix structure. The dimension of a blocking particle must be significantly greater than that of a typical particle – perhaps by a factor of at least 3-5. Thus the MBT material described in this paper can be viewed in terms of its flow characteristics as 2-D or 3-D blocking (or semi-blocking) particles (typical particle size > 3 mm) in a matrix of fines (D_{50} ~ 1 mm). 1D particles are assumed to be neutral as far as fluid flow is concerned. Particles of a given material and size are classified in terms of their impact on fluid flow in Table 6, which gives the distribution in each category as a proportion of the total dry mass. In total, potentially blocking components comprise 36.9% of the sample by dry mass, 9% from which could be potentially reinforcing elements. The oveall percentage of reinforcing particles is 12.9% and matrix material takes 58.1%. The relative size needed for a particle of a given dimensionality to be considered as blocking is currently being investigated by means a laboratory study using controlled synthetic wastes.

A cumulative PSD, indicating the distribution by particle size of matrix material, potentially reinforcing elements and potentially flow blocking or impeding (semi-blocking) elements is presented in Figure 1. This is in essence a simplification of the categorisation scheme proposed by Dixon and Langer (2006), in which the types of component that processing has removed from MBT waste have been eliminated.The distinction between compressible and incompressible particles has for the time being been neglected: research into its importance for an MBT and its quantification is currently in progress.

6. CONCLUSIONS

Mechanical biological treatment (MBT) of municipal solid waste (MSW) reduces the particle size and eliminated certain components – in particular, large and crushable elements from the material. Much of the MBT residue is too small to be able to distinguish, visually, the parent material and whether the particle is likely to be compressible or incompressible. However, it is possible to identify visually the dimensionality (shape) of the larger particles, and to make at least a preliminary assessment of whether these could act as reinforcing elements (sticks, strings or sheets, increasing the shear strength of the material) or elements that block or impede flow (sheets or large, bulky/rotund particles).

Particles in the latter category made from impermeable materials such as plastic and metal will block flow, while particles made from less impermeable materials such as textiles and perhaps paper or card may merely impede it.

In terms of the dimensionality of the particle proposed by Kölsch (1995), 0D particles form a matrix of particles smaller than a minimum significant dimension (in the case of the MBT investigated in this study, the D_{50} of the matrix material was about 1 mm). 1D and 2D particles are potentially reinforcing (and either rigid or extensible), while 2D and 3D particles are potentially flow-blocking or flow-impeding.

The minimum size of 1D, 2D and 3D reinforcing and blocking/impeding particles is under investigation, but has been taken as 3 times the D_{50} size of the matrix as a working hypothesis in this paper.

These observations have been used to develop a simplified version of the classification system relating particle shape to mechanical properties of the waste proposed by Dixon and Langer (2006). The simplified classification is suited to MBT, and does not need to consider particles removed from raw MSW by processing. These include large and crushable particles. The importance of being able to distinguish between compressible and incompressible matrix particles is currently under investigation, along with a way of making this distinction by observation or simple experiment.

ACKNOWLEDGEMENTS

The work described in this Paper was carried out as part of EPSRC research grant EP/E041965: Science and strategies for the long-term management and remediation of landfills.

REFERENCES

Ashby, M.F. & Jones, D.R.H. (1986) Engineering Materials 2: An Introduction to Microstructures, Processing and Design, Oxford, England, Pergamon Press.

Bauer, J., Münnich, K. & Fricke, K. (2005) Influence of hydraulic properties on the stability of landfills. T. H., Cossu, R. & Stegmann, R. (Eds.). Proceedings Sardinia 2007, Eleventh International Waste Management and Landfill Symposium. S. Margherita di Pula, Cagliari, Italy CISA, Environmental Sanitary Engineering Centre, Italy.

BS1377 (1990) Methods of test for Soils for civil engineering purposes Part 2: Classification tests. British Standard 1377-2:1990. United Kingdom.

Dixon, N. & Langer, U. (2006) Development of a MSW classification system for the evaluation of mechanical properties. Waste Management, 26**,** 220-232.

EC (1999) Council Directive 1999/31/EC on the Landfill of Waste. Official Journal of the

European Communities.

Grisolia, M., Napoleoni, Q. & Tancredi, G. (1995) Contribution to a technical classification of MSW: he use of triaxial tests for the mechanical characterization of MSW. In Christensen, T. H., Cossu, R. & Stegmann, R. (eds.) Proceedings Sardinia 1995, Fifth International Waste Management and Landfill Symposium. S. Margherita di Pula, Cagliari, Italy. CISA, Environmental Sanitary Engineering Centre, Italy.

Juniper (2005) 'Mechanical-Biological Treatment: A guide for decision making processes, policies and markets'. Sheppards Mill, Uley, Gloucestershire, GL11 5SP, UK, Juniper Concultancy Services Ltd.

Kölsch, F. (1995) Material values for some mechanical properties of domestic waste. In Christensen, T. H., Cossu, R. & Stegmann, R. (Eds.) Proceedings Sardinia 1995, Fifth International Waste Management and Landfill Symposium. S. Margherita di Pula, Cagliari, Italy, CISA, Environmental Sanitary Engineering Centre, Italy.

Kuehle-Weidemeir, M. (2005) Online measurement of gaseous emissions from mechanical-biological waste treatment (MBT). T. H., Cossu, R. & Stegmann, R. (Eds.) Proceedings Sardinia 2005, Tenth International Waste Management and Landfill Symposium. S. Margherita di Pula, Cagliari, Italy; 3 - 7 October 2005, 2005 by CISA, Environmental Sanitary Engineering Centre, Italy.

Landva, A. & Clark, J. (1990) Geotechnics of waste fills - theory and practice, American Society for Testing and Materials, Baltimore, pp. 86-103.

Michalowski, R.L. & Zhao, A. (1996) Failure of fiber-reinforced granular soils. Journal of Geotechnical Engineering, 122**,** 226-234.

Münnich, K., Bauer, J. & K., F. (2005) Investigation on relationship between vertical and horizontal permeabilities of MBT wastes. T. H., Cossu, R. & Stegmann, R. (Eds.) Proceedings Sardinia 2005, Tenth International Waste Management and Landfill Symposium. S. Margherita di Pula, Cagliari, Italy CISA, Environmental Sanitary Engineering Centre, Italy.

Siegel, R.A., Robertson, R.J. & Anderson, D.G. (1990). Geotechnics of waste fills – theory and practice. In Landva & Knowles (eds) Geotechnics of waste fills. ASTM Special Publication STP1070. American Society for Testing and Materials, Baltimore, pp. 259-284.

Xie, M., Aldenkortt, D., Wagner, J-F., Rettenberger, G (2006) Effect of plastic fragments on hydraulic characteristics of pretreated municipal solid waste. Can. Geotech. J., 43**,** 1333–1343

10. References

ABFABIV 2001. Ordinance on environmentally compatible storage of waste from human settlements and from biological waste-treatment facilities. *Annex 2. Allocation criteria for landfills for mechanically and biologically pre-treated waste.* Federal Ministry of the Environment, Nature conservation and Nuclear Safety, Germany.

ACHARYA, T. & RAY, A. K. 2005a. Image Segmentation. *Image Processing.* John Wiley & Sons, Inc.

ACHARYA, T. & RAY, A. K. 2005b. Recognition of Image Patterns. *Image Processing.* John Wiley & Sons, Inc.

ALLAIRE, S. E., ROULIER, S. & CESSNA, A. J. 2009. Quantifying preferential flow in soils: A review of different techniques. *Journal of Hydrology,* 378**,** 179-204.

AMOS, C. L., SUTHERLAND, T. F., RADZIJEWSKI, B. & DOUCETTE, M. 1996. A rapid technique to determine bulk density of fine-grained sediments by X-ray computed tomography. *Journal of Sedimentary Research,* 66**,** 1023-1024.

ANDERSON, S. H., PEYTON, R. L., WIGGER, J. W. & GANTZER, C. J. 1992. Influence of aggregate size on solute transport as measured using computed tomography. *Geoderma,* 53**,** 387-398.

ANDREINI, M. S. & STEENHUIS, T. S. 1990. Preferential paths of flow under conventional and conservation tillage. *Geoderma,* 46**,** 88-102.

ASTM 1441-00 2005. Standard Guide for Computed Tomography (CT) Imaging. United States.

ASTM D 2434-68 1968. Standard Test Method for Permeability of Granular Soils (Constant Head). *Reapproved 2000.* United States.

BARLAZ, M., HAM, R. & SCHAEFER, D. 1989. Mass-Balance Analysis of Anaerobically Decomposed Refuse. *Journal of Environmental Engineering,* 115**,** 1088-1102.

BARLAZ, M. A., HAM, R. K. & SCHAEFER, D. M. 1990. Methane production from municipal refuse: A review of enhancement techniques and microbial dynamics *Critical reviews in Environmental Control* 19**,** 557-584.

BEALL, J. L., GORDON I. T., GOURNAY, J. P., KIRKLAND, B. L. & WHITE, J. V. 1996. Analysis of porosity in lower Ismay phylloid algal packstone using high-resolution computed x-ray tomography. *American Association of Petroleum Geologists, Annual Meeting Abstracts* 5**,** 13.

BEAVEN, R. P. 1996. Evaluation of geotechnical and hydrogeological properties of wastes. *Engineering Geology of Waste Disposal, Geological Society Engineering Geology Special Publication,* 11**,** 57-65.

BEAVEN, R. P. 2000. *The hydrogeological and geotechnical properties of household waste in relation to sustainable landfilling.* Thesis for the degree of Doctor of Philosophy, University of London.

BEAVEN, R. P. & POWRIE, W. Hydrogeological and Geotechnical Properties of Refuse Using a Large Scale Compression Cell. Proceedings Sardinia 95, Third International Lnadfill Symposium, 2-6 October 1995 S.Margherita di Pula, Cagliari, Italy.

BENDZ, D. & SINGH, V. P. 1999. Solute transport under steady and transient conditions in biodegraded municipal solid waste *Water Resources Research,* 35**,** 2333-2345.

BENSON, C. H., BARLAZ, M. A., LANE, D. T. & RAWE, J. M. 2007. Practice review of five bioreactor/recirculation landfills. *Waste Management,* 27**,** 13-29.

BEVEN, K. & GERMANN, P. 1982. Macropores and Water Flow in Soils. *Water Resources Research,* 18**,** 1311-1325.

BOADU, F. K. 2000. Hydraulic Conductivity of Soils from Grain-Size Distribution: New Models. *Journal of Geotechnical and Geoenvironmental Engineering,* 126**,** 739-746.

BOUWER, H. & RICE, R. C. 1984. Hydraulic Properties of stony Vadose Zone *Ground Water* 22**,** 696-705.

BROOKS, R. A. The physics of computer assisted tomography. 1977 Electro Conference Record, 19-20 April 1977 New York, NY, USA. Electro, 23/1/1-23/1/6.

BROOKS, R. A., MITCHELL, L. G., O'CONNOR, C. M. & DICHIRO, G. 1981. On the relationship between computed tomography numbers and specific gravity. *Physics in Medicine and Biology,* 26**,** 141.
BROUERS, F. & SOTOLONGO-COSTA, O. 2006. Generalized fractal kinetics in complex systems (application to biophysics and biotechnology). *Physica A: Statistical Mechanics and its Applications,* 368**,** 165-175.
BS 1377-2 1990. Methods of test for Soils for civil engineering purposes Part 2: Classification tests. *BS 1377-2:1990.* United Kingdom.
BS 1377-4 1990. Methods of test for Soils for civil engineering purposes —Part 4: Compaction- related tests. *BS 1377-5:1990.* United Kingdom.
BS 1377-5 1990. Methods of test for Soils for civil engineering purposes —Part 5: Compressibility, permeability and durability tests. *BS 1377-5:1990.* United Kingdom.
BS 1881: PART 131 1998. Testing Concrete —Part 131: Methods for testing cement in a reference concrete *BS 1881: Part 131:1998.* United Kingdom.
BS ISO 9276-1 1998. Representation of results of particle size analysis Part 1: Graphical representation. *BS ISO 9276-1:1998.* United Kingdom.
BS ISO 9276-2 2001. Representation of results of particle size analysis Part 2: Calculation of average particle sizes/diameters and moments from particle size distributions *BS ISO 9276-2:2001.* United Kingdom.
BS ISO 9276-3 2008. Representation of results of particle size analysis Part 3: Adjustment of an experimental curve to a reference model. *BS ISO 9276-3:2008.* United Kingdom.
BS ISO 9276-5 2005. Representation of results of particle size analysis Part 5: Methods of calculation relating to particle size analyses using logarithmic normal probability distribution *BS ISO 9276-5:2005.* United Kingdom.
BS ISO 23909:2008 2008. Soil quality-Preparation of laboratory samples from large samples. *BS ISO 23909:2008.* United Kingdom.
CAICEDO D, M., WATSON, G. V. R., RICHARDS, D. J. & POWRIE, W. 2010. Exploring the use of Micro-focus Computed Tomography for a better conceptual understanding of flow and structure in landfilled waste in the context of post-closure management for landfills. *1st International Conference on Final Sinks.* Vienna, Austria.
CAICEDO, D. M., SANDOVAL, J. J., WATSON, G. V. R., RICHARDS, D. J. & POWRIE, W. 2010. Exploring the use of a modified dye-adsorption method for the study of landfilled waste structure and some implications for post-closure management in landfills. *Global Waste Management Symposium* San Antonio, Texas.
CAICEDO, D. M., WATSON, G. V. R., RICHARDS, D. J. & POWRIE, W. 2011. Exploring the use of Micro-focus Computed Tomography for a better conceptual understanding of structure in landfilled waste in the context of post-closure management for landfills. *Sustainable Environmental Research,* 21**,** 1-10.
CHEN, C., PACKMAN, A. I. & GAILLARD, J.-F. 2009. Using X-ray micro-tomography and pore-scale modeling to quantify sediment mixing and fluid flow in a developing streambed. *Geophysical Research Letters,* 36.
CHO, G.-C., DODDS, J. & SANTAMARINA, J. C. 2006. Particle Shape Effects on Packing Density, Stiffness, and Strength: Natural and Crushed Sands. *Journal of Geotechnical and Geoenvironmental Engineering,* 132**,** 591-602.
CHOUDALAKIS, G. & GOTSIS, A. D. 2009. Permeability of polymer/clay nanocomposites: A review. *European Polymer Journal,* 45**,** 967-984.
CLAYTON, C. R. I., SIMONS, N. E. & MATTHEWS, M. C. 1982. *Site Investigation,* London, Granada Publishing.
COLLINS, R. E. 1961. *Flow of Fluids through porous materials,* New York, Reinhold Publishing Corporation.

CRAWFORD, J. W., RITZ, K. & YOUNG, I. M. 1993. Quantification of fungal morphology, gaseous transport and microbial dynamics in soil: an integrated framework utilising fractal geometry. *Geoderma,* 56**,** 157-172.

CRESSWELL, A., BARTON, M. E. & BROWN, R. 1999. Determining the maximum density of sands by pluviation. *Geotechnical Testing Journal* 22**,** 324-328.

CRONICAN, A. E. & GRIBB, M. M. 2007. Literature review: equations for predicting hydraulic conductivity based on grain-size data.

CUBRINOVSKI, M. & ISHIHARA, K. 2002. Maximum and minimum void ratio characteristics of sands. *Soils and Foundations,* 42**,** 65-78.

D'AMICO, K. L., DUNSMUIR, J. H., FERGUSON, S. R., FLANNERY, B. P. & DECKMAN, H. W. 1992. The Exxon microtomography beam line at the National Synchrotron Light Source (invited). *Review of Scientific Instruments,* 63**,** 574-577.

DANIEL, D. E. 1993. State-of- the art: Laboratory hydraulic conductivity tests for saturated soils. *In:* DANIEL, D. E. & TRAUTWEIN, S. J. (eds.) *Proceedings of the Symposium in Hydraulic Conductivity and Waste Contaminant Transport in Soil ,1993.* San Antonio, Texas: ASTM.

DARCY, H. 1856. *Les Fontaines Publiques de la Ville de Dijon,* Paris, Victor Dalmont.

DE GRYZE, S., JASSOGNE, L., SIX, J., BOSSUYT, H., WEVERS, M. & MERCKX, R. 2006. Pore structure changes during decomposition of fresh residue: X-ray tomography analyses. *Geoderma,* 134**,** 82-96.

DENISON, C. & CARLSON, W. D. 1997. Three-dimensional quantitative textural analysis of metamorphic rocks using high-resolution computed X-ray tomography: Part II. Application to natural samples. *Journal of Metamorphic Geology,* 15**,** 45-57.

DENISON, C., CARLSON, W. D. & KETCHAM, R. A. 1997. Three-dimensional quantitative textural analysis of metamorphic rocks using high-resolution computed X-ray tomography: Part I. Methods and techniques *Journal of Metamorphic Geology,* 15**,** 29-44.

DERESIEWICZ, H. 1958. Mechanics of granular matter. *Advances in Applied Mechanics,* 5**,** 233-306.

DEVAUX, M. F., TARALOVA, I., LEVY-VEHEL, J., BONNIN, E., THIBAULT, J. F. & GUILLON, F. 2006. Contribution of image analysis to the description of enzymatic degradation kinetics for particulate food material. *Journal of Food Engineering,* 77**,** 1096-1107.

DIXON, N. & JONES, D. R. V. 2005. Engineering properties of municipal solid waste. *Geotextiles and Geomembranes,* 23**,** 205-233.

DIXON, N. & LANGER, U. 2006. Development of a MSW classification system for the evaluation of mechanical properties. *Waste Management,* 26**,** 220-232.

DIXON, N., LANGER, U. & GOTTELAND, P. 2008. Classification and mechanical behavior relationships for municipal solid waste: Study using synthetic wastes. *Journal of Geotechnical and Geoenvironmental Engineering,* 134**,** 79-90.

DONOHUE, T. J. & WENSRICH, C. M. 2008. A numerical investigation of the void structure of fibrous materials. *Powder Technology,* 186**,** 72-79.

DONOHUE, T. J. & WENSRICH, C. M. 2009. Improving permeability prediction for fibrous materials through a numerical investigation into pore size and pore connectivity. *Powder Technology,* 195**,** 57-62.

DULLIEN, F. A. L. 1992. *Porous Media: Fluid Transport and Pore Structure,* San Diego, California.

DUNCAN, T. V. 2011. Applications of nanotechnology in food packaging and food safety: Barrier materials, antimicrobials and sensors. *Journal of Colloid and Interface Science,* 363**,** 1-24.

DUNSMUIR, J. H., FERGUSON, S. R., D'AMICO, K. L. & STOKES, J. P. X-Ray Microtomography : A New Tool for the Characterization of Porous Media SPE Annual Technical Conference and Exhibition, 1991 Dallas, Texas. Society of Petroleum Engineers, Inc, 423.

ELEAZER, W., ODLE, W., WANG, Y.-S. & BARLAZ, M. 1997. Biodegradability of Municipal Solid Waste Components in Laboratory-Scale Landfills. *Environmental Science & Technology,* 31**,** 911-917.

EMERSON, W. W. & MCGARRY, D. 2003. Organic carbon and soil porosity. *Australian Journal of Soil Research* 41**,** 107-118.

ENVIRONMENT AGENCY, U. K. 2009. A technical assessment of leachate recirculation. Environment Agency, Rio House, Waterside Drive.
EUROPEAN UNION 1999. EU Directive 1999/31/EC on the landfill of waste. Official Journal of the European Communities.
FELSKE, C., KRAFT, E., ZEISS, C. & BIDLINGMAIER, W. Geometric characterisation of residential waste with special consideration to the fluid flow behaviour in landfills. *In:* CISA, E. S. E. C., ITALY, ed. Proceedings Sardinia 2001, Eighth International Waste Management and Landfill Symposium, 1-5 October 2001 2001 S.Margherita di Pula, Cagliari, Italy. 405-414.
FERNANDO, S., POWRIE, W., WATSON, G. & RICHARDS, D. J. The Impact of the reinforcing content on the shear strength of mechanically biologically treated waste. Third International Workshop " Hydro-Physico-Mechanics of Landfills", 10-13 March 2009 2009 Braunschweig, Germany.
FETTER, C. W. 1999. *Contaminant Hydrogeology,* New Jersey, USA, Prentice Hall
FLURY, M. & FLÜHLER, H. 1995. Tracer Characteristics of Brilliant Blue FCF. *Soil Science Society of America Journal,* 59**,** 22-27.
FLURY, M., FLÜHLER, H., JURY, W. A. & LEUENBERGER, J. 1994. Susceptibility of soils to preferential flow of water: A field study. *Water Resources Research,* 30**,** 1945-1954.
FREDRICKSON, G. H. & BICERANO, J. 1999. Barrier properties of oriented disk composites. *Journal of Chemical Physics,* 110**,** 2181-2188.
FREEZE, R. A. & CHERRY, J. A. 1979. *Groundwater,* Englewood Cliffs, New Jersey, Prentice Hall.
GAILLARD, J.-F., CHEN, C., STONEDAHL, S. H., LAU, B. L. T., KEANE, D. T. & PACKMAN, A. I. 2007. Imaging of colloidal deposits in granular porous media by X-ray difference micro-tomography. *Geophys. Res. Lett.,* 34**,** L18404.
GARNER, M. R. 1953. The Preparation of Latex Casts of Soil Cavities for the Study of Tunneling Activities of Animals.
GERMÁN-HEINS, J. & FLURY, M. 2000. Sorption of Brilliant Blue FCF in soils as affected by pH and ionic strength. *Geoderma,* 97**,** 87-101.
GOKTEPE, A. B. & SEZER, A. 2010. Effect of particle shape on density and permeability of sands. *Proceedings of the Institution of Civil Engineers: Geotechnical Engineering,* 163**,** 307-320.
GRADER, A. S., CLARK, A. B. S., AL-DAYYANI, T. & NUR, A. Computations of porosity and permeability of sparic carbonate using multiscale CT images. International Symposium of the Society of Core Analysts, 27-30 September 2009 2009 Noorwijk ann Zee, The Netherlands.
GRISOLIA, M., NAPOLEONI,Q., TANCREDI,G. Contribution to a Technical Classification of MSW. 2-6 October 1995 1995 S.Margherita di Pula, Cagliari, Italy. 703-710.
GÓMEZ-HERNÁNDEZ, J. & GORELICK, S. 1989. Effective groundwater model parameter values: influence of spatial variability of hydraulic conductivity, leakance, and recharge. *Water Resources Research,* 25**,** 405-419.
HALL, D. H., DRURY, D., GRONOW, J. R., POLLARD, S. J. T. & SMITH, R. 2007. Estimating Pollutant Removal Requirements for Landfills in the UK: III. Policy Analysis and Operational Implications. *Environmental Technology,* 28**,** 25-32.
HANGEN, E., GERKE, H. H., SCHAAF, W. & HÜTTL, R. F. 2004. Flow path visualization in a lignitic mine soil using iodine-starch staining. *Geoderma,* 120**,** 121-135.
HAZEN, A. 1911. Discussion of Dams on sand foundations. *Transactions of American Society of Civil Engineers,* 73**,** 199-203.
HAZEN, A. 1914. Storage to be provided in impounding reservoirs for municipal water supply. *Transactions of American Society of Civil Engineers,* 77**,** 1539-1669.
HEIJS, A. W. J., DE LANGE, J., SCHOUTE, J. F. T. & BOUMA, J. 1995. Computed tomography as a tool for non-destructive analysis of flow patterns in macroporous clay soils. *Geoderma,* 64**,** 183-196.
HERDAN, G. 1960. *Small Particle Statistics* Bath, Great Britain, Butterworths.
HILLEL, D. 1998. *Environmental Soil Physics,* San Diego, California, USA, Elsevier.
HUBBERT, M. K. 1940. The Theory of Ground-Water Motion. *Journal of Geology,* 48**,** 785-944.

HUDGINS, M. & HARPER, S. Operational characteristics of two aerobic landfill systems. Proceedings Sardinia 99. Seventh International Waste Management and Landfill Symposium, 1999 S.Margherita di Pula, Cagliari, Italy. 327-333.

HUDSON, A. P. 2007. *Evaluation of the vertical and horizontal hydraulic conductivities of household wastes.* Thesis for the degree of Doctor of Philosophy, University of Southampton.

HUDSON, A. P., BARKER, J. A. & BEAVEN, R. P. Preliminary Tests Investigating the Dispersion of Leachate Injection in Unsaturated Waste. Waste 2010: Waste and Resource Management-Putting Strategy into Practice, 28-29 September 2010 2010 Stratford-upon-Avon, Warwickshire, England.

HYSLIP, J. P. & VALLEJO, L. E. 1997. Fractal analysis of the roughness and size distribution of granular materials. *Engineering Geology,* 48**,** 231-244.

IVANOVA, L. K. 2007. *Quantification of Factors Affecting Rate and Magnitude of Secondary Settlement of Landfills.* Thesis for the degree of Doctor of Philosophy, University of Soutampton.

IVANOVA, L. K., RICHARDS, D. J. & SMALLMAN, D. J. 2008. The long-term settlement of landfill waste. *Proceedings of Institution of Civil Engineers: Waste and Resource Management,* 161**,** 121-133.

JOHNSON, C. A., SCHAAP, M. G. & ABBASPOUR, K. C. 2001. Model comparison of flow through a municipal solid waste incinerator ash landfill. *Journal of Hydrology,* 243**,** 55-72.

KAK, A. K. & SLANEY, M. 1988. *Principles of Computerized Tomographic Imaging,* New York, IEEE Press.

KETCHAM, R. A. & CARLSON, W. D. 2001. Acquisition, optimization and interpretation of X-ray computed tomographic imagery: applications to the geosciences. *Computers & Geosciences,* 27**,** 381-400.

KETELSEN, H. & MEYER-WINDEL, S. 1999. Adsorption of brilliant blue FCF by soils. *Geoderma,* 90**,** 131-145.

KETTRIDGE, N. & BINLEY, A. 2008. X-ray computed tomography of peat soils: Measuring gas content and peat structure. *Hydrological Processes,* 22**,** 4827-4837.

KETTRIDGE, N. & BINLEY, A. 2011. Characterization of peat structure using X-ray computed tomography and its control on the ebullition of biogenic gas bubbles. *Journal of Geophysical Research G: Biogeosciences,* 116.

KLYMKO, P. W. & KOPELMAN, R. 1982. Heterogeneous exciton kinetics: triplet naphthalene homofusion in an isotopic mixed crystal. *The Journal of Physical Chemistry,* 86**,** 3686-3688.

KOPELMAN, R. 1986. Rate processes on fractals: Theory, simulations, and experiments. *Journal of Statistical Physics,* 42**,** 185-200.

KOPELMAN, R. 1988. Fractal Reaction Kinetics. *Science,* 241**,** 1620-1626.

KORFIATIS, G. P., DEMETRACOPOULOS, A. C., BOURODIMOS, E. L. & NAWY, E. G. 1984. Moisture transport in a solid waste column. *Journal of Environmental Engineering,* 110**,** 780-796.

KORVIN, G. 1992. *Fractal Models in the Earth Sciences,* Amsterdam, Elsevier.

KRUMBEIN, W. C. 1936a. Application of logarithmic moments to size-frequency distributions of sediments.

KRUMBEIN, W. C. 1936b. Application of logarithmic moments to size-frequency distributions of sediments. *Journal of Sedimentary Petrology,* 6**,** 35-47.

KRUMBEIN, W. C. 1938a. Size frequency distributions of sediments and the normal phi curve.

KRUMBEIN, W. C. 1938b. Size frequency distributions of sediments and the normal phi curve. *Journal of Sedimentary Petrology,* 8**,** 84-90.

KRUMBEIN, W. C. & MONK, G. D. 1942. Permeability as a Function of the Size Parameters of Unconsolidated Sand. *Transactions of American Society of Civil Engineers,* 151**,** 153-163.

KÖLSCH, F. 1995. Material values for some mechanical properties of domestic waste. *In:* CHRISTENSEN, T. H., COSSU, R. & STEGMANN, R. (eds.) *Proceedings Sardinia 1995, Fifth International Waste Management and Landfill Symposium.* S. Margherita di Pula, Cagliari, Italy: CISA, Environmental Sanitary Engineering Centre, Ital.

LAMBE, T. W. 1951. *Soil Testing for Engineers,* New York, John Wiley & Sons, Inc.

LANDVA, A. O. & CLARK, J. I. 1990. Geotechnics of Waste Fill. *Geotechnics of Waste Fills-Theory and Practice* Pittsburgh, PA, USA: Publ by ASTM, Philadelphia, PA, USA.

LEE, J. S., GUIMARAES, M. & SANTAMARINA, J. C. 2007. Micaceous sands: Microscale mechanisms and macroscale response. *Journal of Geotechnical and Geoenvironmental Engineering,* 133**,** 1136-1143.
LIPSIUS, K. & MOONEY, S. J. 2006. Using image analysis of tracer staining to examine the infiltration patterns in a water repellent contaminated sandy soil. *Geoderma,* 136**,** 865-875.
MANDELBROT, B. B. 1982. *The fractal geometry of nature* San Francisco W.H. Freeman.
MANTELL, C. L. & SALZBERG, H. W. 1958. *Engineering Materials Handbook*, ECS.
MARTIN, D. J. 1999. Mass transfer limitations in solid-state digestion. *Biotechnology Letters,* 21**,** 809-814.
MARTIN, D. J. 2001. The Site of Reaction in Solid State Digestion: A New Hypothesis. *Trans IChemE,* 79**,** 29-37.
MAXWELL, J. C. 1954. *Treatise on Electricity and Magnetism,* New York, Dover Publications, Inc.
MCCULLOUGH, E. C. 1975. Photon Attenuation in Computed Tomography. *Medical Physics (Woodbury),* 2**,** 307-320.
MCDOUGALL, J. 2007. A hydro-bio-mechanical model for settlement and other behaviour in landfilled waste. *Computers and Geotechnics,* 34**,** 229-246.
MCDOUGALL, J. R. & PYRAH, I. C. 2004. Phase relations for decomposable soils. *Geotechnique,* 54**,** 487-493.
MCDOUGALL, J. R., PYRAH, I. C., YUEN, S. T. S., MONTEIRO, V. E. D., MELO, M. C. & JUCA, J. F. T. 2004. Decomposition and settlement in landfilled waste and other soil-like materials. *Geotechnique,* 54**,** 605-609.
MERAZ, R. L., VIDALES, A. M. & DOMINGUEZ, A. 2004. A fractal-like kinetics equation to calculate landfill methane production. *Fuel,* 83**,** 73-80.
MICHALOWSKI, R. L. & ZHAO, A. 1996. Failure of fiber-reinforced granular soils. *Journal of Geotechnical Engineering,* 122**,** 226-234.
MOONEY, S. J. & MORRIS, C. 2008. A morphological approach to understanding preferential flow using image analysis with dye tracers and X-ray Computed Tomography. *CATENA,* 73**,** 204-211.
MOONEY, S. J., MORRIS, C. & BERRY, P., M. 2006. Visualization and quantification of the effects of cereal root lodging on the three-dimensional soil macrostructure using x-ray computed tomography. *Soil Science,* 171**,** 706-718.
MORIASI, D. N., ARNOLD, J. G., VAN LIEW, M. W., BINGNER, R. L., HARMEL, R. D. & VEITH, T. L. 2007. Model Evaluation Guidelines for Systematic Quantification of Accuracy in Watershed Simulations *Transactions of the ASABE,* 50**,** 885-900.
MORRIS, C. & MOONEY, S. J. 2004. A high-resolution system for the quantification of preferential flow in undisturbed soil using observations of tracers. *Geoderma,* 118**,** 133-143.
MUNYANKUSI, E., GUPTA, S. C., MONCRIEF, J. F. & BERRY, E. C. 1994. Earthworm Macropores and Preferential Transport in a Long-Term Manure Applied Typic Hapludalf. *Journal of Environmental Quality,* 23**,** 773-784.
NAKAMURA, M., CASTALDI, M. J. & THEMELIS, N. J. Measurement of Particle Size and Shape of New York City Municipal Solid Waste and Combustion Residues Using Image Analysis. Proc. 16th Japan Society of Waste Management Experts (JSMWE) Fall Conference, 2005 Sendai, Japan. Earth Engineering Center and Department of Earth and Environmental Engineering, 1-3.
NAYAGUM, D., WHITE, J., ZARDAVA, K. & BEAVEN, R. 2010. The use of a numerical model to extrapolate laboratory scale results on waste to full scale landfill remediation applications. *Global Waste Management Symposium.* San Antonio, Texas.
NIELSEN, L. E. 1967. Models for the Permeability of Filled Polymer Systems. *Journal of Macromolecular Science: Part A - Chemistry,* 1**,** 929-942.
NIXON, M. & AGUADO, A. 2008. *Feature extraction & Image Processing,* Oxford, Elsevier.
PAGLIAI, M. & VITTORI, A. L. 1993. Influence of waste organic matter on soil micro-and macrostructure. *Bioresource Technology,* 43**,** 205-213.

PARKER, L. J., WHITE, J. K. & POWRIE, W. The measurement of the geotechnical and hydrogeological properties of degrading solid waste Sardinia 1999, Seventh International Waste Management and Landfill Symposium, 1999 S. Margherita di Pula, Cagliari, Italy; 4-8 October 1999.

PELT, W. R., BASS, R. L. & BLACKARD, A. L. 1990. Landfill Air Emissions Estimation Model User´s Manual. *In:* AGENCY, U. E. P. (ed.).

PERFECT, E. & KAY, B. D. 1995. Applications of fractals in soil and tillage research: a review. *Soil and Tillage Research,* 36**,** 1-20.

PERRET, J. S., PRASHER, S. O. & KACIMOV, A. R. 2003. Mass fractal dimension of soil macropores using computed tomography: from the box-counting to the cube-counting algorithm.

PEYTON, R. L., HAEFFNER, B. A., ANDERSON, S. H. & GANTZER, C. J. 1992. Applying X-ray CT to measure macropore diameters in undisturbed soil cores. *Geoderma,* 53**,** 329-340.

POPE. J.A. 1999. *Medical Physics: imaging* Oxford, Heinemann Educational Publishers.

POWRIE, W. 1997. *Soil Mechanics : Concepts and applications 2nd Edition,* Abingdon, Oxon, Spon Press.

POWRIE, W. & BEAVEN, R. P. 1999. Hydraulic properties of household waste and implications for landfills. *Proceedings of the Institution of Civil Engineers, Geotechnical Engineering,* 137**,** 235-247.

POWRIE, W., BEAVEN , R. P., WATSON, G. V. R., RICHARDS, D. J., BARKER, J. A., WHITE, J. K., ATKINSON, T. C., WOODMAN, N. D. & MUNNICH, K. Landfill Science Research Needs: After the EU Landfill Directive. Proceedings Sardinia 2007, Eleventh International Waste Management and Landfill Symposium, 1 - 5 October 2007 2007 S. Margherita di Pula, Cagliari, Italy.

POZDNIAKOV, S. & TSANG, C. F. 2004. A self-consistent approach for calculating the effective hydraulic conductivity of a binary, heterogeneous medium. *Water Resources Research,* 40.

QUINTON, W. L., HAYASHI, M. & CAREY, S. K. 2008. Peat hydraulic conductivity in cold regions and its relation to pore size and geometry. *Hydrological Processes,* 22**,** 2829-2837.

RAVINDRA, P. V., RAO, D. P. & RAO, M. S. 1997. Liquid flow texture in trickle-bed reactors: An experimental study. *Industrial & Engineering Chemistry Research,* 36**,** 5133-5145.

REES-WHITE, T. The examination of 3 leachate wells exhumed from a landfill. Waste 2004, September 2004 2004 Stratford uppon Avon.

REZANEZHAD, F., QUINTON, W. L., PRICE, J. S., ELLIOT, T. R., ELRICK, D. & SHOOK, K. R. 2010. Influence of pore size and geometry on peat unsaturated hydraulic conductivity computed from 3D computed tomography image analysis. *Hydrological Processes,* 24**,** 2983-2994.

SANTAMARINA, J. C. & CHO, G. C. Soil behaviour: The role of particle shape. Advances in Geotechnical Engineering: The Skempton Conference, 2004 London. Thomas Telford, 604-617.

SATO, H. & SUZUKI, S. 2003. Fundamental study on the effect of an orientation of clay particles on diffusion pathway in compacted bentonite. *Applied Clay Science,* 23**,** 51-60.

SHIPITALO, M. J., NUUTINEN, V. & BUTT, K. R. 2004. Interaction of earthworm burrows and cracks in a clayey, subsurface-drained, soil. *Applied Soil Ecology,* 26**,** 209-217.

SIDDIQUI, A. 2011. *Biodegradation and Settlement Behaviour of Mechanically Biologically Treated (MBT) Waste.* Thesis for the degree of Doctor of Philosophy, University of Southampton.

SIEGEL, R. A., ROBERTSON, R. J. & ANDERSON, D. G. 1990. Geotechnics of waste fills – theory and practice. *In:* LANDVA & KNOWLES (EDS) GEOTECHNICS OF WASTE FILLS (ed.) *ASTM Special Publication STP1070.* Baltimore: American Society for Testing and Materials.

STOLTZ, G., GOURC, J.-P. & OXARANGO, L. 2010. Characterisation of the physico-mechanical parameters of MSW. *Waste Management,* 30**,** 1439-1449.

SWEENEY, S. M. & MARTIN, C. L. 2003. Pore size distributions calculated from 3-D images of DEM-simulated powder compacts. *Acta Materialia,* 51**,** 3635-3649.

TURCOTTE, D. L. 1986. Fractals and Fragmentation. *Journal of Geophysical Research-Solid Earth and Planets,* 91**,** 1921-1926.

TYLER, S. W. & WHEATCRAFT, S. W. 1989. Application of Fractal Mathematics to Soil-Water Retention Estimation. *Soil Science Society of America Journal,* 53**,** 987-996.

TYLER, S. W. & WHEATCRAFT, S. W. 1992. Fractal Scaling of Soil Particle Size Distributions: Analysis and Limitations *Soil Science Society of America Journal,* 56**,** 362-369.

VAN OMMEN, H. C., DEKKER, L. W., DIJKSMA, R., HULSHOF, J. & VAN DER MOLEN, W. H. 1988. A new technique for evaluating the presence of preferential flow paths in nonstructured soils. *Soil Science Society of America Journal,* 52**,** 1192-1993.

VELKUSHANOVA, K., CAICEDO, D., RICHARDS, D. J. & POWRIE, W. A detailed characterisation of an MBT waste. Proceedings Sardinia 2009, Twelfth International Waste Management and Landfill Symposium, 5-9 October 2009 2009 S. Margherita di Pula, Cagliari, Italy.

WALL, D. K. & ZEISS, C. 1995. Municipal Landfill Biodegradation and Settlement. *Journal of Environmental Engineering-Asce,* 121**,** 214-224.

WANG, Z. & FENG, H. 2010. Fractal kinetic analysis of the enzymatic saccharification of cellulose under different conditions. *Bioresource Technology,* 101**,** 7995-8000.

WANG, Z., XU, J.-H., FENG, H. & QI, H. 2011. Fractal kinetic analysis of polymers/nonionic surfactants to eliminate lignin inhibition in enzymatic saccharification of cellulose. *Bioresource Technology,* 102**,** 2890-2896.

WASHINGTON, C. 1992. *Particle size analysis in pharmaceutics and other industries: Theory and Practice* Chichester, West Sussex, England.

WATSON, G. V. R., POWRIE, W. & BLADES , A. P. Particle scale classification and identification of the structure of processed municipal solid waste by CT scanning. *In:* HYODO, M. A. N., ed. International Symposium on Geomechanics and Geotechnics of Particulate Media 2006 Yamaguchi, Japan.

WATSON, G. V. R., POWRIE, W. & BLADES , A. P. An investigation into the effects of degradation on waste structure. Proceedings Sardinia 2007, Eleventh International Waste Management and Landfill Symposium, 1 - 5 October 2007 2007 S. Margherita di Pula, Cagliari, Italy.

WEILER, M. & FLÜHLER, H. 2004. Inferring flow types from dye patterns in macroporous soils. *Geoderma,* 120**,** 137-153.

WELLINGTON, S. L. & VINEGAR, H. J. 1987. X-Ray Computerized Tomography *Journal of Petroleum Technology* 39**,** 885-898.

WERTH, C. J., ZHANG, C., BRUSSEAU, M. L., OOSTROM, M. & BAUMANN, T. 2010. A review of non-invasive imaging methods and applications in contaminant hydrogeology research. *Journal of Contaminant Hydrology,* 113**,** 1-24.

WHITE, H. E. & WALTON, S. F. 1937. Particle Packing and Particle Shape *Journal of the American Ceramic Society,* 20**,** 155-166.

WHITE, J., ROBINSON, J. & REN, Q. 2004. Modelling the biochemical degradation of solid waste in landfills. *Waste Management,* 24**,** 227-240.

WHITE, J. K. & BEAVEN, R. P. The role of pore space geometry, waste descriptors, and micro-scale network modelling in the design of macro-scale landfill modesl. Global Waste Management Symposium, September 7-10 2008 Colorado, USA

WILSON, W. S. 1991. Advances in Soil Organic Matter Research: The Impact of Agriculture and the Environment. *In:* ROYAL SOCIETY OF CHEMISTRY, U. (ed.). Cambridge: Woodhead Publishing Ltd.

WITHJACK, E. M. 1988. Computed Tomography for Rock-Property Determination and Fluid-Flow Visualization. *SPE Formation Evaluation,* 3**,** 696-704.

WU, Q., BORKOVEC, M. & STICHER, H. 1993. On Particle-Size Distributions in Soils. *Soil Science Society of America Journal,* 57**,** 883-890.

XIE, M., ALDENKORTT, D., WAGNER, J.-F. & RETTENBERGER, G. 2006. Effect of plastic fragments on hydraulic characteristics of pretreated municipal solid waste. *Can. Geotech. J.,* 43**,** 1333–1343

XU, F. & DING, H. 2007. A new kinetic model for heterogeneous (or spatially confined) enzymatic catalysis: Contributions from the fractal and jamming (overcrowding) effects. *Applied Catalysis A: General,* 317**,** 70-81.

YAMADA, H., TAMURA, K., WATANABE, Y., IYI, N. & MORIMOTO, K. 2011. Geomaterials: their application to environmental remediation. *Science and Technology of Advanced Materials,* 12.

ZEISS, C. & MAJOR, W. 1992. Moisture flow through municipal solid waste: patterns and characteristics. *Journal of Environmental Systems* 22.

ZIMMERMAN, R. W. 1996. Effective conductivity of a two-dimensional medium containing elliptical inhomogeneities. *Proceedings of the Royal Society of London Series a-Mathematical Physical and Engineering Sciences,* 452**,** 1713-1727.